PART I.

GEOLOGY OF THE MANICOUAGAN-MUSHALAGAN LAKES STRUCTURE

PART II.

GEOCHRONOLOGY OF THE MANICOUAGAN-MUSHALAGAN LAKES STRUCTURE

Thesis by

Stephen Howard Wolfe

In Partial Fulfillment of the Requirements

for the Degree of

Doctor of Philosophy

California Institute of Technology

Pasadena, California

1972

(Submitted September 20, 1971)

ACKNOWLEDGEMENT

The completion of this thesis would not have been possible without the aid, both financial and intellectual, from many sources.

I am indebted to my advisor, G. J. Wasserburg, for financial support, laboratory facilities and guidance during the geochronological phase of the work. I would like to thank E. M. Shoemaker for stimulating my interest in the problem, for extensive and constructive criticism concerning the geological aspects of the study, and for help in obtaining support from the U.S.G.S. John Huneke provided invaluable advice and guidance with the geochronological laboratory work, and Grenville Turner supplied guidance without which the Ar^{40}-Ar^{39} studies would not have been possible. A. L. Albee was a continuing and non-grudging source of information concerning electron microprobe procedures, and L. T. Silver took time for informative and stimulating discussions of the problem.

My wife, Ronny, put up with me during much of the work, typed three drafts of the tome and did most of the figure drafting. Many of the technical people from the department, P. Young, V. Nenow, L. Ray, A. Chodos, E. Bingham and T. Wen, were extremely helpful during the course of the work.

These thesis studies were carried out with the support of the California Institute of Technology. The U. S. Geological Survey provided financial support and paid for field expenses during

the field work in the summers of 1965 and 1966. Most of the work was supported by National Science Foundation grants GP-19887 and GP-9114 and National Aeronautics and Space Administration contract NAS 9-8074.

ABSTRACT

The Manicouagan-Mushalagan Lakes structure is an area of anomalous geological features in the Grenville Province terrain of northeastern Canada. Three features of this structure have been revealed by geological studies:

(1) The Grenville gneisses and anorthosites which outcrop in the area between the arcuate lakes have been shock metamorphosed.

(2) The shocked Grenville gneisses are covered by a thin, discontinuous layer of shock breccia and thin outcrops of Ordovician limestone.

(3) An annular-shaped body of Permo-Triassic, igneous, andesitic rock, which shows no signs of shock metamorphism, overlies the shocked gneisses, the shock breccia and the Ordovician limestone. This rock (monzonite) is 800 feet thick at a maximum.

The shocked basement rocks in the structure were most probably caused by the impact of an extraterrestrial body, but the origin of the igneous rock unit is not completely understood. This latter unit has been hypothesized to be either (1) a shock-melted breccia or (2) a later, secondary igneous event occurring at the crater site due to disruptions of the earth's thermal regime around the impact site. A geochronological study of this structure was made to determine which, if either, of the above modes of formation for the igneous material is likely.

Ar^{40}-K^{40} data for the igneous material and rock units related to it yield a well-defined crystallization age of 210 ± 4 m.y. Ar^{40}-Ar^{39} data for this unit indicate that it has experienced no subsequent metamorphism. Argon isotopic ages obtained for a series of shock-sequence anorthosites do not indicate a well-defined time of shock metamorphism; the ages could characterize a system shocked at any time between 320 and 210 m.y. ago which then suffered a secondary gas loss. It is shown that anorthosites yielding ages between 280 and 320 m.y. probably underwent complete or nearly complete outgassing at the time of shock. These latter ages should therefore yield a good impact age. The time interval within which the impact took place is thought to be 280-320 m.y. ago.

The Ar^{40}/Ar^{39} data show unexpected evidence for the occurrence of a secondary event at about 100-110 m.y. which affected the anorthosites in the crater but not the igneous monzonite.

Since it is not possible to say with certainty when the meteoritic impact took place, the difference between the monzonite formation time and the impact time is unclear. The suggested impact time is, however, significantly earlier than the crystallization time of the igneous material. This suggests that a secondary formation mode for this material is more likely than an impact melt formation mode. A secondary mode is also compatible with evidence that the monzonite formed in a subsurface environment with $po_2 < 0.2$ atm.

This study is the only case where the hypothesis of impact-melt formation of igneous rocks has been subjected to careful scrutiny. The fact that the observed data does not obviously conform with and may contradict the predictions of this theory suggests that the theory should be subjected to closer scrutiny.

The Ar^{40}-Ar^{39} studies clearly show that the shock-metamorphic process produces a very complicated series of changes. It is also shown that a simple model of thermal outgassing of a shocked system is inadequate to explain the results observed.

TABLE OF CONTENTS

INTRODUCTION

The Manicouagan-Mushalagan Lakes area (51°31'N latitude, 68°W longitude) was originally recognized to be a region of aberrant geology by Hammond (1945). Hammond noted extensive outcrops of "volcanic"-appearing material between the two lakes. The unusual rock deformations, which are present in the area, were not observed. The original theory that the structure is meteoritic in origin was probably inspired by the circularity of the two lakes when viewed on aerial photographs. Beals et al. (1963) originally suggested that the Manicouagan-Mushalagan Lakes area was of meteoritic origin. Rose (1955) had previously considered a meteoritic impact origin for the area, but he thought it to be untenable. Subsequent investigations have revealed that "shock"-deformational features, similar to those found in other meteoritic impact sites, are indeed present in the basement complex exposed in this structure (Currie, 1964; Dence, 1965; Wolfe, 1966; Bunch et al., 1967; Murtaugh and Currie, 1969; Wolfe and Hörz, 1970). Further study of the "volcanic" material, however, has revealed none of the planar features, partial vitrification or extensive fracturing normally observed in shocked materials. This poses a dilemma: the most likely origin of shock-deformation features in terrestrial rocks is the impact of a large, meteoritic mass. Although such an event would explain many of the anomalous features of the Manicouagan-Mushalagan Lakes structure, it does not explain how the apparently igneous or "volcanic" material

originated. It is primarily this question which has prompted the research for this thesis.

The earth has experienced, during the last 70 years, the impacts of two large extraterrestrial bodies whose masses exceeded 10^5kg. The effects of these hint at what could be expected to occur during impacts of still larger bodies. The Tunguska meteorite in 1908 was probably a small, cometary object (Krinov, 1966) whose mass has been estimated at about 10^7kg (Krinov, 1963). Effects from this comparatively small body were wide ranging and violent as summarized by Krinov (1966) in his book, Giant Meteorites. They included the observable passage around the earth of an atmospheric pressure pulse (recorded at about 0.2 milibars in England), a seismic tremor recorded as a mild shock 900 km away, and the blowing over of many objects and people 60 km away. The most spectacular optical effects were the passage of the fireball through the atmosphere and the remaining dust train. Subsequent "white nights" probably resulted from stratospheric dust from the comet's tail and ablated from the body. The Tunguska object disintegrated aerially near the ground, probably due to its small size. Although it produced no craters, large areas of trees were blown over in the impact area due to the explosion.

In 1947 a small shower of iron meteorites fell in eastern Siberia. The estimated size of the original body was about 10^5kg. This meteorite broke up in the atmosphere and

produced only small craters, the largest being about 30 meters in diameter. Noise, dust, and slight seismic disturbances accompanied this fall; however, the magnitude of the effects produced was much less than that observed for the Tunguska body (Krinov, 1963).

These two objects are small, indeed, when compared to the 10^8kg body which probably formed Meteor Crater (Shoemaker, 1963). They appear even more insignificant when compared to the estimated 10^{12}kg body which would form a feature like Manicouagan (see Part I , Chapter 1).

Bodies impact the earth at between 10 and 70 km/sec; hence, the amount of energy dissipated is proportional to the mass of the body (within a factor of 50). It can be assumed that, regardless of the kinetic energy of an impacting body, energy is similarly partitioned between the processes which take place in the impact. From this one may conclude that an impacting 10^{12}kg body would produce air waves about 10^5 as energetic as those of the Tunguska body, and earthquakes would be universally felt. The dust cloud remaining would be at least as dense, and probably denser, than that produced by the Tunguska body since the impact would scatter much fine dust or water high into the atmosphere. If the impact site were located in an area covered by water, a significant amount of energy could still be transmitted to the underwater surface, and a tremendous quantity of water would be blown up into the atmosphere. Ice crystals formed from this water would temporarily refrigerate the earth by reflecting solar energy and, in the long term, deluge the

earth in the polar regions. The great water wave traveling outward would be responsible for inundation of large areas.

The extent of the effects which would be produced by such an impact is largely speculative. It is very possible, however, that resultant air waves could kill much of the existing fauna on the earth's surface, earthquakes would be triggered and produced worldwide, and dust in the atmosphere could result in major climatic changes. Dust or ice and clouds mantling the earth might sufficiently reduce solar flux, thereby producing a continental glaciation or extended pluvial periods. For these "immediate effects", one might be able to find evidence of glaciations, climatic changes, or mass faunal extinction in the sedimentary record.

In addition to the "immediate effects" discussed briefly above, one might ask what the long-term disturbances produced by a very large impacting body would be. These effects can be inferred from the present-day appearances of craters which presumably appeared quite differently at an earlier time.

The Nördlinger Ries is presently expressed as a shallow basin with a rim about 400-500 feet higher than its reasonably flat bottom (Hörz, 1965; Bucher, 1963). Large craters initially resemble wide, flat-bottomed basins. Such basins could be expected to become centers for sedimentation due to the inward drainage from the rim. Outside the rim, drainage would be away from the crater. In large craters, sediments may be preserved

in impact-originated basins during periods when the rest of the area is being denuded. Circular, isolated outcrops of sediments in old meteorite basins can be found in certain areas. Many younger craters (Meteor and Wolf Creek) contain pluvial lakes (Baldwin, 1949), and the Rieskessel contains Pleistocene lake beds (Bucher, 1963). Flynn Creek Crater in Tennessee contains "preserved" sediments (Roddy, 1968). For very large craters ($>$20 miles in diameter), a logical post-impact event would be an isostatic uplifting of the central area and a flattening of the crater profile (Dence, 1965). As the central part of the crater becomes uplifted, sediments would be removed from the center; however, evidence of the original drainage directions should be preserved. The drainage divide on the rim produced shortly after the original basin was excavated would probably persist long after the original crater was uplifted, provided the platform it formed on remained reasonably stable.

Perhaps the most interesting long-term effect likely to result from an impact is the production of a "lava"-like material which lies on the crater floor. Such flat-lying, extrusive-appearing units have been known for a long time to line lunar craters (Dietz, 1946); however, Sudbury (French, 1967) and Manicouagan are the only suspected terrestrial craters which show any closely analogous material in the crater. At present, the only real evidence that these materials are related to the impact events is that the "lavas" are spatially confined to vicinities

immediately surrounding the areas of highly shocked rocks. The origin of these lava-like materials is a very interesting question because its resolution would yield some real data on a terrestrial event which has, as its root cause, interactions of the earth with other bodies in the solar system.

The problem of whether or not terrestrial effects of large meteorite impacts are present is the most interesting question which the information in this thesis can touch on. In general, geological arguments tend to assume some initial cause or event, the extrusion of lavas, the intrusion of a large batholith or the breaking up of a primitive proto-continent, and describe the sequence of resulting effects. The reason for the initial event is not generally considered. Impacting objects may be partly or totally responsible for such events. If so, the fact that the earth is part of the solar system will once again be emphasized. It has been suggested that continental drift was initiated by an impact event (Kelly, 1955). Whether or not this is true remains to be seen, but the idea raised is an intriguing one, and the interaction of the earth with the solar system is a subject for further research.

Two modes of formation of the extrusive units mentioned above have been suggested:

(1) That they arise from shock breccias and shock melt collecting in the crater, melting together and then crystallizing to produce the material presently observed.

(2) That they are due to the extrusion of terrestrial, magmatic material into the crater. The emplacement of this material is strongly affected or controlled by some feature of the impact.

The suggestion has also been made that the material in the crater is a terrestrial, volcanic rock, and that an explosive phase of the volcano which erupted the lava formed the crater. This theory is discounted because no known terrestrial explosions attain sufficient intensity to produce the observed deformations (Roddy, 1968).

Based on consideration of the above, in May of 1966 this thesis problem was formulated in which the author undertook to answer the following questions:

(1) Are the evidences of "shock" deformation at Manicouagan real? Stated otherwise, have shock waves deformed the basement? If so, what else have they done?

(2) At what time did the deformations take place?

(3) At what time did the monzonite body crystallize?

(4) Is there a time difference between the crystallization of the monzonite and the deformation? If so, what is it?

The method of attack can be described as twofold:

(1) A study of the petrographic nature of representative samples from the rock units exposed in the crater in order to determine whether or not this structure really involved shock processes in its formation and what insights into its origin could be obtained. This part of the work is described in Part I of the thesis.

(2) A geochronological study of deformed samples was made in an effort to determine the time of deformation. A parallel study was made of the apparently igneous "lava" exposed in the crater in order to determine its time of formation. The hope was that these two ages would be unambiguously indicated, and that the second, third, and fourth questions posed above could thereby be answered. The efforts to resolve these questions are described in Part II of this thesis.

DETAILED OUTLINE OF PART I

Detailed Outline of Part I -- Continued.

Detailed Outline of Part I -- Continued.

Detailed Outline of Part I -- Continued.

Detailed Outline of Part I -- Continued.

Detailed Outline of Part I -- Continued.

Detailed Outline of Part I -- Continued.

CHAPTER 1

Geology of the Manicouagan-Mushalagan Lakes Structure

Introduction:

The Problem --

In the northeastern part of Quebec, southeast of the Grenville Front, two narrow, arcuate lakes outline a polygonal or roughly circular area about 36 miles in diameter in which outcrops atypical of the Grenville Province are present. The center of this feature, termed the Manicouagan-Mushalagan Lakes structure, is located about 600 miles northeast of Montreal (68°30'W long, 51°30'N lat) in the subarctic belt of Canada.

Outside the two large lakes, calcareous or quartzo-feldspathic metasedimentary and metaigneous gneisses of amphibolite and granulite grade can be found over distances of 200 miles in any direction from the structure. Potassium-argon isotopic ages determined for rocks external to the crater indicate that major metamorphism of these rocks took place about 955 m.y. ago (Stockwell, 1970). Interior to the two lakes, extensive outcrops of a Triassic igneous rock are found. Basement gneisses inside the crater display unusual microscopic deformation features which are not found in other regionally metamorphosed terrains. Along the interior margins of the two large lakes, small outcrops of fossiliferous Ordovician limestone occur.

The contrast between the rock types inside and outside of the two large lakes strongly suggests that the geological processes operative within the structure have been very different from the processes involved in the development of the rocks external to the structure.

Previous Work --

The presence of the two lakes is not indicated on the 1865 geological map of Canada. Map 91A (1913) shows the two large lakes as lying in an area of undifferentiated Grenville-type gneisses. Although easily visible on global maps, the extremely poor knowledge of the area both cartographically and geologically delayed the first serious investigations of the area until 1945 when W. P. Hammond (1945) undertook a study of the area in a master's thesis. Hammond was prompted by the prospecting work of W. I. Keith for the Mining Corporation of Canada (unpublished report) as well as by some preliminary reconnaissance work along the shore of Manicouagan Lake done by C. Faessler (1933). In his study, Hammond noted that there were outcrops of "Proterozoic lava" within an area limited to the interior of the two lakes. He recognized that these lavas were different from the surrounding Grenville Province rocks, and that small, isolated outcrops of Ordovician limestone occurred on the interior margins of Manicouagan and Mushalagan Lakes. Hammond attributed these peculiarities to subsidence of a dome of extrusives in an area interior to the lakes. He felt that the interior of the lakes had been a basin in which the thin Ordovician limestone had been

preserved. He also felt that the original basin was formed by a caldera subsidence.

Prompted by the circularity of the two lakes, the Dominion Observatory of Ottawa employed E. R. Rose to geologically investigate the structure. In his preliminary map, Rose (1955) discounted a meteoritic theory of origin for this structure but realized that the rock interior to these two lakes was very different from the Precambrian gneisses and anorthosites and resembled a younger intrusive or extrusive. Rose interpreted the anorthosite in the center of the structure and the trachyandesite (his terminology for the younger intrusive) as being part of one and the same post-Paleozoic intrusive unit which was intruded into the gneisses of Grenville Province. He believed that the andesites and anorthosites intruded and had originally overlain the Ordovician limestone and hence were younger than it. He interpreted the present expression of the structure as having been caused by erosion along fault and joint planes around the resistant igneous intrusive.

In 1959 the Quebec-Cartier Mining Company commenced iron mining operations on a recently discovered metamorphic iron shale outcrop 40 miles to the northeast. A mining settlement, Gagnon, was built on Barbelle Lake. Developmental plans for the area included a hydroelectric power plant. In 1960 construction began on a 700-foot hydroelectric dam at the southern juncture of the two lakes. Subsequent flooding of areas marginal to the lakes by

the impounded waters of the Manicouagan and Mushalagan Lakes prompted a geological survey of the shoreline edges of the lakes by Jean Berard in 1962. Previous preliminary maps of the lower area of the Hart Juane River (which flows into Manicouagan Lake) by L. Kish (1962) covered an area of the "trachyandesite" outcrops inside the lakes.

From 1962 onward an impetus was provided for the study of meteoritic impact sites (suspected or proven) by the Apollo Project, as well as by questions raised on contradictory conclusions drawn by previous investigators, The Manicouagan-Mushalagan Lakes area then became an active site for further research by numerous investigators, including teams from the Dominion Observatory of Ottawa (Dence, 1965; Beals et al., 1963; Beals, 1965).

In 1965 after arrangements for appointment as a temporary field geologist with the U. S. Geological Survey in Menlo Park had been made by E. M. Shoemaker, the field investigations for this thesis commenced. Subsequent field work was done in the summers of 1966 and 1968. In 1968 a large collection of samples was made for geochronological study which was already in progress under the supervision of G. J. Wasserburg.

The Manicouagan-Mushalagan Lakes area is located in the northern subarctic belt of Canada. Geological work is limited by snow cover to the period of May 15 through September 15. The ground is permanently frozen from a level of about two feet below the surface, causing surface drainage and swampy conditions to be prevalent.

Extremely thick vegetative cover consisting mainly of stunted black spruce, birch, tamarack, alder, and moss make travel difficult and limited to foot and canoe. The area is completely devoid of roads or permanent settlement. The nearest town, Gagnon, lies 40 miles to the northeast. Gagnon was founded in 1958 and has a population of approximately 3500. The residents are mostly resettled French Canadians employed nearly exclusively by the Quebec-Cartier Mining Company. In order to pursue geological investigation, the most effective method is for an individual to arrange for chartered light aircraft (i.e. Beavers) to deposit him with enough supplies for a one- to two- week tent camp on the shores of one of the moderately sized lakes near a region of interest. One can then make foot and canoe traverses over a four- to six- mile area around his site. Frequent heavy rainstorms (one day out of three) and clouds of biting insects further complicate geological field work.

The Setting of the Manicouagan-Mushalagan Structure in Grenville Province:

Grenville Province in a Broad View --

In Fig. 1 the location of the Manicouagan-Mushalagan Lakes structure is shown. The structure occurs in an area of the Canadian Shield known as the Grenville Province. Grenville Province appears as a roughly elongate area of the Canadian Shield. On the northwest, Grenville Province rocks yield to rocks of the Superior and Nain Provinces. The boundary between these provinces is a fault zone, or zone of rapid change in

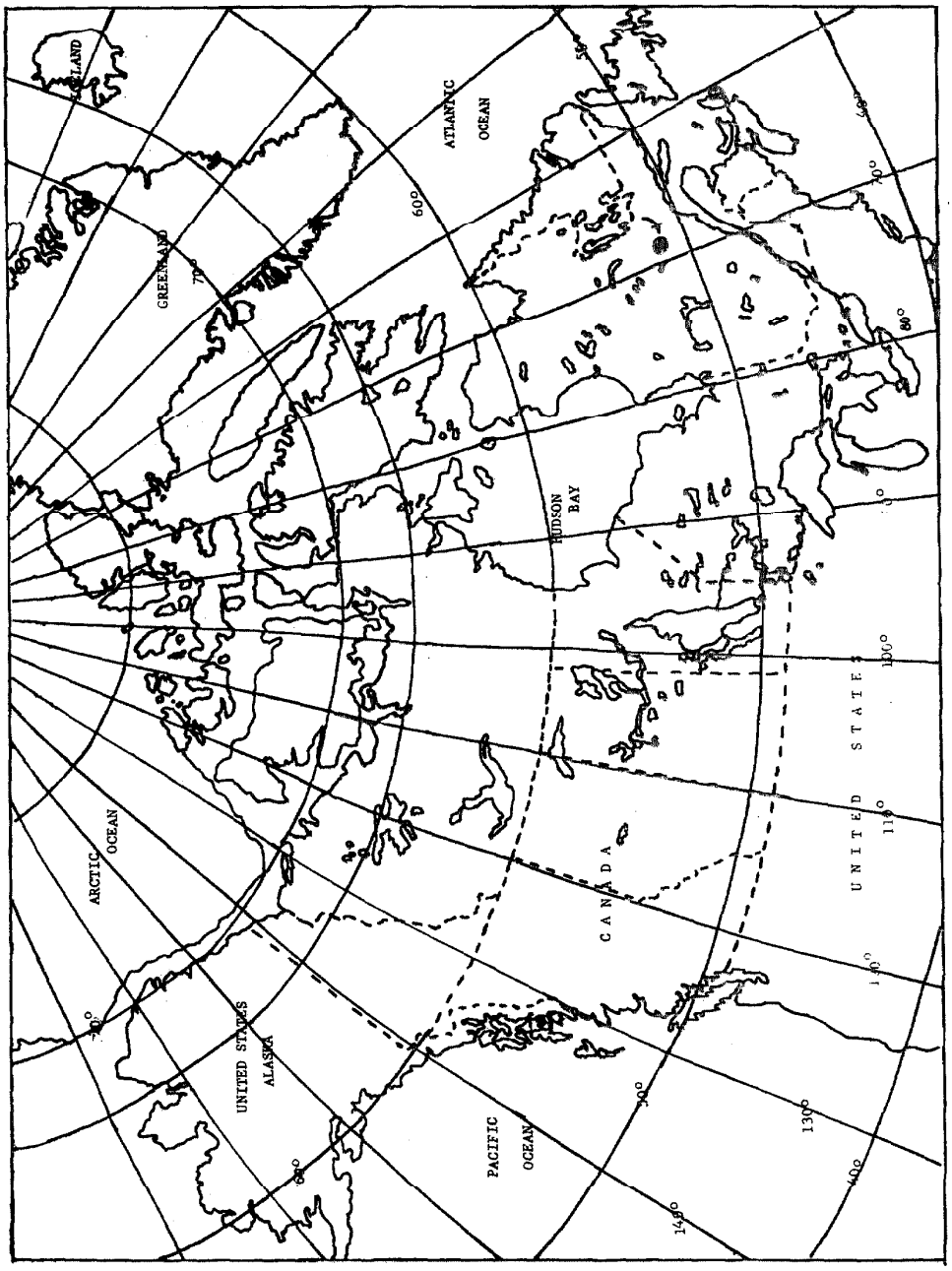

LOCATION OF MANICOUAGAN-MUSHALAGAN LAKES STRUCTURE
(DOT WITH ARROW)

FIG. 1

metamorphic grade, known as the Grenville Front. Grenville Province borders the St. Lawrence River on the southeast. It has been suggested (Kumarapeli and Saull, 1966) that the St. Lawrence flows in part of a rift valley system. A series of normal faults which form the north wall of this rift valley also mark the southeastward limit of rocks of Grenville Province. This line of normal faults, which extends to the south along the eastern side of the Adirondack Mountains, has been referred to as the Laurentian Escarpment (Kumarapeli and Saull, 1966). On the southwest, Paleozoic sediments cover the Precambrian Shield rocks. The Atlantic Ocean forms the geographic boundary of Grenville Province on the northeast. The rocks of the province, however, may extend as far as Greenland and possibly Norway (Kulp and Neumann, 1961).

Although Grenville Province is defined above in a restricted sense, it has been forcibly argued by many workers that Grenville-type rocks are quite widespread (see Wasserburg et al. (1962) and Wasserburg (1966)).

Rocks of Grenville Province --

Metamorphic: The majority of Grenville Province rocks are metamorphic. These rocks are gneisses, both metasedimentary and metaigneous, with bodies of anorthosite, granite and gabbro. Although trends are highly variable, a general N-S or NW-SE trend is exhibited by the fold axes, planes of shistosity, and gneissosity. In contrast, the trends of such features in the Superior Province

north of the Grenville Front are predominantly E-W and NE-SW. Folding tends to be tighter with steeper dips in Grenville Province than in Superior Province. As a whole, folding and gneissosity trends are extremely variable in Grenville Province. In the Manicouagan area, however, NW-SE directions are dominant. The gneisses of Grenville Province are typically of amphibolite to granulite grade. Some of the rocks are granitic or seyenitic plutons. Extensive discussions of the metamorphic rocks of Grenville Province can be found elsewhere (Stockwell, 1970).

Isotopic ages obtained for Grenville Province rocks (mostly by K-Ar methods) cluster reasonably tightly around 955 m.y., although a spread from 800-1100 m.y. is seen. The time of the Grenville Orogeny is taken as 955 m.y. (Stockwell, 1970).

Igneous: The Canadian Shield is largely free of Paleozoic or younger igneous activity. The Grenville Orogeny is the most recent period of extensive igneous and metamorphic activity on the shield. Minor igneous activity has, however, taken place on the shield. This activity is widespread in location and in times of occurrence.

Large areas of the shield, especially Superior and Churchill Provinces, have been intruded by diabase dike swarms (Fahrig et al., 1965; Fahrig and Wanless, 1963). These dikes, which mineralogically resemble tholeiitic basalts, are vertical or steeply dipping bodies. Individual dikes may extend for over 100 miles with widths exceeding 500 feet (Fahrig et al., 1965). Fahrig and Wanless (1963) have obtained potassium-argon ages ranging from 2500 m.y. to 600 m.y. for dike swarms in various localities of the Canadian Shield.

Diabase dikes of Paleozoic and younger ages appear southeast of the St. Lawrence River. In particular, a dike with a 207 m.y. age is located 500 miles southeast of the Manicouagan area on Prince Edward Island (Poole, 1970). An E-W trending diabase dike with a 194 m.y. age occurs in southern Nova Scotia (Wanless et al., 1968). Another diabase dike which is 138 m.y. old can be found on the north shore of Anticosti Island (Wanless et al., 1967). The Monteregian Hills east of Montreal represent another set of intrusive rocks of Mesozoic age which are adjacent to the shield. On the basis of rubidium-strontium studies, Fairbain et al. (1963) have suggested that these bodies were intruded about 113-124 m.y. ago. An intrusive body at Oka, west of Montreal, intrudes a Precambrian outlier of Grenville Province (Gold and Vallee, 1969). Fairbain et al. (1963) have obtained a 114 m.y. age for the carbonatite body at Oka and suggest that this complex is contemporaneous with the intrusives of the Monteregian Hills. It is probable that Paleozoic intrusive bodies exist in other localities within Grenville Province.

It has been proposed by Fahrig and Wanless (1963) that diabase dikes may have been originally feeder dikes for plateau basalt flows. They suggest that these flows have been eroded and were originally much more extensive than they are today. If this is true, then the present appearance of the shield which is largely devoid of Paleozoic extrusive rocks may be somewhat unrepresentative of its previous appearance. The presence of large numbers of diabase dikes with very different ages, as well

as intrusive complexes with Paleozoic and younger ages, suggests that igneous events (at least small-scale events) occur on the Shield.

Sedimentary: Paleozoic sedimentary rocks are present in Grenville Province, but such rocks are rare. Extensive outcrops of Paleozoic sedimentary cover are found on the southeastern and southwestern borderlands of the Canadian Shield and on the Hudson Bay lowlands (Norris and Sanford, 1968). Paleozoic cover on the shield proper, however, occurs only in a limited number of localized depressions.

It is generally thought (Williams, 1970) that some time during the Middle Ordovician a shallow sea covered the area which currently comprises the Canadian Shield. Deposition of the marine limestones, characteristic of the Middle Ordovician in southeastern Canada, also took place at this time. Sedimentation on the shield and in Hudson Bay and Moose River Basins continued until a gradual uplift of the shield areas began. This uplift was followed by erosional removal of the sedimentary cover from most of the shield. Sedimentary deposition continued to the south of the shield and in Hudson Bay and Moose River Basins. There are about a dozen localities on the Canadian Shield where Ordovician sediments are found lying uncomformably on Precambrian Grenville gneisses. These include: Lake Temiskaming, Lake St. John, Gilmour Lake, Clearwater Lake, Lake Nipissing, Mattawa River, Waswanipi Lake, and Manicouagan-Mushalagan Lakes (Norris and Sanford, 1968; Kranck and Sinclair, 1961; Williams, 1970). The outcrops of Lake St. John, Lake Nipissing, and Lake Temiskaming are thought to be

segments down-dropped in graben faults and thereby protected from erosional removal (Kumarapeli and Saull, 1966). The reason for existence of the other outcrops is more open to question. Brent Crater (Gilmour Lake), in which the thickest sequence on the shield is found, is thought to be a meteorite crater in which the Ordovician sequence was deposited and preserved.

The period during which part or all of the Canadian Shield was covered by Paleozoic sediments is difficult to ascertain. The thinnest sequence observed, that at Clearwater Lake, contains only Upper Ordovician limestones. The thickest sequence of Paleozoic sediments, that found in the Moose River Basin, has members of Upper Ordovician to Upper Devonian ages (Norris and Sanford, 1968). The best statement which can be made is that a Paleozoic sedimentary cover existed on some part of the shield from about 470 m.y. (Middle Ordovician) to about 360 m.y. (Upper Devonian). (Age-stratigraphy correlations after Wanless et al., 1970). The lowermost member of these sequences is invariably Middle or Upper Ordovician in age.

Summary: The vast majority of rocks outcropping in Grenville Province are high-grade metamorphic rocks with bodies of cogenetic igneous granite, seyenite, and gabbro. These rocks yield a rather consistent isotopic age of about 955 m.y., the time of the Grenville Orogeny. Younger igneous rocks in Grenville Province are diabase dikes and some alkaline intrusive stocks. Paleozoic sediments are presently limited to relatively few localized

depressions.

Rocks of the Manicouagan-Mushalagan Lakes Area (A Broad View) --

Metamorphic: The basement units of the area are rock types which are very commonly observed in the Grenville Province. They include: granitic gneisses; amphibolitic gneisses; hornblende-biotite-plagioclase gneisses; granulitic gneisses; anorthosites; gabbroic anorthosites (see Fig. 2c). The gneisses display extensive variations since they are generally composed of mafic-rich bands alternating with rocks rich in quartz and potassium feldspar. A typical variation in the gneisses would be from a quartz-feldspar-biotite gneiss in quartz- and feldspar- rich bands to a biotite-hornblende gneiss with minor plagioclase (see Appendix). Amphibolites are frequently interlayered with the biotite-hornblende-plagioclase gneisses. The granulite facies gneisses also show large variations in mafic mineral content. The gabbroic anorthosite and anorthosite which occur in the area are more uniform in mineral composition, although these also have mafic-rich bands.

The Grenville-type basement rocks are subdivided, partly on the basis of composition and partly by metamorphic grade, into five units. Units #1, #2, and #3 are gneisses with variable compositions which are characterized by different metamorphic grades. Units #4 and #5 are anorthosite and gabbroic anorthosite, respectively; these units are fairly homogeneous in character throughout the areas in which they outcrop (see Fig. 2c).

A sketch map of the Manicouagan-Mushalagan Lakes structure is shown in Fig. 2. This map includes data from Murtaugh and Currie (1969), Murtaugh (1968), Berard (1962), and Kish (1962). The major features of the area are shown in Figs. 2a, 2b, and 2c.

The gneisses of the Manicouagan area exhibit steeply dipping or vertical, N or NW trends in their foliations. These trends are fairly consistent, although E and NE trends have been observed by Murtaugh and Currie (1969). Original sedimentary layering, where observable, parallels the gneissosity (Murtaugh and Currie, 1969).

Basement rocks in the region of the structure show a general increase in metamorphic grade in a NE direction. West and just east of Mushalagan Lake, quartz-plagioclase-biotite gneisses of the almandine-amphibolite facies occur. (Facies definition after Turner and Verhoogen, 1960). (Units #1 and #2, Fig. 2c) *Granulite facies gneisses and anorthosite occur in a broad band* of outcrops through the center of the structure (Units #3 and #4, Fig. 2c).

On the eastern edge of the map area, extending somewhat into the interior of the lakes, extensive outcrops of gabbroic anorthosite and norites are found (Unit #5, Fig. 2c). This massif, which ranges 40 miles east of Manicouagan Lake has been mapped by Kish (1962, 1963, 1965). Well east of this area (just south of Petit Lac Manicouagan), the gabbroic anorthosite massif contains

an olivine-pyroxene rock (Kish, 1965) which may represent eclogite facies metamorphic grade.

The most recent gravity map of Canada shows a regional positive Bouguer Anomaly (Bouguer Anomaly Map, 1970) which coincides with the eastern extremity of the gabbroic anorthosite. It is possible that the eastern end of the massif is underlain by an extensive body of dense, high-grade metamorphic rocks.

A whole rock potassium-argon age of 932 m.y. was obtained for an anorthosite exterior to the ring of the lakes (Part II, this work). This age is close to the time generally accepted for the Grenville Orogeny (955 ± 50 m.y.; Stockwell, 1970). The similarity of the anorthosite age with the time of the Grenville Orogeny supports the correlation of this rock with other rocks of the Grenville Province. A correlation of the whole series of cogenetic basement gneisses and anorthosite in the area with Grenville Province rocks has already been inferred from structural and petrographic evidence. The 932 m.y. age provides further support for this correlation.

Superimposed on the variations in metamorphic grade and composition, the rocks interior to the two lakes show evidence of "shock"* deformation ranging from barely detectable to extremely

---

* The use of the term, "shock", involves an inference which has yet to be justified. In the interest of verbal economy, however, the term will be retained in this general description and will be justified in the section involving specific descriptions of the rock units.

severe, along with varying amounts of contact metamorphic effects. Shock effects include: extensive microscopic fracturing of the rock; development of macroscopic shatter cones; development of microscopic, closely spaced planar shock lamellae; partial or complete isotropization of isolated grains of minerals within a rock without evidence of melting or flowage in the rock. Thermal effects observed range from slight oxidation of mafic minerals to complete recrystallization of the rock. Both extreme shock deformation and heating lead to the same end product, i.e. molten rock. It is often difficult therefore, to decipher which type of deformation has been predominant. When the deformations due either to shock effects in the materials or to thermal effects are small, the original material can generally either be identified or its identify inferred. This situation often holds in the stream cuts and eroded openings in the monzonite body, thus making identification of basement types under the body possible. In some cases, however, the original nature of the rock within the lakes is undiscernible.

Sedimentary: Hammond (1945), Rose (1955), and Berard (1962) observed fossiliferous Ordovician limestone outcrops along the inner margins of the two lakes. Murtaugh and Currie (1969) have mapped these bodies and observed minor outcrops in the mouths of nearly all larger stream valleys which join the two large lakes. They have also observed that the maximum thickness of stratigraphic section in any outcrop is

about 75 feet. Murtaugh and Currie (1969) have stated that the limestones have been tilted and deformed and lie unconformably on the Precambrian basement. Fossils within this unit are of Middle Ordovician age.

Igneous: Large regions interior to the two lakes are covered by an irregular, flat-lying sheet of massive, completely crystalline igneous material (monzonite). This substance either lies directly on the Precambrian basement or is separated from it by a thin layer of reddish breccia. The monzonite is a fine- to medium-grained, plagioclase-sanidine-augite-hypersthene rock which mineralogically somewhat resembles a tholeiitic diabase. The rock is significantly more potassic and acidic than most tholeiitic diabases and could be classified as a trachybasalt (Table 4, Appendix).

Potassium-argon age studies of this rock yield an age of 210 $\pm$ 4 m.y. (Part II). This Triassic age is not obviously correlative with any igneous feature in Grenville Province proper.

Wanless et al. (1968) have reported an age of 665 m.y. for a small diabase dike which occurs on the outer edge of Manicouagan Lake. Murtaugh and Currie (1969) have mapped other occurrences of similar small dikes. They interpret these as being members of a minor diabase dike swarm. These features are distinctly older and appear unrelated to the monzonite.

The Manicouagan-Mushalagan Structure (Typical or Atypical of Grenville Province)--

It is worthwhile to consider in more detail whether or not the features present in the Manicouagan-Mushalagan Lakes structure are really unusual to Grenville Province.

Paleozoic intrusive rocks and Ordovician sediments are found elsewhere on the Canadian Shield. These features, therefore, cannot be considered too uncommon. Sediments and igneous rocks are widely dispersed in Grenville Province, and the isolated occurrence of either type of rock is not, per se, unexpected. The coexistence of igneous rocks and sediments is more distinctive. Igneous rocks are found coexisting with Ordovician limestone only at Clearwater Lake, Lake Nipissing, and Brent Crater.

The deformational features found in the basement gneisses are highly distinctive. Features similar to those found at Manicouagan are observed only in a relatively small number of localities throughout the world. In these localities, basin-like depressions occur with unusual microscopic deformation features in the rocks exposed. These localities are thought to be meteorite impact sites. The theory that the Manicouagan area is of impact origin has gained favor chiefly because of the presence of microscopic deformation features in the basement rocks.

Paleozoic igneous activity in other parts of the shield consists of diabase dike swarms, alkaline stocks and plugs and carbonatite complexes. Although the igneous body found at Manicouagan might be forced into an association with the diabase dikes, this body neither closely resembles an alkaline intrusive stock nor a diabase dike. The age of the Manicouagan body, 210 m.y., is distinctly different that the ~ 115 m.y. age of the Monterregian intrusives or the 560 m.y. age of the intrusive body at Lake Nipissing. Diabase dike swarms of Triassic age have not been reported in Grenville Province. As previously pointed out, however, dikes approximately 200 m.y. old are found just outside the Grenville Province in Nova Scotia and on Prince Edward Island.

It has been suggested (Dence, 1965) that the igneous rocks at Manicouagan are totally melted impact breccias. This mode of origin for these rocks does not imply any relation between the Manicouagan igneous body and other igneous bodies found on the Canadian Shield.

The sediments preserved in small blocks on the inner margins of Manicouagan and Mushalagan Lakes are Middle Ordovician in age. During the Middle Ordovician, most or all of the Canadian Shield was an area of sedimentary accumulation. The Ordovician sequence preserved at Manicouagan is rather thin (75 feet), as opposed to the rather thick (504 feet) sequence preserved in the Gilmour Lake (Brent Crater) outlier. The thin sequence suggests that

previous to the Middle Ordovician, Manicouagan was not a structure in which a thick, carbonate sequence could have accumulated. The existence of limestone at Manicouagan, however, implies that the area became a structural low before the carbonate sequence had been erosionally removed. The latest period during which sediments were present in this part of Grenville Province is difficult to determine. This period, however, was probably not too much later than Upper Devonian. Upper Devonian (~ 350 m.y.) sediments are the youngest sediments found in sequences on the margins of the shield (Norris and Sanford, 1968). This suggests that a major uplift of the shield and the beginning of erosional denudation dates back to this time. The scattered outcrops of deformed, tilted, and brecciated limestone present at Manicouagan were probably part of a thin, sedimentary veneer present on the margins of the impact site previous to the impact. They have since been preserved on the margins of the basin produced by the impact event.

Manicouagan-Mushalagan Lakes Area -- A Detailed Description:

General Statement --

Fig. 2a is a generalized geological map of the Manicouagan-Mushalagan Lakes area. This map is a composite of Figs. 2b and 2c . Fig. 2b is a topographical map of the area. Fig. 2c is a map of Precambrian units exposed in the area, and the distribution of Paleozoic units is displayed in Fig. 2a. The rock units present in the structure are discussed in terms of (1) Precambrian basement units and (2) Paleozoic and later units.

Precambrian Basement Units --

General Description: Fig. 2c shows the inferred configuration of the basement rocks exterior to the lakes and under the monzonite body. The contacts among the Precambrian units are gradational; those shown are approximately located.

Units #1, #2, and #3 are all highly variable in composition. For the purpose of this map, these units are distinguished on the basis of metamorphic grade. Units #4 and #5 display a much greater degree of homogeneity than Units #1 through #3. Although some variation in the mafic mineral content between outcrops in Units #4 and #5 is observed, they are mapped as single units.

In the map area, metamorphic isograds more or less follow a NW-SE trend. This trend parallels the general trend of foliations in the gneisses exposed. The metamorphic grade increases from west of Mushalagan Lake toward the central anorthosite body. The grade then decreases somewhat east of this body. Continuing

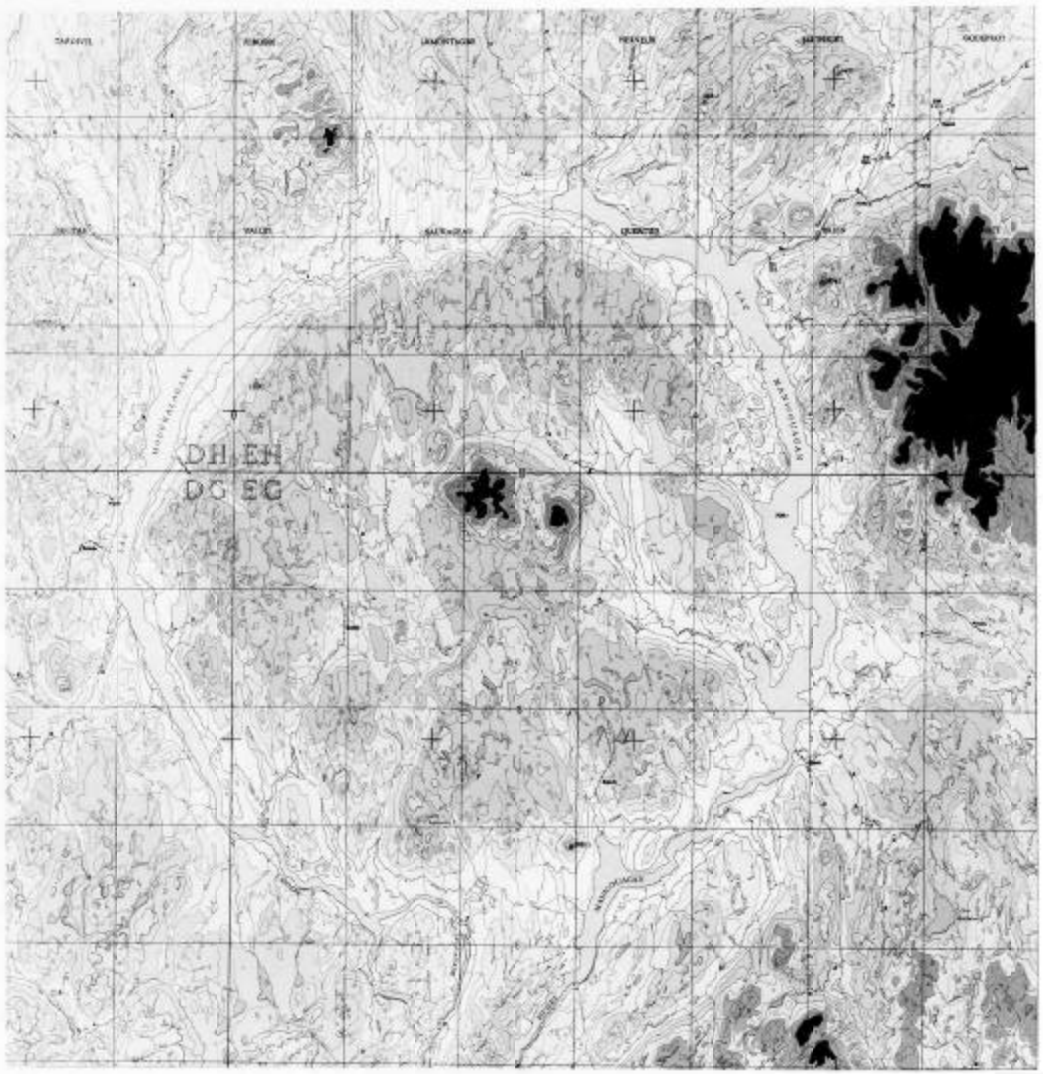

MAP OF
MANICOUAGAN - MUSHALAGAN LAKES
STRUCTURE

0 5 10 miles
0 4 8 12 16 km
scale

3200 - 3600
2800 - 3200
2400 - 2800
2000 - 2400
1600 - 2000
1200 - 1600
below 1200

feet above mean sea level

ELEVATIONS

Unit No 1 Almandine - Amphibolite grade quartzo-feldspathic gneiss (Kyanite - Almandine Subfacies)

Unit No 2 Almandine - Amphibolite grade gneiss (Sillimanite - Almandine - Orthoclase Subfacies)

Unit No 3 Granulite Facies quartzo-feldspathic gneiss (Pyroxene - Hornfels Subfacies)

Unit No 4 Anorthosite

Unit No 5 Gabbroic Anorthosite

Ordovician Limestone

Shock Breccia

Igneous Material (Monzonite) Subunits not differentiated

Dots indicate presence of deformations due to shock intensities greater than 100 kilobars

LEGEND

34a

FIG. 2a

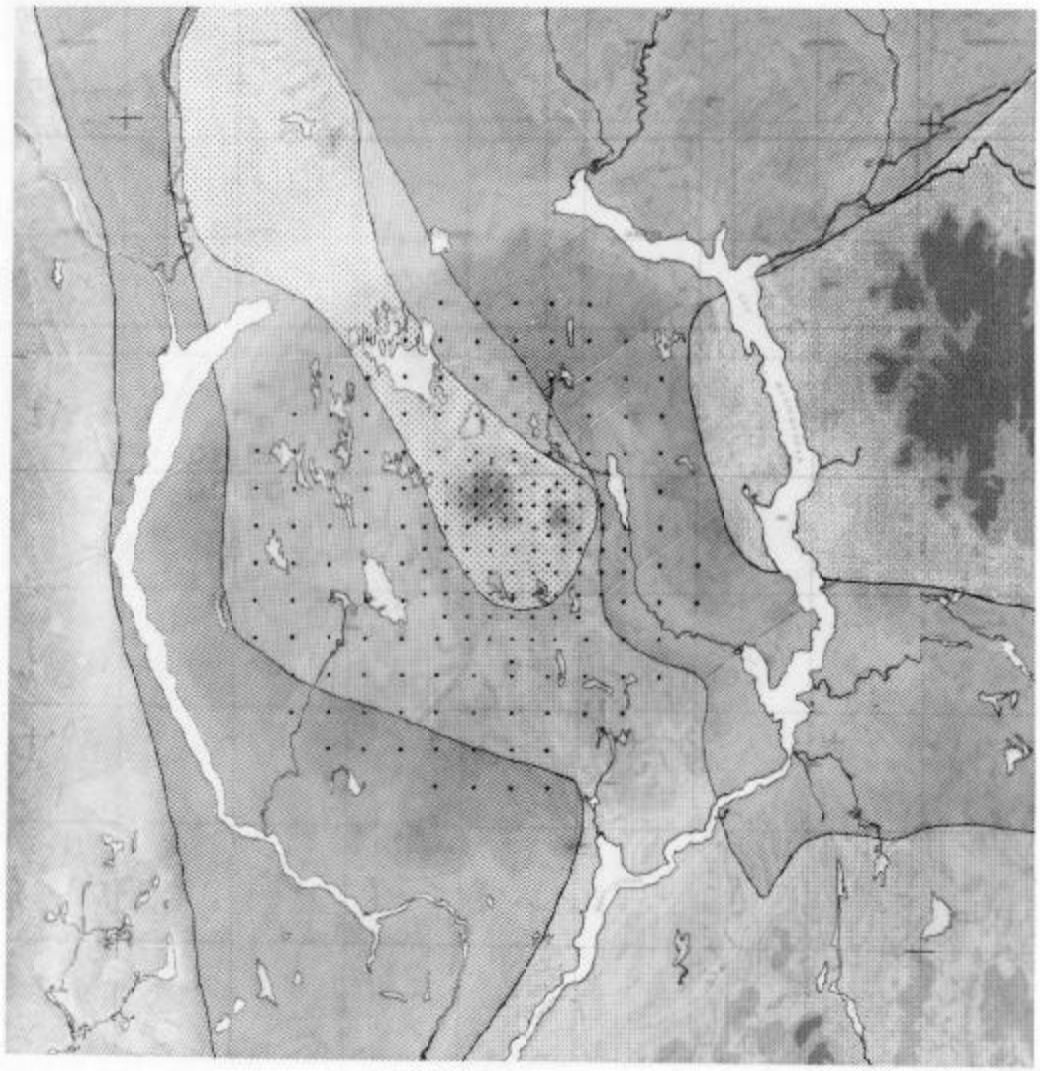
MAP OF
MANICOUAGAN - MUSHALAGAN LAKES
STRUCTURE
0 5 10 miles
0 4 8 12 16 km
scale
feet above mean
sea level
ELEVATIONS
Unit No 1 Almandine-Amphibolite grade quartzo-feldspathic gneiss (Kyanite-Almandine Subfacies)
Unit No 2 Almandine-Amphibolite grade gneiss (Sillimanite-Almandine-Orthoclase Subfacies)
Unit No 3 Granulite Facies quartzo-feldspathic gneiss (Pyroxene-Hornfels Subfacies)
Unit No 4 Anorthosite
Unit No 5 Gabbroic Anorthosite
Ordovician Limestone
Shock Breccia
Igneous Material (Monzonite) Subunits not differentiated
Dots indicate presence of deformations due to shock intensities greater than 100 kilobars
LEGEND

FIG. 2b

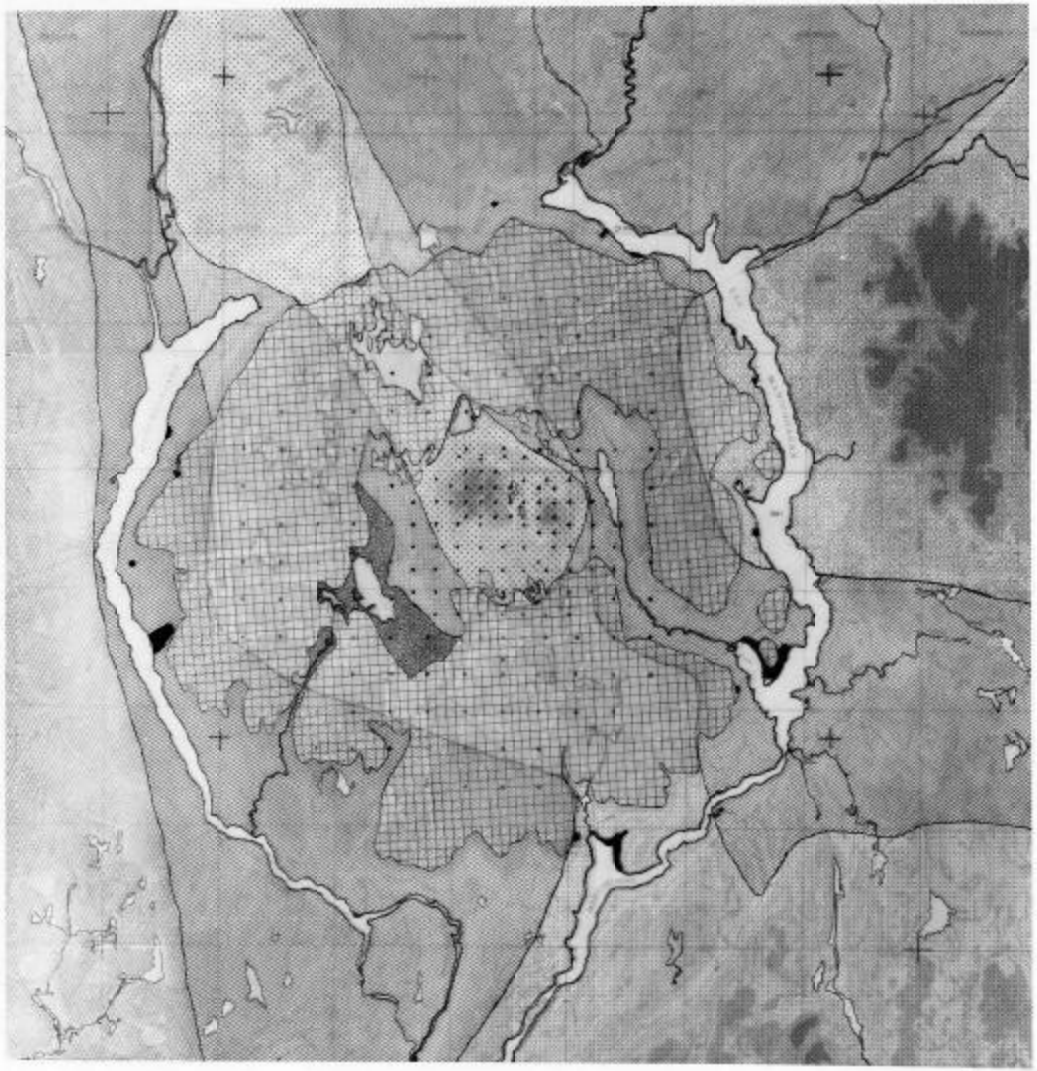

MAP OF
MANICOUAGAN - MUSHALAGAN LAKES
STRUCTURE

0 5 10 miles
0 4 8 12 16 km
scale

3200-3600
2800-3200
2400-2800
2000-2400
1600-2000
1200-1600
below 1200
feet above mean sea level

ELEVATIONS

Unit No 1 Almandine-Amphibolite grade quartzo-feldspathic gneiss (Kyanite-Almandine Subfacies)

Unit No 2 Almandine-Amphibolite grade gneiss (Sillimanite-Almandine-Orthoclase Subfacies)

Unit No 3 Granulite Facies quartzo-feldspathic gneiss (Pyroxene-Hornfels Subfacies)

Unit No 4 Anorthosite

Unit No 5 Gabbroic Anorthosite

Ordovician Limestone

Shock Breccia

Igneous Material (Monzonite) Subunits not differentiated

Dots indicate presence of deformations due to shock intensities greater than 100 kilobars

LEGEND

FIG. 2c

northeastward, there is an abrupt increase in metamorphic grade as the gabbroic anorthosite massif is approached. As mentioned previously, the eastern end of this massif coincides with a regional positive Bouguer gravity anomaly. This anomaly is possibly indicative of a subsurface body of dense, high-grade metamorphic rock. Occasional surface exposures of eclogite-grade, garnet-pyroxenites in this area provide some support for the above hypothesis.

Unit #1: Unit #1 is a quartz-feldspar-biotite gneiss. It outcrops over a broad area west of Mushalagan Lake (Fig. 2c) The rock is fine- to medium- grained, grey or pinkish-white in outcrop with layers enriched in mafic minerals forming bands 1 cm to 1 ft. wide. In hand specimens, bands (about 1-2 mm in thickness) rich in fine-grained biotite impart a gneissic texture to the rock. Rocks of this unit are highly variable and range from granitic gneisses to biotite-rich rocks and amphibolites.

Typical assemblages which occur are: (1) quartz, plagioclase (An_{25-30}), microcline, and biotite; (2) plagioclase, quartz, biotite, hornblende, and chlorite. Garnet is rare but has been observed in some rocks from this unit (Murtaugh, 1965). The assemblages of this unit are characteristic of the kyanite-almandine subfacies of the almandine-amphibolite facies (defined according to Turner and Verhoogen, 1960). Quartz observed in rocks from this unit sometimes appears strained but shows no closely spaced, parallel, shock lamellae (see Appendix: Samples #1 and #NT-8).

Unit #2: Unit #2 occurs in a narrow band along Mushalagan Lake as well as in an arcuate area east of Mont de Babel. In hand specimen, rocks from this unit are fine- and medium- grained with white quartz and feldspar interbanded with black biotite. Biotite bands define a gneissosity, and medium-grained, reddish garnets are scattered throughout the rock.

Unit #2 is a medium-grained, quartz-feldspar-biotite-garnet gneiss. Rocks from this unit display highly variable amounts of potassium feldspar. Proportions of mafic minerals, compared to quartz and feldspar, are also quite variable. Typical assemblages observed are: (1) quartz, orthoclase, plagioclase, and minor amounts of hornblende and garnet; (2) quartz, plagioclase, biotite and garnet; (3) quartz, orthoclase, plagioclase, biotite, hornblende and garnet. Plagioclase in these rocks is An_{25-30}. Potassium feldspar is present as orthoclase. Orthoclase sometimes contains 50-100 μ blebs of exsolved sodium feldspar. Large, anhedral garnet grains (up to 4 mm in a dimension), which contain numerous inclusions of quartz and plagioclase, comprise 15% of the mode of some rocks. Quartz from rocks near the contact of this unit with Unit #3 has a lensoid, elongate habit. In other areas, quartz grains are generally equi-dimensional.

The assemblages observed in these rocks are characteristic of a slightly higher metamorphic grade than that observed in Unit #1. The grade corresponds to the sillimanite-almandine-muscovite and the sillimanite-almandine-orthoclase subfacies of the almandine-amphibolite facies (defined after Turner and

Verhoogen, 1960).

Unit #2 is microscopically distinguished from Unit #1 by the presence of orthoclase rather than microcline. The coarser grain size and larger content of garnet found in Unit #2 rocks compared to rocks from Unit #1 provide macroscopic distinguishing features.

Rocks from outcrops of Unit #2 in the area east of Mont de Babel show abundant "shock"-deformational features as well as contact metamorphic effects due to the monzonite body. Some samples from outcrops in the band just east of Mushalagan Lake show these effects also. These features are discussed below in the sub-section describing deformations. (See Appendix also: Samples #NT-1, #13-8-4, #24-7-5, Shatter cone, #25-20-3, and #4-20-1).

Unit #3: Unit #3 outcrops in a broad band extending through the center of the structure. Outcrops of this unit occur between Unit #2 and the anorthosite. This unit mantles the anorthosite.

Unit #3 is a medium-grained, grey or yellowish, pyroxene-bearing, granulite-grade gneiss. In hand specimen, the rock shows a foliation defined by the segregation of mafic minerals into 1-3 mm bands several centimeters apart. Macroscopically, Unit #3 appears somewhat different from Unit #2. The plagioclase appears greyish or yellowish in hand specimens of the unit; this contrasts with the whitish appearance of feldspar and quartz in hand specimens of Unit #2. Microscopically, the presence of pyroxene is a

diagnostic, distinguishing feature.

Unit #3 is highly variable in composition, as are Units #1 and #2. Assemblages which are observed in this unit include: (1) quartz, orthoclase, plagioclase, garnet, and hornblende; (2) quartz, orthoclase, plagioclase, biotite, garnet, diopside, hornblende, and hypersthene; (3) plagioclase, biotite, garnet, hornblende, diopside, and minor scapolite. The first assemblage is sometimes referred to as a seyenitic gneiss. Charnockitic gneiss and anorthositic gneiss are terms frequently applied to the second and third assemblages, respectively. Most rocks observed from the central part of the structure tend to conform to the third assemblage, although some gneisses conforming to the first assemblage are also observed. Rocks from the southeastern part of the structure and southeast of Manicouagan Lake contain both hypersthene and diopside and conform to the second assemblage. On the microscopic scale, garnet in this unit occurs in subhedral to euhedral grains which contain noticeably fewer inclusions than the garnet in Unit #2. Potassium feldspar is orthoclase perthite, which often contains sub-equal amounts of host and exsolved phase (mesoperthite). Plagioclase is generally An_{30-35} and shows better-developed albite twinning than plagioclase from Units #1 or #2. Quartz is elongate and lensoid rather than equant.

The assemblages from this unit conform to the pyroxene hornfels subfacies of the granulite facies of regional metamorphism (defined after Turner and Verhoogen, 1960). Pyroxene is sometimes

present in minor amounts in rocks which are transitional from Unit #2 to Unit #3.

An extensive area of outcrops of Unit #3 lies within the two lakes. Rocks in this area contain microscopic deformation features found in other suspected meteorite impact sites. They also display contact metamorphic effects which are due to the overlying monzonite. The observed shock effects will be discussed in the section on deformation. Thermal effects observed mainly include: (1) oxidation of mafic mineral phases (garnet, hornblende, biotite, and pyroxene) to black opaque forms pseudomorphous after the original grain; (2) partial or total recrystallization of quartz and feldspar to masses of crystallites. These thermal effects often make it difficult or impossible to infer the original nature of the rock (see Appendix: Samples #12-20-8, #NT-7 and #15-7-3).

A large percentage of the rocks found in Units #2 and #3 consists of calcareous gneisses. These gneisses consist of about 60-80% of plagioclase, very little quartz or potassium feldspar, and 20-40% mafic minerals. In Unit #2, mafic minerals found are garnet, biotite, and hornblende. In Unit #3, the mafic minerals garnet, biotite, hornblende, and diopside appear. The calcareous gneisses from Unit #3, with 80-85% plagioclase and 15-20% mafic minerals, are essentially equivalent to rocks of Unit #4. These gneisses are in gradational contact with rocks from Unit #4.

Unit #4: Unit #4 is the anorthosite which outcrops in an elongate, pinched-in body. The southern end of this body lies approximately in the center of the two lakes. This anorthosite is a medium- to fine- grained, plagioclase-garnet-pyroxene-scapolite rock. The unit generally appears as pinkish, whitish, or greyish in outcrop with banding on a scale which varies from one centimeter to several feet. The mafic-rich bands are composed mainly of garnets and pyroxene with some minor amounts of biotite and hornblende. Rocks rich in biotite and hornblende are more common near the edges of the massif. These "border" phases contain about 20-40% mafic minerals and are transitional to rocks of Unit #3. Rocks from this unit are somewhat variable in composition. For the purpose of this work, however, the biotite- and hornblende-rich phases occurring near the edge of the massif are lumped together with the "normal" anorthosite which contains about 85-95% plagioclase and 5-15% mafic minerals. The anorthosite unit forms prominent highlands, both inside and outside the crater. These highlands are probably due to the fact that the anorthosite has greater resistance to erosion than the surrounding gneisses have.

Macroscopically, Unit #4 is differentiated from Unit #3 by its smaller modal percentage of mafic minerals. Along transition zones between the units, in which the mafic mineral contents of rocks are about 15-25%, it is difficult to distinguish between the two units. Microscopically, the two units are distinguishable

by the lower mafic content of Unit #4 compared to Unit #3. The plagioclase in Unit #4 is andesine or labradorite; oligoclase is present in Unit #3.

In thin section, the anorthosite is typically about 85% albite-twinned plagioclase, An_{50-55}. About 15% of the rock is composed of garnet and pyroxene (diopside) with accessory scapolite, hornblende, and some sphene. The plagioclase occurs in 1 mm grains with intergranular, sodium- or potassium- rich feldspar in strings or elongate blebs between the grains. The assemblages present in rocks of Unit #4 are characteristic of the granulite facies of regional metamorphism. This anorthosite appears to be a product of high-grade, regional metamorphism of calcareous gneisses, rather than an intrusive body.

The southern end of the anorthosite body lies approximately in the center of the two lakes and contains rocks displaying the microscopic deformation features characteristic of "shock" metamorphism. The textures observed in these rocks provide strong evidence supporting the impact origin of the structure. These textures are discussed in the section on deformation.

Contact-metamorphic textures are not observed in rocks of Unit #4 within the central massif. On the east and southeastern margins of the massif, anorthosite is locally in contact with monzonite. In these areas, recrystallization of plagioclase and blackening of mafic minerals can be observed. Thermal alterations are also observable in anorthosite northwest of the central block. These alterations can be seen in the rocks from the narrow band

of outcrops between the two parts of the body.

Unit #5: Unit #5 is a gabbroic anorthosite. This unit outcrops marginally west of Manicouagan Lake. It also outcrops in a more or less rectangular massif, south of the Hart-Juane River, extending eastward from Lake Manicouagan. Rocks of this unit are very resistant to erosion and the highest peaks in the map area occur in the gabbroic anorthosite massif.

In hand specimen, rocks from this unit are medium-grained with yellowish or greenish-yellow plagioclase and black pyroxene. They are composed of about equal amounts of mafic minerals and lighter plagioclase. Most of the outcrops appear massive and unfoliated.

The characteristic assemblage of this rock is plagioclase, hypersthene, and diopside. Some rocks contain minor biotite and quartz. Kish (1962, 1963, and 1965) has observed garnet in rocks from this unit, but garnet is markedly less abundant than in other units. Plagioclase is about An_{55}. Some samples show abundant calcite in thin section. A border phase of this rock contains large (3 mm), irregular grains of hypersthene and small (0.2 mm) grains of diopside in a ground mass of 2 mm, equant An_{55} grains. Kish (1962, 1963, and 1965) has mapped the gabbroic anorthosite from Manicougan Lake to its eastern extremity, southwest of Petit Lac Manicouagan. In the eastern part of the massif, high-grade, granulite-facies assemblages and intrusive olivine gabbros are present. These assemblages may represent the highest regional

metamorphic grades in this sector of Grenville Province.

Unit #5 is fairly easily distinguished from the other units in the field area by its relative lack of foliation and its higher content of mafic minerals.

Some samples from this unit have bent plagioclase grains, undulous extinction, and cataclastic textures but lack the closely spaced, parallel fractures observed in rocks from the interiors of the lakes. Kish (1963) has mapped a large fault along the course of the Hart-Juane River and observed mylonitized and chloritized rocks in the massif. The shearing observed in the samples studied is probably due to the Hart-Juane River fault.

The above units comprise the Precambrian, Grenville-type, metamorphic rocks in the Manicouagan-Mushalagan Lakes area. The Manicouagan-Mushalagan structure is unique because of (1) the unusual microscopic deformations observed in the Precambrian rocks and (2) because of the unusual Paleozoic rock sequence present in the area.

Paleozoic and Younger Rocks of the Structure --

Ordovician Limestone: Along the inner margins of Manicouagan and Mushalagan Lakes, numerous, isolated outcrops of Ordovician limestone occur. Major outcrops of limestone are indicated in Fig. 2d.

During the course of this work, only two of these outcrops were sampled. Murtaugh and Currie (1969), however, have mapped numerous occurrences of the limestone. Outcrops range in size from about 100-200 yards up to a maximum of about a mile. The maximum vertical thickness of any outcrop is about 75 feet. Outcrops of Ordovician limestone are limited to within two miles of the inner lake shores; no outcrops have been observed in the central part of the structure. The outcrops are located near the original inner shorelines of the two lakes and are limited to regions below 1200 feet in elevation. At present, they are submerged by water which has been impounded as a result of the hydroelectric dam at the mouth of Manicouagan and Mushalagan Lakes.

Individual outcrops of the limestone unconformably overlie the Precambrian basements. Bedding planes in the outcrops strike in variable directions (NW-SE to E-W) and frequently dip away from the structure at angles of 25-80^{o} (Murtaugh and Currie, 1969). Murtaugh and Currie also noted that the rocks have been tilted and deformed. Sandstones and shales were found by these authors at the basal parts of some limestone sequences.

Some outcrops of this unit are overlain by fine-grained, igneous material. Kish (1965) observed a large block of limestone surrounded by fine-grained monzonite, and Murtaugh and Currie (1969) show some outcrops of the limestone overlain by the igneous material.

In hand specimen, the limestone is fine- or medium- grained and ranges from a dark grey to a dirty cream color. The material has beds from 1 in. to 4 ft. thick and is fairly fossiliferous (Berard, 1962). Murtaugh and Currie (1969) interpret the fossils present in the limestone as a fauna transitional between that common in Ordovician outcrops around Lac St. Jean and an "Arctic Ordovician" fauna found at Clearwater Lake (Kranck and Sinclair, 1963).

In thin section, the limestone consists almost entirely of fine-grained calcite. Some cryptocrystalline quartz is present in shell casts. In general, calcite does not display shock damage as well as silicates , since it tends to yield plastically by gliding. Shock-deformed calcite, however, develops microscopic twin lamellae within grains (Roddy, 1968). Twin lamellae have been observed in calcite from this limestone (Roddy, personal communication). No microscopic planar features were observed in the occasional quartz.

Ordovician limestones present both at Lac St. Jean and at Clearwater Lake are of Middle Ordovician age (Kranck and Sinclair, 1963). The Middle Ordovician era corresponds to a period of about 440-460 m.y. ago (Wanless et al., 1970).

Shock Breccia: A thin, discontinuous layer of rock-fragment breccia occurs underlying the monzonite in the central part of the structure. The thickness of this layer, when present, is variable and ranges from a few feet up to 60 feet in a few localities. The layer appears in a roughly annular ring around the central anorthosite

massif and thins out completely near the western, eastern, and southern extents of the monzonite. Where the breccia is absent, fine-grained members of the monzonite unit either lie directly on the basement anorthosites or are in contact with the Paleozoic limestone. The shock breccia is exposed more extensively west of Mont de Babel than it is to the east. Several spectacular outcrops occur east of Lac Chastelaird. The areal extent of the shock breccia is indicated in Fig. 2a. The most extensive outcrops of this rock occur around Lake Chastelaird.

A typical outcrop of this unit appears as a jumbled mass of rock fragments enclosed in a matrix of fine-grained, reddish material. These fragments of rock range in size from several meters down to a few centimeters. Some fragments observed are rounded, some are angular; others are contorted, elongate, and wavy. Most of the fragments display a foliation similar to that of the basement gneisses and the foliations of the fragments are oriented randomly in an outcrop. Boulders of shock breccia are extremely common along the shore of Lake Chastelaird. They can also be found in the southwestern part of the crater.

The breccia is generally in gradational contact with underlying basement rocks. In an outcrop, the size of the included rock chunks continues to increase downward until more or less homogeneous basement rocks are observed. Where observable, the upper contact of the breccia with the overlying monzonite is also gradational. The lower layers of the monzonite contain many inclusions; at successively higher levels in a breccia outcrop,

the reddish, inclusion-rich matrix of the breccia appears to grade into the black, inclusion-rich, fine-grained monzonite.

In hand specimen, rocks of this unit appear to be composed of a reddish, fine-grained matrix enveloping contorted (1-10 cm) fragments of lithic material. Closer inspection of the reddish matrix which envelops and surrounds the rock chunks reveals that the matrix itself is a breccia on a finer scale. The matrix consists of 0.5 to 5 mm pieces of white rock enveloped in an aphanitic, reddish material.

In thin section, the rock fragments within the unit are seen to reflect the mineralogy of the underlying basement, although the fragments are often nearly unrecognizable. Quartz and plagioclase in these fragments are generally tan to brown and frequently exhibit the closely spaced, parallel fractures observed in the other shocked rocks. Mafic minerals in fragments appear as black, opaque grains pseudomorphous after hornblende, biotite, garnet, or pyroxene from the unaltered basement rock. Microscopically, the reddish matrix is an aggregate of particles ranging in size from 0.1 to 2 mm which are enveloped in material that is too fine-grained to distinguish. Identifiable fragments in the reddish matrix are small, contorted rock fragments, individual mineral grains, or groups of grains.

Igneous Material, The Monzonite :

(a) Areal extent. The monzonite is the igneous rock present in the Manicouagan-Mushalagan Lakes structure. Rocks of this unit outcrop in a roughly annular-shaped area between the central anorthosite massif and the inner shores of the two large lakes (see Fig. 2a). Within this annular area, the monzonite body has a very irregular form. The present irregular form is probably due to erosional dissection of a more complete, annular, sheet-like mass. Vertical thickness of outcrops in this unit range from a few feet to about 700-800 feet.

A series of high, steep cliffs occur along the inner shores of the two lakes. These cliffs are the outer limit of the monzonite body. Outcrops of this material are limited to the interior of the lakes. Most outcrops have the form of high, N-S, elongate hills with steep northward- or southward- pointing snouts.

(b) Appearance. In hand specimen, the material is a black, massive, fine- to medium- grained, equigranular, plagioclase-pyroxene-quartz rock. The material weathers brown or yellow-brown. In the upper levels of this unit, some coarse-grained rocks can also be found.

(c) Similarities to an extrusive. Most of the features of the Manicouagan igneous body are similar to those expected for a material which cooled on the earth's surface. Lower layers of the body contain fine-grained and glassy phases indicative of rapid cooling along chilled contacts. On the outer edge of the body,

where thin layers of igneous material overly shocked basement rock, the rock contains abundant vesicles and has a rounded, irregular surface resembling that of pahoehoe flows. The vesicles are strongly suggestive of gas exsolution from the material in a low-pressure, surface environment. No evidence of any rock unit which originally covered the monzonite has been found on the exposed upper surface of the body.

Although many features of the material suggest surface cooling, it is medium- and occasionally coarse- grained. Such large grain sizes are most frequently observed in rocks from intrusive bodies rather than in surficially cooled material. While referring to this rock as monzonite is somewhat misleading, the term emphasizes the large grain sizes present.

(d) Sub-units. The macroscopic textures of rocks from the unit vary somewhat. The unit can be subdivided, mainly on the basis of grain size, into three sub-units: (1) a fine-grained, inclusion-rich, lower sub-unit; (2) a medium-grained sub-unit; (3) a coarse- and medium- grained upper sub-unit.

Currie (1965) has referred to "several distinct flows" in the igneous material. Murtaugh and Currie (1969) consider the igneous material to be composed of two units with an "abruptly gradational contact". The observations made in this study suggest that the sub-units of the monzonite are in gradational contact. If the sub-units of the monzonite are composed of different extrusive flows, then the flows must have occurred over a

short enough time span such that most of them did not cool sufficiently rapidly for fine-grained rocks to form.

Every outcrop of monzonite sampled in this study showed an upward increase in grain size, but the relative thickness of fine-, medium-, and coarse- grained material varied between outcrops. Near Lake Mushalagan, in the southwestern part of the structure, a 700-ft.-thick sequence is observed. In this sequence, about 15 ft. of fine-grained, inclusion-rich material grade into about 600 ft. of medium-grained material. The upper 125 ft. of the sequence is medium- to coarse- grained. An outcrop on the south shore of Lake Du Chenouy, in the interior of the structure, contains only about 25 ft. of fine- to medium-grained material enveloping blocks of basement rock . The fine-grained rock grades into 300 ft. of medium-grained, inclusion-free material.

The size of inclusions observed in the lower layers of the monzonite seems to be smaller in outcrops near the large lakes than in outcrops nearer the center of the structure. Included fragments near the outer lakes range from a few centimeters to a meter. Nearer the center of the structure, however, fragments range in size from a few centimeters up to 10 meters.

The lower layers of the fine-grained unit contain many inclusions and vesicles. Some outcrops of this material display almost columnar jointing. In a large stream valley in the northwestern part of the structure, pods and small stringers of

a conchoidally fracturing, black, holohyaline material occur in the fine-grained sub-unit.

The medium-grained material contains a few inclusions, but they are extremely rare. Coarse-grained rocks, occasionally exposed on the tops of the highest hills in the interior of the structure, contain no inclusions.

(e). Thermal effects. The thermal effects of the monzonite on the rocks it is in contact with appear to be much more extensive near the center of the structure than near Manicouagan or Mushalagan Lake. A 1-cm inclusion of basement rock in an outcrop of the fine-grained sub-unit near the edge of the structure shows only minor blackening of mafic minerals and very little recrystallization of the quartz and feldspar. Near the center of the structure, a 10-meter inclusion of anorthosite, surrounded by monzonite, is nearly completely recrystallized (see Appendix, Anorthosite Hornfels). Near contacts of the monzonite with anorthosite, in and around the central anorthosite massif, the anorthosite has been recrystallized to a hard, aphanitic hornfels up to 40 feet from the contact. Murtaugh (1970) has described what he interprets as dikes of monzonite in anorthosite (northeast of the central massif); around the monzonite dikes, anorthosite has recrystallized for distances of more than five times the dike width from the dike contact.

(f) Structural relations. The monzonite body is essentially flat-lying with a maximum thickness of about 800 ft. Monzonite overlies Precambrian gneisses and Ordovician limestone near the margins of the structure. In the central part of the structure, monzonite overlies a thin layer of shock breccia or rests directly on shocked Precambrian basement. The contact of the fine-grained sub-unit of the monzonite with the underlying gneisses occurs at about the 1300-ft. elevation near the lakes. The shock breccia-monzonite contact occurs at the 1500-ft. level near Mont de Babel. The contact of the monzonite with shock breccia appears gradational near the center of the structure. Near the inner shores of the two large lakes, where fine-grained monzonite is in contact with lightly shocked gneisses, however, the monzonite contact is quite sharp.

The monzonite is massive and structureless, and its black color contrasts with the underlying units.

(g) Mineralogy and lack of "shock"-deformational features. Rocks from this unit have a very consistent mineralogical mode. Minerals present are invariably plagioclase, sanidine, augite, hypersthene, quartz, and magnetite-ilmenite. Hydrous phases such as biotite or hornblende have not been observed.

Compositions of minerals from rocks of all three sub-units are very consistent. Plagioclase, both in the cores of rimmed grains and when sub-ophitically enclosed in augite, is about An_{52-55}. Sanidine rims of feldspar grains are about Or_{50} near the

edge of the plagioclase core and about Or_{70} on the outer edge of the rim. Augite has the composition $En_{47}Fs_{18}Wo_{35}$. Both hypersthene and pigeonite have the composition $En_{58}Fs_{38}Wo_4$ (see Appendix, Sample #5-32-1). Compositions determined for pyroxenes in all three sub-units are closely similar. Grains of an altered iron-magnesium silicate are present in coarse- and medium- grained rocks. This material has an Mg:Ca:Fe ratio similar to pigeonite in the rock but contains significant Al_2O_3 and H_2O. This mineral may be altered pigeonite or olivine, perhaps iddingsite or bowlingite.

Microscopic textures observed in the unit vary somewhat between sub-units but all rocks lack evidence of shock. Apart from the inclusions which are found in the fine-grained, lower levels of the monzonite, none of the rocks from this unit display the microscopic deformational shock features which are so common in the shocked basement rocks. Some rocks in the fine-grained unit are isotropic. These rocks are volcanic glasses and not diaplectic (shock-formed) glasses. They are completely glassy and do not contain isotropic phases coexisting with crystalline phases as is the case with the maskelynitized anorthosite. No closely spaced, parallel fractures were observed in grains of quartz or plagioclase. Fracturing of individual mineral grains is limited to the normal cleavage directions.

(h) Microscopic textures. The texture which is fairly characteristic of the monzonite unit as a whole is developed best in the medium-grained sub-unit. In this rock, laths of plagioclase feldspar which are rimmed by an overgrowth of sanidine form a

groundmass containing intergranular augite, hypersthene, quartz, pigeonite, and magnetite-ilmenite grains. Augite grains are larger than hypersthene grains and sub-ophitically enclose unrimmed plagioclase laths. The medium-grained member of this unit is holocrystalline and has few or no inclusions of basement rocks (see Appendix: Sample 5-32-1).

The coarse-grained and medium-grained members of the monzonite unit have similar fabrics and differ mainly with respect to grain sizes. Both units lack inclusions of basement rocks.

In contrast to the above two sub-units, the fine-grained sub-unit contains numerous inclusions of basement rocks. Some inclusions are rounded, some angular, and, in many instances, they are contorted and distended. Many of the inclusions display microscopic shock deformation features such as extensive fracturing and development of planar shock lamellae. Apart from the inclusions present, the fine-grained sub-unit has a somewhat different fabric than the other sub-units. Some fine-grained rocks near the lake consist of a few phenocrysts of quartz and sanidine in an aphanitic groundmass. In thin section, the volcanic glasses from this unit have holohyaline textures with perlitic cracks. Other rocks from the fine-grained unit consist of intergranular hypersthene, augite and magnetite in a groundmass of plagioclase laths, with some intersertal alkali feldspar. Phenocrysts of hypersthene, augite, plagioclase, sanidine, and quartz-sanidine

intergrowths are also present.

(i) Chemical composition and variation. Chemical analyses for the medium- and coarse- grained sub-units are given in Table 4 of the Appendix; two analyses of rocks in the fine-grained sub-unit are given in Table 5. Analyses for all sub-units of the monzonite are fairly close in composition. The rock contains about 59% SiO_2 which classifies it (using fine-grained, extrusive rock terminology) as andesitic. Its K_2O content is much higher than most andesites, and its Al_2O_3 content is slightly lower (Larsen, 1938).

All sub-units of the monzonite have quartz in the norm, and normative feldspar for all the rocks is about $Ab_{.47}An_{.26}Or_{.27}$. Neither the medium-grained rock nor the coarse-grained rock analysis contains normative magnetite, although cubic (spinel-series) iron oxide is evident in the magnetite-ilmenite intergrowths present in these rocks. One fine-grained rock does contain magnetite in the norm. The presence of hematite in most norms suggests fairly oxidizing conditions during formation of this material.

The monzonite body has not undergone extensive differentiation during its formation. SiO_2 contents show an increase of about 2-3 % from the fine-grained to the coarse-grained material. The K_2O contents show only a 10% increase, i.e. 3.0 to 3.3 %, between the fine-grained lower layers and the coarser-grained upper layers. MgO contents of the lower layers are 4.6% as compared to 3.2% for the uppermost layers of the body. By contrast, rocks from the

differentiated Palisade sill of New Jersey show a 300% increase in K_2O content and a 60% decrease in MgO content between extreme rock types (Turner and Verhoogen, 1960). The thicknesses of both these bodies are comparable; the Manicouagan body is 700-800 ft. thick while the Palisade sill is about 1000 ft. thick.

Shock Deformation Features in the Basement Complex --

General statement: Rocks from the Manicouagan-Mushalagan Lakes structure exhibit a general set of microscopic features unlike those normally observed in regional or contact metamorphic environments. These features include: (1) kinkbanding in biotite; (2) development of extensive microscopic fractures in mineral grains within the rock; (3) development of closely spaced, parallel fractures along planes of specific crystallographic orientation in quartz, feldspar, and scapolite; (4) partial or complete transformation of plagioclase to an isotropic material (diaplectic glass). The transformation of plagioclase to diaplectic glass takes place without destruction of grain textures, change of chemical composition, or destruction of the textures of coexisting pyroxene and garnet . Features similar to those described above have been observed in laboratory shock-loading experiments (Hörz and Ahrens, 1969; Hörz, 1968; Short, 1968; Milton and DeCarli, 1963) as well as in rocks around nuclear explosion craters (Cummings, 1965; Short, 1968; Carter, 1965). The occurrence of diaplectic glasses, however, has not been observed in experiments other than shock-loading experiments. The textural observations suggest that basement rocks of the Manicouagan-Mushalagan Lakes structure

have been subjected to shock wave deformation.

The purpose of this section is to detail evidence indicating the presence of shock deformation and to present as much quantitative information as possible concerning the intensity of shock-metamorphic effects present.

A chart showing microscopic shock-deformational features observed in different minerals is presented in Fig. 4. The shock pressure regimes at which various phenomena are thought to occur are also shown in Fig. 4. Features present in rocks from the Manicouagan-Mushalagan area are compared with features observed in shocked materials from other localities. Detailed descriptions and photomicrographs of samples are presented in the Appendix. Sample locations are indicated in Fig. 3.

The microscopic deformation features are displayed best in Unit #4, the anorthosite. Deformation features are less evident but observable in both Units #2 and #3. The latter two units display blackening of mafic minerals and recrystallization of quartz and feldspar, probably due to heating by the overlying monzonite. Both of these alterations of textures tend to obliterate evidence of microscopic shock features. Most anorthosite samples have not been thermally altered.

Description of Textures :

(a) Unit #1. Rocks from Unit #1 outcrop outside the crater and show no unusual textures. Quartz sometimes displays undulous extinction, but this feature is frequently observed in metamorphic terrains. In the rocks studied, biotite is unbent and shows no

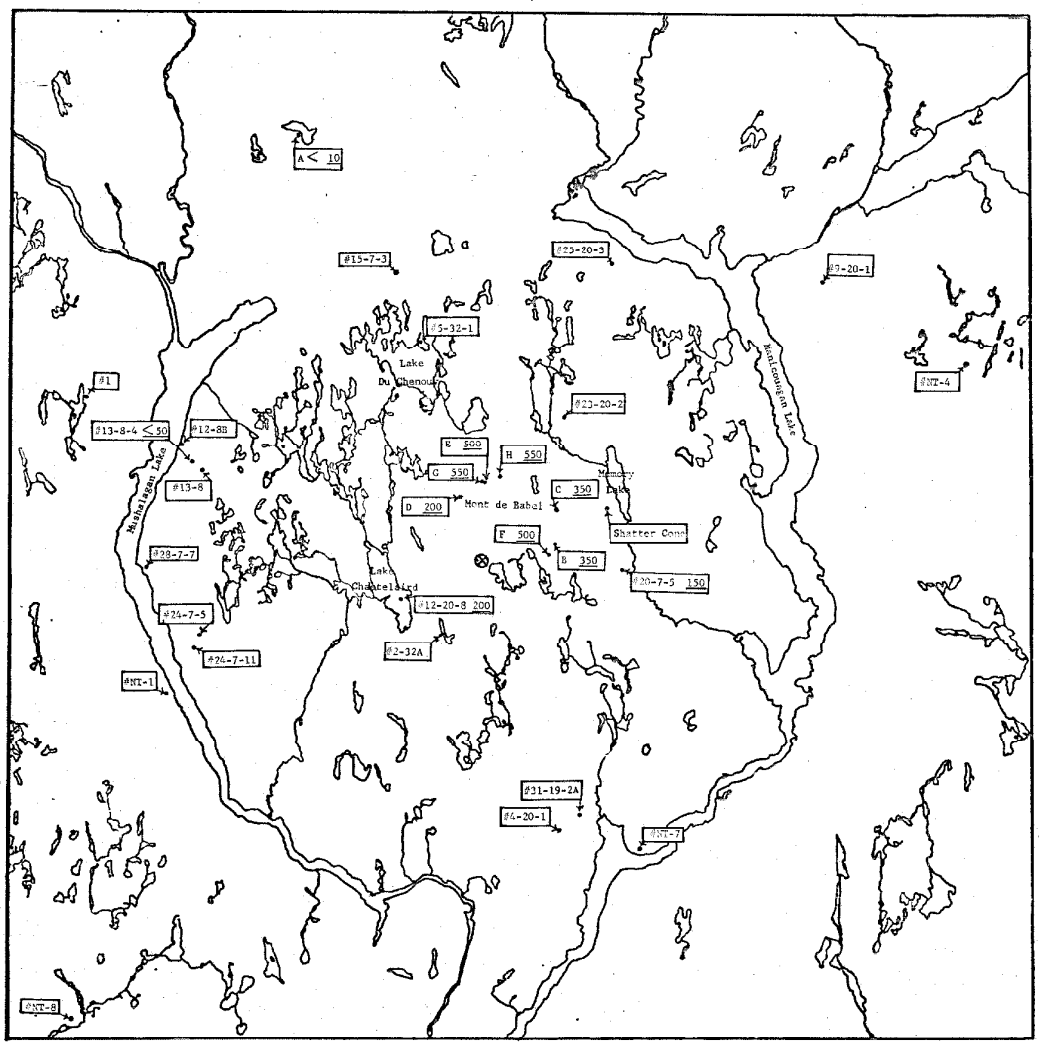

MANICOUAGAN-MUSHALAGAN LAKES STRUCTURE--SAMPLE LOCATION MAP

FIG. 3

kinkbands.

(b) Unit #2, Sample #13-8-4. Rocks from Unit #2 outcrop both east and west of Mont de Babel. Some gneisses in Unit #2 are overlain by the monzonite body and show contact-metamorphic textures in addition to unusual deformational features.

Sample #13-8-4 is an autobreccia. In hand specimen, the rock is an aggregate of fragments of fine- to medium- grained gneiss. These fragments range from 1-5 cm in size, and the gneissosity of individual fragments is oriented randomly. The material enclosing the gneiss fragments is somewhat finer grained and contains a larger percentage of dark minerals then gneiss fragments contain.

In thin section, the individual fragments are seen to be quartz-orthoclase-plagioclase-biotite gneisses. The material between the fragments is a melange of fine quartz, biotite, garnet, plagioclase, and orthoclase grains. There is no preferred orientation of mafic grains in the inter-fragmental material. This contrasts with the regular orientation of biotite and hornblende within individual grain fragments.

Mineral grains in the inter-fragmental material are jumbled together, and biotite is frequently bent. In the gneiss fragments, biotite is unbent. Plagioclase grains are not extensively fractured, and brownish, low-index material is absent. Closely spaced, parallel fractures are absent from quartz, both in the inter-fragmental material and in the gneiss fragments.

(c) Unit #2, east of Mushalagan Lake. Rocks from Unit #2 which outcrop in the area east of Mushalagan Lake display some closely spaced, parallel fractures in quartz and some bending of biotite. Most rocks from this area also show some degree of alteration due to the overlying monzonite. This alteration consists of blackening of the mafic minerals and slight recrystallization around the edges of quartz and feldspar.

(d) Unit #2, Sample #20-7-5. Sample #20-7-5 is from just east of the central massif. This rock exhibits alterations due to the monzonite body and microscopic deformational effects. Black, opaque grains, pseudomorphous after garnet and biotite, comprise the mafic minerals. Most quartz grains have a rim of recrystallized material and also show at least one set of closely spaced, parallel fractures. Almost every quartz grain in the rock exhibits at least one set of closely spaced, parallel fractures, and some grains contain as many as four intersecting sets. Poles of these fractures, measured in 20 grains, averaged 18-25^{o} inclination from the c-axes. Plagioclase is about An_{25}; it is in the high-albite structural state. In contrast to the quartz, plagioclase and orthoclase do not display closely spaced, parallel fractures. Kinks in the blackened, biotite-shaped grains may exist but cannot be seen.

(e) Unit #3, in general. Rocks from Unit #3 flank the central anorthosite massif. Over a large part of the area in which these rocks outcrop, they are overlain by monzonite. In areas overlain by the monzonite, rocks show blackening of the mafic minerals and

recrystallization of the feldspars. These thermal alterations conceal the microscopic deformation features which may have existed within the grains previous to the monzonite formation. In some rocks, however, thermal alterations are minimal, and microscopic deformation features can be observed. These deformational features include: bending and kinking of biotite; fracturing of plagioclase grains; development of closely spaced, parallel fractures. The parallel fractures are more frequently present in quartz but are also occasionally observed in plagioclase. Partial isotropization of grains is observed in some rocks from the unit.

(f) *Unit #3, Sample #12-20-8.* *Sample #12-20-8 (from a* small island in the southeast part of Lake Chastelaird) is from an erosional window in the monzonite and illustrates deformational features frequently found in Unit #3. The outcrop itself exhibits rock structures described by Dietz (1959 and 1963) as shatter cones.

In thin section, the mafic minerals in the rock are not blackened, and the rock texture does not appear to have been thermally altered. Plagioclase, garnet, and hornblende show many more fractures per unit area than do grains of these minerals in rocks exterior to the lakes. Many plagioclase grains contain numerous, closely spaced, parallel fractures. In some albite-twinned grains, the fractures are developed only in one set of twin orientations. Areas with extensive development of parallel fractures often merge into tannish, low-index areas. Plagioclase

grains frequently contain regions of this tannish or brownish material; both its index and birefringence are lower than in the host grain. Sometimes the brownish material is isotropic. The tan regions sometimes occur over whole grains with the adjacent grains being unaffected. In other cases, the regions are limited to one set of albite twin orientations.

Quartz is not present in this sample. In other rocks from Unit #3, quartz displays closely spaced, parallel, fractures.

Biotite, when oriented edgewise, displays bands approximately 30^{o} to the cleavage which have a different extinction position than the main part of the grain. These features are similar to kinkbands (Cummings, 1965).

The microscopic, deformational features observed in anorthosites from the central massif are illustrated by the set of samples discussed below. Complete petrographic descriptions of these rocks are found in the Appendix. Locations of these samples are shown in Fig. 3.

(g) Unit #4, Sample A. Exterior to the two lakes, the anorthosite appears to be fresh with few fractures. Fractures in plagioclase occur mainly along the (001) plane. The plagioclase has uniform, non-undulating extinction, and no closely spaced, parallel fractures are present. Scapolite displays normal birefringence, non-undulous extinction and has no closely spaced, parallel fractures.

(h) Unit #4, Sample D . Sample D illustrates the least intense deformations observed in the anorthosite suite. In hand specimen, this sample is indistinguishable from unshocked anorthosite. In thin section, grain boundaries are preserved, and plagioclase exhibits non-undulous extinction. Fractures within grains are more extensive than in plagioclase from anorthosite exterior to the lake and occur along both (001) and (010). A tan or light brown material occurs either in patches around mafic grains or as isolated patches within individual plagioclase grains. This material has an index of 1.509 which is distinctly lower than the mean index of 1.560 of the plagioclase enveloping it. The tan and brownish material is either isotropic or has a lower birefringence than the host plagioclase. Microprobe beam scanning pictures suggest that this material has about the same chemical composition as the plagioclase (see Appendix, Sample D). Parallel, closely spaced fractures appear in plagioclase with traces of the fractures aligned parallel to the albite twin composition plane. These fractures are frequently limited to one set of twin orientations. One set of twin lamellae in a grain is often densely packed with parallel fractures and may appear tannish and isotropic.

No maskelynite is observed in this material. Garnets show strong fracturing but are chemically homogeneous (see Appendix).

(i). Unit #4, Samples B and C. Samples B and C are totally maskelynitized anorthosites. In these samples, the grain boundaries of the plagioclase can be discerned, although the grains themselves

have been transformed to a water-clear, isotropic glass, n = 1.537. The index of this glass is greater than the 1.533 index of refraction for a plagioclase glass of similar composition (An_{55}) which has quenched from a melt. Grain boundaries are visible because the albitic feldspar on the edges of the plagioclase grains is birefringent. The albitic feldspar often shows closely spaced, parallel fractures. General fracturing and closely spaced, parallel fractures are absent in maskelynite. Parts of some maskelynite grains are birefringent plagioclase and display both albite twinning and closely spaced, parallel fractures.

Garnet in the maskelynitized anorthosite is a darker red-brown and more heavily fractured than garnet in anorthosites exterior to the structure. It is also also isotropic and displays no heterogeneity in composition.

A detailed study of the scapolite deformations present in Samples B and C is presented in Chapter 2. Two results of this study show (1) that the isotropic plagioclase (maskelynite) has the same chemical composition as the plagioclase in other anorthosites from the massif and (2) that closely spaced, parallel fractures occur in the scapolite of this rock (see sample descriptions in Appendix). Scapolite from this rock shows no chemical heterogeneity on a 100μ scale.

(j) Unit #4, Samples E and F. Samples E and F do not exhibit brecciation in hand specimens. Neither sample displays macroscopic signs of melting or plastic flow.

In thin section, plagioclase in these rocks is birefringent with uniform, non-undulous extinction. Albite-twinned grains occur infrequently compared to Sample D or anorthosite outside the lakes. Closely spaced, parallel fractures, similar to those observed in Sample D, are extremely rare. Plagioclase has a composition of An_{55} (see Appendix, Table 3) and a mean index of refraction of about 1.552. A series of curved, concentric fractures is present in some plagioclase grains. Optical properties of this material are anomalous: a 2V of 0 to 30^{o}(+) is observed in contrast to the 2V = 85^{o}(+) characteristic of normal plagioclase (Deer et al., 1963). The interiors of grains have peculiar branching strings of 10 μ bubbles. Brownish material with a lower refractive index than plagioclase occurs both between grains and as isolated patches in some grains. This brownish material is isotropic or has very low birefringence. No maskelynite is present in this sample.

Scapolite in the rock is charged with inclusions; individual grains are composed of mosaics of fine crystallites with differing optical orientations. The sulfur content of these scapolites is extremely heterogeneous. A single grain contains well-defined 20 - 50 μ domains. Some domains have chemical compositions similar to scapolite from Sample A. Other domains within the same grain have very different chemical compositions than scapolite (see Appendix, Sample E).

Grains pseudomorphous after garnet from other anorthosites in the massif are present in these samples. This pseudomorphous material is isotropic and has a composition similar to the garnet from other anorthosites in the massif (see Appendix, Sample E). These grains may be garnet, but no x-ray data is available to determine their crystal structure. Regions, 20 - 50μ in a dimension, display concentrations or depletions of Fe, Mg, Ca, Al, and Si compared to other regions of the grain (see Appendix, Sample E). The heterogeneous distribution of elements within a single grain is not observed in the garnets of Samples A, D, B, or C.

(k) Unit #4, Samples G and H. Both Samples G and H are breccias which occur in isolated pods and lenses within the central anorthosite massif. These pods and lenses are not discernibly related to the monzonite and do not appear to be pipes of volcanic breccia. In hand specimen, these breccias appear as jumbles of whitish rock fragments in a reddish or (less frequently) greyish matrix. Both rounded and angular fragments are present in the breccias, and some fragments have elongate, distended forms. Bands of mafic minerals in the fragments appear twisted and bent.

Thin sections of Samples G and H contain contorted grains of reduced birefringence plagioclase in a matrix of aphanitic, reddish or greyish material. The contorted plagioclase frequently displays undulous extinction but no closely spaced, parallel fractures. Plagioclase "grains" are actually domains of 20-50μ

plagioclase crystallites. These domains are about 0.5 - 1 mm in a dimension and are pseudomorphous after plagioclase grains from other anorthosites. Crystallites within each domain are in more or less uniform alignment and are probably part of the same original grain. No maskelynite is present in these rocks.

Euhedral, isotropic garnet grains such as those occurring in other anorthosites from the massif do not exist in either Sample G or Sample H. Opaque grains pseudomorphous after garnet are found in the breccias. Electron beam scans of these opaque areas in Sample G reveal small blebs of iron and magnesium oxide surrounded by material of highly variable but approximately garnet composition. Electron beam scan studies of Sample H reveal a large number of slightly nickeliferous,iron sulfide balls, both in the matrix material and imbedded in garnet pseudomorphs (see Appendix, Samples G and H). The significance of these iron sulfide balls is unclear, although El Goresy et al. (1968) have reported pyrrhotite spherules of similar composition imbedded in glasses from the Ries Basin in Germany.

Aphanitic matrix material comprises about 50% of both Samples G and H. Contorted mineral fragments are frequently observed in the aphanitic material.

Correlation of Observed Deformational Features with Shock Features --

The features described above are identical to those produced in laboratory shock-loading experiments and those

observed in naturally shock-loaded materials occurring at suspected meteorite impact sites. Similar features have also been observed in rocks subjected to intense stress waves produced by nuclear explosions.

Some of the features observed in these samples have also been observed in rocks subjected to the static loading conditions found in geological tectonic environments. In contrast, all of the above-described features have been observed in shock-loaded materials. Microscopic fractures, kinkbands in biotite, and planar features in quartz fall into the former category. Diaplectic phases and planar features in plagioclase have been observed only in shock-loaded material.

Increases in the frequency of fractures within mineral grains of experimentally shocked rocks have been observed by Short (1968). An increased density of microscopic fractures is also observed in shock-metamorphosed rocks from the Ries Basin in Germany (W. v. Engelhardt and Stöffler, 1968). Kinkbands similar to those described in Sample #12-20-8 have been observed in tectonic environments as well as in laboratory shock experiments (Hörz and Ahrens, 1969). The closely spaced, parallel fractures which were observed in quartz from Sample #20-7-5 are identical to the planar features produced in experimentally shock-loaded quartz (Hörz, 1968). Fractures similar to "planar features" have been observed in tectonically deformed rocks and statically loaded quartz (Carter, 1965). Extensive development of planar features in quartz, however, occurs only in shock-deformed rocks (Carter, 1968). Planar feature poles in

experimentally shocked quartz occur most frequently at angles of about 23° to the quartz c-axis (Hörz, 1968). Planar feature pole angles to the c-axis in quartz from rocks of suspected meteorite impact sites also peak at about 23° (Robertson et al., 1968). Angles of planar feature poles to the c-axis in quartz measured in Sample #20-7-5 peak at about 23°.

The closely spaced, parallel fractures observed in plagioclase from Sample #12-20-8 and the anorthosite (Sample D) have been observed in rocks from the Ries Basin by Engelhardt and Stöffler (1968). These authors have also observed the peculiar tendency for parallel fractures and low-index material to affect only one twin orientation of an albite-twinned plagioclase grain. Closely spaced, parallel fractures in plagioclase grains have not been reported from tectonically deformed areas.

Textures such as those observed in the maskelynitized anorthosite have not been observed in tectonic or volcanic environments. Glasses of roughly plagioclase composition may be found in rocks that have been completely melted and rapidly cooled. These volcanic glasses, in which the entire rock is melted and quenched, are distinctly different from the maskelynite-bearing rocks found at Manicouagan. In the maskelynitized anorthosite, non-crystalline plagioclase glass (Bunch et al., 1967) coexists with crystalline minerals which have retained their original textures and optical properties. Volcanic glasses are holohyaline rocks with no crystalline phases.

In Chapter 2, studies of scapolite which coexists with maskelynite in the maskelynitized anorthosite are described. The scapolite is crystalline, apart from containing "planar features" frequently found in shocked tectosillicates, and exhibits unaltered optical properties. The fact that scapolite, which incongruently melts at 860°C (Deer et al., 1963), is unmelted and coexists with maskelynite of composition An_{53} suggests that the maskelynite formed at temperatures below ~ 850°C. Material of An_{53} composition must be quenched from temperatures of about 1300°C in order to form a thermal glass. The apparent low temperature indicated for maskelynite formation suggests that this material did not result from thermal processes. Textures similar to those found in maskelynitized anorthosite from Manicouagan have been produced by shock-loading a specimen of stillwater gabbro (Milton and DeCarli, 1963). After having been shocked, the plagioclase of the gabbro was entirely transformed to a clear, vitreous material. This vitreous material coexisted with fractured but otherwise unaltered mafic minerals. Plagioclase glass, coexisting with unaltered mafic minerals, has also been observed in rocks from the Ries Basin in Germany, as well as in other suspected meteorite impact craters. Since maskelynitized rocks are easily produced by shock processes but are not known to result from thermal processes, their presence strongly suggests shock deformation.

The striated, conical fractures observed in many of the rock outcrops in the Manicouagan-Mushalagan structure are identical

to the "shatter cones" (Dietz, 1959, 1963, and 1968) frequently found at suspected meteorite impact sites.

The similarity of the microscopic features present in Manicouagan rocks to the high-strain-rate, high-pressure deformations produced by shock waves very strongly suggests that the basement rocks of this structure have been subjected to shock-wave metamorphism. As will be discussed later, the most likely terrestrial source of shock waves is the impact of a hypervelocity, extra-terrestrial object. Strain rates in geological tectonic environments are much smaller than strain rates during shock deformations. Extensive microscopic fractures, kinkbands in biotite, and microscopic planar features in quartz occur predominantly in shock wave-deformed rocks, but they may also be found in tectonically deformed rocks. The presence of the features mentioned above in rock minerals is, therefore, not incontrovertible evidence that the rock has experienced shock-wave deformation. Macroscopic shatter cone development in rocks and microscopic planar features in plagioclase, however, have only been observed at suspected meteorite impact sites (Dietz, 1963; Engelhardt and Stöffler, 1968). Maskelynitized rocks are limited to (1) probable impact sites where shock metamorphism is suspected to have occurred and (2) to laboratory shock-loading experiments where the rocks are known to have been shock metamorphosed. In the basement rocks of the Manicouagan-Mushalagan Lake structure, the presence of an association of features which are either (1) known to be exclusive products of shock-wave deformations or (2) known to be associated with

shock-wave deformation leaves little doubt that these rocks have been subjected to shock metamorphism.

Several quartz-bearing, shocked gneisses from Units #2 and #3 were examined for traces of coesite and stishovite using x-ray diffraction techniques. No traces of these minerals were found. Such high-pressure polymorphs of quartz might not be present at Manicouagan because most of the highly shocked rocks (i.e. those shocked to pressures $>$ 200 kb) are non-quartzose. Thermal metamorphism of shocked rocks by the overlying monzonite may have caused any polymorphs originally produced by the impact to transform to α-quartz.

Estimation of Shock Intensity:

(a) General statement. The experimental shock studies which have been made on various minerals permit at least a semi-quantitative estimation of shock intensity experienced by a rock based on observed microscopic features. Fig. 4 is a compilation of data which pertains to the estimation of shock intensities from observed deformations. The sources of information are discussed in the caption. The shock pressure estimates based on these features are shown in the lower entries of the table.

(b) Sample A. The anorthosite exterior to the crater show no visible signs of shock. It has a fracture density comparable to that of rocks 40 miles distant from the structure. The few biotites present displayed no kinkbands. This sample probably experienced shock pressures lower than 10 kb.

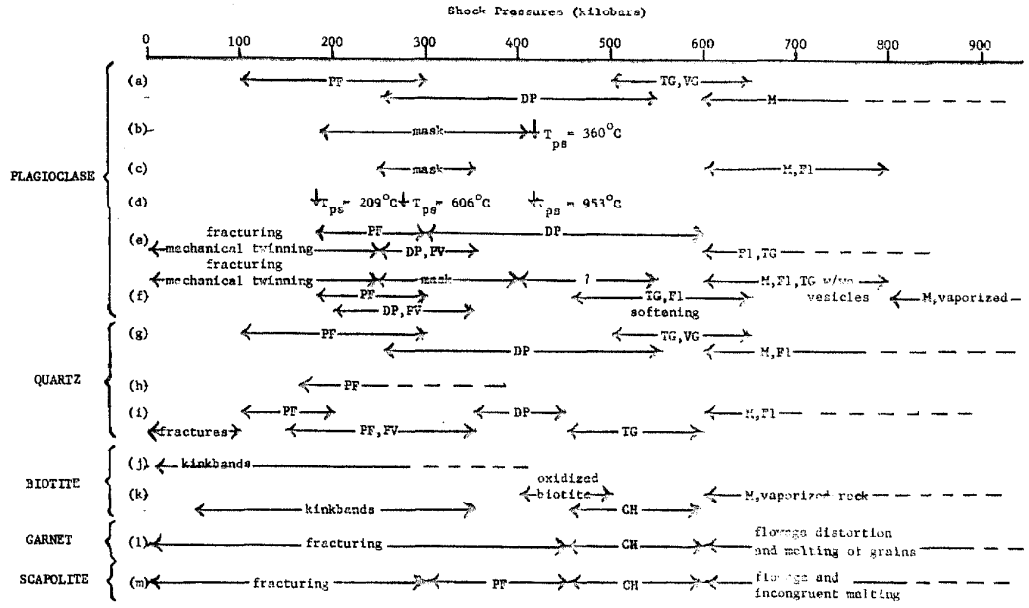

A ↔ Anorthosite exterior to lakes.

D Slightly ⟷ shocked anorthosite.

B,C Maskelynitized ⟷ anorthosite.

E,F Anorthosite with no PF, chemically heterogeneous ⟷ garnet and scapolite.

G,H Breccias: Rock appears softened. ⟷

#12-20-8 Shocked ⟷ granulite-grade gneiss.

#20-7-5 Shocked ⟷ gneiss from Unit #2.

#13-8-4 ⟷ Gneiss autobreccia.

Abbreviations used:

PF = Planar features. DP = Diaplectic phases. CH = Chemical heterogeneity.
Mask = Maskelynite production. Fl = Flowage. M = melt. TG = Thermal glass.
VG = Vesicular glass. FV = Partial vitrification. T_{ps} = Post-shock temperature.

FIGURE 4.

CORRELATION OF KNOWN SHOCK FEATURES WITH DEFORMATIONS
OBSERVED IN MANICOUAGAN ROCKS AND MINERALS

FIGURE 4

Correlation of Known Shock Features with
Deformations Observed in Manicouagan Rocks and Minerals

(a) Deformation scheme of Engelhardt and Stöffler (1968); based on shocked plagioclase from the Ries Basin.

Stage I, 100-300 kb: Plagioclase displays bending, undulous extinction and extensive micro-fracturing. Planar features and regions of lowered birefringence develop along planes (001), (010), (100) and $(1\bar{2}0)$.

Stage II, 250-550 kb: Diaplectic phases develop. One set of albite twin lamellae in albite-twinned grains becomes preferentially isotropized.

Stage III, 500-650 kb: Normal thermal glass, often containing vesicles, is produced.

Stage IV, 600-1000 kb: Melting of the rock, with development of heterogeneous rock fragment-melt breccias (Fladlen). Vaporization of the rock also occurs in this pressure range.

(b) Data of Ahrens et al. (1969). Transformation to maskelynite in oligoclase begins at about 180 kb; complete transformation to maskelynite during shock takes place at 417 kb. Post-shock temperature at 417 kb is 330-400°C.

(c) Observations of shocked stillwater gabbro, Milton and DeCarli (1963). Plagioclase (An_{80}) transforms completely to maskelynite at 250-350 kb. At 600-800 kb, shocked rock contains vesicular thermal glass quenched from melted plagioclase. Temperatures implied at 600-800 kb by the melting are 1300-1700°C.

(d) Temperature revision of temperature values in (b), Ahrens (1971). Post-shock temperatures are 209, 606 and 953 °C at pressures of 180, 272 and 417 kb, respectively. These are probably overestimates of the post-shock temperatures.

(e) Deformation scheme of Chao et al. (1970), based on recent shock-loading experiments with plagioclase, and post-shock temperatures

in (b). 0-250 kb: microfractures, extinction variation, and mechanical lamellar twins. 200-300 kb: planar features form in birefringent plagioclase. 250-350 kb: partial transformation to diaplectic glasses. Transformation often takes place selectively along one set of twin lamellae in albite-twinned grains. 275 - ~ 600 kb: complete transformation to diaplectic glass occurs. ~ 500- ~ 1000 kb: flowed and vesicular plagioclase glasses occur. 700 - ~ 900 kb: melted rock.

(f) Preferred scheme. Based on the scheme of Chao et al. (1970) for low pressures but including other data in the pressure region above 400 kb. 0-200 kb: fracturing, mechanical twinning, and extinction variations. 200-300 kb: planar features. 200-350 kb: partial vitrification, transformation to diaplectic phases along one set of twin lamellae. 250-400 kb: formation of maskelynite. 400-500 kb: ? Disappearance of planar features and development of low 2V plagioclase. 450-650 kb: local development of thermal glass, minor plastic deformation, softening and incipient flowage. Based on the temperature revisions of Ahrens (1971), the softening range of plagioclase (temp. ~ 700°C) is probably 500-600 kb rather than 600-700 kb as suspected by Chao et al. (1970). 600-800 kb: plagioclase melts and flows. Thermal glasses with and without vesicles occur. > 800 kb: melts and vaporized melts of the total rock.

(g) Quartz deformations after the scheme of Engelhardt and Stöffler (1968). Stage I, 100-300 kb: planar features, lower densities and refractive indices. Stage II, 250-550 kb: transformation to diaplectic phases. Presence of coesite and stishovite in some glasses. Stage III, 500-650 kb: melting of quartz production of thermal glasses with or without vesicles. Stage IV, 600-1000 kb melting and flowage of quartz. Production of fladlen.

(h) Data from Hörz (1968). Planar features in quartz form only above 162 kb shock pressures.

(i) Quartz deformation scheme of Chao (1968). 0-100 kb: normal and fractured quartz. 100-200 kb: planar features. 150-350 kb: planar features with some partially isotropic quartz. 350-450 kb: diaplectic quartz. 450-600 kb: melted quartz and quartz glass (lechatlierite). > 600 kb: melted and vesicular quartz. Lechatlierite: vaporized quartz at highest shock pressures.

(j) Data from Hörz and Ahrens (1969). Lower pressure limit for the formation of kinkbands is about 9 kb.

(k) Biotite deformation scheme after Chao (1968). 0-50 kb: normal biotite. 50-350 kb: biotite with kinkbands and lowered birefringence. 400-500 kb: oxidized, opaque biotite and mixtures of magnetite and glass. 450-600 kb: chemically heterogeneous mixtures of magnetite, glass, and melted rock. > 600 kb: melted and vaporized material.

(l) Probable sequence of deformations in garnet. 0-450 kb: fracturing of grains occurs. (Planar features observed in this pressure range in quartz, feldspar and scapolite have not been found in garnet.) 450-600 kb: the residual temperature of the garnet is high enough to cause breakdown of the garnet and cause individual grains to decompose to a chemically heterogeneous mixture of phases. Chao (1968) observes similar effects in shocked biotite and amphibole. Above 600 kb the garnet melts and flows yielding distorted grains.

(m) Probable sequence of deformations in scapolite. A parallel sequence of deformations is observed in scapolite. 0-300 kb: grains are micro-fractured. 300-450 kb: planar features develop in scapolite (Wolfe and Hörz, 1970). 460-600 kb: The scapolite shows chemical heterogeneity. Scapolite melts incongruently at 860°C (Deer et al., 1963), hence the post-shock temperature of scapolite in the pressure range 450-600 kb must exceed this value. > 600 kb: scapolite grains melt and decompose. Flowage distorts and elongates grains.

Shock pressure ranges estimated for some of the samples petrographically studied are indicated in this figure. The pressure assignments are discussed in the text.

(c) Sample D. The slightly shocked anorthosite contained no maskelynite but displayed abundant micro-fractures and planar features. Many albite-twinned plagioclase grains with one set of isotropic or low-index, twin lamellae were observed. This sample has probably been shocked to between 150 and 250 kb. These limits correspond roughly to the regime of planar features in plagioclase suggested by Chao et al. (1970).

(d) Samples B and C. Both Samples B and C are totally maskelynitized anorthosites. Planar features occur in plagioclase which has not been transformed to maskelynite, but they are absent from the maskelynite. No flowage or vesiculation is present. Both scapolite and garnet are chemically homogeneous. These maskelynitized anorthosites have probably been shocked to pressures between 300 and 400 kb. Three-hundred kilobars is the lower limit for maskelynite formation (Chao et al., 1970). Although the upper shock pressure limit of 400 kb, shown in Fig. 4, is somewhat uncertain, this upper limit is probably less than 500 kb. Thermal glasses are present above 500 kb (Engelhardt and Stöffler, 1968), and no thermal glass is present in this sample. The data of Ahrens et al. (1969) suggests that above 400 kb the post-shock temperatures of plagioclase will rapidly increase to $> 900^{\circ}C$. Since scapolite in the rock probably did not reach $900^{\circ}C$, the upper pressure limit for this rock is believed to be about 400 kb.

(e) Samples E and F. In hand specimen, Samples E and F show no signs of flowage or vesiculation. Both of these samples contain material which has plagioclase composition but very small optical 2V. This anomalous plagioclase is not maskelynitized, and no planar features are found. Garnet and scapolite in this anorthosite both display chemical heterogeneity on a 100μ scale. The chemical heterogeneities observed in these minerals are not observed in Samples A, B, C, or D (see Appendix).

An estimation of the shock pressure experienced by Samples E and F is difficult to make since the features observed in these samples have not yet been reported in samples from areas other than Manicouagan. (Dworak (1970) has also observed similar uniaxial plagioclase from Manicouagan.) The shock pressures experienced by Samples E and F must be higher than those experienced by the maskelynite samples; the chemical heterogeneity present in garnet and scapolite implies that these samples experienced higher temperatures than the maskelynite. The higher temperatures are presumed to be due to greater shock pressures. A rough assignment of the shock pressure is 450-600 kb. The lower pressure limit of 450 kb is about the upper limit for maskelynite formation; the upper pressure limit of 600 kb corresponds to the pressure at which significant flowing and vesiculation begin to occur (Engelhardt and Stöffler, 1968) (see Fig. 4).

(f) Samples G and H. On a hand specimen scale, both Samples G and H (breccias) are composed of elongate mineral fragments which appear to have been softened. These fragments suggest plastic flow of the rock.

Microscopically, both breccias show textures similar to those observed in Fladle from the Ries (Engelhardt and Stöffler, 1968). Some grains of plagioclase are decomposed into clusters of small crystallites, a texture which suggests recrystallization within the grain. Other plagioclase grains are elongate, bent, and display undulous extinction. Garnet in these breccias has apparently undergone quite extensive decomposition during the shock process.

These features suggest temperatures high enough to soften plagioclase and decompose garnet but not high enough to produce total melting and vesicular plagioclase glass. The shock pressure experienced by these samples is roughly estimated at between 500 and 800 kb. Post-shock temperatures at 500 kb are 700 - 800 ^{o}C, the temperature range in which plagioclase begins to soften (Chao et al., 1970). Eight-hundred kilobars is an approximate upper limit for the shock pressure. At 800 kb, melting and vesicular thermal glasses would probably be more extensive than they are in these samples. These samples have textures similar to the fladle of the Ries. Fladlen are believed to have experienced shock pressures of between 600 and 1000 kb (Engelhardt and Stöffler, 1968).

(g) Sample #12-20-8. Sample #12-20-8 displays planar features in plagioclase and some isotropic or low-index, brownish plagioclase. Albite-twinned plagioclase grains often have one low-index set of twin lamellae. Biotite shows kinkbanding. These features are roughly comparable to the deformations found in Sample D of the anorthosite (i.e., deformations which appear between 150 and 250 kb shock pressure.

(h) Sample #20-7-5. Sample #20-7-5 shows planar features in nearly every quartz grain. No low-index or isotropic quartz is present. The planar features are predominantly oriented with poles inclined about 23° to the quartz c-axis. Planar features are absent in plagioclase. Chao et al. (1970) suggest that about 200 kb is the lower limit for planar feature formation in plagioclase. Hörz (1968) observed planar features in quartz shocked to greater than 162 kb. Based on these observations, Sample #20-7-5 must have experienced a shock intensity of between 150 and 200 kb.

(i) Sample #13-8-4. Sample #13-8-4 is an autobreccia. Biotite from this sample is bent and frequently displays kinkbands. Planar features are absent from both quartz and feldspar. This rock probably experienced shock pressures of less than 50 kb.

Correlation of Shock Effects with Position: The center of the structure is indicated in Fig. 3 with an "X". The underlined numbers in Fig. 3 are the shock intensities believed to have been experienced by the sample shown. The shock effects observed in the basement rocks tend to become more extreme as the point "X" is

approached. Shock pressures of over 600 kb have been experienced by some rocks in the central massif, while gneisses on the inner shore of Manicouagan Lake appear to have been shocked to less than about 50 kb. Sample #1, which is from an outcrop about four miles northwest of the north shore of Mushalagan Lake, experienced a shock pressure of only 10 kb or less. Samples located more than five miles from the outer lake shores have no detectable shock-metamorphic effects. It appears that the outer shores of the two lakes mark the limit of deformations due to shocks greater than ~ 10 kb. Shock pressure isobars in the basement rocks of the structure probably form concentric rings around the central massif. An exact correlation of sample location with deformation intensity cannot be made, however, because of the limited sampling in this study.

Samples which have been severely deformed often occur only a short distance from others which show only moderate deformation. This is especially true of the rocks from the central anorthosite massif. The variability in shock effects over small distances is probably due to variations in the effective shock impedance of the anorthosite massif. Such variations could result from joint planes and mafic mineral bands.

The general localization of intense shock-metamorphic effects in the central part of the structure strongly suggests that the energy source which produced the deformations was centrally located in the structure rather than being dispersed throughout

the structure. This centralization of deformations is a requisite feature of craters which have been formed by meteorites.

Structures, Faults, Joints, and Possible Meteoritic Material --

Detailed studies of structures in the gneisses and anorthosites were not made. It was generally observed that the basement rocks in the area tend to show a rather consistent NW-SE pattern of foliation. The foliation is steeply dipping or vertical. Alternation of mafic-rich layers and leucocratic layers in the gneisses is a widespread phenomenon.

It has been suggested by Currie (1965) that Manicouagan and Mushalagan Lakes are located in fault valleys. The fault valleys are supposed to be part of a ring fault which surrounds the structure. The basement rocks near these lakes, however, do not display cataclastic features. It is therefore thought unlikely that such a ring fault exists.

Kish (1962) has mapped a very large, normal fault along the banks of the Hart-Juane River. Some samples from the gabbroic anorthosite massif just south of the river resemble cataclastic rocks.

Jointing in the area produces traces which weather preferentially. Preferential weathering along joint planes is probably responsible for the predominance of cliff escarpments with strikes near 025, 335, 300, and 230 ^{o}.

No fragments of meteoritic iron have been found associated with any of the rock units exposed in the crater. Microscopic

fragments of Ni-rich iron may occur in the matrix of the shock breccia unit which underlies the monzonite. In reflected light, thin sections of this material sometimes show 50 μ , spherical, highly reflective materials. The chemical composition of these materials, however, is unknown.

As mentioned previously, one anorthosite breccia (Sample H) contains balls of slightly nickeliferous iron sulfide. The composition of these balls was determined to be: 50% S, 39% Fe, 1% CaO, 4% SiO_2, 5% Al_2O_3, and 1% MgO. (Values as wt. %) This material is about 93 atomic percent FeS_2 with about 7 atomic percent of the material composed of a silicate. The Ni content of these balls is less than 1%.

It is unclear whether or not this iron sulfide is of extra-terrestrial origin. El Goresy et al. (1968) reported the presence of a somewhat similar material in glasses from the Ries Crater. They have observed material of approximately FeS composition with 0.9% nickel. FeS_2 was not found in other anorthosites from the massif.

Summary of Stratigraphic Relations --

The Structure in General: Units within the Manicouagan-Mushalagan structure are exposed in an essentially horizontal sequence. Grenville-type gneiss and anorthosite form the basement complex of the structure. A thin, discontinuous layer of shock breccia and limestone blocks unconformably overlies the Precambrian basement. The thickness of this layer does not exceed 70 feet.

The limestone blocks occur along the interior of the two lakes, while the shock breccia layer occurs in an annulus which rings the central massif. Limestone blocks always occur on the Precambrian basement and have not been observed resting on shock breccia. The monzonite forms a much thicker layer, up to 800 ft. thick, which overlies both the shock breccia and the Ordovician limestone as well as the Precambrian basement gneisses.

The Monzonite Body: The lower sub-unit of the monzonite contains many inclusions and appears to grade downward into the shock breccia. The contact between the monzonite and the Precambrian basement is sharp and easily distinguishable. On the outer margins of the monzonite sheet, flow structures are visible along the contact of the Precambrian gneisses and the fine-grained sub-unit of the monzonite. The medium-grained monzonite overlies the fine-grained sub-unit, and it, in turn, is overlain by coarse-grained monzonite. The upper sub-unit of the monzonite appears to be the top of the monzonite sequence. No blocks or patches of non-igneous material, other than glacial till, are found stratigraphically above the monzonite. Glacial boulders of monzonite are found on the top of the anorthosite body, suggesting that the upper surface of the monzonite was exposed and being eroded 10,000 years ago.

Implications of the Detailed Observations:

General Statement --

A broad, regional picture of Grenville Province and a detailed description of the rock units found in the Manicouagan-Mushalagan Lakes Structure have now been presented. With this information, some features of the history of the Manicouagan-Mushalagan structure can be deduced. In this section, three questions will be considered:

(1) What are the implications of the shock-metamorphic effects?

(2) What are the age relations which can be deduced from the presence of the Ordovician limestone along Manicouagan and Mushalagan Lakes?

(3) What is the nature of the igneous body of the Manicouagan-Mushalagan Lakes structure?

Implications of the Shock-Metamorphic Effects --

Meteoritic Impact:

Arguments have already been given which relate the microscopic, deformational features in the basement to high-strain-rate, shock-wave deformations. An extraterrestrial body impacting the earth's surface at velocities of from 10-70 km/sec will produce shock deformations in rocks around the impact point (Shoemaker, 1963). For this reason, the presence of shock-deformational features in the basement rocks of the Manicouagan-Mushalagan Lakes structure suggests that this area has been impacted by a meteorite. Some considerations, however, should be given to

the question of whether or not meteorite impact is the only process which can produce the deformations observed.

The question posed above is essentially the question which must be answered in determining the origin of the "crypto-volcanic" structures on the earth. These structures are non-volcanic, circular depressions where no evidence of meteoritic matter exists. Examples of "crypto-volcanic" structures in the United States include Wells Creek, Middleboro, Howell, Serpent Mound, and the Manson structure (Baldwin, 1963). Rocks from these structures show no shock deformations, but the basins have structural similarities to meteoritic impact basins. For the purpose of this paper, meteoritic impact basins are considered to be basins in and around which meteoritic, nickel-rich iron exists. The meteoritic, nickel-rich iron can exist either as microscopic, metallic fragments in glass, or in the form of nickel-iron fragments lying on the ground around the crater. The Ries Crater in Germany is an example of the first type of occurrence of nickel iron (El Goresy et al., 1968) while Meteor Crater in Arizona is probably the best-known example of the second type of occurrence (Shoemaker, 1963).

The origin of "crypto-volcanic" structures has been considered in detail by various authors. Several comprehensive reviews of this subject are available (Baldwin, 1963; Bucher, 1963; Dietz, 1963b). No attempt will be made here to consider all the mechanisms of formation which have been proposed for the origins

of these structures.

Three points should be considered if one is to make the assumption that an internal source of shock waves produced the rock textures observed at Manicouagan-Mushalagan:

(1) The maskelynitized rocks at Manicouagan would require pressures of at least 250 kb for formation (Chao et al., 1970; Milton and DeCarli, 1963). Other rocks from the structure would require even higher formation pressures.

(2) Pressures of 250 kb are not known to occur in any surface or near-surface terrestrial environment. Pressures of this magnitude are found within the earth only at depths of about 1000 km where temperatures are thought to be $\sim 2200^{\circ}C$ (Stacy, 1969). The maximum tensile strength of any rock is about 25 kb at $20^{\circ}C$ (Clarke, 1969). The tensile strength of all materials decreases with increasing temperature. It is difficult to see how pressures of 250 kb, which are prevalent only at depths of 1000 km within the earth, could be contained in any geological material, transferred to the surface, and suddenly released.

(3) Diatreme formation most closely resembles the elusive "explosive" eruptions described by Bucher (1963) and Currie (1965). Such eruptions are supposed to be the causes of "crypto-volcanic" structures. Diatremes result when high-pressure gases from volatile-rich magmas are vented at the earth's surface. The typical surficial expression of a diatreme is an irregular pipe or plug of breccia. This breccia contains fragments of the rock which

the gases have "cored" through during their ascent to the surface (Shoemaker et al., 1962).

The observed features present in diatremes are significantly different from the features observed in "crypto-volcanic" structures. Neither the wall rock around the breccia pipe nor the wall rock fragments within the breccia display microscopic, shock-metamorphic features. Exposed breccia pipes of known diatremes do not exceed two miles in diameter; most are less than one-half mile in diameter. Surface outlines of diatremes are often highly irregular (Wyllie, 1967) rather than nearly circular as are the "crypto-volcanic" structures.

It is concluded that no process other than a meteorite impact produces in surficial rocks the high-pressure, high-strain-rate deformations which are naturally associated with meteorite impacts. In view of this, it follows that the rocks of the Manicouagan-Mushalagan Lakes structure have been shock metamorphosed by the impact of an extra-terrestrial body.

Dimensions of the Original Crater: The present diameter of the Manicouagan-Mushalagan Lakes structure is about 60 km when measured between the outer shores of the two lakes. The original diameter of the structure was larger than its present diameter as the present erosional surface corresponds to a level below the original surface of the crater. It has been suggested that this structure was originally about twice the present diameter (Murtaugh, 1970; personal communication).

The original floor of the crater corresponds roughly to the bottom of the shock breccia layer. This stratigraphic level topographically occurs at about 1300 ft. The shock breccia layer of Manicouagan now extends discontinuously as far as the inside of the lakes, i.e. the present shock breccia layer was originally a continuous layer ~ 46 km in diameter. Using Brent Crater in Ontario (Dence, 1968) as a scaling model, one can estimate that the original crater was around 70 km in diameter. This estimate of the diameter is compatible with the observation that shock intensities of less than 10 kb were experienced about 37 km from the structure center, i.e. at the location of Sample #1.

Since impact craters have similar morphologies (Baldwin, 1963), estimates of dimensions of the original crater at Manicouagan can be made by using appropriate scaling laws and dimensions of well-exposed craters.

Using the depth-to-diameter relation of Baldwin (1949) and assuming a 70-km original diameter of the crater, the original depth of the Manicouagan structure must have been about 3.4 km. Baldwin's revised (1963) depth-to-diameter relationship suggests an original depth of 5.1 km for a 70-km structure. Beals et al. (1963) have shown that well-preserved Canadian craters fit Baldwin's 1949 curve more closely than his revised curve. The estimate of 3.4 km for the original depth of the structure is thought most accurate.

An order of magnitude estimate for the energy of the body causing the original crater can also be made. Using the scaling technique suggested by Shoemaker (1963), which involves scaling the dimensions and explosive energy of a nuclear explosion crater, a kinetic energy of 2.5×10^{27} ergs is indicated for the impacting body. Baldwin (1963) suggests scaling from the known parameters of chemical explosive craters. His scheme suggests a value of about 4.7×10^{27} ergs for this energy. An estimate of about $4 \pm 2 \times 10^{27}$ ergs for the kinetic energy of the impacting body causing the original 70-km diameter Manicouagan Crater seems most reasonable.

Meteorites impact the earth at speeds ranging from 10 km/sec to about 70 km/sec (Millmann, 1963), and an average speed of an impacting body is taken as about 30 km/sec. Using the above estimates of energy, the mass of the impacting body can be inferred to be between 0.25 and 4×10^{15} gm; an average value of 0.9×10^{15} gm is appropriate.

About 92% of the meteorites impacting the earth are stones, while only 7% are irons (Brown, 1960). These types of bodies have densities of 3.6 and 7.8 gm/cm^3, respectively. Considering the above parameters, the body which caused the original Manicouagan Crater must have been between 0.2 and 0.64 km in radius. A stone meteorite traveling at 30 km/sec would have been 0.4 km in radius. If a cometary object impacted the Manicouagan area, this object was probably about 0.3 km in radius.

Age Implications of the Ordovician Limestone --

The Ordovician limestone which occurs in the Manicouagan-Mushalagan structure suggests a time "window" during which the meteoritic (or cometary) impact must have occurred.

In the earlier discussion of the Canadian Shield rocks, it was pointed out that remnants of more extensive sedimentary cover occur at about a dozen localities on the Canadian Shield. These sedimentary remnants invariably contain a lowermost member of Middle or Upper Ordovician age.

Present locations of Ordovician limestone are indicated in Fig. 5. It can be seen that this limestone occurs on the borderlands of the Canadian Shield as well as at various localities throughout the shield. The pattern of occurrence strongly suggests that the Paleozoic sedimentary outliers on the shield are part of a once-continuous cover of Ordovician limestone over the shield and the borderlands. This cover has since been mostly removed from the shield. The original thickness of this cover and the period before which the material was erosionally removed is a matter of speculation.

The existence of the Ordovician limestone at Manicouagan attests to the fact that during the Middle Ordovician the sea, from which deposition took place, covered the present site of the Manicouagan-Mushalagan Lakes.

The limestone at Manicouagan comprises a rather thin sequence (75 ft. thick). The outcrops of limestone have been brecciated and deformed; the bedding

planes in individual outcrops generally dip away from the center of the structure at angles ranging from 20-70° (Murtaugh and Currie, 1969). Microscopically, these limestones show increased grain twinning which is known to occur in shocked limestone.

The thin, scattered, and deformed limestone sequence present at Manicouagan contrasts to the thick, undeformed, horizontally bedded sequence which would be expected if there had been a meteoritic impact basin present at Manicouagan previous to Middle Ordovician time. For example, the Ordovician limestone present at the Brent Crater (Gilmour Lake) in Ontario forms a flat-lying sequence with a maximum thickness of 850 ft. (Beals et al., 1963). The Brent Crater sequence is what would be expected if the sediments were deposited in a previously formed impact basin. Limestone outcrops at Manicouagan were probably once part of a thin, sedimentary veneer present on the Precambrian surface at the time of the impact. Although limestone blocks occurring on the margins of the impact basin were tilted and deformed during the impact, they were not moved very far from their original locations. The deformed blocks may have subsequently slumped into the crater, or they may have been the downwarped part of a ring anticline such as that present at the Odessa Crater in Texas (Roddy, 1968). In any event, they were stratigraphically lowered during the impact and thereby preserved from the general erosion of the surrounding areas.

Based on the above considerations, the impact event at Manicouagan must have taken place after Middle Ordovician time. The earliest time at which the Manicouagan impact could have taken place, however, is not very well defined. The sequence at Manicouagan is quite thin and could have been deposited over a short time interval, probably less than 15 m.y. (Poole et al., 1970). It is not clear (1) whether the sediments present at Manicouagan at the time of impact were the eroded remnants from a more extensive sequence or (2) whether the limited succession comprised all that had been originally deposited after Middle Ordovician time. Since it is unknown which of the above two conditions prevailed, the duration of the time interval after Middle Ordovician, before which the probable pre-impact configuration of the rocks at Manicouagan was present, is unknown. About the best statement which can be made concerning the impact time, on the basis of the stratigraphic evidence, is that the impact took place after the end of the Ordovician era, i.e. less than 430 m.y. ago.

The Igneous Body (Monzonite) at Manicouagan --

Association with Shock-Deformed Rocks: The body of igneous rock present in the Manicougan-Mushalagan Lakes structure forms a layer up to 800 ft. thick. Its original volume was probably greater than 700 km^3. The igneous rock outcrops entirely within the circle defined by Manicouagan and Mushalagan Lakes. Since

these lakes also mark the outer extent of shock-deformational features, there is a strong suggestion that the shocked rocks and the igneous rock are genetically related. The nature of this relationship, however, is not entirely clear.

Stratigraphic Age: Within the crater, the igneous material sometimes overlies the shock breccia. In other cases, it overlies scattered outcrops of Ordovician limestone or unconformably overlies the Precambrian basement rocks. Since the body overlies the limestone, its age must be less than 430 m.y. In Part II, a study of the potassium-argon age of this rock yielded a value of 210 m.y. which is compatible with this stratigraphic age.

Other Igneous Bodies: As was pointed out previously, Paleozoic, igneous, intrusive or extrusive rocks are not extensive on the Canadian Shield. Localities at which igneous rocks ($\equiv$ as rocks solidified from a melt) with ages between 100 and 300 m.y. occur, on and near the Grenville Province, are shown in Fig. 5. Igneous rocks represented are of very divergent types; rock types are not differentiated in this figure. Three igneous occurrences, i.e. Manicouagan-Mushalagan Lakes, Clearwater Lake, and Mistastin Lake,are other sites of suspected meteorite impacts.

The Question of Extrusive Rock Association: The igneous material at Manicouagan is not easily classified on the basis of normal extrusive rock classification, although many external features of an extrusive, igneous body are exhibited. These features include: (1) flow structures at its base;

FIG. 5

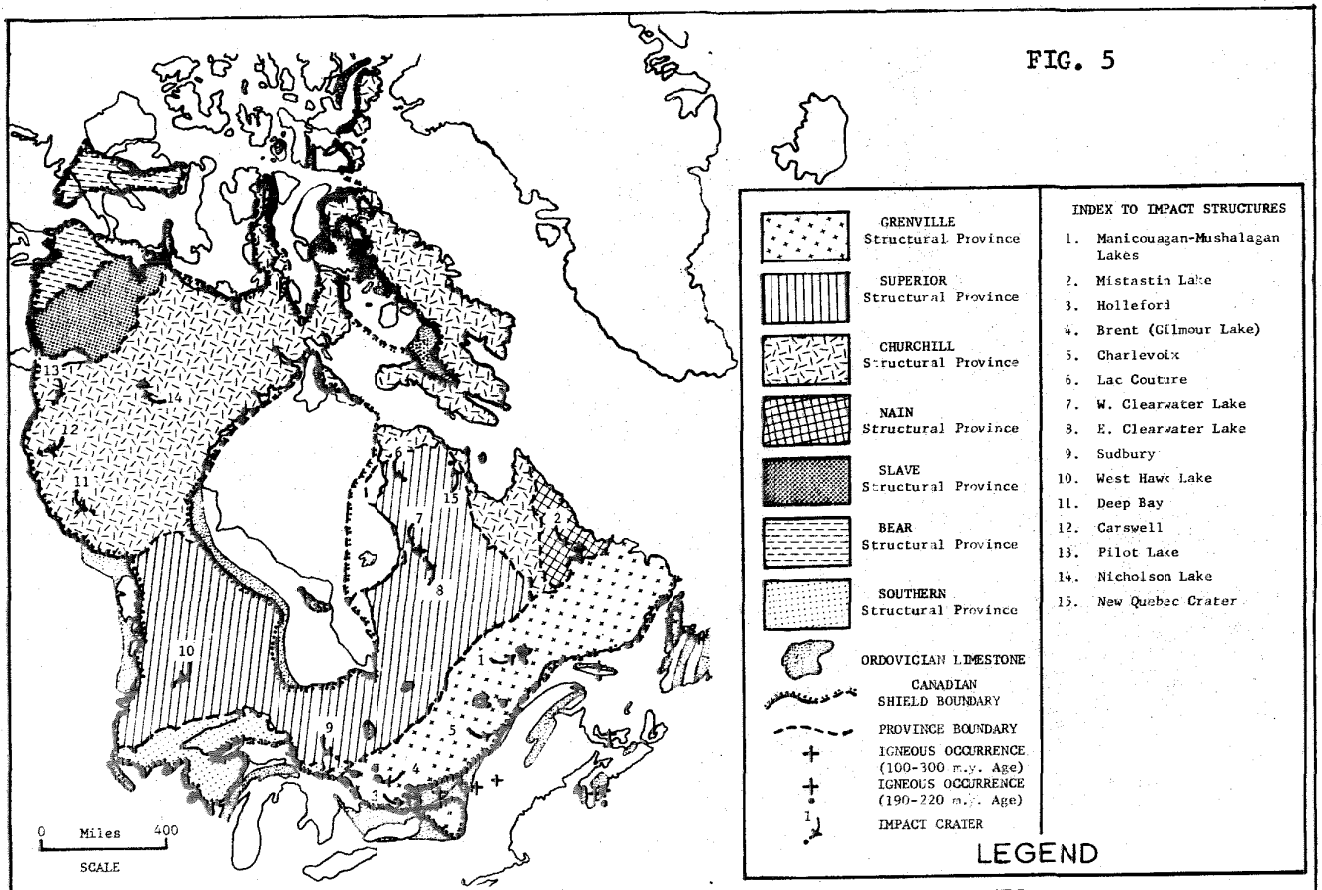

LOCATION OF CANADIAN SHIELD IMPACT STRUCTURES, IGNEOUS OCCURRENCES AND ORDOVICIAN LIMESTONE

(2) vesicles in the lower layers of the rock; (3) lack of evidence along its top of any material that it could have been intruded into. If this rock is classified according to its silica content (59%), it could be considered equivalent to an andesite or a latite (Williams et al., 1958). The material at Manicouagan is quite different from andesites or quartz latites, which are generally encountered, for three reasons:

(1) There is a general lack of porphyritic textures; most rocks from all of the sub-units appear more or less equigranular.

(2) Although the SiO_2 content of the rock is appropriate for an andesite, its K_2O content is much higher and its Al_2O_3 content somewhat lower than the values generally observed in basalt-andesite-rhyolite associations such as those of the Western Cascades (Peck et al., 1964). The indications of "dry" conditions during the crystallization of this "monzonite" include both the presence of pigeonite and the lack of hydrous phases. Dry conditions are atypical of the calc-alkali (basalt-andesite-rhyolite) rock series (Kuno, 1968).

(3) There is an extreme variation in grain size over the 800-ft. thick section of this rock which is exposed. Fine-grained sub-units contain holohyaline rocks, while the stratigraphically higher sub-units contain medium- and coarse- grained rocks. The general predominance of medium- and coarse- grained rocks is more characteristic of shallow-intrusive rather than extrusive rocks. Medium- and coarse- grained textures are especially

anomalous in a surface-cooled material with a SiO_2 content (60%) appropriate to an andesite. The"monzonite" term was chosen for the rock mainly because of its similarities to a shallow-intrusive rock.

Theories of Origin of the Body: The fact that the igneous material present at Manicougan-Mushalagan is limited to the area between the two lakes has been generally recognized in the theories of origin suggested for this material. All of these theories are, naturally, tied to theories concerning the formation of the depression within the two lakes which the monzonite is confined to. Four modes of formation have been suggested for the monzonite:

(1) Dence (1968) has suggested that this material may represent a remelted mass of brecciated and shock-heated rock which collected in the crater at the time of the meteorite impact. In addition to lightly shocked rocks, which remained relatively cool during the impact, the breccia is supposed to contain a significant proportion of material shock heated to super-geological temperatures. The total thermal energy in the breccia is thought to be sufficient for complete remelting of the mass. Subsequent cooling and crystallization of the mass would then produce the igneous material presently observed.

(2) Another mode of formation has been suggested by Dietz (1964) as well as others. In this mode of formation, a magma is presumed to have ascended along weaknesses in the crust caused by the meteorite impact. This magma would then have been extruded

on the floor of the crater within the basin, forming a flat-lying pool of melt covering the crater floor. The magma then cools and crystallizes on the surface.

(3) Currie (1965) suggests that the igneous material is a magma which was extruded during the last phase of violent, "phreatic", volcanic eruptions. The initial volcanic explosions which occurred during these eruptions are presumed to have produced the shock-metamorphic deformations observed in the basement rocks of the crater. According to Currie, the basin presently seen resulted from the down-dropping of a ring graben.

A more recent, thoughtful discussion of a mechanism similar to Currie's has been presented by Bostock (1969). Bostock's discussion deals with the formation of the Clearwater Lake Crater.

(4) Both Hammond (1945) and Rose (1955) believed that the igneous material at Manicouagan was the result of normal volcanic processes. Both felt that the structural basin at Manicouagan resulted from caldera subsidence after the extrusion of the volcanic material.

The theories of origin for the monzonite body, proposed by Hammond and Rose, do not account for the presence of the shock deformations found in the basement rocks and must be discarded.

As pointed out earlier, no known geological process other than meteorite impact can produce conditions necessary for the formation of the shock deformation features in the Manicouagan basement rocks. The "phreatic" explosions described by Currie

(1965) involve an unknown geological process. These explosions do not satisfactorily account for the shock-deformation features present in the basement rocks. Since the "phreatic" eruptions do not account for the observed features at Manicouagan, this theory of formation must be rejected.

The first two suggested origins of the body are the most probable. Both involve the impact of a meteorite, and this accounts for the shock-deformational features present in the basement rocks at Manicouagan. The two mechanisms differ, however, concerning the extent to which the impact is involved in the formation of the igneous body. In the first case, the meteoritic impact supplies the energy which brecciates, mixes, and melts the rocks in the crater to form the monzonite. In the second case, the molten monzonite is produced by terrestrial thermal processes, but its emplacement is controlled by features which are due to the meteoritic impact.

Implications of the Shock-melt Origin of the Monzonite: If the assumption is made that the Manicouagan body resulted from the collection, melting, and recrystallization of shock breccias within the crater, then: (1) The composition of the igneous material should represent the average composition of the original basement rocks excavated from the crater. (2) The impactite melt would be expected to contain some partially assimilated inclusions of shock-deformed basement rocks, especially in the more rapidly cooled lower parts of the body. (3) The monzonite would not necessarily be related to other igneous

rocks on the Canadian Shield. (4) The mineral assemblage present in the igneous material should represent an equilibrium mineral assemblage, crystallized from a pool of completely molten rock, under conditions of 1 bar total pressure and 0.2 atm partial pressure of oxygen. The initial temperature of this melt is a function of the amount of energy generated by the impact and is not dependent upon the thermal regime of the earth. The melt, therefore, may have originally possessed a temperature significantly greater than the 1000-1200°C temperature which is typical of extrusive lavas. (5) The crystallization age of the igneous material would closely represent the time of the meteoritic impact and shock metamorphism. There could be a time difference of a few million years, at most, between the impact time and the age of the body. This time would be required for the cooling of the impactite melt from its original temperature to an argon-retentive temperature.

Implications of the Impact-induced Volcanism Origin of the Monzonite: If the monzonite of Manicouagan is derived from a magmatic material whose emplacement is affected and not caused by the meteoritic impact, then: (1) the composition of the body might or might not resemble the composition of a melt derived from excavated country rocks. One might reasonably expect the body to resemble igneous material commonly observed at other locations on the Canadian Shield, e.g. tholeiitic diabase. The composition of the original magma, however, could have undergone

significant alteration by assimilation of rock near the crater during its emplacement. (2) The crystallization age of the body could be more than a few million years younger than the time of shock metamorphism. (3) The age of the monzonite would probably be more or less contemporaneous with other extrusive rock found on or near the Canadian Shield. Some tectonic feature which controls the emplacement of both the Manicouagan body and other contemporaneous igneous bodies would probably be present but might be difficult to recognize. (4) The mineralogy of the monzonite would probably be similar to the mineralogy of extrusive volcanic rocks and would represent subsurface equilibrium conditions. Initial temperatures of the material would fall in the 1000-1200^{o}C range.

Evaluation of the Evidence: It is difficult to assess, with the information presently at hand, which set of features listed above best describes the igneous material at Manicouagan. Part of this difficulty is due to the fact that much uncertainty exists concerning the formation conditions of magmas and impact melts. The temperatures and oxygen fugacities which exist in a cooling impact melt may not differ significantly from those which exist in an extruded magma cooled on the earth's surface. If this is true, the two different mechanisms of formation suggested for the monzonite would yield very similar rocks. In spite of the above difficulties, an evaluation of the monzonite with respect to the above criteria will be attempted.

An average composition of the rocks which would have been excavated from this crater during a meteorite impact has been determined by Currie (1971). Currie claims that the composition of the monzonite differs significantly from the average of basement rocks in the crater. The compositional differences which he alludes to are small, and insufficient data are presented with which to fully justify his conclusion. The chemical composition of the monzonite is much more silicic and potassic than that of tholeiite which is the most frequently observed igneous rock on the Canadian Shield. It is possible to imagine some process whereby material of originally basaltic or tholeiitic composition assimilates granitic rock and changes in composition until it has a chemical composition close to that of the monzonite. There is, however, no a priori reason to believe that this mechanism took place.

The lowermost layers of the monzonite contain abundant inclusions of shock-deformed basement rocks. These are enveloped in a matrix of fine-grained, igneous material. The inclusions are interpreted by advocates of the "shock-melt" hypothesis as being shocked rock fragments which have been only partly assimilated in the rapidly cooled part of the body. It is also possible to interpret these inclusions as being fragments of shocked rock entrained by the first extrusive flows of the igneous material.

In principle, it should be possible to distinguish critical features of the history of the monzonite body at Manicouagan by

the mineralogy of the monzonite. In practice, however, this is often difficult to do. Mineralogical studies of this body have not been extensively pursued, and further work along these lines may clarify the nature of this body.

Although the three sub-units of the monzonite have different grain sizes, they have uniform mineralogical compositions. Feldspars consist of laths of plagioclase (An_{55}) jacketed with sanidine (Or_{50} - Or_{70}). Pyroxenes consist of augite, pigeonite, and hypersthene; the latter two are chemically identical. Magnetite-ilmenite intergrowths and quartz are secondary phases. The Mg/Mg + Fe ratio for pigeonite and hypersthene is about 0.67, while for the augite this ratio is about 0.73. These values of the magnesium distribution coefficient fall on a curve of distribution coefficients determined for coexisting pyroxenes in extrusive and intrusive rocks (Kretz, 1963). The above values are compatible with a crystallization temperature of 900-1100°C for the monzonite. The pyroxene compositions are compatible with the original formation of the monzonite body, having taken place in a subsurface environment similar to that in which other intrusive and extrusive rocks form. It is not known, however, whether pyroxenes of these compositions could also crystallize from a melt that formed and cooled entirely on the surface.

The igneous material at Manicouagan contains abundant magnetite-ilmenite intergrowths. Magnetite-ülvospinel, solid solutions are the original forms of these magnetite-ilmenite intergrowths.

The original solid solutions form under very low oxygen fugacities present in the crust (Buddington and Lindsley, 1964). Hematite would be the stable iron oxide if the monzonite had crystallized on the surface exposed to atmospheric oxygen (MacChesney and Muan, 1959).

Hörz (1965) has shown that impact breccias from the Ries Crater undergo a rapid oxidation of FeO to Fe_2O_3 when heated in the atmosphere. Shock breccia aggregates would be expected to contain mostly Fe^{+3} iron since these have been at an elevated temperature, during cooling, while exposed to atmospheric oxygen. Chemical analyses of shock breccias from Manicouagan show a much higher Fe^{+3}/Fe^{+2} atomic ratio than do the original basement rocks from which the breccias form (see Currie (1971), his pseudotachylite = shock breccia -- Table 4). These observations suggest that shock breccias in real craters will contain iron predominantly in the Fe^{+3} oxidation state and hematite as the normative iron oxide. The fact that magnetite exists as a stable phase in the monzonite suggests that the original formation of this material took place in a subsurface environment with $PO_2 \sim 10^{-10}$ atm rather than at the surface where $PO_2 = 0.2$. When observed in the field, the presence of magnetite rather than hematite in the monzonite body is evidenced by the black, not red, color of rocks from this unit. The underlying shock breccia, which cooled on the surface, is red suggesting that the iron oxide in the shock breccia is hematite rather than magnetite.

The possible association of the Manicouagan body with other igneous occurrences on the shield is a matter for debate. The sites at which igneous activity occurred between 100 and 300 m.y. ago are shown in Fig. 5. Crosses with dots below them indicate activity in the 190-220 m.y. range. There seems to be a weak clustering of Triassic events around the southeastern edge of the shield, but no compelling correlation exists between the Manicouagan igneous body and other Triassic events.

Triassic and Jurassac intrusive diabases are widespread along the eastern edge of North America and along the western edge of Africa (May, 1971). May has correlated Triassic dikes in eastern North America as far north as Nova Scotia. His correlation can be continued further north to the 207 m.y. dike on Prince Edward Island (Poole et al., 1971). An extension of the dike pattern even further northward may become evident with new data on the Arctic regions. Although a correlation of the igneous material at Manicouagan with this widespread system of Triassic-Jurassic intrusive bodies is possible, such a correlation is presently speculative.

Mistastin Lake in Labrador, which is another suspected meteoritic impact site, contains igneous material which overlies shocked basement rocks. The structure has a diameter of about 26 km and presents many similarities to the Manicouagan structure (Taylor and Dence, 1969). The Mistastin Lake igneous material has a chemical composition only slightly less silicic and potassic

than the Manicouagan monzonite (Currie, 1971). The igneous rock at Mistastin Lake has a potassium-argon age of 202 m.y. (Taylor and Dence, 1969). As is the case with Manicouagan, this igneous body might also be hypothetically correlated with the diabase dike system suggested by May (1971).

An attempt has been made to determine the time of shock metamorphism of the basement rocks. This attempt is discussed in the second part of this thesis. The data suggests that the shock event took place between 70 and 100 m.y. before the monzonite crystallized, but it was not possible to uniquely define a shock age. Extreme values obtained for the shock age could be interpreted as indicating that the time of shock metamorphism and the crystallization age of the monzonite are the same. If the shock-metamorphic event and the monzonite have discernibly different ages, then the monzonite must have originated from volcanic processes with its emplacement controlled by crustal weaknesses caused by the impact. If the age determined for the shock metamorphism and the monzonite crystallization age appear identical, then formation of the monzonite from an impact melt seems most likely. In the latter case, the possibility still exists that the monzonite was extruded very shortly after the impact. Considering the precision of the potassium-argon analyses, an interval of ~ 10 m.y. between the two events would not be discernible.

Possible History of the Crater: A reasonably complete geological history of the structure can be constructed with the information currently available. Unfortunately, several important details of this history still remain uncertain.

After the regional metamorphism during the Grenville Orogeny, and subsequent erosion, a thin layer of limestone was deposited at the site of the present structure. This occurred about 440 m.y. ago (Middle Ordovician). At some time between 210 and 440 m.y. ago, the site was impacted by an extra-terrestrial body. This impact left a flat-bottomed basin about 70 km in diameter with a central depth of about 3.4 km. On the inside edges of this basin, an irregular band of brecciated and upturned limestone remained from the previous sedimentary veneer.

Opinions diverge concerning the appearance of the crater after the impact. Advocates of the "impact melt" theory claim that the floor of the crater was partly covered with a pool of melted rock about 1 km deep. According to this view, there was a central uplift in the central part of the crater, and the pool of melt formed an annular ring around this. Subsequent cooling and crystallization of the melt pool produced the igneous rock which is presently found within the crater. Erosion has deeply dissected the monzonite, and drainages which developed around the edges of the melt pool presently form Manicouagan and Mushalagan Lakes.

An alternative theory of the crater history after the impact which is thought to be more likely follows. Some aspects of the crater history according to this view are speculative and must be inferred from scanty evidence. This view of the crater history postulates that the original breccia layer which covered the crater floor was much thinner (about 50-100 meters). This breccia layer contained some shock-melted material but was not totally molten. After the impact event, the resultant basin may have had a central uplift and probably became a large circular lake. Isostatic uplift of the structure which took place over a period of $\sim 10^5$ years resulted in this lake becoming progressively shallower at its center. Concurrently, valleys were being cut in the original crater rims by streams draining both into and away from the original basin. At some time well after the impact event, these valleys had become deep enough so that drainage out of the basin occurred. The breaching of the crater rim caused drainage of the lake then present, and erosion of the newly exposed crater floor began. Central parts of the crater were more heavily eroded since isostatic uplift was greater in the central regions of the basin than along the margins of the basin.

According to the "impact-induced volcanism" theory, the impact took place about 280-310 m.y. ago, and erosional and isostatic modification of the original crater took place for some unknown period after this. During this period, the original basin was modified to a ring-shaped depression which resulted from the

central floor of the original basin bulging upward.

At around 210 m.y. ago, a fairly large amount of tholeiitic magma was mobilized below the crust. This is evidenced by the large number of Triassic intrusive bodies along eastern North America. Some of this magma ascended along structural weaknesses below the Manicouagan Crater site. During its ascent this magma, which may have been tholeiitic originally, assimilated a fairly large amount of crustal, granitic composition material; the final composition of the material became andesitic. The Manicouagan magma reached the surface about 210 m.y. ago, probably with a large proportion of the material partially crystallized. Initial flows of the material entrained fragments of the shocked Grenville Province basement rocks; these flows cooled rapidly and formed the lower, fine-grained sub-unit of the monzonite. The fissures from which these flows were erupted were located in the central part of the structure. Subsequent flows of "monzonite" overlaid the original flows. The flows were confined to a roughly annular depression around the central, uplifted part of the original crater floor.

After the emplacement of the monzonite, erosional dissection of the original body began.

Much of the drainage in the crater was away from the central part of the structure; the drainage out of the crater developed along a set of valleys between the outer limit of the monzonite body and the remains of the inner walls of the original crater depression. These valleys have persisted to the present and today

form the elongate, arcuate Manicouagan and Mushalagan Lakes. These two elongate lakes,which are essentially wide, deep rivers, have developed preferentially along joint directions common in the region. This preferential erosion along joint planes resulted in the present, roughly octagonal form of the lakes.

The Geochronological Problem: The previous discussion presents sufficient background to raise the question which is fundamental in deciding between the (two) formation modes discussed above: At what time were the Grenville-type basement rocks deformed, and how does this time compare with the crystallization time of the monzonite? The experimental effort made to answer this is discussed in Part II. In brief, it involves (1) the selection of various samples of deformed basement rocks which had been apparently unaffected by the thermal effects of the monzonite and (2) the subsequent determination of their isotopic ages. The age converged upon by the most highly deformed samples is presumably the age of this "shock"-deformation event. Rocks from the anorthosite massif, which has the best-defined sequence of deformations, were used for the "shock sequence". Rocks from the anorthosite unit also display the least visible thermal effects due to the monzonite. This "shock" age was then compared with the isotopic age of the monzonite. The relationship between the ages would hopefully enable an accurate and complete discussion of the history of this crater to be made.

CHAPTER 2

Shock Effects in Scapolite*

Various minerals, when subjected to the high pressures and strain rates of shock waves, develop unique deformation features so far not observed in any endogenous or exogenous geological process but meteorite impact. The general trends of progressive shock deformation have been well documented, and various stages of shock metamorphism can be established (Stöffler, 1966; Chao, 1967; Dence, 1968). Tectosilicates such as quartz and feldspar exhibit a variety of deformation features which are used as diagnostic criteria for the degree of shock damage. However, detailed knowledge of other mineral species is either scarce or completely missing.

In order to more specifically study the deformations observed in basement rocks of the Manicouagan structure, the maskelynitized anorthosite was closely compared with anorthosite exterior to the crater which appears extremely similar in mineral textures and mineral composition. In the maskelynitized anorthosites, closely spaced parallel fractures occur in some untransformed regions of plagioclase grains and in some scapolite grains. This chapter describes some deformation features in scapolite from the central anorthosite of the Manicouagan-Mushalagan Lakes structure in Quebec, Canada (see also Dworak, 1969). This mineral was

---

* Most of this chapter is taken from "Shock Effects in Scapolite" by Stephen H. Wolfe and Fred Hörz, Amer. Mineral. 55 (1970), 1313-1328.

investigated, using standard universal stage, electron microprobe and Debye-Scherrer x-ray techniques; the enveloping maskelynite was also microprobe analyzed and compared with plagioclase from exterior anorthosites as part of this study. The general features of the unaltered anorthosite and the maskelynitized anorthosite, in which these scapolites are found, are described in Chapter 1.

Sample Description:

Fig. 2 (Chapter 1) shows the general geological setting of the Manicouagan structure, as well as the locations of the anorthosites studied. The geology has been discussed as well as the regional setting of the anorthosites. Anorthosite from both inside and outside the structure is about 85% plagioclase (An_{53-55}), the grains generally showing a bimodal size distribution with means about 0.5 and 1.5 mm. Larger grains are mostly albite and Carlsbad twinned (see Appendix -- Samples A, B, and C). Clinopyroxene (approximately $Ca_{.4}\ Fe_{.2}Mg_{.4}\ SiO_3$) is present in 1-mm grains which are often rimmed by subhedral or euhedral grains of garnet. Feldspar, of more potassic or more sodic composition, is present in minor amounts as small, elongate grains along the edges of the plagioclase. Scapolite is a rather frequent accessory mineral with rounded, subhedral grains generally 0.5 to 1 mm in size. Apatite, as well as some hornblende and biotite, are present in minor amounts.

Anorthosite inside the crater shows all stages of shock metamorphism from the merely fractured to the shock-melted

stage. In a few localities in the central anorthosite massif, the material is strikingly altered (Wolfe, 1966), and about 99 % of the plagioclase has been transformed to a water-clear glass of high refractive index, i.e. maskelynite (Tschermak, 1872; Duke, 1968), "diaplectic" feldspar glass (v. Engelhardt et al., 1967), or "thetomorphic" feldspar (Chao, 1967). This Manicouagan material has been described by Bunch et al. (1967).

Optical Studies:

About 50% of the scapolite which occurs in the isotropic material from the center of the structure exhibits closely spaced sets of planar features resembling those known from shocked quartz and feldspars. This scapolite is optically very uniform with no evidence of reduced birefringence or extensive fracturing, although undulous extinction is sometimes observed. For the most part, scapolite from both inside and outside the crater appears nearly identical. Measurements of refractive indices obtained on isolated grains with immersion techniques are listed in Table 1. An appreciable amount of scapolite in the central anorthosite exhibits sets of planar features. One and two sets occur frequently (both shocked grains used for index determination displayed two sets of planar features), while grains with three sets are rare. These features (see Fig. 1) are identical to "planar features" (Carter, 1968), "planar elements" (v. Engelhardt and Bertsch, 1969), or "shock lamellae" (Chao, 1967). They are of the

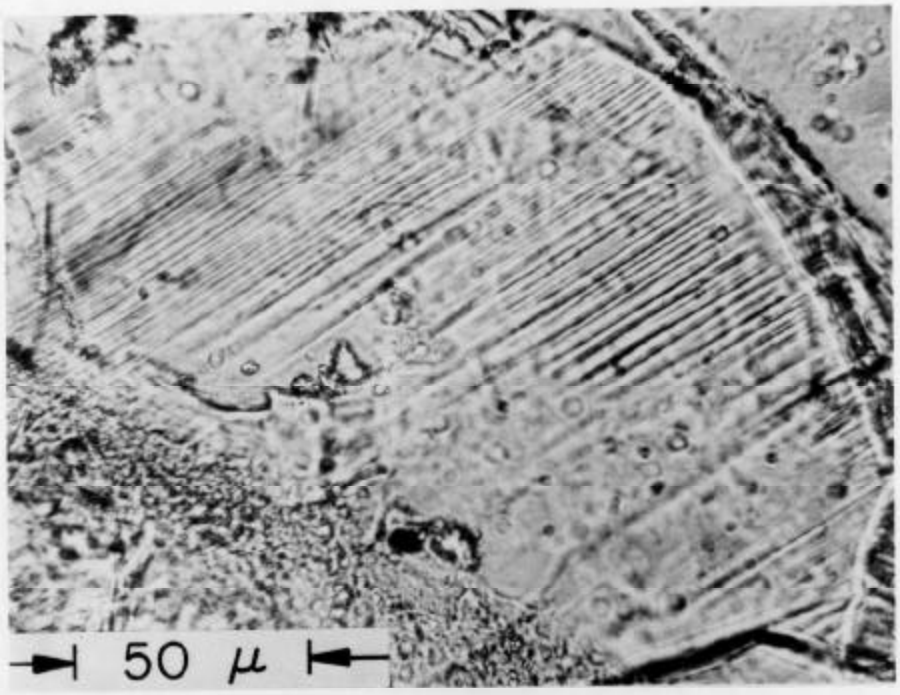

A ↑

FIG. 1

↓ B

undecorated type. As in quartz and feldspar (see French and Short, 1968; Stoffler, 1967), most of the measured inclinations of planar feature poles to the optic (c-axis) in scapolite coincide with angles of rational crystallographic planes (Fig. 2). The majority of planar features in scapolite occur along planes of the general crystallographic form (001), $\{102\}$, $\{101\}$ and $\{100\}$.

In order to identify the specific crystallographic directions of these features, inclination measurements and angular relations in the aximuth plane have been plotted on a stereonet for grains with two or three sets of planar features (Fig. 3) (about 65% of all the measured grains). Grains showing only one set of features were omitted since their azimuth values are ambiguous. Plots for grains with two or three sets of planar features retain the angular relations between the measured elements. Unfortunately, these scapolites displayed no prominent cleavage which would have allowed orienting each individual stereoplot with the (100) pole (the prominent cleavage direction of scapolite). We, therefore, arbitrarily decided to have at least one of the measured features coincide with the $[010]$ zone; the measured inclinations to the optical axis suggested preference of the $[010]$ zone over the $[110]$ zone.

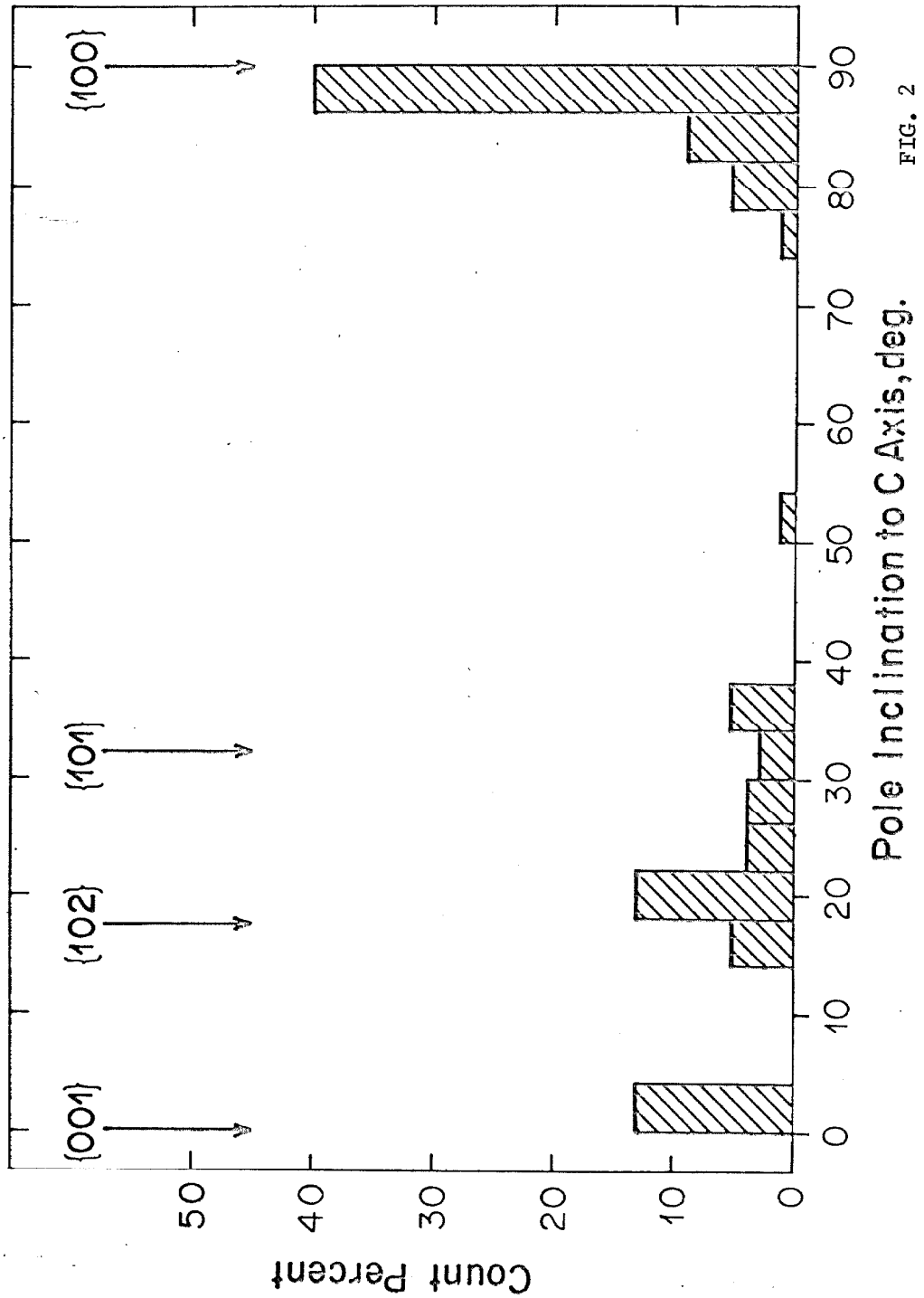
{100}
{101}
{102}
{001}
0
10
20
30
40
50
Count Percent
0
10
20
30
40
50
60
70
80
90
Pole Inclination to C Axis, deg.

FIG. 2

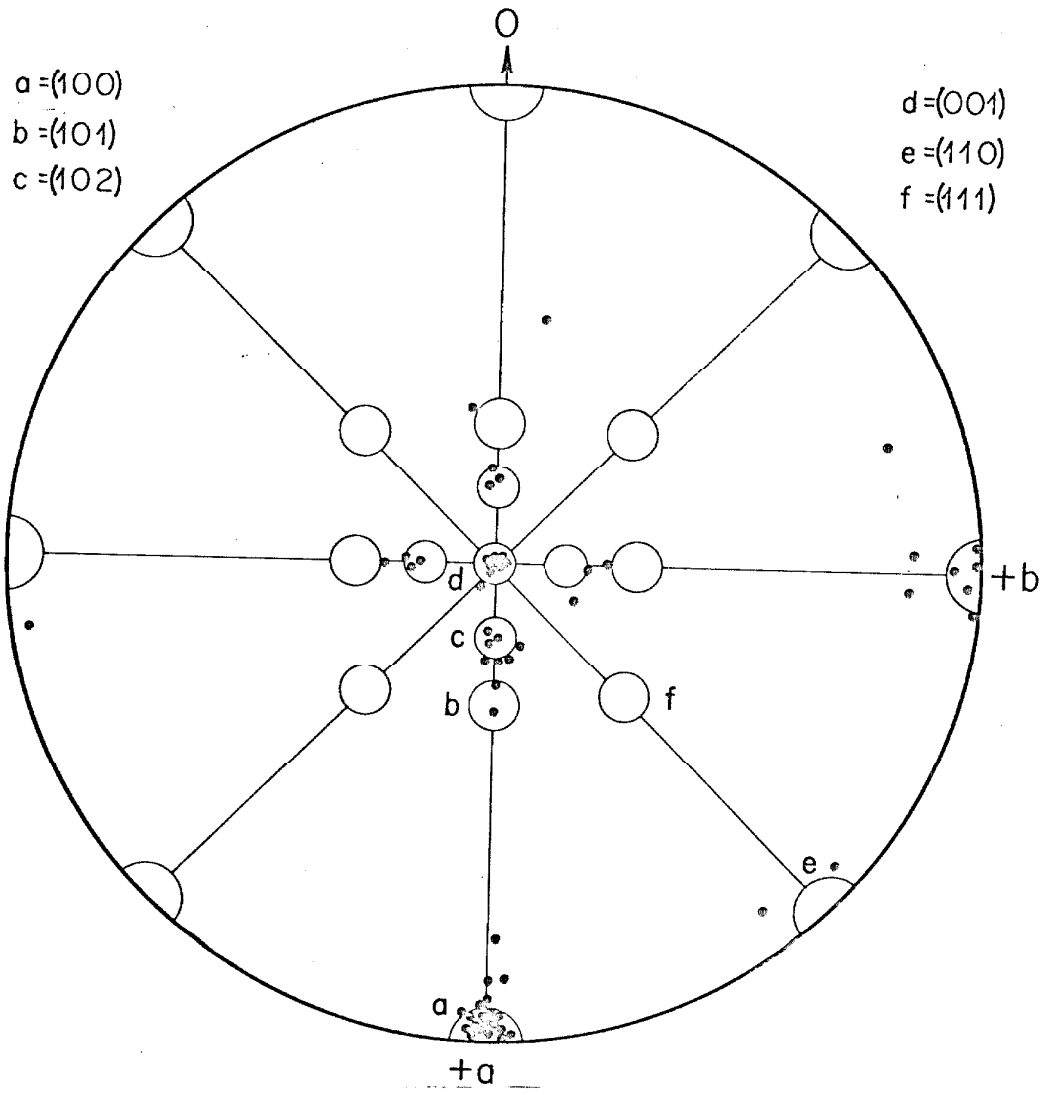

FIG. 3

TABLE 1.

Refractive Indices and Cell Parameters of Shocked and Unshocked Scapolite

	Refractive Index		Birefringence			$2\theta_{400}-2\theta_{112}$ (deg.)
	$N_\alpha \pm .002$	N_β	ΔN	a = b	c	
Unshocked I	1.588	1.551	0.037	12.1108	7.5816	3.500
Unshocked II	1.589	1.551	0.038	±.0400	±.0240	
Shocked I	1.586	1.550	0.036	12.1574	7.5631	3.400
Shocked II	1.587	1.548	0.039	±.0050	±.0244	

Accordingly, we could demonstrate (see Fig. 2) that planar features in scapolite are parallel to the planes (100), (101), (102), (001) or their symmetrically equivalent forms. The only features parallel to planes of the $[110]$ zone seem to be of the type (110). Table 2 shows the absolute and relative frequencies of planar features using the data reduction scheme of v. Engelhardt et al. (1968).

Chemical Composition:

Chemical compositions of coexisting scapolite and plagioclase in both shocked and unshocked anorthosite were determined using an ARL-EMX electron microprobe. Both phases were analyzed in each of three shocked and two unshocked rocks. For samples #41-#44, three scapolite and two to three plagioclase grains were analyzed, while for samples #48 and #50 only one grain of each phase was run. Each analysis consits of data averages from approximately six $20\mu^2$ areas of the grain; mineral standards were used and oxide contents were determined (for SO_3 anhydrite with 58.81 % SO_3 was the standard used). Data obtained, after correcting for background and deadtime, were reduced to oxide contents using the procedure of Bence and Albee (1968).

The averages of the grains analyzed in each sample are shown in Table 3, as well as standard deviations (in percent) calculated from the observed variations among grains in the same sample. The scapolite data are also shown in terms of the normalization: Si + Al = 12.00 atoms, as suggested by Evans et al.

TABLE 2.

Frequencies of Planar Features in Scapolite*

	A	B	C	D	E
{100}	135	35	50.0	25.9	36.5
{101}	140	8	11.4	5.7	7.9
{102}	140	17	24.3	12.1	17.1
(001)	34	9	12.9	26.5	37.4
{110}	136	1	1.4	0.7	1.0
		70	100.0	70.9	99.9

*For data reduction scheme, see v. Engelhardt et al. (1968).

A = Number of observable planes after correcting for blind circle of universal stage.

B = Number of actually observed planar features.

C = $(B/\sum B) \cdot 100$ = Apparent frequency.

D = $(B/A) \cdot 100$ = Unnormalized probability.

E = $(D/\sum D) \cdot 100$ = True frequency or probability.

(1969). The number of Ca, Si, Ca + Na + K (= $\sum$W site) and S atoms, as well as the meionite contents, are also shown. These values are averages of values observed for grains in the same sample. The CO_2 values shown are not measured, but they are estimated from the stoichiometry proposed by Evans et al. (1969)

$$(C + S = \frac{(Ca + Sr)}{3}) \quad .$$

This procedure is used in order to estimate the total oxide content, exclusive of H_2O; contents of from 0 to 1.3 percent are indicated. The analyses indicate a value of Me_{72-79} which is in good agreement with the refractive indices and the $2\theta_{400} - 2\theta_{112}$ calculated from the Debye-Scherrer patterns (see Table 1).

These analyses, with the exception of #41, #48, and the low sulfur areas of #50, are in good agreement with the stoichiometry of Evans et al. (1969); #48 and #41 show somewhat lower W site summations than those normally observed by Evans (3.92 - 4.06), but #50 is quite anomalous.

Sample #50 is an anorthosite which appears to have been more severely shocked, or at least to have attained a higher temperature, than either #41 or #44 (see Appendix -- Sample E). It was analyzed to check for selective volatilization at higher shock intensities. The plagioclase appears to have melted and produced a thermal glass along the grain boundaries, and the plagioclase grains themselves display anomalous optical characteristics with 2V ranging from 30 to 0 degrees (cf. normal An_{55} has

2V ~ 80°). The garnets in this sample are very heterogeneous with localized concentrations of Fe, Ca, Mg and Al on a 20 μ to 50 μ scale. The scapolite grains are also heterogeneous with areas 10 μ to 40 μ in dimension containing 7.5 % SO_3 ("high S" areas in Table 3), while other parts of the grain ("low S" areas) have non-detectable SO_3 concentrations. This heterogeneity in the scapolite and garnet is not observed in the unshocked anorthosites or in the maskelynitized samples (#41, #44 and #48). The high sulfur areas of the scapolite in #50 conform well to the stoichiometric relations, but the low sulfur areas do not. It is not clear what these low sulfur areas are; they may represent some intermediate breakdown stage of scapolite.

Sample #48 is cut from a chip adjacent to #41 and was analyzed to see if the anomalies in #41 are real; they appear to be.

From this data, it is evident that the compositions of plagioclase and scapolite, in both the maskelynitized and unshocked anorthosites, are not grossly different and, in fact, are quite similar. The differences that exist do not appear to be systematic. The lower Na_2O and SO_3 contents of #41, compared to #42 and #43, might be attributed to some process of selective volatilization, but the K_2O content is not lower, and the scapolite SO_3 content in #44, which is similarly shocked, is higher than in #42. In #50, both Na_2O and K_2O contents are similar to the unshocked rocks, and heterogeneities in SO_3 content

TABLE 3.

Microprobe Analyses of Manicouagan Scapolites and Plagioclases

(Oxides as Wt. %)

Scapolite								
	Shocked					Unshocked		
Sample	#44	#41	#48	#50 High S	#50 Low S	#43	#42	Standard Deviation (%)
SiO_2	44.9	45.4	45.5	45.3	51.9	45.1	45.3	2
Al_2O_3	26.8	27.2	27.6	26.0	29.2	26.1	26.6	2
Na_2O	3.30	2.57	3.04	3.52	3.12	3.66	3.33	5
K_2O	0.15	0.15	0.15	0.16	0.13	0.10	0.20	8
CaO	17.7	18.2	17.5	17.2	14.8	17.1	17.3	2
SO_3	4.04	2.67	2.71	7.52	0.0	6.61	3.45	5
Total	96.9	96.2	96.5	99.7	99.2	98.7	96.2	
CO_2^+	2.5	2.8	2.8	0.0	--	1.0	2.5	

(TABLE 3 -- continued)

Sample	Shocked #44	Shocked #41	Shocked #48	Shocked #50 High S	Shocked #50 Low S	Unshocked #43	Unshocked #42	Standard Deviation (%)
$\sum$ Oxides $-H_2O$	99.4	99.0	99.3	99.7	99.2	99.7	98.7	
$\sum$ W site	4.01	3.80	3.81	4.02	3.07	4.06	3.95	
Ca	2.98	3.00	2.88	2.91	2.21	2.91	2.90	
S	0.48	0.31	0.31	0.89	0	0.77	0.40	
Si	7.04	7.04	7.00	7.15	7.21	7.14	7.09	
% Me	74.2	78.9	75.5	72.3	71.9	71.5	73.4	

Plagioclase

Sample	Shocked #44	Shocked #41	Shocked #48	Shocked #50	Unshocked #43	Unshocked #42	Standard Deviation (%)
SiO_2	53.6	54.6	55.2	55.2	55.6	55.0	3
Al_2O_3	28.8	28.4	28.2	28.4	27.0	27.6	5
Na_2O	4.51	4.79	5.07	5.12	5.56	5.09	6
K_2O	0.55	0.52	0.60	0.52	0.33	0.37	15
CaO	11.5	11.3	10.7	10. 7	10.7	10.9	5

(TABLE 3 -- continued)

	Plagioclase						
	Shocked				Unshocked		
Sample	#44	#41	#48	#50	#43	#42	Standard Deviation (%)
Total	99.0	99.6	99.8	99.9	99.2	99.0	
% An	56.6	54.1	52.0	51.9	50.5	53.0	

+ CO_2 values are estimated from the scapolite stoichiometry proposed by Evans et al. (1969).

rather than general volatile losses are observed.

A more likely interpretation of the data would be that the composition of phases in both the shocked and unshocked rocks are roughly similar and that the variations observed are mainly due not to the shock metamorphism but to preexisting variations in the anorthosite massif. Any selective volatilization at shock intensities which produce maskelynite has, at most, marginal effects on chemical composition. Production of heterogeneous phases seems to occur before systematic volatile loss takes place.

Experimentally produced shock waves of 300-450 kb amplitude are known to produce isotopic feldspar phases (Milton and DeCarli, 1963). Neither the short "in-shock" temperature pulse of 400-500°C (Ahrens et al., 1969), nor the residual temperature of the material (~ 100°C) is sufficient to selectively alter the composition of these minerals (see, also, Duke, 1968).

Cell Parameters and Other X-Ray Data:

Scapolite grains were picked from shocked and unshocked anorthosite and crushed to a fine powder. X-ray patterns were obtained using Cu K_α radiation in a 114-mm camera. These photographs are shown in Fig. 4. It can be seen that shocked and unshocked material appear quite similar except for the absence of high-angle "back" reflections in the shocked material. The weakening or disappearance of back reflections is observed

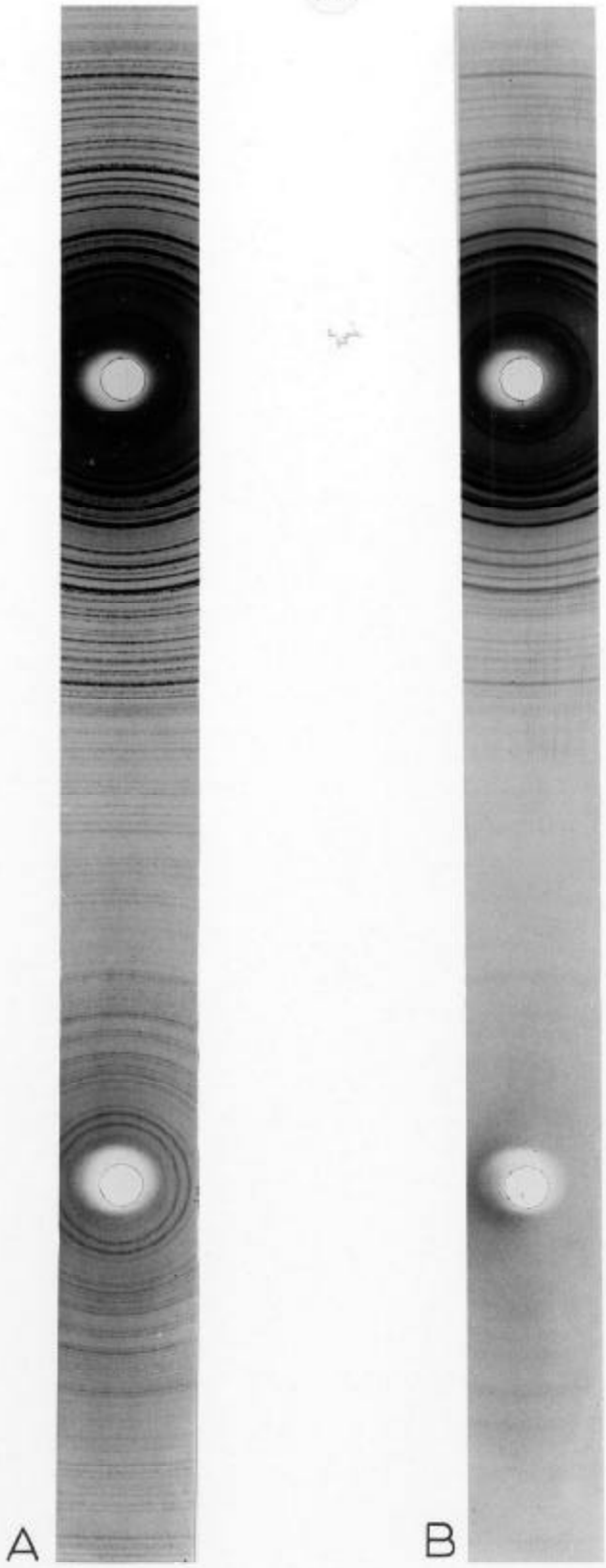

FIG. 4

in cold-worked metals (Cullity, 1959), as well as in shocked quartz (Chao, 1968; Dachille et al., 1968; Bunch, 1968) as a result of destruction of the crystal's long-range order. The cell parameters for both the shocked and unshocked materials are given in Table 1. The values are near those reported for the meionite and member of the series and, as such, agree with other parameters observed for this material.

Discussion and Conclusions:

As has been mentioned earlier, anorthosite inside and outside the crater is believed to have formed at the same time and to have been shock metamorphosed at a later time. Scapolite is probably primary, having been formed during the Grenville metamorphism and was present previous to the shock event.

The presence of planar features in the plagioclase and pyroxenes and the presence of diaplectic feldspar phases (v. Engelhardt, 1967) is felt to be convincing evidence that the anorthosite within the structure has been shock metamorphosed. The closely spaced planar features in scapolite are identical to those reported from other silicates, the shock origin of which has been demonstrated in the laboratory by Short (1968), Müller and Defourneaux (1968) and Hörz (1968).

Recovery shock experiments by Milton and DeCarli (1963) on feldspar (250-350 kb) and equation of state data of Ahrens et al. (1969) indicate that diaplectic feldspar glasses form in response to shock pressures in the range of 300-400 kb. Ahrens

et al. give 300 kb as the lower limit for the formation of diaplectic glasses and 450 kb as the pressure at which melting begins. Genuine melting was not observed in samples #41, #44 or #48. These data and the highly fractured condition of the coexisting pyroxenes (Carter, Raleigh and DeCarli, 1968) indicate that the anorthosite was probably shocked to about 400 kb. Compared to plagioclase, which is completely transformed to diaplectic glass at these pressures, scapolite shows only minor shock damage. This is quite surprising; one might expect it to show similar behavior since scapolite and plagioclase have many structural similarities.

Both tectosilicates are composed of tetrahedra of four coordinated Al and Si atoms. If scapolite is viewed along the c-axis and plagioclase along a direction parallel to the a-axis, they are both seen to consist of stacks of four-membered rings of AlO_4 and SiO_4 tetrahedra which are linked in directions perpendicular to the stacking axes. The Ca, Na and K ions are located approximately on planes which run parallel to the stacking axes and between adjacent rows of stacks. When viewed in these directions, scapolite displays its fourfold rotation axis, and plagioclase is seen to have very nearly tetragonal symmetry. The main difference between the two structures is that in scapolite alternate stacks of rings are found to consist of only one-half as many four-membered rings in the stack. The resulting cavities in these stacks are filled with ions such as

Cl^-, F^-, $Co_3^=$, SO_4^- (Papike and Stephenson, 1966; Papike and Zoltai, 1965; and Deer et al., 1963). In contrast to plagioclase, shocked scapolite in Manicouagan anorthosite is not vitreous and shows essentially unchanged cell parameters, indices of refraction, birefringence and chemical composition. As far as can be ascertained, the only changes that took place during shock deformation were development of planar features and erasure of the back reflections in the Debye-Scherrer powder patterns.

Three possible explanations for this apparent anomaly are:

(1) There might be a gross shock (acoustical) impedance mismatch between scapolite and plagioclase such that scapolite actually experienced much lower shock pressures than did the enveloping plagioclase.

(2) It is possible that scapolite is more resistant to shock deformation than is plagioclase, with the ionic sublattice acting as a "stabilizer".

(3) The presence of ionic bonds (i.e. Ca - CO_3 or Na - Cl) in scapolite tends to make the mineral behave in a plastic fashion. These bonds would ease gliding and increase recrystallization rates, thus preventing total lattice breakdown.

In view of the underlying structural similarities of scapolite and plagioclase and the small density differences (about 2%), the first explanation seems unlikely, but it cannot be discarded until elastic constants and equation of state data for scapolite are known. These data are not presently available.

TABLE 4

Frequencies (Count %) of Planar Features in Grains Displaying One, Two, or Three Sets of Planar Features

	No. of Grains	Crystallographic Orientations					
		{100}	{101}	{102}	(001)	{110}	Irrational
1 set	17	71	6	23	0	0	0
2 sets	25	36	12	18	14	2	18
3 sets	4	50	8	25	17	0	0

Structural similarities and similar hardnesses seem to exclude large strength differences between the two, an indication that the second suggestion is unlikely as well. Due to the lack of more information about scapolite, the last explanation seems most likely at the present.

It has been shown (Müller and Defourneaux, 1968; Robertson et al., 1968; Hörz, 1968) that quartz develops differing sets of planar features with differing shock pressures. The data for scapolites, presented here, indicate that this mineral may also show such behavior. If the reasonable assumption is made that in a given rock progressively fewer grains experience shock pressures of increasing intensity, then the data of Table 4 suggest that,as scapolite undergoes progressively higher shock pressures, planes with face poles at lower inclinations to the c-axis become populated with planar features, i.e. (101) and (102). This behavior is similar to that observed in quartz. If scapolite were an abundant rock-forming mineral, it might conceivably be used to establish a shock metamorphic subclass in the 300 - 400 kb range with planes parallel to (100) appearing first, followed by a variety of other planes.

The data in Table 5 for scapolite, plagioclase and quartz strongly suggest that there is a basic difference between the formation mechanisms of cleavage and planar features. Various authors (Carter, 1968; v. Engelhardt and

Bertsch, 1969) have discussed the optical characteristics which distinguish these two types of planar elements. In scapolite it is observed that cleavage takes place along planes with low numbers of Si-O bonds per unit area. Planar features, on the other hand, occur frequently along planes with high Si-O bond densities. This behavior is similar to that observed in plagioclase (Stoffler, 1967) and quartz (Robertson, et al., 1968; Hörz, 1968). Table 5 lists the relative tendencies for formation of frequently observed cleavages and planar features in scapolite, plagioclase and quartz, and bond densities along the planes involved.

Some authors have suggested that slip or glide mechanisms are responsible for the formation of planar features (Chao, 1968; Carter, 1968; v. Engelhardt and Bertsch, 1969). This theory is compatible with the experiments of Hörz (1968) and Müller and Defourneaux (1968) who found that in quartz, planar features form only under shock pressures of amplitudes greater than 120 kb. Therefore, their formation occurs outside the elastic region of quartz (Hugoniot Elastic Limit ~ 100 - 110 kb, Wackerle, 1962). This hypothesis is supported by the observation that, for silicates, planes with high Si-O bond densities are, in general, planes along which the lattice repeat distance is the shortest, and, in analogy with metals, slip would be

TABLE 5.

Cleavages, Planar Features, and Si-O Bond Densities for Scapolite, Plagioclase and Quartz

	Plane	Cleavage	Planar Features (%)	Si-O Bonds/ 100 Å^2
		(Data from this paper)		
	(100)	Excellent	34	3.01
	(110)	Good	1	4.26
SCAPOLITE*	(001)	None	38	5.44
	(101)	None	10	4.62
	(102)	None	16	5.23
		(Data from Stoffler, 1967)		
	(100)	None	10	6.62
	(010)	Good	11	3.84
PLAGIOCLASE*	(001)	Perfect	25	3.82
	(1$\bar{2}$0)	None	10	4.35
	(110)	Poor	0	3.85
		A B	A B	
	(0001)	37 26	31 22	9.60
	(10$\bar{1}$0)	4 --	2 --	7.55
QUARTZ**	(10$\bar{1}$2)	5 2	14 15	8.15
	(10$\bar{1}$3)	3 2	38 44	8.90
	(10$\bar{1}$1)	19 47	6 5	5.90

A = Data from Hörz (1968); B = Data from Robertson et al. (1968).

*Cleavages are normal (static) cleavages.

**Cleavages are shock induced.

expected to occur in these directions.

In accordance with this hypothesis, and on the basis of their optical investigations, v. Engelhardt and Bertsch (1969) have suggested that planar features are the traces of high pressure phases which nucleate, preferably along these planes, due to the increased dislocation densities caused by the gliding process. These high-pressure polymorphs convert, upon pressure release, partially or completely to disordered phases (Müller, 1969; Hörz, 1968).

According to the data in Table 5, some other mode of formation seems probable. Since planes with high bond densities are also the planes with the highest densities of silicon and oxygen, they would be logical nucleation sites for high-pressure polymorphs. Such planes might also show short-range order analogies to the dense phases. The data of Ahrens et al. (1969) indicate that a phase change takes place in quartz at approximately 120 kb, i.e. just slightly above the Hugoniot Elastic Limit. This is also in agreement with the observed minimum pressures for the planar feature formation. According to this hypothesis, compression only without gliding is required for the formation of high-pressure phases.

On the basis of the existing data, it is difficult to say which, if either, of these two hypotheses is correct. Both lead to high-pressure polymorphs along crystallographic planes which, upon pressure release, relax to highly disordered phases.

Summary:

Planar features observed in scapolite of the Manicouagan-Mushalagan anorthosite are oriented principally along symmetrical equivalents of the planes (100), (001), (102) and (101) in that order of frequency. Shocked scapolite is chemically very similar to unshocked scapolite and shows very little structural damage. Scapolite in shocked rocks might conceivably be used to define a shock-metamorphic subclass in the 300-400 kb range.

APPENDIX

UNIT #1

Sample #1: Granitic Gneiss

This material is a fine- to medium- grained, grey or pinkish grey, gneissic-appearing rock. The rock is composed mostly of fine- to medium- grained feldspar and quartz. Some fine-grained black biotites, segregated in bands, give the rock a gneissic texture.

In thin section, the rock is composed of about 35% of fine- to medium- grained quartz; about 20% of fine-grained microcline; about 10% of fine- to medium- grained orthoclase perthite; about 20% of fine-grained plagioclase (An_{25-30}) and about 15% of fine- or medium- grained biotite. Quartz is generally 0.5 to 1.5 mm and frequently shows undulatory extinction. Potassium feldspar exists both as 0.25-to 0.5-mm irregular grains of crosshatched-twinned microcline and as orthoclase with exsolved stringers of albitic feldspar. Plagioclase is about 0.5 to 1 mm, generally rounded with poorly developed albite twinning. The biotite is brown and generally elongate. Traces of chlorite are intergrown with some biotite.

The texture of the quartz and feldspar-rich bands of the rock is granoblastic. The biotite segregates into bands, and these give the rock an overall gneissic texture.

Sample #NT-8:
Quartz-Feldspar-Biotite Gneiss

In hand specimen, this material is a fine-grained, grey and black gneissic rock. Bands of fine-grained, black, flaky biotite alternate with bands of fine-grained, white or grey quartz and feldspar. The banding defines a foliation in the rock.

In thin section, the rock is composed of about 20% plagioclase, 40% quartz, 15% hornblende, 15% biotite and 10% chlorite. Plagioclase is fine-grained, anhedral and about An_{30} in composition. Quartz is fine- to medium-grained, anhedral and shows no planar features or undulatory extinction. Hornblende may be either elongate or equant. It is fine- to medium- grained and green or brown. Biotite is fine-grained, elongate and displays no kinkbands. Chlorite is fine-grained, elongate and displays an anomalous blue under crossed polarizers.

The texture of the rock is gneissic. Bands (about 1 mm wide) contain predominantly biotite, hornblende and chlorite. These bands define the foliation of the rock. The mafic-rich bands alternate with 1- to 2- mm bands of equigranular quartz and plagioclase. Biotite, chlorite and hornblende are elongated along the direction of the bands, while in the leucocratic bands quartz and plagioclase are mostly equi-dimensional. A few quartz grains in the leucocratic material are elongated along the direction of foliation.

UNIT #2

Sample #28-7-7:
Quartz-Plagioclase Biotite-Garnet Gneiss

Macroscopically, the sample is a medium- and coarse- grained, grey and black gneiss. It appears to be composed of about 45% of fine- to medium- grained, greyish or whitish quartz and plagioclase and about 45% of medium-grained, black, flaky biotite. Medium- and coarse- grained, reddish garnets make up the remainder of the rock.

In thin section, the rock is seen to consist of about 35% of fine- and medium- grained quartz, 20% of medium-grained plagioclase, 35% of elongate, fine- and medium- grained biotite, and about 10% of medium- and coarse- grained garnet. Trace amounts of orthoclase, muscovite, and apatite are present.

The rock has an approximately equigranular gneissic texture. Biotite is segregated into bands with its elongation along these bands.

The quartz in the rock occurs as small, rounded, 0.1-to 0.2-mm grains which are included in plagioclase, and also as larger, 0.5-to 2-mm, irregular, anhedral grains. The quartz is unstrained and shows no closely spaced parallel fractures. Plagioclase occurs in equant or slightly elongate 1-mm grains. These grains show well-developed albite twinning and are about An_{30-35} in composition. Biotite is generally elongate, about 0.5 x 1 mm. The biotite is unbent, brown, and often contains small zircon grains. Large

(up to 3 mm), subhedral or anhedral, neutral-colored garnets which contain inclusions of muscovite plagioclase and quartz are scattered throughout the rock. Some muscovite is intergrown with the biotite. Very minor amounts of orthoclase occur as 0.1-mm equant grains included in plagioclase grains or interstitial to the quartz and plagioclase.

Sample #13-8-4:
Granitic Gneiss Auto-breccia

In hand specimen, the rock is a breccia composed of fragments of grey and white, fine- and medium- grained gneiss. Fragments range in size from about 1 cm up to about 10 cm, with the foliation of different fragments within the breccia oriented in different directions. Individual gneiss fragments contain 1-mm bands of fine-grained, black biotite and hornblende alternating with 1-3 mm bands of fine- and medium- grained, white quartz and feldspar. A few large porphyroblasts of garnet are seen in the hand specimen.

In thin section, the rock is composed of about 25% of fine-grained orthoclase, 25% of fine-grained plagioclase, 25% of fine- and medium- grained quartz, 15% of fine- and medium- grained hornblende, 10% of fine-grained biotite, and a few percent of medium- and coarse- grained garnet. Orthoclase is anhedral, equant and non-perthitic. Plagioclase is anhedral with some grains being equant and some being elongate ; albite twinning is well developed. The plagioclase does not contain planar features or low-index lamellae. The composition of the plagioclase is about An_{25-30}.

Quartz is anhedral; both elongate and equant grains are found. Some undulatory extinction occurs in quartz, but no planar features are observed. Hornblende is anhedral and elongate. Biotite is subhedral and elongate. A few biotite grains are bent, but most are not. Many biotite grains contain poorly developed kinkbands; grains with well-developed kinkbands and grains without kinkbands also occur.

The rock texture consists of two elements: the gneiss fragments and the inter-fragmental material. Gneiss fragments consist of nearly undeformed,gneissic-textured rock fragments. Fragments about 0.5 to 1 cm in a dimension occur in this thin section. Gneiss fragments consist of a granoblastic matrix of quartz, plagioclase and orthoclase, with bands of biotite,hornblende and garnet in the matrix. Biotite and hornblende are oriented with their elongation along the extension of the bands. Fragment minerals are unbent, unfractured and show no planar features. Biotite in the gneiss fragments frequently displays poorly developed kinkbands.

The inter-fragmental material is made up of plagioclase, orthoclase, quartz, biotite, hornblende and garnet grains of widely divergent sizes. Very small grains and a low-index pore filling occur in the interstices between larger grains. Mineral grains are oriented randomly in the inter-fragmental material; biotite and hornblende show no preferred orientation such as they do in

the gneissic fragments. Quartz in the inter-fragmental material sometimes displays undulatory extinction but no planar features. Inter-fragmental biotite is often bent and occasionally displays well-developed kinkbands.

The minerals of this sample do not show extensive microfracturing, although kinkbands are often present in biotite. No planar features or isotropic material is present in the rock. The above features suggest that the rock has probably experienced shock pressures greater than 10 kb but less than ~ 50 kb. More extensive microfracturing would be expected to occur if a shock pressure greater than 50 kb had been experienced.

The mafic minerals of the rock are undarkened, suggesting that heating and oxidation has probably not occurred.

Sample #24-7-5:
Plagioclase-Hornblende-Biotite-Orthoclase-Quartz Gneiss

In hand specimen, the rock is a fine- to medium- grained, grey and black gneiss. The rock contains layers a few centimeters thick which consist predominantly of fine-grained hornblende and biotite. These layers alternate with layers, also a few centimeters thick, which contain mostly white and grey feldspar. Bands of fine-grained biotite and hornblende in the mafic-poor layers define a foliation which parallels the layering of the rock.

In thin section, the rock is composed of about 35% medium-grained plagioclase, 15% fine- and medium- grained orthoclase, 10% fine-grained quartz, 15% fine-grained biotite, 20% fine- to medium-

grained hornblende and about 5% fine- and medium- grained garnet. Plagioclase is equant, anhedral, and shows well-developed albite twinning. The composition of the plagioclase is about An_{25-30}; it exhibits no planar features. Orthoclase is roughly equant, anhedral and contains a few 10-20 μ blebs of exsolved plagioclase. Quartz is equant, anhedral and occurs as interstitial grains between feldspars. The quartz is unstrained and exhibits no planar features. Biotite is elongate and subhedral. Biotite grains are unbent but display well-developed kinkbands. Hornblende is generally elongate and anhedral. Hornblende is typically pleochroic in olive brown, yellow brown, and reddish brown; many grains have dark or nearly opaque edges. Garnet is fine- to medium- grained, equant and anhedral. Grains generally appear in groups which may be partly decomposed relicts of larger, porphyroblastic grains.

The rock displays a granoblastic to gneissic texture. Quartz-feldspar layers of the rock consist of a fine- to medium- grained, granoblastic matrix of plagioclase, orthoclase and quartz. Bands of hornblende and biotite are segregated from the quartz-feldspar layers. These bands are generally a few millimeters wide , a few millimeters apart, and parallel to the layers. Biotite and hornblende are oriented with grains elongated along the bands. Groups of garnet grains occur predominantly in the quartz-feldspar layers.

In the mafic-rich layers of the rock, the mafic-rich bands are closely spaced and form a lepidoblastic matrix of biotite and hornblende which contains equant, plagioclase grains.

The feldspars of the rock are fairly extensively fractured, but no planar features occur in either quartz or feldspar. No isotropic phases are present. Based on the absence of planar features and the presence of kinkbands in biotite, the shock intensity experienced by the rock is estimated to be between 20 and 150 kb. The blackened, nearly opaque edges of hornblende grains suggest that the hornblende has been partially oxidized, probably as a result of heating by the overlying monzonite.

Sample #NT-1:
Quartz-Plagioclase-Orthoclase Gneiss

In hand specimen, the rock is a fine- to medium- grained, tannish to pinkish gneiss. It is composed chiefly of grey quartz and tannish feldspar, with some hornblende. The hornblende is segregated into poorly defined sheets which give the rock a poorly defined foliation. A few medium- to coarse- grained garnets are visible in the hand specimen.

In thin section, the rock is composed of about 45% medium-grained perthitic orthoclase, 25% fine- and medium- grained quartz, 20% fine-grained plagioclase, 4% fine- to medium- grained hornblende and 1-2% medium-grained garnet. Plagioclase is anhedral, of about An_{20} composition, and shows poorly defined albite twinning. Quartz occurs both in 1-mm grains and in small, rounded grains within plagioclase. It is anhedral, unstrained and contains no closely spaced, parallel, planar features. Orthoclase is anhedral and contains numerous 30 μ blebs of exsolved plagioclase. Hornblende is generally anhedral, elongate and greenish brown. Garnet occurs as large, rounded, anhedral, pink porphyroblasts which are filled with numerous inclusions of quartz and plagioclase. Accessory minerals are biotite, opaques, and zircon.

The rock has a granoblastic texture. Quartz, plagioclase and orthoclase occur in an equigranular intergrowth. Hornblende tends to be elongate with its elongation parallel to the foliation of the rock. Elongate quartz also shows a sub-parallel alignment with

this foliation. The porphyroblasts of garnet occur irregularly throughout the section.

Sample #4-20-1:

In hand specimen, the rock is a white and black, fine-grained gneiss. Well-defined, 1-mm bands of black biotite alternate with 2- to 3- mm bands of whitish quartz and feldspar.

In thin section, the rock is composed of about 25% fine-grained plagioclase, 30% fine- to medium- grained quartz, 25% fine- and medium- grained orthoclase, 15% fine-grained, brown biotite and 5% fine-grained hornblende. Oxides, pyroxene and occasional zircon comprise the secondary minerals. Plagioclase is equant, anhedral and has well-developed albite twinning. The plagioclase composition is about An_{30-35}. Quartz is sometimes equant, but it is more frequently lensoid (0.5 x 4 mm). The quartz displays no planar features. Orthoclase is anhedral and, on some occasions, contains a few exsolved blebs of plagioclase. Biotite is subhedral, elongate and brown. It is unbent and shows no kinkbands. Hornblende is anhedral, elongate and pleochroic in green and brown. Oxides are fine-grained and elongated. A few grains of fine-grained pyroxene are present.

The rock is gneissic textured. Mafic-rich bands, 1 mm thick, alternate with 2- to 3- mm bands of quartz, orthoclase and plagioclase. Mafic bands contain predominantly biotite hornblende and oxides with these minerals elongated parallel to the bands. The quartz-

feldspar bands consist of granoblastic aggregates of orthoclase, quartz and plagioclase. A few orthoclase grains in these bands contain cores of microcline. Quartz in the leucocratic bands frequently occurs as very elongated grains (0.5 x 4 mm). These long grains show undulatory extinction and are composed of different segments with slightly different crystallographic orientations.

Fairly frequent fractures, a few millimeters apart, occur in the section. Brownish staining and alterations occur along these fractures, and some plagioclase grains are fractured along the cracks.

Shatter Cone: Shocked-Granitic Gneiss

In hand specimen, the rock is a fine- to medium- grained, pink and white gneiss. The rock contains predominantly fine- and medium- grained, pink or white feldspar with some white quartz. Thin, discontinuous bands of elongate, black hornblende extend through the rock and define a foliation. The fracture surfaces of the rock display sets of approximately parallel striations. The striations are about 0.5 mm deep, about 1 mm apart and appear to radiate from points on the rock surface. The appearance of the rock surface resembles the surfaces of poorly formed "shatter cones". Shatter cones are described by Dietz (1963).

In thin section, the rock contains about 30% medium-grained quartz, 30% fine- and medium-grained plagioclase, 30% fine- and medium- grained orthoclase, 15% fine- and medium- grained hornblende

and 3-5% fine-grained biotite. Quartz grains are anhedral and appear tan or dusty brown. Most grains are equant, but a few are elongate and lensoid. Almost every quartz grain contains at least one set of closely spaced, parallel, "planar features" (Carter, 1965). Most grains contain 2 to 3 sets. Plagioclase is equant and anhedral. Albite twinning is only rarely present in the plagioclase. Many grains contain parallel, closely spaced fractures, and these fractures seem to be present along (001), (010) and (120)?. Many grains have one set of low-index, brownish lamellae resembling brown, albite twin lamellae. Orthoclase is anhedral; most grains are equant, but a few are elongate. Planar features are absent from the orthoclase. Hornblende is anhedral and elongate. Grains range from dark brown and green to nearly opaque. Biotite is dark brown or nearly opaque.

The rock has a granoblastic to gneissic texture. Most of the rock consists of a fine- to medium- grained, granoblastic matrix of quartz, plagioclase and orthoclase. Poorly defined bands of hornblende extend through this matrix. These bands are the traces of the rock foliation, and hornblende is aligned with its long direction along the bands. The long direction of elongated quartz and orthoclase is sub-parallel to the foliation of the rock.

The plagioclase and orthoclase in the section are strongly fractured, compared to gneisses exterior to the crater. Plagioclase and quartz show abundant planar features, but the rock contains no isotropic phases. An estimate of 150-300 kb can be made for the shock intensity experienced by this rock.

Hornblende in the rock is darkened and sometimes nearly opaque; this alteration is probably due to heating of the rock by the monzonite with consequent oxidation of some mafic minerals.

Sample #20-7-5:
Shocked Quartz-Feldspar-Hornblende Gneiss

In hand specimen, the rock is a reddish-brown and grey, fine- to medium- grained gneiss. The rock consists of 1- to 2- mm bands of reddish-brown, fine- and medium- grained hornblende alternating with 1- to 2- mm bands of fine- to medium- grained, greyish quartz and feldspar. The mafic mineral bands give the rock a well-defined foliation.

In thin section, the rock is seen to be composed of about 25% fine- and medium- grained plagioclase, 15% fine- to medium-grained orthoclase, 30% fine- to medium- grained quartz, 5% fine-grained pyroxene (diopside), 7% opaques pseudomorphous after fine- and medium-grained biotite, 15% opaques pseudomorphous after medium-grained hornblende and 3% opaques pseudomorphous after fine- and medium- grained garnet. Plagioclase is equant, anhedral

and generally displays albite twinning. Plagioclase has a composition of about An_{20-30}. It displays no undulatory extinction, planar features or low-index lamellae. Orthoclase is generally equant and anhedral; grains sometimes contain a few 20 μ blebs of exsolved plagioclase. Quartz is anhedral and most grains are markedly elongate. Almost every grain of quartz contains at least 1 set of closely spaced, parallel fractures. Most grains contain 2 and 3 sets of these features. Universal-stage measurements showed that about 90% of the measured planar feature poles are inclined 18-25° from the quartz c-axis. Almost every grain of quartz is surrounded by a band of low-index, recrystallized material (potassium feldspar?) which is generally about 100 μ wide. Opaques in the rock appear to be pseudomorphous after subhedral biotite, subhedral and anhedral hornblende, and subhedral or euhedral garnet. Inspection of a typical opaque grain shows rounded, black, 10 μ inclusions imbedded in more transparent, brownish material. Almost every opaque grain is rimmed by small, 10-30 μ diopside grains.

The rock has a gneissic texture. Quartz, plagioclase and orthoclase form an approximately granoblastic matrix which contains opaques segregated into bands. The opaque grains are elongate and have their long direction parallel to the banding. Rims of diopside are common around the opaques. The highly elongate, quartz grains in the quartz feldspar matrix

also show orientation of their long direction parallel to the rock foliation. The matrix consists of about 70% of the rock, while the opaque bands comprise the other 30%.

The rock probably started as a quartz-feldspar-biotite-hornblende gneiss. Shock metamorphism caused the planar features present in the quartz. Heating, subsequent to the shock event (due to the overlying igneous material), probably caused partial melting of the rock (producing a small amount of quartz feldspar liquid). Heating also caused the extensive oxidation and disintegration of the hornblende, biotite, and garnet.

Sample #25-20-3: Quartz-Feldspar-Biotite Gneiss

In hand specimen, the rock is a fine- and medium- grained, grey and white gneiss. The rock is very friable and breaks easily into centimeter-sized fragments. It is composed of 1- to 5- mm bands of black biotite and red garnet alternating with irregular, 1- to 5- mm bands composed of grey quartz and white feldspar. Bands of fine, crushed material extend randomly through the hand specimen. The white and grey bands of minerals produce an easily visible foliation of the rock.

In thin section, the rock is composed of about 45% fine- and medium- grained plagioclase, 35% fine- and medium- grained quartz, 10% fine-grained biotite, 5% fine-grained hornblende, 5% fine-grained garnet, and a few percent fine-grained orthoclase. Plagioclase is equant and anhedral with most grains showing well-developed albite twinning. The plagioclase has a composition of about An_{30}. Quartz is anhedral, sometimes equant and sometimes more elongate. It sometimes displays undulatory extinction but has no planar features. Hornblende is anhedral, equant and dark green or brown. Biotite is subhedral and elongate. Most biotite grains are unbent and show numerous kinkbands, although some biotite grains are bent. Garnet is subhedral to euhedral. Orthoclase

is anhedral and contains no exsolved blebs of plagioclase.

The rock has a gneissic texture. Most of the rock consists of a medium-grained, granoblastic matrix of quartz and feldspar with occasional interstitial grains of orthoclase.

Thin, discontinuous bands of biotite, hornblende and garnet extend through this matrix about 3-10 mm apart. Biotite is oriented with its lengthwise direction along the bands. The bands are the traces of the rock foliation, and many quartz grains are elongated sub-parallel to this foliation.

A system of millimeter-wide fractures extends through the section. In these fracture zones, minerals are much more fine-grained than in the rest of the section and are randomly oriented.

The rock shows no blackening of mafic minerals. Micro-fracturing is fairly extensive, but no planar deformation features or isotropic material is present. Biotite is bent in the fracture zones and unbent, but kinkbanded, in most of the rock.

UNIT #3

Sample #23-20-3:
Plagioclase-Hornblende-Garnet Gneiss

In hand specimen, the rock is a dark reddish-brown and white, fine- to medium- grained gneiss. The rock contains 1-mm bands of dark reddish-brown garnet and hornblende, alternating with 1- to 2- mm bands of whitish plagioclase. The banding defines a marked foliation of the rock.

In thin section, the rock is seen to contain 50% fine- to medium- grained plagioclase, 25% opaques pseudomorphous after hornblende, 15% fine- and medium- grained garnet, 5% fine- and medium-grained scapolite and 5% fine- and medium- grained diopside. Plagioclase is equant, anhedral and tannish or clear. Most grains are not albite twinned; they contain regions of low-index material and low-index lamellae which are densely packed with closely spaced, parallel fractures. Plagioclase is about An_{30-40} in composition. Opaques are elongate and anhedral. Some cores of opaque grains can be identified as hornblende. Garnet is subhedral to euhedral, isotropic and strongly fractured. Many garnet grains are stained reddish brown. Diopside is subhedral to anhedral, greenish, and elongate. Scapolite is subhedral or anhedral, and each grain consists of an aggregate of 20-50 μ domains of slightly differing orientation.

The rock has a gneissic texture. Garnet, hornblende and scapolite are segreated into bands about 1 to 2 mm wide.

These bands alternate with bands, 2 to 3 mm wide, which are composed mainly of plagioclase. Elongate mafic minerals are aligned with their long direction parallel to the direction of the foliation. The dark color of the hornblende is probably due to heating by the overlying monzonite and consequent oxidation of iron-rich hornblende.

Sample #NT-7:
Charnockitic Gneiss

In hand specimen, the rock is a fine- to medium- grained, tannish and black gneiss. It is composed of medium- and fine-grained, black pyroxenes and fine- to medium- grained tan or yellow feldspar. Poorly defined, 1-mm bands of black, fine-grained pyroxene alternate with 1- to 2- mm wide bands composed of fine- and medium- grained, tan and yellow feldspar. The banding of the rock defines its foliation.

In thin section, the rock is composed of about 15% fine- to medium- grained hypersthene, 15% fine- to medium- grained diopside, 45% medium- grained mesoperthitic orthoclase, 15% fine-grained plagioclase, 5% fine-grained quartz, 5% fine-grained oxides and trace amounts of biotite, hornblende and zircon. Some slides contain occasional 5-mm porphyroblasts of garnet . Hypersthene is pale pink or grey, elongate, anhedral to subhedral and pleochroic. Diopside is anhedral, elongate and greenish. The mesoperthite is anhedral and elongate with 10-20 μ blebs of exsolved plagioclase in an

orthoclase host. Plagioclase has a composition of about An_{25-35}; it is subhedral or anhedral, equant and displays well-developed albite twinning. Plagioclase contains no planar features or low-index lamellae. Oxide grains are rounded and elongate. Quartz occurs in small, anhedral grains, both within and between plagioclase grains; no planar features were observed in the quartz. Small grains of hornblende or biotite are often associated with the oxides. The few grains of biotite observed show no kinkbands.

The rock has a gneissic texture. Mesoperthite, plagioclase and quartz form a granoblastic matrix in which prisms of pyroxene are aligned parallel to the direction of foliation. The diopside and hypersthene segregate into poorly defined and closely spaced sheets which give the rock its macroscopic gneissosity. Oxides are associated with the pyroxenes and are elongated in the direction of foliation. Mesoperthite is also elongated in the direction of foliation. Hypersthene and diopside are frequently intergrown, and biotite and hornblende typically occur as small grains rimming the oxides.

Sample #15-7-3:
Plagioclase-Orthoclase-Hornblende-Garnet Gneiss

In hand specimen, the rock is a fine- to medium- grained, reddish-brown and white gneiss. Layers a few centimeters thick, composed predominantly of reddish-brown hornblende and garnet, alternate with layers a few centimeters thick which consist predominantly of feldspar. The compositional layers produce a well-defined foliation of the rock, and thin bands of mafic minerals in the feldspar-rich layers parallel this foliation.

In thin section, the rock is seen to be comprised of about 30% fine- and medium- grained plagioclase, 20% medium-grained orthoclase, 13% fine- and medium- grained diopside, 13% fine- to medium-grained garnet, and about 20% fine- and medium- grained, opaque or nearly opaque material which is pseudomorphous after hornblende and biotite. Trace amounts of apatite, hypersthene and oxides are present. Plagioclase is anhedral and equant, showing well-defined albite twinning. It has a composition of about An_{30-40}. Plagioclase displays no planar features and only occasional undulatory extinction. Orthoclase is anhedral and equant or elongate. Diopside is yellowish brown to greenish and is anhedral and elongate. Garnet is equant and subhedral or euhedral. Edges of garnet are frequently altered to a black, opaque material. Some elongate, anhedral, opaque grains have unaltered cores of hornblende. Most opaque grains are too dark to identify the original mineral species. Close inspection reveals that opaque grains consist of numerous small, black inclusions in a low birefringence matrix. Some opaques, pseudomorphous after biotite,

contain unaltered biotite cores. These grains are subhedral and elongate. Some unblackened grains show kinkbands.

The rock texture is gneissic. Feldspar-rich layers of the rock consist of a roughly granoblastic matrix of plagioclase and orthoclase. One-millimeter bands of biotite, hornblende, garnet and diopside extend through the feldspar matrix. The long directions of the elongate mafic minerals are aligned parallel to the bands. The bands of mafic minerals, in turn, are parallel to the macroscopic layering and foliation of the rock.

Mafic-rich layers consist of a matrix of hornblende, biotite, diopside and garnet. This matrix encloses some equant plagioclase grains. The elongation of hornblende, diopside and biotite grains in the matrix parallels the foliation of the rock. Orthoclase is generally absent from the mafic-rich layers.

All minerals in the rock are fairly extensively fractured, and most of the mafic minerals are blackened, probably due to oxidation during heating of the rock by the overlying monzonite.

Sample #12-20-8: Shocked Granulite-Grade Gneiss

In hand specimen, the rock is a fine- to medium- grained, greyish and pinkish gneiss. The rock is comprised predominantly of greyish, fine- and medium- grained plagioclase with broad bands and lenses of whitish and pinkish potassium feldspar. Fine- and medium- grained biotite and garnet are segregated into poorly defined sheets ~ 1 cm apart, and these sheets define a foliation. The rock tends to break from the outcrop, yielding surfaces with slightly curved striations. The striations appear to join at a point. These fracture surfaces resemble parts of shatter cones as described by Dietz (1963).

In thin section, the rock is comprised of about 35% medium-grained plagioclase, 30% fine- and medium- grained orthoclase, 15% medium-grained garnet, 7% fine-grained biotite, 7% fine- and medium- grained hornblende, 2% fine-grained quartz, 3% fine-grained diopside and traces of scapolite zircon and apatite. Plagioclase is equant and anhedral; most grains are albite twinned. The plagioclase composition is about An_{25-35}. Many plagioclase grains display closely spaced, parallel fractures along the (100) and (010) planes, and these fractures are frequently densely packed in one set of albite twin lamellae while only sparingly present in the other set of lamellae. In some cases, whole grains are densely packed with fractures. Regions densely packed with fractures have

lower birefringence than plagioclase. No clear maskelynite is present. Orthoclase is equant and anhedral and contains very few exsolved plagioclase blebs. Orthoclase shows no closely spaced fractures. Garnet is subhedral to euhedral, strongly fractured and contains a few inclusions. Biotite is elongate and subhedral with most grains displaying kinkbands. Hornblende is anhedral and elongate. Pyroxene is greenish, strongly fractured and anhedral. Scapolite is equant and anhedral with a few grains displaying poorly developed planar features.

The texture of the rock is granoblastic to gneissic. The plagioclase and orthoclase form a granoblastic matrix. Garnet, biotite, hornblende and diopside are segregated into bands about 1 mm wide and about 1 cm apart in this matrix. These latter bands define the foliation of the rock. The biotite and hornblende are aligned with their long directions along these bands, but in many cases the alignment of these minerals is not very pronounced.

UNIT #4

Sample A:

Outside (Unshocked) Anorthosite

Macroscopic:

In hand specimen, the material is whitish or greyish white; fine- to medium- grained. It consists predominantly of fine- to medium- grained plagioclase, with bands of fine- and medium- grained reddish garnets and greenish pyroxenes. The banding of mafic minerals gives the rock a gneissose appearance. These bands of dark minerals are evident on a 1-cm scale in hand specimen, while in the outcrop bands of mafic-rich rock, 1 to 10 feet thick, alternate with lighter, mafic-poor material.

Microscopic:

In thin section, the rock is seen to consist of 80-85% fine- to medium- grained, clear, albite-twinned plagioclase (An_{55}) with about 15% of fine- or medium- grained pink garnet and greenish pyroxene. One to two percent of the mode is comprised of fine- and medium- grained scapolite and dark green hornblende. Accessory minerals consist of intergranular potassium feldspar, sphene, apatite, and occasional biotite.

The rock has a gneissic texture which results from the segregation of garnet , pyroxene and hornblende into bands with elongation of the pyroxene along them. The plagioclase is nearly equigranular with 0.5-to 1.5-mm equant grains. Pyroxene is elongate , anhedral, 0.5 x 1 mm, and often occurs rimmed by subhedral or euhedral 0.5-to 1-mm garnets. Hornblendes are equant and tend to segregate with the mafic-rich materials. Scapolites are rounded,

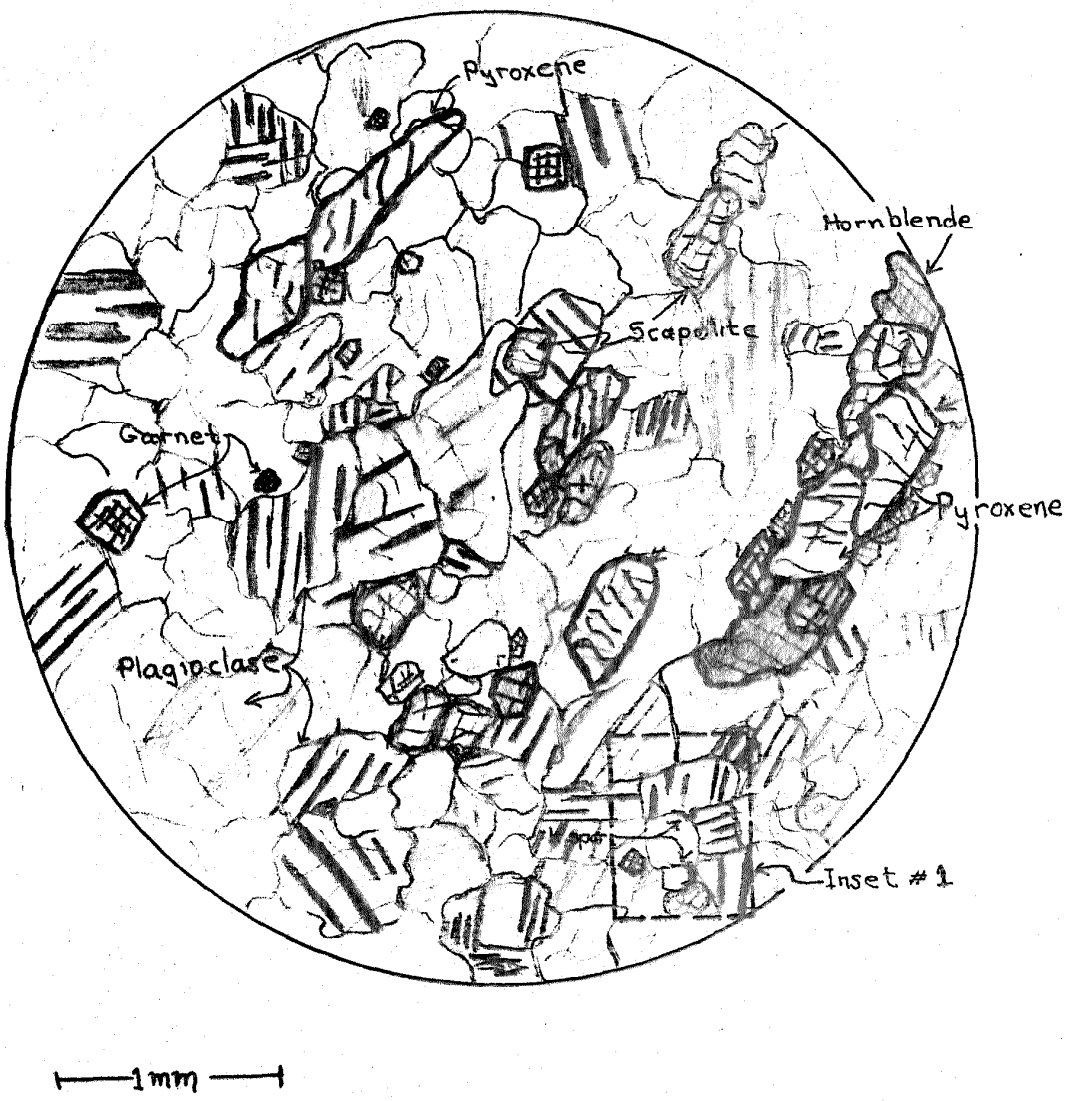

FIG. 1

GENERALIZED VIEW OF

UNSHOCKED ANORTHOSITE

SAMPLE A

0.5 - 1 mm,and also tend to predominate in the mafic-rich bands. Small (0.1 to 0.2 mm), euhedral garnets are found scattered throughout the plagioclase groundmass, while the larger, subhedral garnets more commonly rim the pyroxene. Fig. 1 illustrates the general textural features of this rock.

Plagioclase:

Plagioclase grains are clear, equant, and rounded, with some very large (1 to 1.5 mm) grains but with a fairly large number of clusters containing smaller (0.2 to 0.7 mm) grains. Albite and pericline twinning occurs; carlsbad twinning is less frequent. Fracturing is not extensive. The plagioclase has composition An_{51} determined by microprobe studies (see Table 1).

Potassium Feldspar:

Small, elongate stringers and blebs, generally 50 to 100μ in a dimension, of potassic feldspar, 2V = 20-40°(-), occur between larger plagioclase grains. Some of these small grains occur in the area shown in Inset I (see Fig. 2(a,b). The appearance of plagioclase and smaller garnet grains in the rock can also be seen in this figure (Fig. 2). The potassium-rich feldspar grains do not show clearly under crossed Nicols, but they can be identified by their lower index compared to the plagioclase. These grains are evident in the electron beam scan pictures of areas between plagioclase grains (Fig. 2). The homogeneous potassium concentration of plagioclase is also evident. If the intergranular phase, which comprises 1 to 2 % of the mode, at most, contains

10% K_2O, then some 30-40% of the potassium and argon in the rock might reside in this intergranular phase.

Garnet:

Garnet appears as clear, uniformly colored, pinkish grains without inclusions. Larger (0.7 - 1 mm), subhedral to anhedral grains are generally associated with the mafic bands in the rock, often rimming the pyroxene . Smaller (0. -0.5 mm) grains are generally scattered throughout the main plagioclase mass (see Fig. 2). A microprobe analysis of a garnet grain from this rock was obtained (Table 1). These garnets are about 43% almandine, 29% pyrope, and 28% grossularite.

Pyroxene is 0.5 to 1 mm, elongate and anhedral, with birefringence ~ 0.020 (2V = 45-60° +). The grains have a greenish color and are not twinned. Nearly all of the grains occur in the mafic-rich bands. Some pyroxene grains contain small inclusions. A microprobe analysis of a pyroxene indicates a Di_{77} Hd_{23} composition for this material, with a 6.5% Al_2O_3 content. The Al_2O_3 composition suggests that approximately 14% of the tetrahedrally coordinated sites in the lattice of this material are occupied by Al.

Scapolite:

Scapolite grains, 0.2 - 0.7 mm, generally rounded and subhedral, occur in the main mass of plagioclase as well as in the mafic-rich bands. They are clear with a birefringence ~ 0.020, uniaxial(-) character and uniform extinction. Microprobe analyses

of the scapolite from this rock (Table 1) indicate that it is about 75% meionite, and that it contains about 6.5% sulfur. The sulfur-rich nature of scapolite from this rock correlates with high sulfur content in other scapolite from rocks of this massif.

Hornblende:

Pleochroic green and green-brown hornblende is sometimes found associated with the pyroxene. It is anhedral and 0.5 - 0.7 mm in a dimension.

Other Data:

Two bulk chemical analyses: one for this sample and one for a sample whose location was 3 miles NNE of it (Location A; see Fig. 3, CHAPTER 1, PART I) are listed in Table 2. The analyses of these two anorthosites appear quite similar. The potassium concentration suggested by the analyses is higher than the value obtained from isotope dilution methods (0.54% K vs. 0.45% K by isotope dilution). Within the error limits claimed by the analyst, however (± 0.2% absolute), the two values are compatible.

FIGURE 2.

Electron Beam Scans of Unshocked Anorthosite Showing Potassium-Rich Intergramular Feldspar

Scale: A and B; as indicated under A. All others; as indicated under D (175 μ field of view).

A and B: Photomicrographs of ~ 1 mm field of view; A, plane light; B, crossed Nicols. Arrows point to small euhedral garnet. Dark finger in lower right is ink reference mark on slide. Plagioclase grain outlined in black on B. Areas outlined by white dots on B are fields scanned with electron beam scans. Upper area is field scanned in C, D, and E. Lower dotted area is field scanned in F, G, and H.

C: Upper area in B, calcium radiation. White outlines potassium-rich area.

D: Upper area, sodium radiation. White outlines potassium-rich areas.

E: Upper area, potassium radiation.

All fields scanned are oriented so that they are the mirror image of the area shown on B. (When the area outlined on B is viewed so that the slant-cut corner is in the upper left, then the right side of the electron beam scan field corresponds to the top of the area with its slant-cut corner matching the slant-cut corner of picture B.)

F, G, and H: Lower area in picture B, viewed with calcium, sodium, and potassium radiation, respectively. Potassium-rich areas are outlined in white.

The potassium-rich, sodium-and calcium-depleted areas are the intergranular feldspar. Note that sodium and calcium concentrations are homogeneous in the plagioclase.

TABLE 1.

Chemical Analyses for Unshocked Anorthosite[a]

Oxide	[b] Plagioclase	[c] Scapolite	[d] Pyroxene	[e] Garnet	Total Rock	[f] Total Rock Sample 7-20-4	[g] Error %
SiO_2	55.6	45.1	50.6	39.3	54.7	54.8	0.5
Al_2O_3	27.0	26.1	6.49	22.2	26.1	26.9	0.3
CaO	10.7	17.1	22.5	10.4	10.9	10.9	0.3
Na_2O	5.56	3.66	--	--	4.4	4.5	0.2
K_2O	0.33	0.10	--	--	0.65	0.60	0.2
MgO	--	--	12.6	7.85	1.0	0.6	0.3
FeO	--	--	6.86	20.7	1.3	1.0	0.2
TiO_2	--	--	--	--	0.18	0.13	0.2
MnO	--	--	0.05	0.43	0.02	0.02	0.02
SO_3	0.05	6.61	--	--	--	--	--
P_2O_5	--	--	--	--	0.03	0.03	0.05
Fe_2O_3	--	--	--	--	0.3	0.25	0.2
H_2O	--	--	--	--	0.3	0.3	0.2
Total	99.2	98.7	99.1	101.0	100.0	99.9	

(TABLE 1 -- continued.)

(a) Values indicated in weight percent oxides. Dashes indicate unmeasured values. Analytical errors for the microprobe analyses are generally ± 3% (standard deviation). Errors for total rock analyses (in absolute percent) are indicated in last column.

(b) Indicated composition is $An_{56.6}$.

(c) Indicated composition is 71.5% meionite.

(d) Composition $(Ca_{.379}\ Mg_{.351}\ Fe_{.107}(CaAl)_{.143})SiO_3$ or $Di_{77}\ Hd_{23}$.

(e) Composition indicated is: Almandine, 43.3%; Pyrope, 28.8%; Grossular, 27.7%; Spessartine, 0.9%.

(f) Values for Sample 7-20-4; 3 miles NNE of this sample.

(g) Errors for total rock analyses in absolute percent. Chemical analyses are by M. Weibel, ETH, Zurich, Switzerland. Financial support by National Aeronautics and Space Administration Contract NAS 9-8074 and National Science Foundation Grant GA-12916 awarded to G. J. Wasserburg.

Sample D:

Slightly Shocked Anorthosite

Macroscopic:

In hand specimen, the rock is whitish or slightly pinkish, fine- to medium- grained and consists predominantly of plagioclase with bands of fine- and medium- grained greenish pyroxene and hornblende giving the rock a gneissic appearance. Some fine-grained, reddish garnet is present. The foliation which appears in hand specimen, due to segregation of mafic minerals, also appears in outcrop. One-to ten- foot thick layers of mafic-rich rock alternate with more leucocratic bands.

Microscopic:

In thin section, the material consists of about 80-85% 0.5-1.0 mm, anhedral, equant plagioclase with ~ 5% garnet, 5-10% pyroxene, and 5% hornblende. Garnet , pyroxene , and hornblende are generally rounded and equant with grain sizes ranging between 0.5 and 1.5 mm. Scapolite is an abundant secondary mineral in smaller (0.5 to 0.75 mm), anhedral grains. Brownish isotropic material and some zeolite occur surrounding the garnet and pyroxene . Fig. 3 shows a generalized view of features found in a thin section of this rock.

The rock texture is gneissic. Some parts of the rock which have few mafic minerals tend to have an almost granitic texture. Garnet and pyroxene are segregated into bands with hornblende found predominantly in the bands as well.

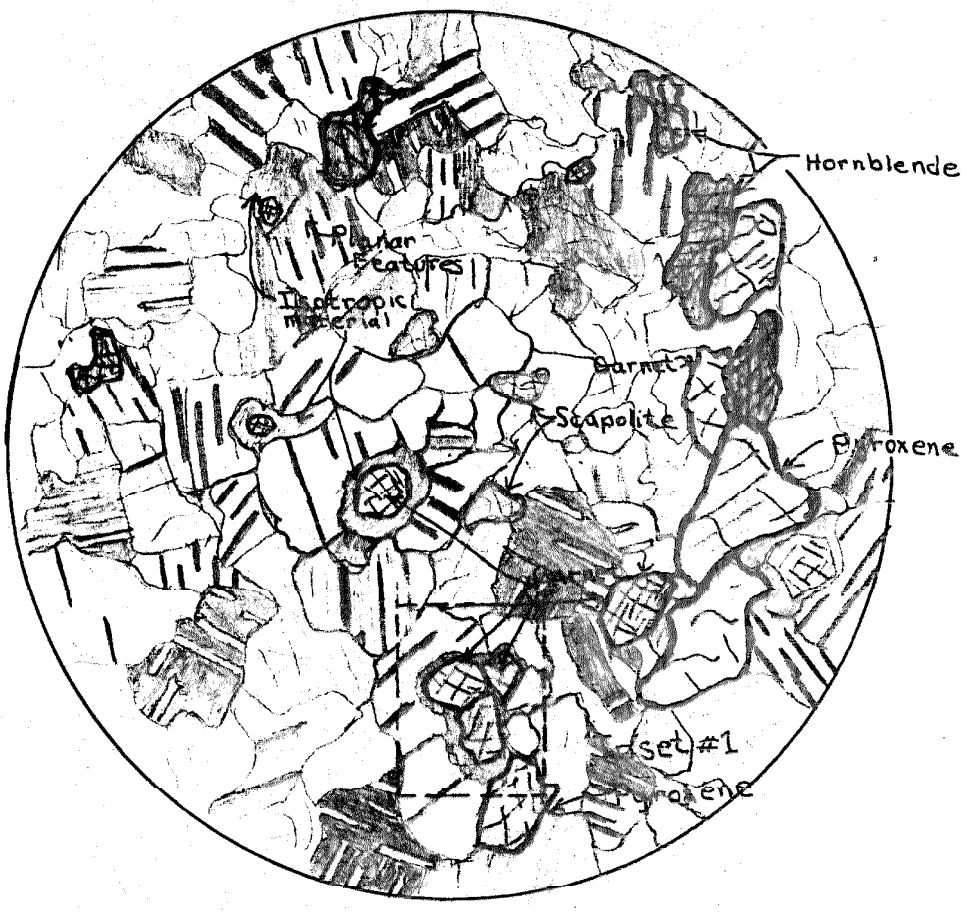

GENERALIZED VIEW OF SAMPLE D

SLIGHTLY SHOCKED ANORTHOSITE

FIG. 3

Plagioclase:

Plagioclase is equant, 0.5 - 1.5 mm in a dimension, and albite- and pericline- twinned. It frequently displays closely spaced, parallel fractures. In Fig. 4 (b and e) microscope views of an area of a thin section (outlined as inset 1 in Fig. 3) which display typical features of this plagioclase are shown. The fracturing of the plagioclase is fairly extensive. Closely spaced, parallel fractures which are visible in 4b and 4e are frequently parallel to the (010) of the plagioclase and occur only in one twin sector of the grain. For the most part, plagioclase in this rock displays uniform extinction (4e).

Isotropic Material:

Small patches of brownish or tannish material (n = 1.510) occur in small areas (0.2 - 0.7 mm) of the plagioclase or more frequently as embayments surrounding mafic minerals (Fig.4(b and e). Electron beam scanning pictures of the edge of an embayed garnet (Fig. 4) enable one to conclude that this material has roughly the same chemical composition as the plagioclase, with the exception that it may be slightly higher in aluminum concentration (Fig. 4i). The tan material sometimes merges into planar feature regions of the plagioclase ; it may be degraded feldspar.

Zeolite:

Small patches of clear, birefringent material ($\triangle n \sim 0.020$, $2V = 20\text{-}50^{\circ}+$) which occur around garnet or pyroxene

are probably zeolite (thomsonite?) This mineral is probably secondary.

Garnet:

Garnets is pink; in plagioclase grains it tends to be small (0.1 - 0.5 mm) and euhedral, but when associated with the mafic bands it is larger (0.7 - 1.2 mm) and more anhedral. As stated above, it is often rimmed by a "glass halo", especially euhedral grains in the plagioclase ground mass. As evidenced in the electron beam scanning pictures (Fig. 4), these garnets are chemically homogeneous and do not show irregular concentrations of Fe and Mg which are found to occur in more highly shocked materials.

Scapolite:

Rounded, clear scapolites (0.5 - 1 mm) occurs in the main mass of plagioclase as well as being associated with the mafic-rich bands. They have birefringence $\triangle n \sim 0.020$ and are uniaxial (-).

Hornblende:

Anhedral, elongate grains of highly pleochroic hornblende can be found in the sample. They are 0.5 x 2 mm, with a pleochroic formula: red-brown; chocolate brown, tan-yellow. They are most often intergrown with pyroxene in the mafic-rich bands.

Pyroxene:

Light green, diopsidic pyroxene in anhedral, equant, 0.7- to 1.5-mm grains is generally found in the mafic-rich bands. This pyroxene has 2V ~ 40-60°+ and, in some cases, shows extensive parallel

fractures which might be planar features.

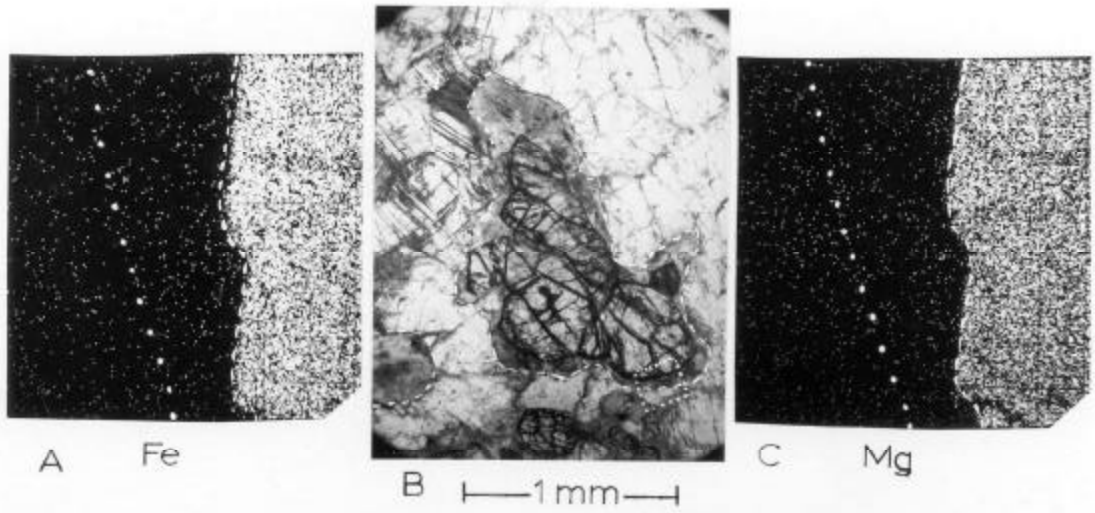

FIG. 4

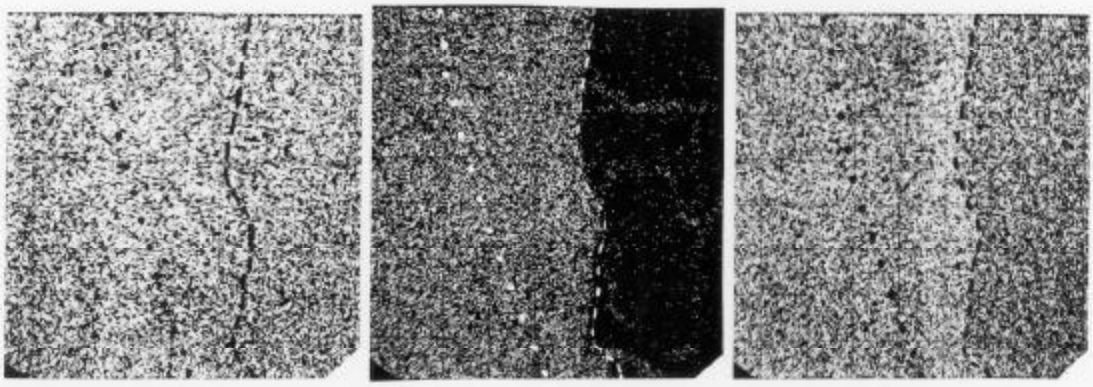

FIGURE 4.

Electron Beam Scans of Garnet from the Slightly Shocked Anorthosite Showing Chemical Homogeneity of Garnet

Scale: B and E; as indicated for B. All others; as shown for picture H (175 electron beam scan fields).

B and E: Photomicrographs of area of thin section indicated as inset #1 on Fig. 3. B is in plane light, E is under crossed Nicols. White dots outline electron beam scanned field. Arrows point to closely spaced, parallel fractures in plagioclase. Here these fractures grade into isotropic material.

B: Dashed outline is limit of brownish material around the garnet. Note that this material appears isotropic in picture E.

E: Dashes outline garnet; dots and dashes outline pyroxene in the group of grains shown. The tannish, low-index material surrounding the grains is mostly isotropic.

A, C, D, F, G, H, and I: Electron beam scan fields of the area outlined in white dots on pictures B and E. Dashes mark the edge of the garnet grain (outlined by dashes in Picture E), dots mark boundary of isotropic material with plagioclase (outlined by dashes in Picture B).

A: Iron radiation.

C: Magnesium radiation.

D: Potassium radiation.

F: Calcium radiation.

G: Silicon radiation.

H: Sodium radiation.

I: Aluminum radiation. Note the apparently aluminum-enriched band in the isotropic material next to the garnet grain edge.

The dotted outline of the EBS field (shown in pictures B and E) is a mirror image of the area shown on the actual scans. The right-hand edge of the dotted outline and the upper edge of the electron beam scan fields coincide, and the slant-cut corners of each coincide. The garnet can be seen to be of homogeneous composition, without iron "hot spots". The chemical composition of the isotropic material appears similar to that of the juxtaposed plagioclase.

Sample C

Maskelynitized Anorthosite

Macroscopic Characteristics:

In hand specimen, the rock is a fine- to medium- grained, equigranular rock consisting predominantly of clear, milky, or (in some cases) slightly salmon-colored maskelynite with fine- to medium- grained garnet and fine-grained, greenish pyroxene making up the rest of the rock. The rocks show a definite, well-developed foliation both in hand specimen and outcrop scale. In hand specimen, laminae rich in garnet and pyroxene give the rock a distinct gneissic structure. The maskelynite displays well-developed choncoidal cleavage. Most of the rocks from this outcrop resemble a quartzite with layers of fine-grained garnet and pyroxene.

Microscopic Characteristics:

In thin section, the sample is a holocrystalline, gneissic, fine- to medium- grained rock with a well-defined foliation due to the presence of mafic layers (see Fig. 5). About 80 to 85 % of the rock consists of fine- and medium- grained, clear, equant, anhedral maskelynite. Five to 10 % consists of subhedral or euhedral, fine- and medium- grained garnet, and about 5% consists of greenish, elongate, medium- or fine- grained diopside. Approximately 1 to 5 %, clear, anhedral or subhedral scapolite is a constant accessory, and dark green hornblende is sometimes present in minor (1 to 2 %) amounts. Fine-grained, elongate and clump-like sodic feldspar is present between plagioclase

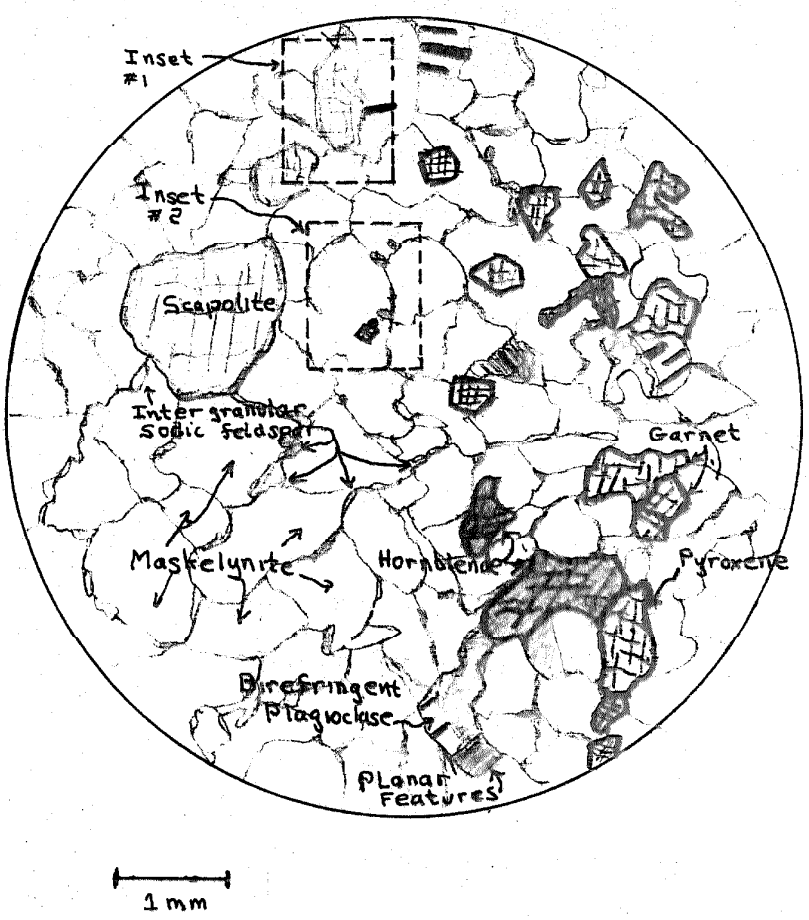

GENERALIZED VIEW OF SAMPLE C

MASKELYNITIZED ANORTHOSITE

FIG. 5

grains. Sphene and apatite are minor accessory minerals. The general textural features are illustrated in Fig. 5.

The maskelynite appears completely dark when viewed under crossed Nicols, except for parts of plagioclase grains which are still somewhat birefringent and the small, birefringent patches of sodic feldspar. These latter outline the maskelynite grains when the section is viewed under crossed Nicols. Pyroxene, hornblende, and scapolite are birefringent as well.

Maskelynite:

Maskelynite occurs in equant, 0.5-to 1.5-mm grains which are clear and isotropic. The original albite twinning which is generally seen in the unshocked plagioclase (see Fig. 1) is not visible in the maskelynite. In some plagioclase grains, however, the original birefringence and albite twinning is preserved either partially or totally. Photomicrographs of inset 1 and inset 2 (insets are outlined in Fig. 5) are shown in Figs. 6(a,b); 7(a,b). An untransformed plagioclase grain is visible in Fig. 6a, as well as a partly transformed grain in which plagioclase and maskelynite exist together. Plagioclase and maskelynite appear to have sharp boundaries on grain edges but generally interfinger within a single grain. An area of closely spaced, parallel, fractures is also visible in 6b. These fractures are visible in some parts of untransformed plagioclase grains, but clear maskelynite shows no cracks or fractures. A microprobe chemical analysis averaged from three grains is given

in Table 2. The material has a composition An_{55} with about 0.45% K. The maskelynite has about the same composition as plagioclase from other rocks in this massif.

Sodium Feldspar:

Small, string-like and irregular grains of more sodic (Ab $>$ 40) feldspar occur in the interstices, between the maskelynite grains. These small grains are about 20-50 μ in a dimension. These feldspars almost always retain their birefringence. Electron beam scanning pictures of areas outlined in inset 2 (Fig. 7) were obtained. The Ca, K, Na maps (Fig. 7 c-f) illustrate the more or less homogeneous, sodium-rich, calcium-poor nature of this material. These interstitial phases are seen to be K-depleted with respect to the maskelynite (Fig. 7).

Garnet:

Garnet is in subhedral crystals 0.5 to 1 mm in size. Most larger grains are found in the traces of the foliation planes. Smaller, euhedral grains occur throughout the main mass of maskelynite. The garnet shows some irregular fractures. The garnet in this rock is homogeneous in chemical composition on a 50 μ scale.

Pyroxene:

Greenish, diopsidic augite occurs in small, equant, 0.5-mm grains (1 to 5 % of the mode) in the mafic-rich bands of the rock. The grains appear optically homogeneous although they are strongly fractured.

Scapolite: Scapolite is a common accessory mineral which occurs in equant (0.5 - 1.5 mm), rounded, subhedral or anhedral grains. Grains occur both in the main mass of the maskelynite and associated with the mafic-rich bands. Scapolite retains its normal birefringence and uniaxial negative character. This scapolite frequently shows closely spaced, parallel fractures (see CHAPTER 2, PART I). Inset 1 shows several scapolite grains (see Fig. 6a). Chemical analyses, given in Table 2, show that the scapolite contains about 4.5% SO_2 and is about 75% meionite. The sulfur content of this scapolite is similar to that of scapolite found in other parts of the massif.

Two bulk chemical analyses are shown in Table 2. One is for this sample (sample C) and the other is for a nearly identical totally maskelynitized anorthosite (Sample B). Both samples yield very similar ages, and their major chemical composition appears very nearly identical. The elemental concentrations of these maskelynitized anorthosites are similar to the elemental concentrations of the outside anorthosite (Table 1). The water content of this sample (sample C) is about 2%. This probably reflects the greater frequency of fractures found in the material. The K content indicated in the bulk analysis is somewhat higher than that obtained by isotope dilution for the same sample (sample C) (0.50% K in the bulk analysis, compared to 0.414 by isotope dilution). The stated analytical errors are ± 0.2% (absolute) for the K_2O concentration. Within these errors, the two potassium determinations are compatible.

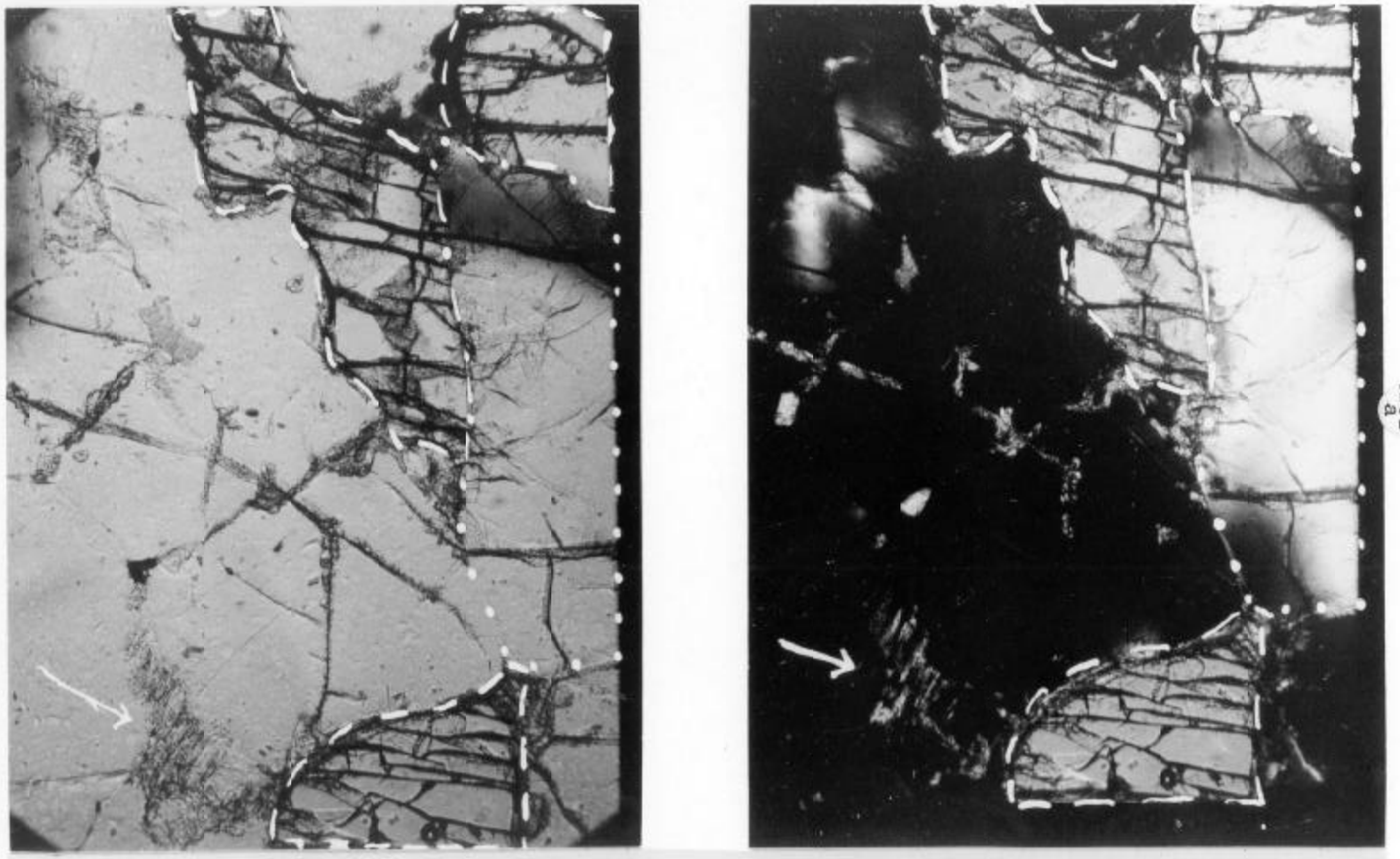

FIG. 6

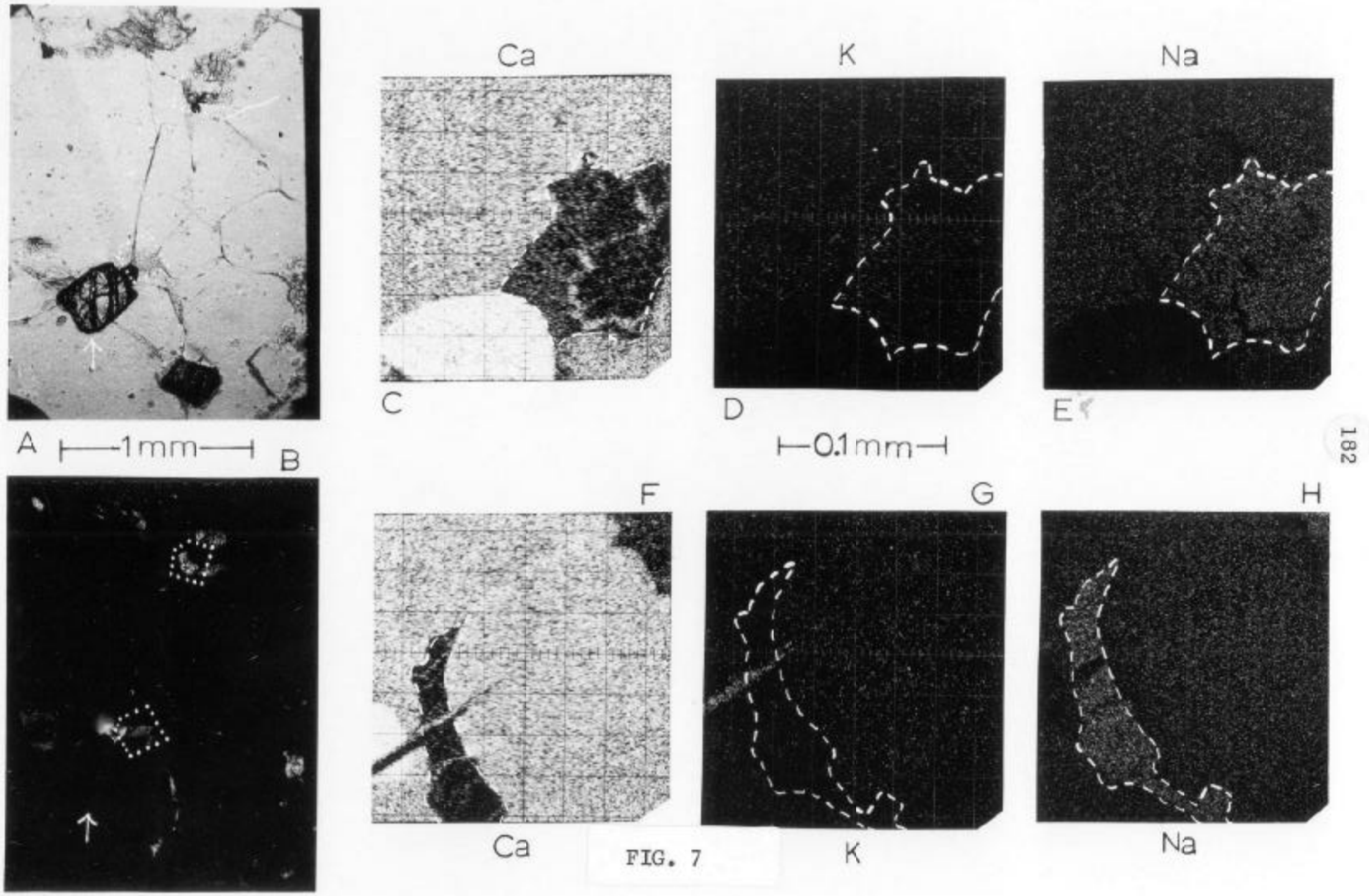

FIG. 7

FIGURE 6.

Photomicrographs of Maskelynitized Anorthosite Showing Maskelynite, Scapolite, and Uncoverted Scapolite

Area outlined as inset 1 in Fig. 5. A,plane light; B,crossed Nicols. Scapolite is outlined with dashes. Dots outline a plagioclase grain which has been mostly unconverted to maskelynite. Arrow points to the edge of a maskelynite grain which has closely spaced parallel fractures.

FIGURE 7.

Intergranular Feldspar in Maskelynitized Anorthosite

A and B: Area outlined as inset 2 in Fig. 5; scale as indicated. A, plane light; B, crossed Nicols. Dotted lines outline areas shown in electron beam scans. Arrows point to a small garnet grain. The small, birefringent grains of intergranular feldspar are most easily seen in B.

C-H: Element maps from the electron beam scans. Scale as indicated under D. All maps are mirror images of the areas outlined with dots. The lower edge of the field is the mirror line, and slant-cut corners of the field should correspond to the slant-cut corners on the dotted outlines.

C, D, and E: Calcium, potassium, and sodium maps, respectively, of the small, equant grain in the lower outline on A and B (near the garnet grain).

F, G, and H: Same elements mapped in the upper outlined area. Calcium-rich (bright) areas in C and F are probably sphene grains. Potassium-rich, accicular grain in G may be a small biotite grain.

Note in each case that the intergranular feldspar has a higher sodium concentration and lower potassium and calcium content than the maskelynite. Maskelynite is An_{50} so that these grains are probably An <30. The intergranular material is sodium rich but appears to contain some exsolved calcic plagioclase.

TABLE 2.

Chemical Analyses of Materials in Maskelynitized Anorthosite[a]

Oxide	[b] Maskelynite C	Maskelynite B	[c] Scapolite C	Scapolite B	[d] Errors	[e] Pyroxene B	[f] Garnet B	[g] Bulk B	Bulk C	[h] Errors
SiO_2	53.6	54.9	44.9	45.5	2	48.5 ± 1	39.8 ± 1	54.8	53.4	0.5
Al_2O_3	28.8	28.3	26.8	27.4	2	7.87 ± 1	22.1 ± 1	27.6	27.7	0.3
CaO	11.5	11.0	17.7	17.9	2	21.8 ± 2	11.0 ± 5	10.7	10.5	0.3
Na_2O	4.51	4.93	3.30	2.80	5	--	--	4.4	5.0	0.2
K_2O	0.55	0.56	0.15	0.15	8	--	--	0.6	0.6	0.2
MgO	--	--	--	--		10.8 ± 6	7.07 ± 6	0.6	0.5	0.3
FeO	--	--	--	--		8.60 ± 3	20.9 ± 2	0.6	0.5	0.2
TiO_2	--	--	--	--		1.0 ± 6	0.1 ± 10	0.10	0.08	0.2
MnO	--	--	--	--		--	--	0.01	--	0.02
SO_3	0.1	0.1	4.04	2.69	5	--	--	--	--	--
P_2O_5	--	--	--	--		--	--	0.03	0.03	0.05
Fe_2O_3	--	--	--	--		--	--	0.1	0.1	0.2
H_2O	--	--	--	--		--	--	0.3	1.8	0.2
Total	99.0	99.7	96.9	96.4		98.6	100.9	99.8	100.2	

(TABLE 2 -- continued)

(a) Oxides are listed as wt. %. Dashes indicate values were not measured.

(b) Indicated composition is $An_{56.6}$ for C, $An_{53.0}$ for B.

(c) Indicated composition is $Me_{74.2}$ for C, $An_{77.2}$ for B.

(d) Standard deviation of values for scapolite and plagioclase indicated in %.

(e) Indicated composition is $(Ca_{.355}Mg_{.307}Fe_{.137}CaAl_{.149})SiO_3$, which is about $Di_{69}Hd_{31}$. ± values are standard deviation of measured value in percent.

(f) Indicated composition is 44.4% almandine; 26.7% pyrope; 29.9% grossularite. ± value is standard deviation in %.

(g) Analyst: M. Weibel, Eidg. Technische Hochschule. Financial support by National Aeronautics and Space Administration Contract NAS 9-8074 and National Science Foundation Grant GA-12916 awarded to G. J. Wasserburg.

(h) Absolute error (%) in value listed for bulk analyses.

Sample B

Maskelynitized Anorthosite

Macroscopic:

This rock is from a spur on the eastern half of the anorthosite massif in the center of the structure. In hand specimen, it is comprised of about 90% clear , fine- and medium-grained maskelynite and 5 to 10 % fine- and medium- grained, reddish garnet. Some medium-grained, greenish pyroxene is visible. The garnets and pyroxene form distinct layers a few millimeters in thickness and one or two centimeters apart. These layers give the rock a distinct gneissic texture. Maskelynite has choncoidal cleavage, and this rock resembles a quartzite with reddish garnet bands.

Thin Section:

In thin section, the rock is seen to consist of about 85 to 90 % clear, equant, fine- and medium- grained maskelynite. Five to 10% consists of fine- to medium- grained, reddish garnets with about 5% of elongate, medium-grained, dark-green pyroxene. Between 1 and 5% of the rock consists of subhedral, 0.2 to 1.0 mm scapolite. Small, elongate strings and blebs of plagioclase (An $<$40) occur between the larger maskelynite grains.

This substance has a granitic texture in those samples which contain few mafic materials. Thin sections of samples which have about 15 modal percent mafics generally display bands of garnet, pyroxene, and hornblende. These samples have a gneissic texture. Fig. 8 (a,b) are large-scale photomicrographs of

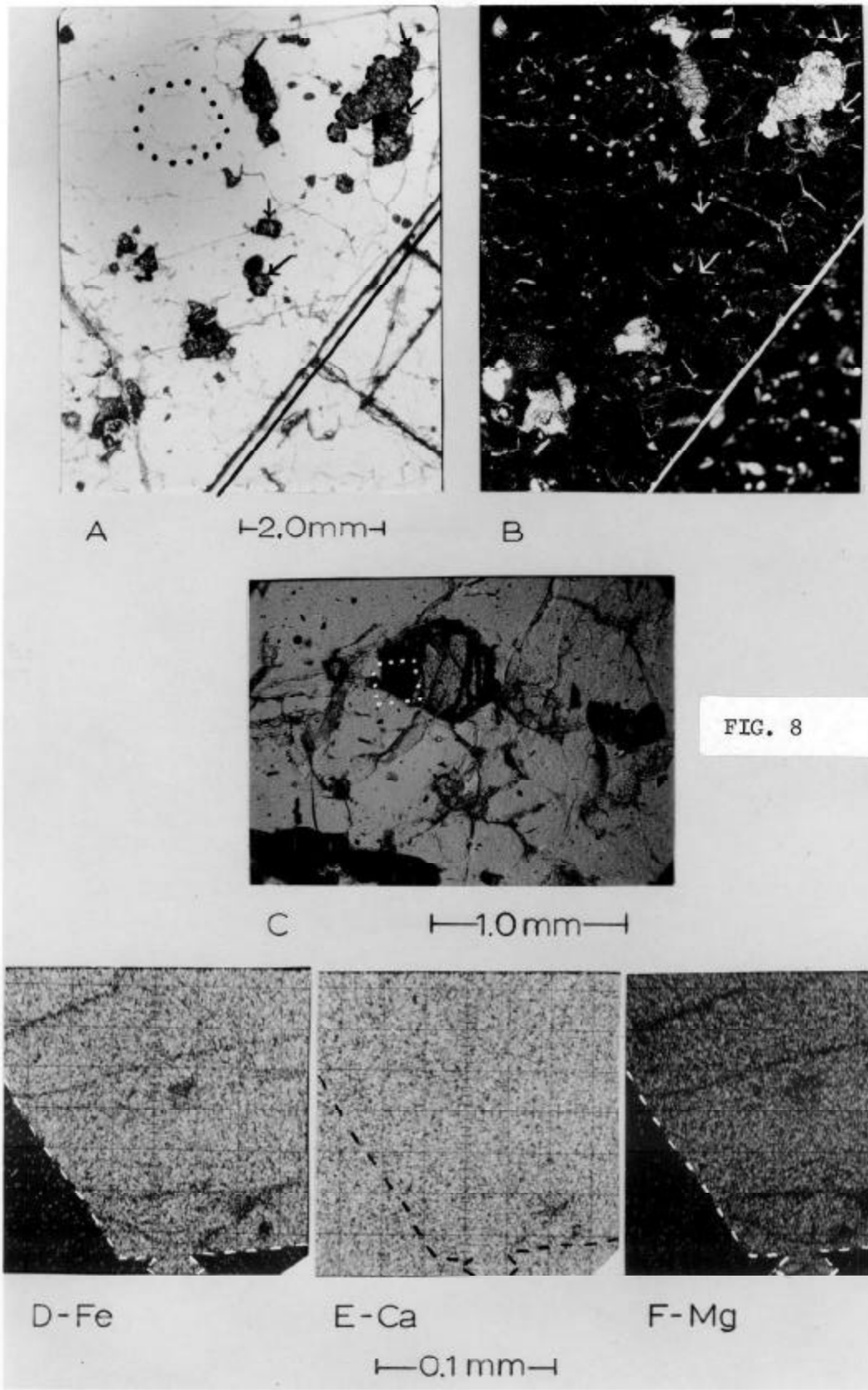

FIG. 8

FIGURE 8.

Broad-Scale Photomicrograph of the Maskelynitized Anorthosite with Detail of Garnet Grain Showing Chemical Homogeneity of the Garnet

A and B: Thin section in plane light (A) and under crossed polarizers (B). Scale is as indicated below A. Heavy line on lower right marks edge of thin section. Most of the thin section is composed of clear, unfractured, isotropic maskelynite. Maskelynite is white in A and black in B. The small, string-like, white grains which show best under crossed polarizers are the calcium-poor, sodic plagioclase grains. These grains occur around the edges of larger maskelynite grains. A maskelynite grain with a nearly continuous string of sodic plagioclase grains around its edges is shown encircled by dots. Pyroxene grains appear dark in A and light in B. A typical pyroxene grain is outlined with dashes. Arrows point to several small, euhedral garnet grains. These appear dark in A and B.

C, D, E, and F: Detail of garnet grain with electron beam scan pictures showing its chemical homogeneity. Scale for C is shown below picture. Scale for D, E and F is shown below E. A small, euhedral garnet grain is shown in plane light in C (dark grey grain in upper center of picture). Area scanned with electron beam is outlined in dots. Electron beam scan pictures of this area, in iron, calcium and magnesium radiation, are shown in D, E and F, respectively. The border of the garnet and the enveloping maskelynite is shown by dashes (area NE of dashed line is garnet). It can be seen that the garnet has a homogeneous distribution of iron, calcium and magnesium with no concentrations or "hot spots" of iron or magnesium (The dark linear EW bands in D and F are fractures in the grain, not element depletions.). The orientation of the electron beam scan pictures D, E and F, with respect to the photomicrograph $(C)_3$ is the same as discussed in Fig. 2.

this sample. The rock appears completely dark under crossed Nicols except for hornblende, pyroxene, scapolite, and sodic feldspar which are birefringent. Under crossed Nicols, the intergranular feldspar outlines the edges of the maskelynite grains since it contrasts with the completely isotropic maskelynite (Fig. 8). Untransformed plagioclase is less abundant in this sample than in Sample C, and only very few parallel fractures are visible in the section. The general features of this sample closely resemble those of Sample C, the location of which is 6 miles to the north. Samples B and C are very similar in hand specimen and in thin section characteristics. They also have very similar potassium-argon ages.

Maskelynite:

Maskelynite occurs as 0.1 - 0.4 and 0.5 - 1.5 mm anhedral grains. Albite twinning is visible only in occasional grains of untransformed plagioclase. Closely spaced,parallel fractures are also visible only in birefringent, untransformed plagioclase. Microprobe chemical compositions,averaged from three maskelynite grains found in two different thin sections of the sample (Table 2, Sample B), indicate that this material has the composition An_{52-54}. This is approximately the same chemical composition as that of the plagioclase in the unshocked anorthosite. A small amount of tan to slightly brown isotropic material is

present in this sample. This isotropic material frequently occurs between maskelynite grains or around mafic grains. It has about the same index of refraction as does the maskelynite.

Plagioclase (An $\leq$ 40):

Small stringers and blebs of plagioclase which are of more sodic composition than maskelynite occur between the maskelynite grains. These are birefringent and frequently exhibit closely spaced,parallel fractures. Electron beam scans of areas which contain this feldspar indicate that the feldspar is sodium enriched and both potassium and calcium depleted with respect to the enveloping maskelynite. This sodium enrichment in the intergranular feldspar was also found in Sample C.

Garnet:

Brown to pink,euhedral garnet , ranging from 0.1 to 0.3 mm, occur in the main mass of the maskelynite. Larger (0.5 - 1.0 mm) subhedral grains are associated with mafic-rich layers and are generally in contact with the pyroxene and hornblende.

A 175 μ field along the edge of a garnet enveloped in maskelynite (Fig. 8) was electron-beam scanned. The element maps obtained are shown in Fig. 8. Iron, calcium, and magnesium appear to be uniformly distributed in this garnet. No "hot spots" which are characteristic of the garnet of the more highly shocked materials can be seen. A microprobe analysis of a garnet grain

from this sample shows that the material is about 45% almandine, 25% pyrope, and 30% grossularite (Table 2).

Scapolite:

Clear, anhedral (0.5 x 1.0 mm) scapolite is present in this sample. Grains of scapolite frequently show closely spaced, parallel fractures (planar features) as are discussed in Chapter 2 of Part I. A microprobe analysis (Table 2) of scapolite from Sample B indicates that the material is about 77% meionite with about 2.7% SO_3. Electron beam scans of the scapolite grains show that the sulfur concentration is homogeneous within the grain.

Pyroxene:

Greenish, elongate (0.5 x 1.0 mm) pyroxene is generally found in the mafic-rich bands of this material. A pyroxene grain analysis indicates a composition of about Di_{69} Hd_{31} with about 15% of the tetrahedrally coordinated sites in the lattice occupied by aluminum atoms. This high concentration of aluminum seems to be characteristic of pyroxene from this massif. Pyroxene in this sample is strongly fractured but retains its normal birefringence and optical character ($2V \sim 45^{o}$,(+) $\Delta n \sim 0.025$). The grains do not display closely spaced, parallel fractures.

Hornblende:

Pleochroic, anhedral, 0.5 mm hornblende often is found in aggregate grains with pyroxene. The hornblende has a pleochroic formula: red-brown, dark green, tan-yellow.

A bulk analysis of Sample B is shown in Table 2.

This material appears chemically very similar to Sample C.

Sample F

Highly Shocked Anorthosite

Hand Specimen:

In hand specimen, the rock is a pinkish or greyish material which is comprised mostly of fine- and medium- grained plagioclase. Also present are a few bands rich in fine- and medium- grained, reddish garnet and greenish pyroxene. The rock tends to cleave rather smoothly in two planes at ~ 90° yielding cleavage surfaces which have a smooth silky lustre. The mafic-rich layers in this material are not well defined, and the foliation of rocks in the outcrop is not very distinct.

Thin Section:

The rock, in thin section, is composed mostly (~ 85%) of anhedral, equant, fine- to medium- grained plagioclase. Fine- and medium- grained, subhedral or euhedral garnet comprises about 10% of the mode, while 3 to 4 % of the rock consists of nearly unrecognizable scapolite. A few percent of medium- grained, dark green pyroxene is present. Intergranular to the plagioclase, some tan, dusty brown, or nearly opaque material is present. This material has an index, n = 1.535 (± 0.001), and is generally present as small, irregular patches or in linear bands which cut through plagioclase grains. Garnet, pyroxene, and hornblende tend to be segregated in bands. These bands give the rock its gneissic texture. Smaller, euhedral garnets occur in the main plagioclase mass. Scapolite is usually associated with these bands. A sketch showing the general textural features of the material is presented

GENERALIZED VIEW
OF SAMPLE F

HIGHLY SHOCKED
ANORTHOSITE

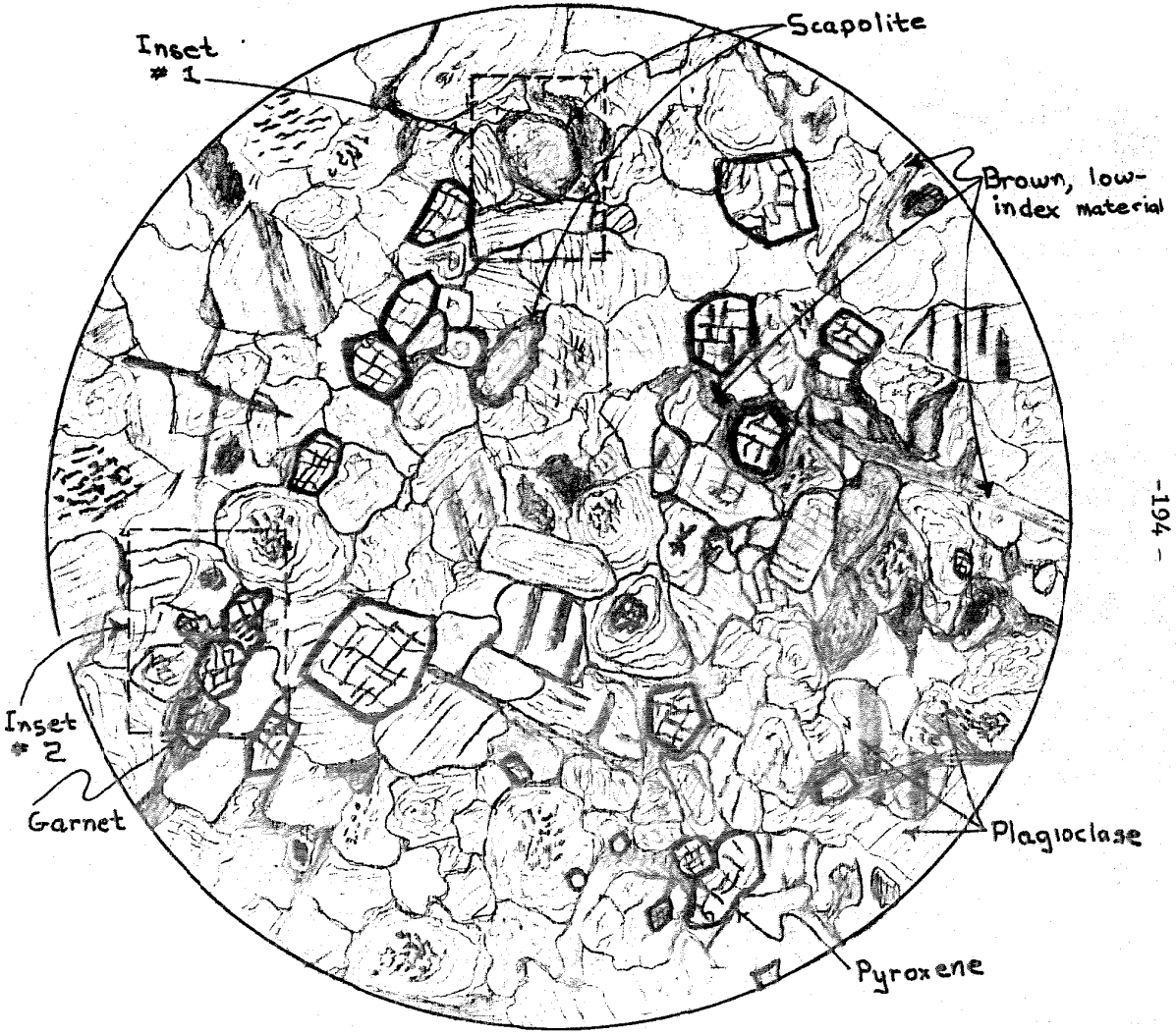

FIG. 9

as Fig. 9.

Plagioclase:

Plagioclase occurs in rounded, equant, anhedral grains; larger grains are 0.7 to 1.5 mm, smaller grains are 0.2 to 0.5 mm. The optical properties of the plagioclase are anomalous. Microprobe analyses of the material (Table 3) indicate a plagioclase, $An_{51.9}$, composition. The chemical analyses of this plagioclase are grossly similar to those of both the unshocked anorthosite and the maskelynitized anorthosite (see Tables 1 and 2). The material has a birefringence of 0.007 but a 2V of from 30^{o} down to 0 (optically +). These properties contrast with normal plagioclase (composition An_{50}) which has a 2V ~ 85^{o} - 90^{o}. Only a few grains in the entire section are albite twinned, and many grains show a peculiar curved fracture pattern. Other grains contain a series of branching chains of 5 to 10 μ bubbles, which resemble worm holes. Several plagioclase grains are pictured in Fig. 10a-b. The small bubbles are visible in several of the grains as are the concentric fractures in the grains. No closely spaced, parallel fractures are found in the plagioclase of this sample.

Potassium-rich Feldspar:

Small, generally elongate, 20 to 100 μ grains of a calcium-poor, potassium-rich feldspar occur between the plagioclase grains. These are clearly visible in electron beam scan pictures of the edge of a plagioclase grain (Fig. 10 c, d, and e). Small grains of calcium-poor feldspar, coexisting with larger grains of

calcium-rich (An_{50}) feldspar, are also characteristic of other anorthosites in the massif. The intergranular feldspar is sodic in the maskelynitized anorthosites but potassium rich in anorthosites outside the crater.

Brown, Low-index Materials:

A tannish or brown, low-index (n - 1.535) material often occurs along plagioclase grain edges. This material is variable in appearance. It is often very dark and sometimes opaque. It always has low birefringence and is isotropic in many cases. Very frequently, brownish material of similar appearance surrounds garnet.

Scapolite:

Rounded, 0.5- x 1- mm grains of scapolite are filled with dark brown, black or opaque inclusions (see Fig. 10a). Grains are most often comprised of aggregates of small crystallites. Some larger crystallites whose optical properties can be measured are uniaxial (-) with $\Delta n \sim 0.025$. The scapolite is heterogenous with respect to its chemical composition. It contains small, 50 μ domains of sulfur-rich material and other sulfur-poor domains. The heterogeneity is evident in the electron beam scan maps of a 175 μ field in a scapolite grain shown in Fig. 10(f-h). Microprobe analyses of both the high- and low-sulfur areas of a scapolite grain are given in Table 3. The compositions of high-sulfur parts of the grain correspond well with scapolite analyses for grains from the maskelynitized anorthosite as well as from

the unshocked anorthosite (Table 1, Table 2). Low-sulfur areas do not correspond well with scapolite composition in other anorthosites.

Garnet:

Dark brown garnet grains, 0.5 to 1.2 mm, are subhedral or euhedral with very dark, nearly opaque edges. Larger grains are found mostly in the garnet pyroxene bands, while smaller, euhedral grains are found within the main mass of plagioclase. Electron beam scan element maps reveal that this garnet is heterogeneous in chemical composition (Fig. 11). Twenty to 40 μ areas are found to be iron-rich, silicon- and aluminum- depleted when compared with the normal garnet composition. These iron "hot spots" are not observed in garnet from the maskelynitized anorthosite, the slightly shocked anorthosite, or the outside anorthosite. The edges of the garnet grains are more heterogeneous than the centers. This effect is apparent in Fig. 11. The results of a microprobe analysis of a garnet grain are shown in Table 3. This garnet is about 40% almandine, 30% pyrope, and 30% grossularite. This composition seems to be characteristic of garnet in other samples from the massif.

Pyroxene:

Some anhedral grains, 0.5 to 0.7 mm in a dimension, occur; these are usually associated with garnet. They are generally dark brown-green and pleochroic. The grains observed appear strongly fractured. A microprobe analysis of a pyroxene grain

is shown in Table 3. The indicated composition ($Di_{77}Hd_{23}$) is compatible with pyroxene from other rocks of this massif (compare Tables 1 and 2). It appears that some 14% of the tetrahedrally coordinated silicon is replaced by aluminum in this material. The high aluminum concentration seems to be characteristic of pyroxene from this massif.

Hornblende:

A few rounded grains of a dark green-brown mineral resembling hornblende are present. Its optical properties are difficult to determine.

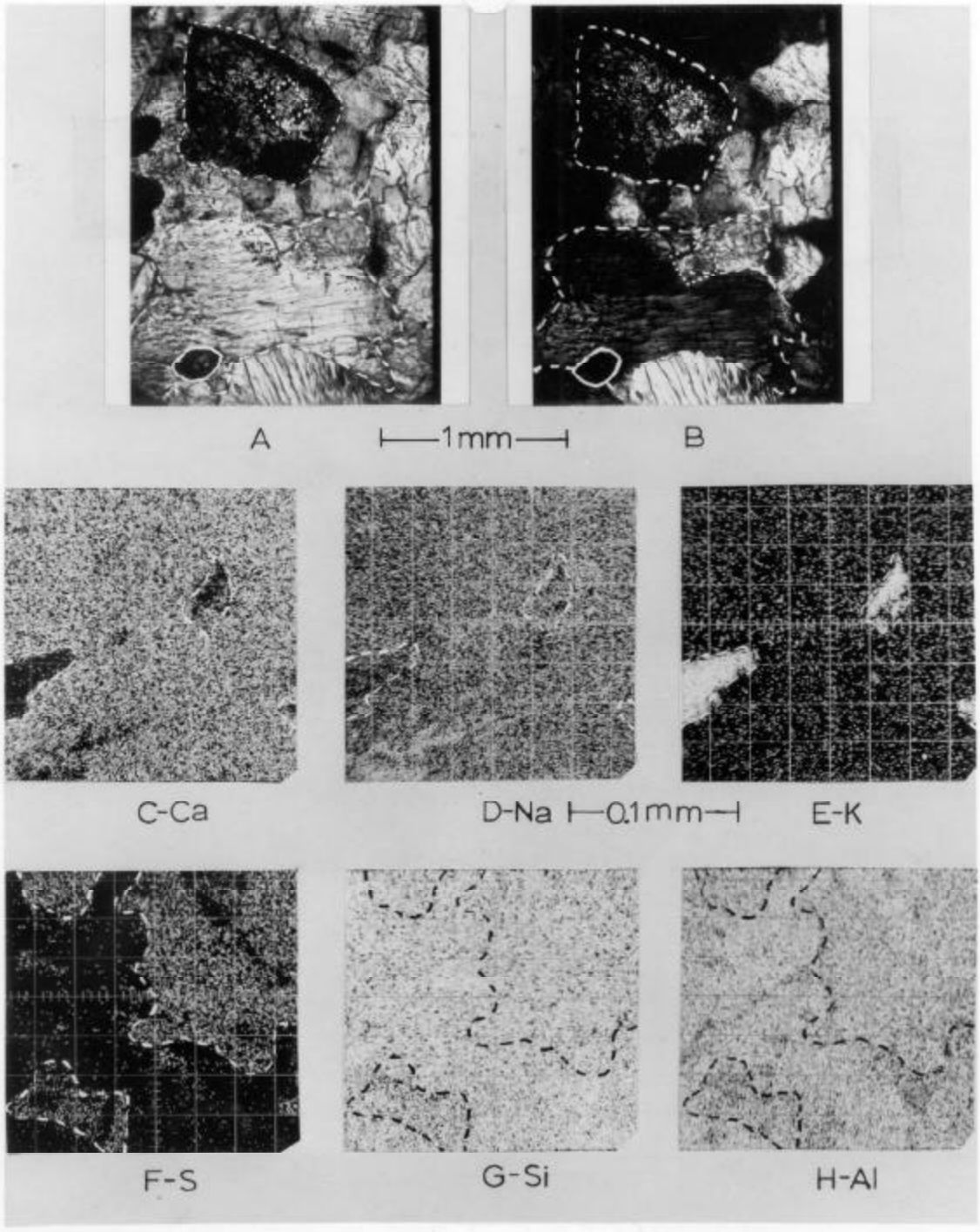

FIG. 10

FIGURE 10.

Intergranular Feldspar and Heterogeneous Scapolite in the Highly Shocked Anorthosite

A and B: Photomicrographs of area of thin section corresponding to Inset #1 in Fig. 9. Scale is indicated between pictures. A, plane light; B, crossed polarizers. Most of the grains in the picture are plagioclase; two plagioclase grains are outlined with dashes. Note the tiny, black, dendritic growths present in the large, outlined grain. Outlined grain indicated by arrow shows curved fracture pattern. A scapolite grain is outlined in the upper part of the picture. Note that this grain appears dark and filled with inclusions. Small grain outlined by solid line is garnet.

C, D, and E: Electron beam scans of the area, outlined by dots, along the boundary between the two outlined plagioclase grains in A and B (lower outlined area). Scale is indicated below D. C, D and E are electron beam scan maps of this area in calcium, sodium and magnesium radiation, respectively. In the beam scan pictures, the small, potassium-rich grains between the plagioclase are outlined with dashes. These grains are potassic feldspar which occurs between the large plagioclase grains. Note that the intergranular feldspar is sodium- and calcium- poor, compared to plagioclase. Most of the scanned area contains plagioclase. Note that the plagioclase seems fairly homogeneous with respect to Na and Ca contents. An irregular area, which is possibly sodium-enriched and calcium-depleted compared to the main part of the plagioclase grain, is seen in the lower left-hand corner of pictures C and D.

F, G, and H: Electron beam scan maps of a region of the scapolite grain shown in A and B. Scale is indicated below picture D. Area shown is the upper dotted region in pictures A and B.

F, G and H are the electron beam scan maps of this region in sulfur, silicon and aluminum radiation, respectively. Areas within the scanned region which are enriched in sulfur are outlined by dashes in F, G and H. There is a marked difference in sulfur content between the high sulfur areas and low sulfur areas in F, but there is little difference in the aluminum and silicon content of the high sulfur and low sulfur areas (pictures H and G). Chemical compositions obtained for the high sulfur and low sulfur areas are given in Table 3.

The orientation of the beam scan pictures compared to the areas outlined in photomicrographs A and B is the same peculiar inversion and twist as indicated in Fig. 2.

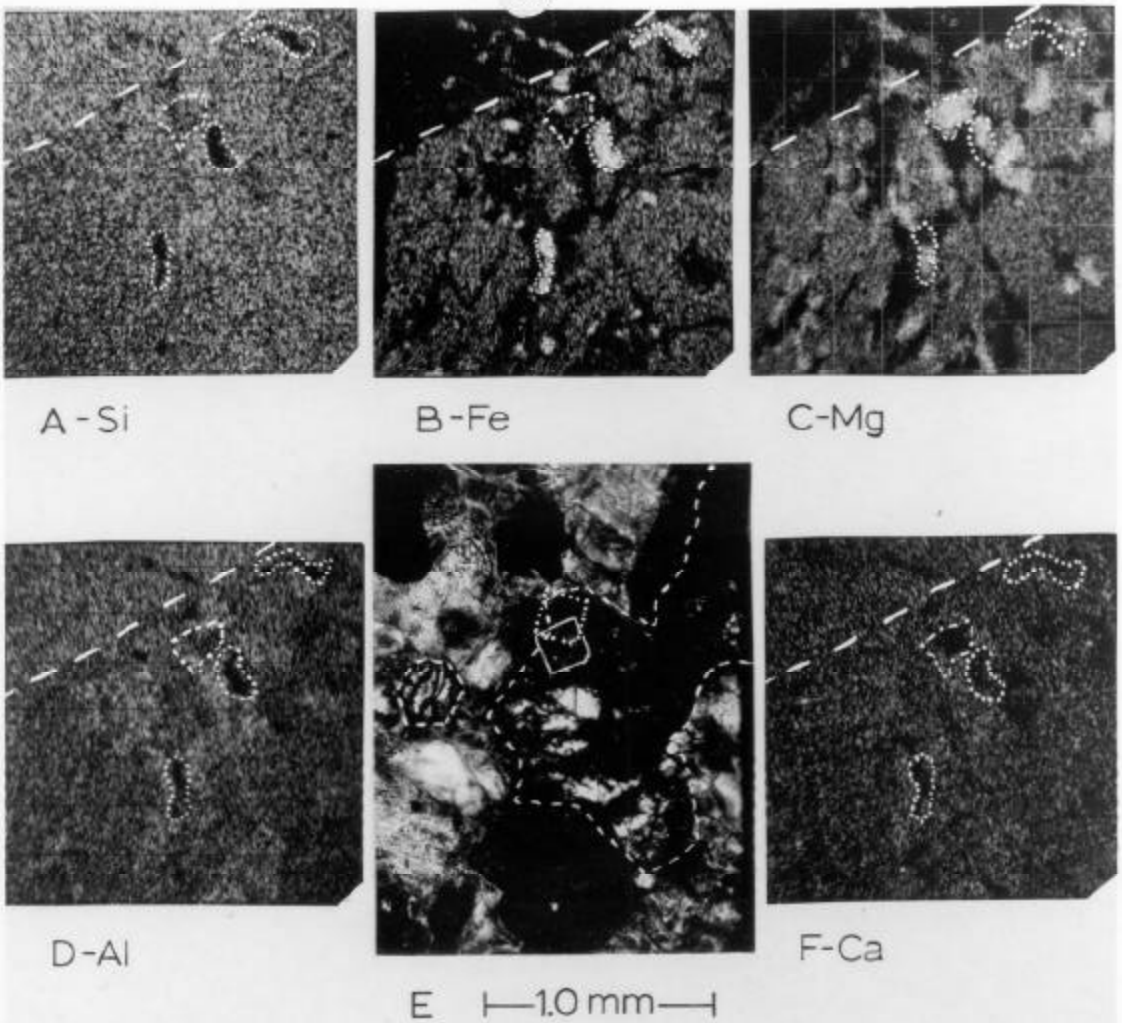

FIG. 11

FIGURE 11.

Electron Beam Scans of Garnet
from the Highly Shocked Anorthosite Demonstrating
Chemical Heterogeneity of this Garnet

E: Photomicrograph of part of thin section in plane light. Scale is indicated below picture. An aggregate of garnet grains and a smaller, euhedral garnet grain are outlined with dashes. Dark areas in grain are darkened, nearly opaque areas. Most of the picture is plagioclase; the darkened patches around the garnet clump are low-index, low-birefringence, brown, plagioclase-composition material. The square areas of the garnet grain, outlined with dots and with a solid line, are the beam-scanned regions of the grain shown in A, B, C, D and F and in G, H and I, respectively. The photomicrograph (E) corresponds to Inset #2 in Fig. 9.

A, B, C, D and F: Electron beam scans of the dot-outlined, square region of the garnet grain. A, B, C, D and F are pictures of the dot-outlined region in silicon, iron, magnesium, aluminum and calcium light, respectively. Scale for A-F is indicated below picture H. The edge of the garnet grain is indicated by dashes in these pictures (garnet is region below the dashed line; altered plagioclase is above and to the left of the line). Iron-rich areas in the grain are outlined with dots; dots and dashes delineate magnesium-rich areas in the grain. The garnet grain contains: (1) 20-50 μ patches which are enriched in iron and depleted in silicon, aluminum and calcium with respect to the majority of the grain. Some (not all) of these patches are outlined in the pictures. (2) Similar-sized patches, enriched in magnesium compared to the rest of the garnet grain, are depleted in iron, calcium and aluminum but contain some silicon. It should be noted that similar electron beam scans of garnet from the maskelynitized anorthosite (Fig. 8) and garnet from the slightly shocked anorthosite (Fig. 4) reveal chemically homogeneous grains with no development of localized

concentrations or depletions of elements. It is thought that the heterogeneities in this garnet are due to incipient breakdown within the grain caused by shock heating.

From the appearance of pictures A, D and F, it can be deduced that the dark, altered plagioclase which borders the garnet grain in these pictures has Si, Al and Ca compositions approximately the same as the garnet (see Table 3 for a garnet analysis). The approximate Si, Al and Ca compositions are compatible with the identification of this brown, low-index, low-birefringence material as altered plagioclase.

G, H and I: Electron beam scan pictures of the solidly outlined square (picture E) in magnesium, iron and calcium radiation, respectively. Scale is indicated below H. This is an overlapping region of the garnet grain, and some of the same patterns appear. Exposure times for pictures G, H and I were somewhat longer than for pictures A-F; hence, the former have somewhat more clarity -- especially the calcium picture (I). The garnet has fairly large homogeneous areas but reveals the same iron-enriched spots. Pictures G and H show that the magnesium-rich regions are calcium depleted but contain some iron.

The beam scan pictures and the photomicrograph (E) have the same inverted orientation relation as indicated in Fig. 2 and Fig. 4. The beam-scan pictures should be imagined to be in a flipped-over, face-down position on the page. The pictures are then rotated about an axis perpendicular to the plane of the page until the slant-cut corners of the picture and the outlined area in E coincide.

TABLE 3.

Chemical Compositions of Materials
in the Highly Shocked Anorthosite

Oxide	(b) Plagioclase	(c) Scapolite		(d) Pyroxene	(e) Garnet
		High S	Low S		
SiO_2	55.2 ± 3	45.3	51.9 ± 2	49.6 ± 1	41.5 ± 10
Al_2O_3	28.4 ± 5	26.0	29.2 ± 2	7.08 ± 3	23.2 ± 9
CaO	10.7 ± 5	17.2	14.8 ± 2	22.4 ± 1	9.51 ± 3
Na_2O	5.12 ± 6	3.52	3.12 ± 5	--	--
K_2O	0.52 ± 15	0.16	0.13 ± 8	--	--
FeO	--	--	--	6.78 ± 1	18.8 ± 21
MgO	--	--	--	12.4 ± 1	8.18 ± 21
MnO	--	--	--	0.05 ± 12	0.3 ± 27
TiO_2	--	--	--	--	--
SO_3	0.05	7.52	0.0 ± 5	--	--
Total	99.9	99.7	99.2	98.3	101.4

(a) Values are in wt.% oxides, dashes indicated unmeasured values. ± values indicate standard deviation errors in %.

(b) Indicated composition is $An_{51.9}$.

(c) Composition for high sulfur scapolite is about 72 % meionite.

(d) Composition is: $(Mg_{0.349}\ Fe_{0.107}\ Ca_{0.374}\ CaAl_{0.157})SiO_3$ which is about $Di_{77}Hd_{23}$.

(e) Composition indicated is: almandine, 41.0; pyrope, 31.8; grossular, 26.6; spessartine, 0.6.

Sample E:
Highly Shocked Anorthosite

Hand Specimen: The sample is a specimen of anorthosite located about 6" from the pseudotachylyte lens which Sample G was taken from. In hand specimen, the rock is a hard, compact, fine- to medium- grained, white and black anorthositic gneiss. The rock is composed predominantly of medium-grained, white or salmon-colored plagioclase with some fine- and medium- grained, brick-red garnet and some fine- and medium- grained black pyroxene. Mafic minerals are segregated into bands, about 1 mm wide and 1 cm apart, which give the rock a poorly defined foliation. Small, 1-2 mm, rounded drops and pods of brick-red "pseudotachylyte" occur scattered throughout the rock.

Cleavage surfaces of plagioclase from this specimen have a peculiar chalky appearance, even in fresh, unweathered samples. The dull-white appearance of the freshly broken surfaces of this rock contrasts sharply with the more lustrous cleavage surfaces of plagioclase in the unshocked or slightly shocked anorthosite (Samples A and D). Garnet likewise displays a duller than average cleavage surface.

Thin Section: In thin section, the rock is seen to contain about 40% brown, low-birefringence material, 40% fine- and medium-grained plagioclase, 7% fine- and medium- grained, greenish diopside, 5% fine- and medium- grained scapolite, and 8% fine- and medium-grained garnet. A small amount of fine- to medium- grained, green or brown hornblende is present. The low-birefringence material forms

a net of thin-to-thick, elongate, continuous bands through the rock. Plagioclase occurs as anhedral, equant grains which do not show well-defined albite twinning. One or two plagioclase grains display closely spaced, parallel fractures. Pyroxene is elongate and anhedral. Grains are usually a dark olive green. Scapolite is subhedral or anhedral and equant. Most grains consist of multiple domains within a single grain. Garnet is clear, subhedral or euhedral and equant.

The fabric of this rock, and many of its mineralogical properties, are similar to those of Sample F. The rock is a gneissic anorthosite with a sieve-like net of brown, low-birefringence material extending through the rock. Bands of brown, low-birefringence material, from 0.1 - 0.5 mm wide, extend continuously through the rock. The intersection of many bands of this material forms a sieve-like net. In some cases, the intersecting bands of low-index material form extensive patches containing only a few isolated regions of clear plagioclase. In other cases, clear plagioclase grains are nearly whole, and only a few thin bands of brownish material cut through the grain. Apart from the brown alteration, the rock texture consists of a medium-grained, granoblastic matrix of plagioclase with 1-mm bands of mafic minerals, 2 - 5 mm apart, extending through the matrix. Diopside, scapolite, garnet and hornblende occur predominantly in these bands. Diopside is elongated in the direction of the bands, and elongated aggregates of garnet grains are also aligned along

the bands.

Brownish, Low-Index Material: The material which comprises the bands is tan to brown and has low birefringence or is isotropic. Its index of refraction is slightly less than 1.54. This material is probably partially vitrified plagioclase. The intimate intermixing of the brown material with plagioclase suggests that it is an alteration of the plagioclase. It is, in part, possibly normal (thermal) plagioclase glass. Electron beam scanning studies of garnet grains in Sample F showed that similar material in that rock has approximately plagioclase composition.

Plagioclase: Plagioclase is generally clear and equant. The plagioclase has anomalously low 2V (i.e. 10-30°+). Only a few grains display albite twinning. Some grains have undulatory extinction, and one or two grains in the slide contain closely spaced planar features. Most grains contain branching strings of 5 μ holes extending throughout cores of the grains.

Pyroxene: Pyroxene is greenish and elongate. Many grains have a series of closely spaced, parallel fractures developed along one crystallographic orientation.

Garnet: Garnet is clear, pink and strongly fractured. A few grains were studied using electron beam scanning techniques, and these grains showed the same iron "hot spots" as observed in garnet of Sample F.

Scapolite: Scapolite is generally clear and anhedral.

Most grains are strongly fractured and appear to be a mosaic of smaller domains. The small domains have varying crystallographic orientation with respect to the larger grain but generally go to extinction more or less simultaneously so that the large grain appears to be mottled. The domains range from equant, 15-20 μ areas to elongate, 20 x 200 μ areas.

Shock Pressure: Assigning a shock intensity to this sample involves the same difficulties as were encountered with Sample E. Neither Sample E nor Sample F contain numerous planar features, maskelynite or indications of plastic flow. The presence of anomalous plagioclase in E and F is difficult to evaluate since such plagioclase has not been reported from shocked materials other than Manicouagan rocks. The chemically heterogeneous garnets in Samples E and F are thought to result from incipient breakdown of these garnets due to high experienced temperatures; the presence of heterogeneous garnets in Samples E and F, but not in the maskelynitized anorthosites, suggests that the former experienced higher temperatures than the latter. Sample E is the least likely rock in the massif to have been heated by the monzonite, and the high indicated temperatures must, therefore, be due to shock heating. Sample E probably was shocked more intensely than the maskelynite but not as intensely as Samples G and H which show evidence of plastic flow.

Sample G:

Red Pseudotachylyte-Shocked Anorthosite Breccia

In hand specimen, the rock is a fine- to medium- grained breccia and consists of a very fine-grained or aphanitic, hard, brick-red matrix which envelops 0.5 mm to 3 mm whitish fragments. Fragments are generally elongate, contorted and bent. Smaller fragments appear to be monomineralic while larger fragments are contorted anorthosite chunks. This sample contains about 80% aphanitic matrix and about 20% distinguishable rock and mineral fragments.

Sample G is from a breccia lens about 6" wide and 2'-3' long in the anorthosite of the central massif. Sample E, discussed previously, is a piece of the wall rock anorthosite in which the above breccia lens occurs.

In thin section, the rock consists of about 55% fine-grained to aphanitic, brown or tannish pseudotachylyte, 5% medium-grained, brown or tan grains, 15% elongated schlieren of plagioclase, about 10% recognizable medium-grained, equant plagioclase and about 5% fine- and medium- grained opaques, some of which are pseudomorphous after medium-grained garnet.

The rock texture is difficult to describe but somewhat resembles a porphyritic texture. The fine-grained, brown or tan material envelops: (1) brown, ovoid, low-index grains; (2) stretched out and contorted schlieren of plagioclase (Typical dimensions of a grain are 0.5 x 3 mm.); (3) occasional 3- to 10- mm recognizable

GENERALIZED VIEW
OF SAMPLE G

RED PSEUDOTACHYLYTE-
SHOCKED ANORTHOSITE
BRECCIA

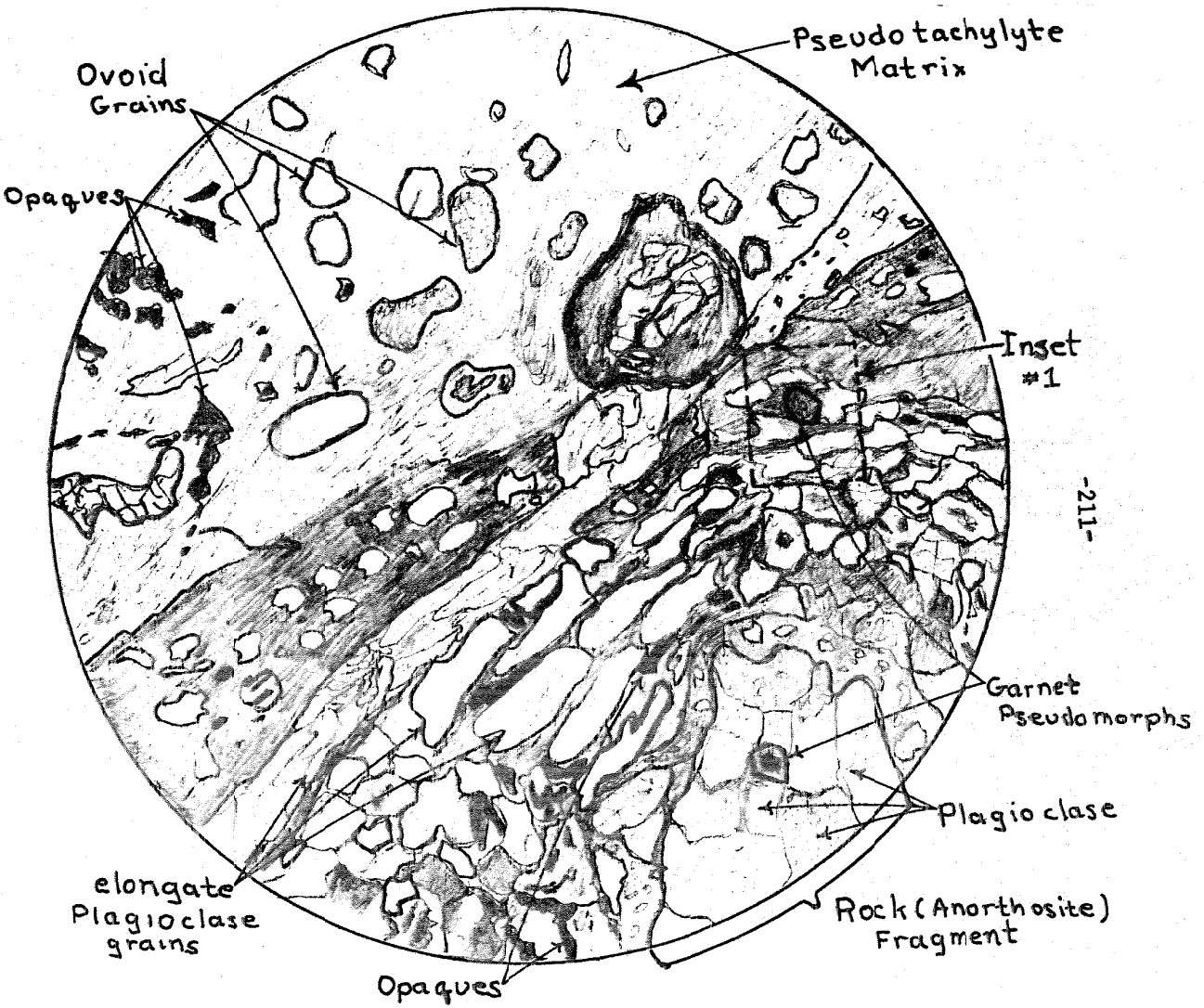

1 mm

FIG. 12

chunks of anorthosite; (4) 0.1- to 0.25- mm, angular, opaque grains. The brown, ovoid grains and the stretched-out plagioclase define what appears to be a direction of flow in the rock. The texture of the rock is illustrated in the generalized thin section sketch shown in Fig. 12.

Fine-Grained Pseudotachylyte: The tannish material which comprises most of the thin section is too fine grained to identify microscopically. The K_2O concentration of the whole-rock breccia (Table 1, CHAPTER 1, PART II) is 0.47%, similar to the anorthosite. This suggests that the breccia matrix has a chemical composition similar to that of anorthosite. The pseudotachylyte matrix probably consists of very finely ground and crushed anorthosite.

Ovoid Grains: The matrix contains a large number of very rounded, equant-to-ovoid, isotropic or very low birefringence grains. These grains range from clear to tan or dark dusty brown and have an index considerably less than 1.562. Some of the ovoid grains have recrystallized to a low-index ($2V \backsim 30\text{-}50^{o}+$) material. These grains are tentatively thought to be droplets of quenched plagioclase glass.

Plagioclase Schlieren: Numerous, elongate, contorted grains of clear to slightly tan, low-index, low-birefringence plagioclase occur in bands in the breccia. Each elongate grain appears to be an aggregate of smaller, 0.1- x 0.3- mm, lensoid grains. The smaller grains show undulatory extinction and have an index less than 1.562. Occasional elongate grains show relict albite twinning.

Anorthosite Fragments: A few, reasonably distinct, unbent, anorthosite fragments are present in the matrix. One fragment, illustrated in Fig. 12, contains 0.5- to 1- mm, equant plagioclase grains and an opaque grain pseudomorphous after garnet. A plagioclase grain from this rock fragment has relicts of albite twinning and a $2V \cong 80^{o}(+)$. Most other grains have $2V \cong 10\text{-}30^{o}(+)$ and consist of many smaller, 20-200 μ crystallites of plagioclase which have approximately the same crystallographic orientation. Several plagioclase grains from this fragment are outlined in Fig. 13. The mosaic structure of grains in the lower part of the field is clearly evident in Fig. 13(b).

Opaques: Many small, generally elongate, often rounded and strung out opaque grains occur in the pseudotachylyte matrix and between grains of elongated plagioclase. Some of the opaques are pseudomorphous after garnet. Fig. 14 shows electron beam scans of one of these garnet pseudomorphs. (This grain is in the part of the section designated as Inset #1 in Fig. 12.) The electron beam scan pictures suggest that the material has Fe, Mg, Ca, Si and Al as major elements. The chemical nature of this material and its garnet pseudomorphism suggest that the grain is decomposed garnet. The iron-rich areas of the grain are outlined in Fig. 14b, and it is seen that these areas correlate with the silicon- and aluminum- depleted areas of the grain. Anorthosite Sample F also contains garnet which displays iron-rich, silicon- and aluminum- depleted regions.

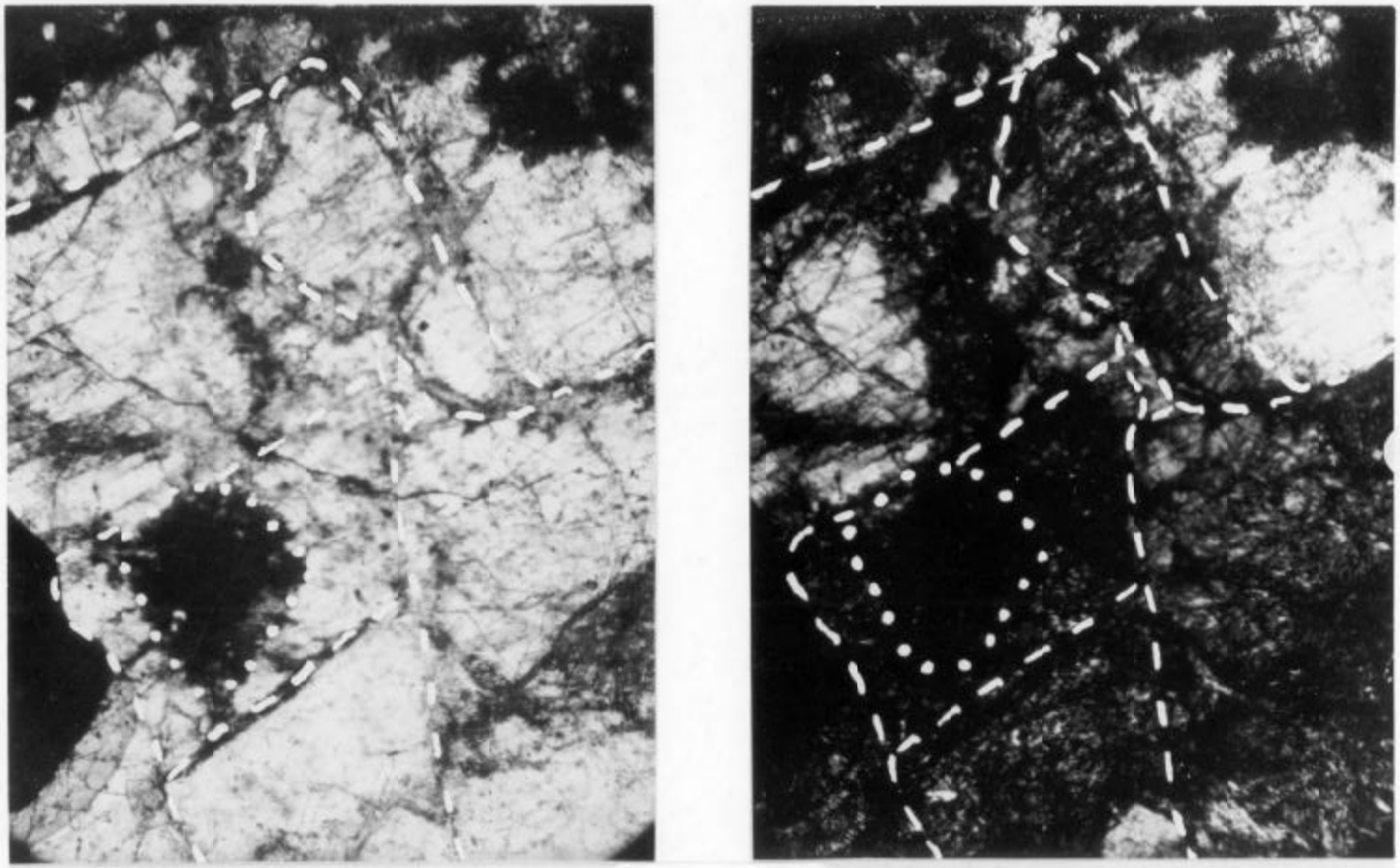

FIG. 13

FIGURE 13

Photomicrograph of Part of a Rock Fragment
Showing Mosaic Structure of Plagioclase in the Fragment

A: A region of the anorthosite fragment indicated in Fig. 12 viewed in plane light. The scale is as shown. The grain outlined with dots is the garnet pseudomorph appearing in Fig. 12. Several plagioclase grains are outlined with dashes. These grains appear strongly fractured.

B: Same field as A, viewed under crossed polarizers. Note that the plagioclase grains in the lower center and lower right-hand corner of the field consist of mosaics of many smaller plagioclase crystallites.

FIG. 14

FIGURE 14.

Electron Beam Scans Showing Breakdown
of Garnet in Anorthosite Fragments from the
Red Pseudotachylyte-Shocked Anorthosite Breccia

B: Photomicrograph (crossed polarizers) of a region of the thin section shown as Inset #1 in Fig. 12. Scale is indicated on photomicrograph. Most of photograph consists of contorted plagioclase schlieren. The peculiar dark patch on the lower edge of the picture is a microprobe reference mark. An opaque grain pseudomorphous after garnet is visible in the center of the photograph. Dots outline the area of this grain which was electron-beam scanned.

A, C, D, E and F: Electron beam scans of the dot-outlined region of the "garnet" grain. Scale for all the beam scans is as shown on E. Pictures A, C, D, E and F are the electron beam scan maps of the outlined area in iron, magnesium, silicon, calcium and aluminum light, respectively. Major elements of the grain are iron, calcium, magnesium, silicon and aluminum, and the approximate chemical composition supports identification of the garnet pseudomorph as garnet. The exact edge of the garnet grain is difficult to locate, but most of the region scanned is part of the garnet pseudomorph. A few (but not all) of the iron-rich areas are outlined with dots, and one magnesium-enriched area is outlined with dots and dashes. It can be seen that two distinct varieties of "hot spots" develop in this garnet. (1) 20μ iron-rich regions which are depleted in silicon, calcium, aluminum and magnesium, compared to other parts of the grain. (2) Magnesium-rich areas which are depleted in calcium and iron but contain silicon and aluminum. Some type of calcium-enriched phase may also develop, but such phases are not apparent in picture E.

The exact chemical composition of the iron-rich and magnesium-rich phases are unknown, but precisely the same sorts of phases are

developed, to a lesser extent, in the garnet of the highly shocked anorthosite (Fig. 11). Similar heterogeneous phases were not developed in garnet from the maskelynitized anorthosite or from the slightly shocked anorthosite.

Orientation of the electron beam scan photographs with respect to the photomicrograph (B) is the same inversion-twist as discussed for Fig. 11.

Sample H:

Greyish Pseudotachylyte-Shocked Anorthosite Breccia

In hand specimen, the rock is a fine- to medium- grained breccia consisting of a very hard, fine-grained, greyish matrix enclosing whitish or greyish rock fragments. The fragments range from 0.2 mm to 3 mm in a dimension and are generally elongated and distorted. Some of these fragments are recognizable pieces of anorthosite which contain bent and twisted bands of mafic minerals.

In thin section, the rock consists of about 40% aphanitic, dark grey matrix, about 45% rock chunks, about 10% ovoid grains of plagioclase and about 5% small plagioclase grains and opaques distributed throughout the matrix. The rock fragments consist of about 80% fine- to medium- grained plagioclase and about 20% fine- to medium- grained opaques pseudomorphous after garnet. The plagioclase in the fragments is equant, anhedral and tannish to dusty brown. Neither planar features nor maskelynite is present in this plagioclase. The opaque grains of the rock fragments have heterogeneous chemical composition; the major elements present are Ca, Al, Si, Mg and Fe. They are, therefore, probably garnet. Most of these grains have 10-30 μ irregular, round blebs of a bronze-colored, highly reflective phase embedded in their outer edges. The blebs are slightly nickeliferous and have an approximate composition: 50% S, 39% Fe, 5% Al_2O_3, 4% SiO_2,

1% CaO and 1% MgO. The ovoid grains in the matrix have n $\sim$ 1.562 and are clear to dusty tannish brown. Some of these ovoid grains are visible in Fig. 15(a). The matrix of the breccia contains innumerable rounded and elongate 20 x 30 μ blebs of opaque material. Electron beam scan pictures of several of these blebs are shown in Fig. 15. The blebs are seen to be slightly nickeliferous iron sulfide, and they may be extraterrestrial material mixed into the breccia during the impact.

The texture of this breccia is very similar to that of the red pseudotachylyte-breccia (see Fig. 12); it is best described as approximately porphyritic. The distorted fragments in the greyish matrix are often stretched and elongated in a single direction, and the rock appears to have flowed plastically.

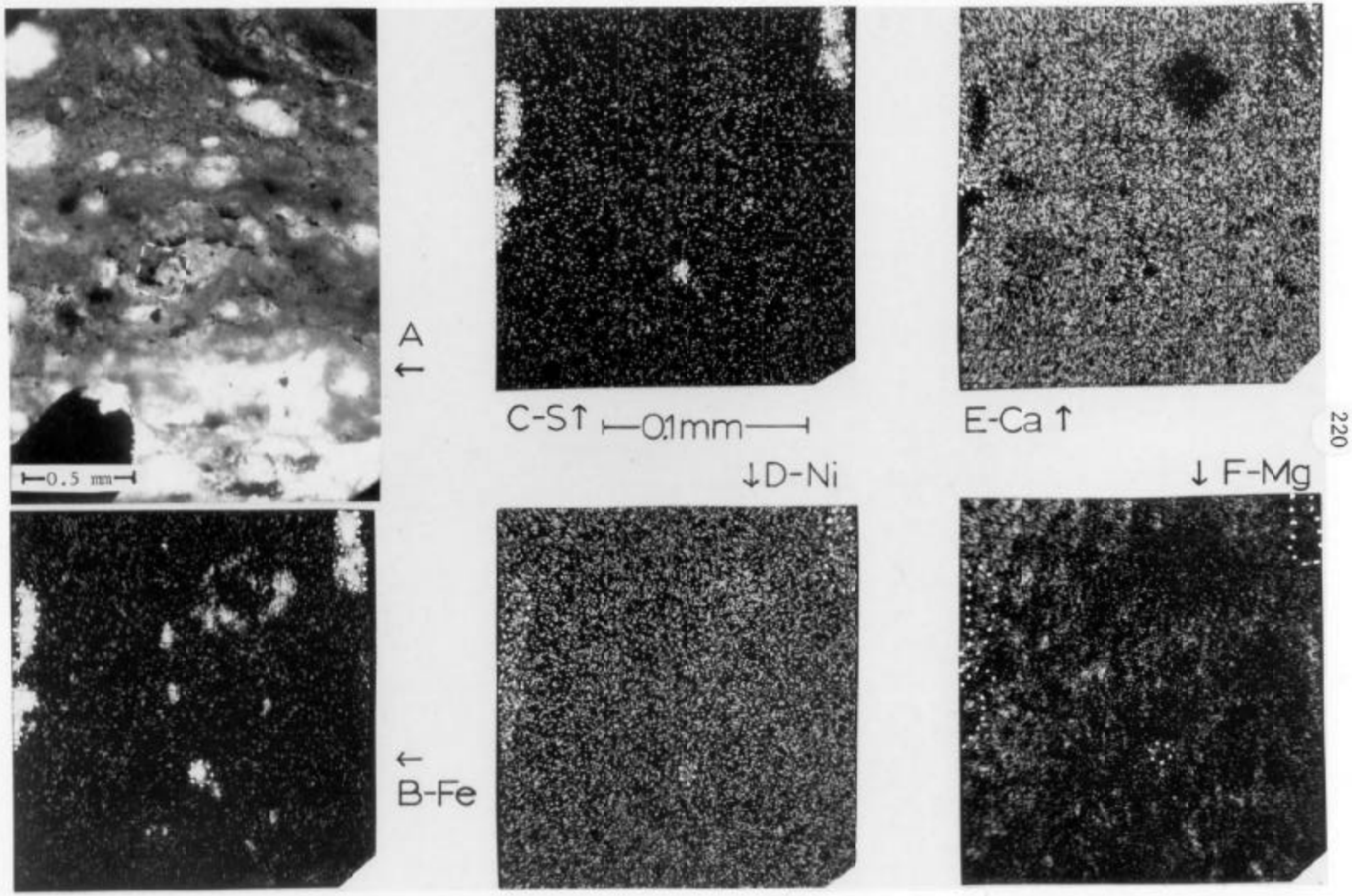

220

FIG. 15

FIGURE 15.

Nickeliferous Iron Sulfide
in the Matrix of the Grey Pseudotachylyte-Shocked
Anorthosite Breccia

A: Photomicrograph of part of Sample H in plane light. The scale is as shown. Most of the field contains dark grey, fine-grained matrix material with small, rounded opaques scattered throughout. Several ovoid and rounded grains are visible in the upper part of the field. The dashed white line outlines the area shown in the electron beam scan pictures. The black, irregular area in the lower left-hand corner of the picture is a microprobe identification mark.

B-F: Element maps of the area shown in Picture A: B -- iron; C -- sulfur; D -- nickel; E -- calcium; F -- magnesium. Scale is as shown under Picture C. Several iron-rich areas in Picture A and corresponding areas in other pictures are outlined with white dots. It can be seen that the small blebs in the matrix are basically iron sulfide. They contain a small amount of nickel. (Most of the Ni radiation in Picture D is background radiation, but the outlined areas are slightly richer in Ni.) The blebs contain very little calcium but may contain some magnesium.

UNIT #5

Sample #NT-4:Anorthositic Gabbro or Norite

In hand specimen, the rock appears as a fine- to medium-grained grey rock. It is composed of approximately equal amounts of medium-grained, greyish to slightly greenish plagioclase and medium-grained black pyroxene. Medium-grained garnet is present in some hand specimens. The rock has a "salt and pepper" appearance and is not noticeably gneissose, although a vague foliation due to bands of pyroxene is present.

In thin section, the rock is composed of about 35% fine- to medium- grained plagioclase, 30% fine- and medium- grained hypersthene, 2% fine-grained biotite, 1% oxides and trace amounts of apatite. The plagioclase is equant, anhedral and albite twinned It has a composition, An_{50-55}. The plagioclase grains are generally slightly bent and display undulatory extinction but no planar features or low-index patches. Numerous, small (10-20 μ), equant plagioclase grains occur along the boundaries of larger grains. The hypersthene is equant, anhedral and pleochroic from grey to red. Diopside is green, anhedral and equant. Quartz is anhedral and equant. It does not have undulatory extinction and displays no closely spaced, parallel fractures. Biotite is equant and elongate. Grains are not bent but occasionally display broad kinkbands.

This rock displays a granoblastic or granular texture. Plagioclase, hypersthene and diopside form a network of equant, interlocking grains. Small grains of plagioclase are almost invariably present along the edges of larger plagioclase grains. Occasional groups of quartz grains are found in the interstices of some plagioclase grains. The few biotite grains do not show a consistent direction of elongation, and the thin section shows no evidence of gneissosity. Most of the plagioclase grains show a gentle bending of their albite-twin lamellae and display some undulatory extinction. These features suggest that the rock has undergone tectonic shearing. This shearing may also be responsible for the kinkbands present in the biotite.

ORDOVICIAN LIMESTONE

Sample #12-8b

In hand specimen, the rock is a cream-to-buff, fine-grained limestone. In outcrop, the rock is moderately thickly bedded (a few inches); hand specimens appear massive. Most specimens show numerous fracture surfaces.

In thin section, the rock is seen to be an organic limestone consisting almost entirely of cryptocrystalline or microcrystalline calcite with a small amount of fine-grained quartz and potassium feldspar. The calcite is anhedral, clear and displays abundant twinning. Quartz is anhedral and granular with no planar features.

The rock consists mainly (about 90%) of a matrix of cryptocrystalline to microcrystalline, interlocking calcite grains and about 10% of 1- to 2- mm casts and shells of organisms replaced by more coarsely crystalline (50-100 μ) calcite grains. A few of the casts appear to be replaced by a single crystal of calcite. Most of the casts and shells appear unbroken, and the rock may therefore be an autochthonous limestone. A few of the casts contain parts which have been replaced by finely crystalline quartz, and a few spots contain some fine-grained, authigenic potassium feldspar.

The organisms present in the rock have been reported to be Middle Ordovician fauna and flora (Murtaugh and Currie, 1969).

Sample #2-32-A: Shock Breccia

In hand specimen, the rock is a breccia consisting of variable proportions of very fine-grained matrix and rock fragments ranging in size from 0.1 mm to several centimeters. The fragments are generally white , contorted and twisted ; bands of reddish microcline, greyish quartz and chalky plagioclase are visible in the larger fragments. The matrix is brick red.

The rock is relatively hard and competent, but it can be broken in the hands. The matrix is hard and compact but contains numerous small vesicles. The minerals in the rock fragments have a chalky luster, and individual grains are not discernible. A few black, elongate grains are visible in some of the larger rock fragments.

In thin section, as was obvious on the scale of the hand specimen, the rock is composed of two distinct textural elements: (1) the larger, lithic rock fragments; (2) the matrix and the small grains and fragments it contains.

A typical rock fragment contains about 50% medium- to coarse-grained quartz, 25% fine- to medium- grained orthoclase, 20% fine- and medium- grained plagioclase and about 5% elongate opaques.

Quartz is tan to brown, lensoid, anhedral and displays undulatory extinction. Grains are birefringent and contain no visible planar features; some grains have a variable index of refraction and contain clumps of minute bubbles. Orthoclase is equant and anhedral. Grains are clear but contain abundant, 20μ

rounded inclusions which appear opaque (These may be bubbles.). Some of the grains contain elongate, 5 μ x 50 μ blebs of higher-index plagioclase. Plagioclase is anhedral and equant or elongate. Grains are clear and contain no visible albite twinning. Many grains contain opaque, rounded inclusions as in the orthoclase; in some cases, grains contain parallel strings of minute, opaque inclusions arranged in a manner suggestive of planar-feature decorations. The plagioclase has anomalous optical properties but an index which is about equal to quartz. Some grains are isotropic, but most are birefringent and have very small, negative $2V\alpha$. The latter are difficult to distinguish from orthoclase, and some orthoclase may be misidentified. The opaque grains are elongate, anhedral and very frequently show irregular arms extending out among the interstices of surrounding grains. These opaques may be pseudomorphous after original hornblendes.

The texture of the rock fragments is granoblastic to gneissic. Nearly continuous bands of elongate quartz grains with minor plagioclase alternate with 2- to 3- mm bands containing predominantly orthoclase and plagioclase. The opaque grains tend to occur in bands with their long directions parallel to the quartz elongation.

In thin section, the matrix material consists of about 50% of aphanitic, dark-to-opaque, low birefringence material and about 50% of both rounded and angular, fine- and medium-grained mineral grains and small fragments of rock. The matrix material is too fine grained to be identified. In reflected light, a few 10 μ anhedral, rounded grains of reflective material are discernible. The grains and fragments in the matrix have a low index and are mostly tannish, anhedral quartz, anhedral plagioclase and orthoclase; also included are a few 1- to 2- mm quartz-plagioclase-orthoclase rock fragments. Grains of the minerals present in the matrix generally have the same appearance as in the rock fragments. Planar features are not apparent in these grains, and most of the smaller grains are not severely contorted. The smaller rock fragments, by contrast, are often severely bent and distended.

The matrix has a poorly sorted clastic texture. The aphanitic matrix material envelops more-or-less randomly distributed, rounded and angular fragments and grains which range from about 20 μ up to 2 mm in size. The matrix also contains large numbers of 10-50 μ vesicles.

Sample #16-7-4:
Anorthosite Hornfels

In hand specimen, the rock is a fine-grained, grey, white and black gneiss. The majority of the rock is composed of very fine-grained or aphanitic grey and white plagioclase. Bands of fine- to medium- grained, black garnet pseudomorphs extending through the rock define a foliation. The rock does not appear to have flowed extensively since the bands of garnet pseudomorphs appear unbent. This rock is extremely hard and breaks only with great difficulty.

In thin section, the rock is composed of about 75% fine-grained plagioclase, 15% opaques pseudomorphous after fine- to medium- grained garnet, 5% fine- and medium- grained diopside, 3% opaques pseudomorphous after fine- and medium- grained hornblende, 2% medium- grained sphene and minor apatite, epidote, zeolite and relict scapolite(?).

The texture of the rock is gneissic. Fine-grained plagioclase forms a granoblastic matrix which contains bands of diopside and opaques pseudomorphous after garnet and hornblende. The granoblastic plagioclase matrix consists of 0.5- to 1- mm domains of small plagioclase grains. These domains are pseudomorphous after plagioclase grains in anorthosite from the central massif. The texture of the rock is illustrated by the photomicrographs in Fig. 13.

Plagioclase: The small crystallites of plagioclase which comprise the larger domains include equant, 5-20 μ grains as well as elongate, 10 x 30 μ grains. Some elongate grains are carlsbad

twinned. Small grains within the domains tend to go to extinction simultaneously so that outlines of the larger grains are readily apparent under crossed polarizers. The larger grains are probably relicts of grains in the rock before it was heated. Several domains of smaller grains are outlined in Fig. 13. Vague remnants of albite twinning can be seen in a few of the domains, and one or two large grains appear to contain relict planar features.

Diopside: Greenish, elongate diopside, 0.1 x 0.2 mm up to 0.5 x 1 mm, occurs in the opaque bands along with garnet pseudomorphs. The larger diopside grains generally consist of a single, unfractured crystal with uniform extinction. Small grains are frequently aggregates of granules. Both large and small grains contain numerous, 10 μ, rounded inclusions of opaque material.

Opaques Pseudomorphous After Garnet: Several opaque grains, pseudomorphous after fine- to medium- grained, subhedral or euhedral garnet are apparent in Fig. 13. On a fine scale, the garnet pseudomorphs consist of a matrix of greenish or greyish material which encloses 5-20 μ, rounded granules of opaque or nearly opaque material. A garnet pseudomorph was electron-beam scanned, and the opaque granules were found to be comprised of an iron-magnesium silicate containing very little calcium or aluminum. The exact chemical composition of the granules was not determined. The matrix of the garnet pseudomorph is a calcium-aluminum silicate. Decomposition products of the garnet in the anorthosite hornfels differ from garnet decomposition products in the highly shocked

anorthosites. These latter are iron rich but silicon and magnesium depleted (Figs. 11 and 14).

Opaques Pseudomorphous After Hornblende: Some of the opaques have rounded, elongate shapes reminiscent of hornblende from other anorthosites. These grains are composed of 20 μ opaque granules in a dark grey or black matrix. The hornblendes are found in mafic bands with diopside and garnet pseudomorphs.

Other Data: The bulk chemical composition of a sample of the anorthosite hornfels is shown in Table 5. Comparison of the hornfels composition with chemical compositions of both shocked and unshocked anorthosite (Tables 1 and 2) shows that the hornfels is compositionally very similar to anorthosites from other parts of the massif. This fact supports the conclusion, already made on the basis of relict textures in the hornfels, that this rock was originally an anorthosite. The rock was heated and nearly totally recrystallized during the cooling of the monzonite. The total iron content of the hornfels is about the same as other anorthosites in the crater, but the hornfels has a higher Fe^{+3}/Fe^{+2} ratio than fresh anorthosites. The high Fe^{+3}/Fe^{+2} ratio suggests that heating of the anorthosite block was a surface or near-surface process in which oxidizing conditions prevailed.

The presence of a few possible relicts of shock features suggests that the rock had been shocked metamorphosed prior to its recrystallization.

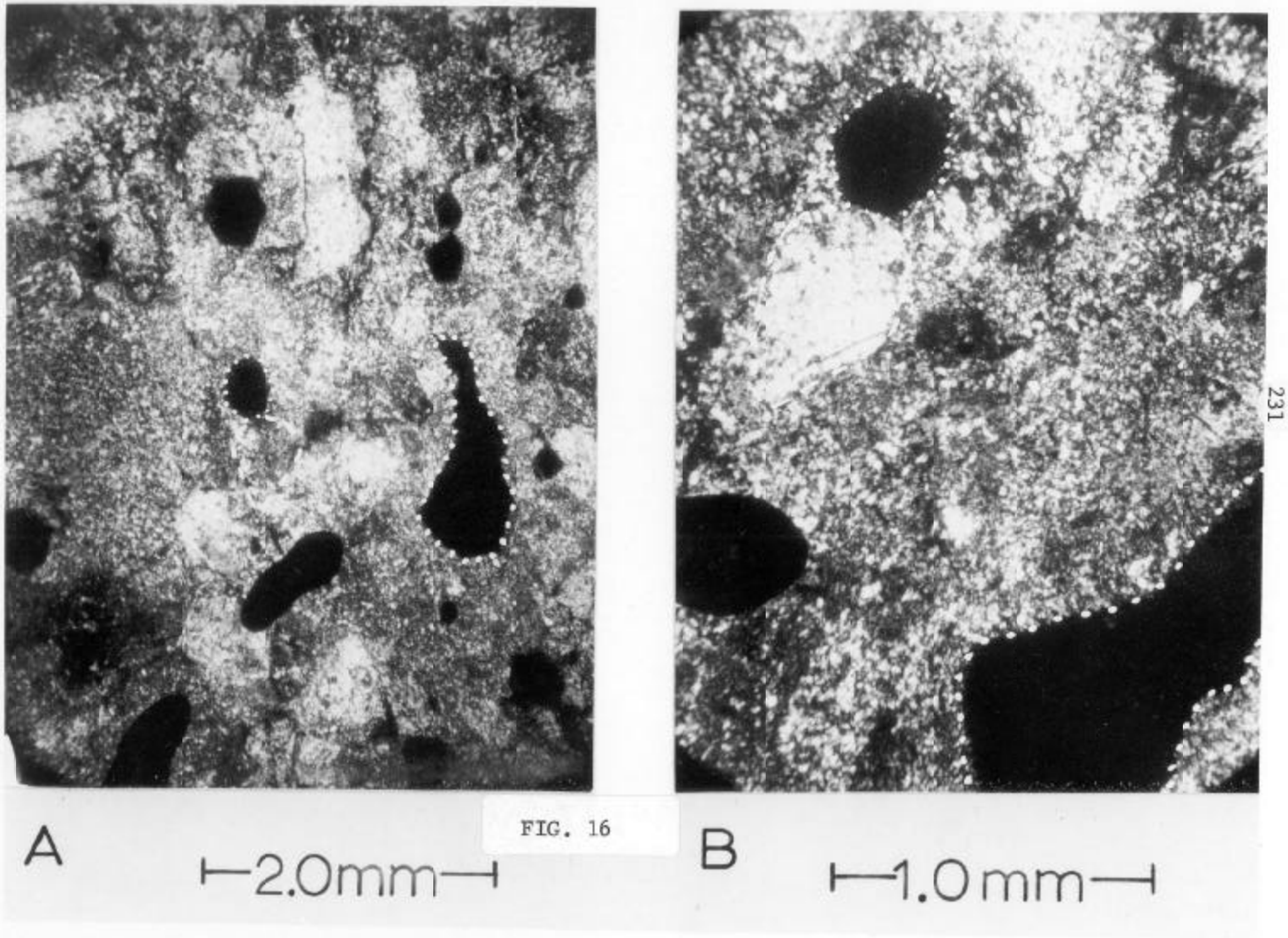

FIG. 16

FIGURE 16.

Mosaic Structure of Plagioclase from the Anorthosite Hornfels

A: Broad-scale photomicrograph (under crossed polarizers) of the anorthosite hornfels. The euhedral black grains, two of which are outlined with dots, are garnet pseudomorphs. The dashed line outlines a plagioclase grain which appears as a granoblastic aggregate of plagioclase granules. More obvious macro-grains are also visible below the outlined grain. (The elongate, black, paramecium-shaped form below the white-outlined plagioclase is a microprobe identification mark.).

B: Photomicrograph of part of the field shown in A under crossed polarizers. The slide orientation is somewhat different than in A, and the magnification is about twice as large. The plagioclase granules in the outlined grain are seen to have more-or-less uniform optical orientation. This suggests that the granules are parts of one original grain. Garnet pseudomorphs are again outlined with dashes.

MEDIUM-GRAINED SUB-UNIT OF THE MONZONITE

Sample #5-32-1

Hand Specimen:

In hand specimen, the material is a massive, fine- to medium-grained, dark grey or black rock. It is composed predominantly (about 70%) of medium-grained, dark grey or greenish-gray plagioclase. Approximately 30% of the rock appears to consist of fine- and medium- grained, black pyroxene prisms. Most outcrops of this material have a dark brown, crumbly, weathering crust developed on them.

Thin Section:

In thin section, the rock contains about 35-40% of medium-grained, albite- and Carlsbad-twinned plagioclase laths; about 25-30% of medium-grained, anhedral sanidine; about 25% of medium and (rarely) coarse-grained, subhedral, clear augite; and 5% of greyish pigeonite and hypersthene. About 3-5% of the mode consists of medium-grained, anhedral quartz, and 1-2% of the mode consists of opaque magnetite, or ilmenite, and magnetite-ilmenite intergrowths. Between 0 and 5% of the mode consists of fine- or medium- grained, fibrous, dark green or brown, altered pigeonite and hypersthene. Apatite is present in trace amounts.

The rock is holocrystalline with an approximately microgranitic texture. About 30% of the rock consists of 1-2 mm of subhedral augite which subophitically encloses unrimmed plagioclase laths. About 60% of the rock is made up of an intergranular matrix of

0.5-x 1-mm plagioclase laths which are rimmed by a 0.5-mm thick mantle of sanidine. Interstitial to the rimmed laths, small, 0.5-mm grains of pigeonite and hypersthene, magnetite and magnetite-ilmenite intergrowths, and 1-mm, irregular intergrowths of quartz and sanidine occur. About 10% of the rock consists of the interstitial phases; 0.5 - 0.5 mm hypersthene and pigeonite occur on the edges of augite grains.

The texture and mineralogy of this rock is very similar to a tholeiitic diabase, although the amount of potassium-feldspar found in this rock is much greater than is normally observed in diabases. The K_2O content of this rock (Table 4) is about 3.2% as opposed to a more normal diabase potassium content of less than 1%. The SiO_2 content of the total rock is about 59%, and this is fairly more siliceous than the typical 48-52% SiO_2 observed for tholeiitic basalts and quartz diabases (Turner and Verhoogen, 1960). Since the K_2O content and SiO_2 contents of this rock are closer to those of a monzonite than those of a diabase, it is referred to as a monzonite even though its texture and mineralogy are closer to that of a tholeiitic diabase.

Fig. 17 is a sketch showing the major textural features of the monzonite.

Plagioclase:

Plagioclase laths (0.25 x 0.5 mm up to 0.5 x 1.5 mm in size) occur as the cores of rimmed feldspars which make up the rock matrix. Unrimmed plagioclase laths of this same size are also subophitically

GENERALIZED VIEW
OF SAMPLE #5-32-1
THE MONZONITE

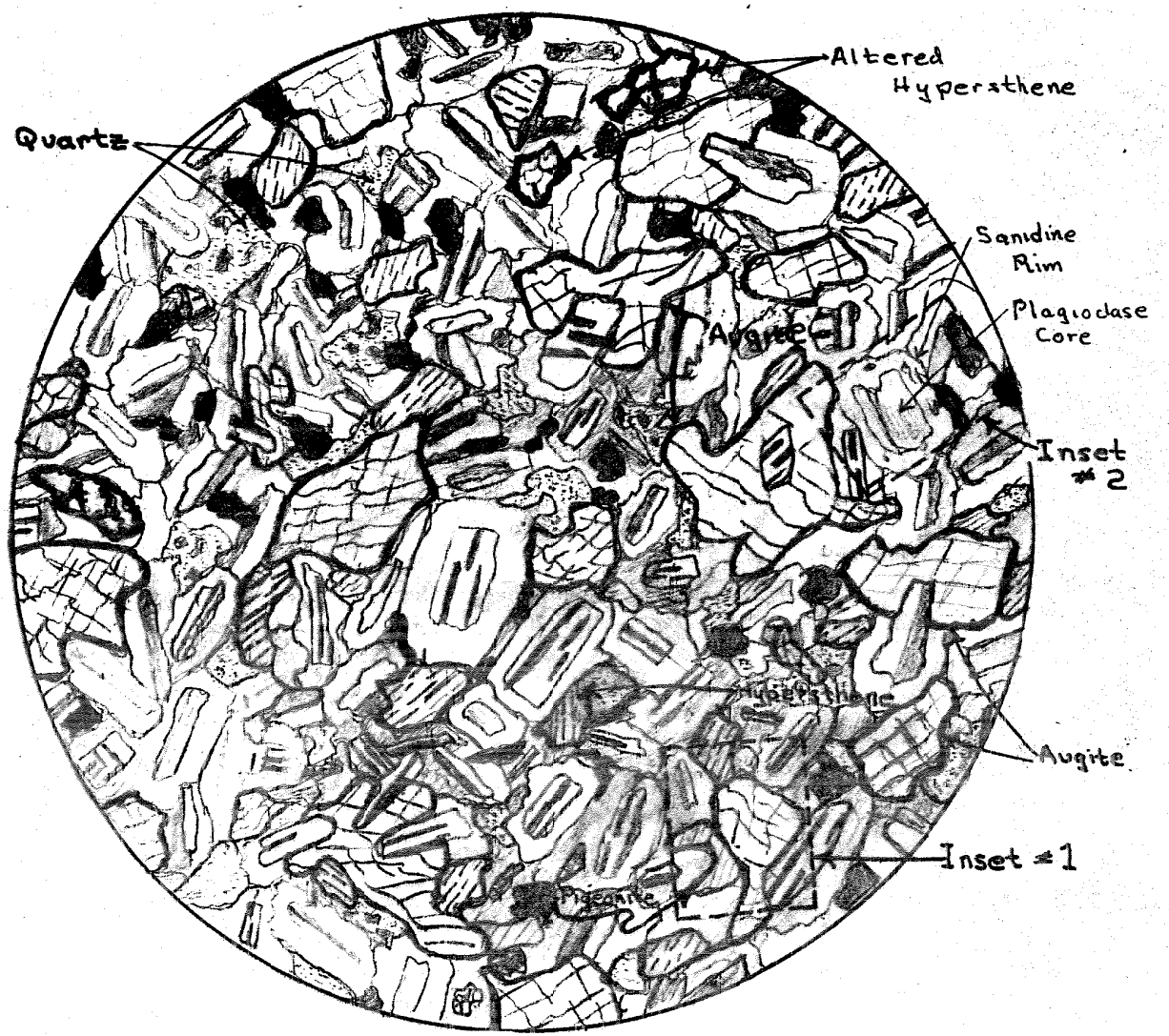

FIG. 17

1 mm

enclosed in augite. A typical, rimmed feldspar lath is shown in Fig. 18. The plagioclase cores have a composition of An_{48-58} and display well-defined Carlsbad and albite twinning. Cores of plagioclase show a gradual zonation from about An_{58} at their centers to about An_{48} near the edge. The composition then shows an abrupt change to the composition of the sanidine which envelops the core. Laths of plagioclase which are subophitically enclosed in augite have compositions of An_{50-54}. They are slightly more sodic at their edges (Table 4).

Sanidine:

The plagioclase laths have an overgrowth of sanidine. The rim of a typical grain is shown in Fig. 18. The sanidine varies somewhat in composition. Near the boundary with the plagioclase lath it is about $An_5Ab_{48}Or_{47}$, while on the outer extremities of the rim it is about $An_2Ab_{28}Or_{70}$. An analysis for some of the potassium-rich sanidine is given in Table 4. Highly potassic sanidine also occurs in grain aggregates with quartz.

Quartz:

Irregular, 0.5 - 0.8 mm grains of quartz are found in the interstices of the matrix of rimmed plagioclase grains. Quartz grains in the interstices are generally associated with irregular, 0.2-mm grains of highly potassic (Or_{70}) sanidine.

Subcalcic Augite:

Anhedral or subhedral, 0.9 - 1.5 mm grains of neutral or slightly pale brown augite which subophitically enclose unrimmed plagioclase laths are the main pyroxene phase. A microprobe analysis of one of these grains, given in Table 4, indicates a composition of $Wo_{.35}En_{.45}Fs_{.15}$, with about 4% of the tetrahedrally coordinated silicon replaced by aluminum. The edges of the grains which sometimes appear stained are about 2% richer in iron than the grain centers. Augite grains are often in contact with hypersthene and pigeonite grains, and these latter generally have the same optical orientation as the augite grains they grow on. Electron beam scan photographs of augite grain contacts with hypersthene and pigeonite are shown in Fig. 19. It can be seen that there is an abrupt transition in composition across the boundary of the two phases.

Hypersthene:

Irregular, 0.3-0.5 mm grains of clear hypersthene are found either interstitial to rimmed plagioclase laths or on the edges of augite grains. Electron beam scan photographs of part of a hypersthene grain are shown in Fig. 19. The parallel, dark streaks visible in the grains appear to be exsolved lamellae of calcium pyroxene. A microprobe analysis of a hypersthene grain is given in Table 4; the composition is about $En_{.58}Fs_{.38}Wo_{.03}$ with about 1% of the tetrahedral silicon replaced by aluminum.

Pigeonite:

Irregular, 0.3-0.5 mm grains of clear pigeonite which closely resemble hypersthene are present. In most cases these can be distinguished from the hypersthene by their nearly uniaxial, optic axis figure. The pigeonite occurs both interstitially to the mantled plagioclase laths and in contact with augite grains. Electron beam scan pictures of a pigeonite grain are shown in Fig. 19. Calcium-rich lamellae occur in this material as in the hypersthene. A microprobe analysis of a pigeonite grain is given in Table 4. The pigeonite has a composition of $En_{.55}Fs_{.39}Wo_{.04}$ which is very similar to that of the hypersthene. For this reason, the hypersthene in this rock is believed to be inverted pigeonite.

Oxides:

Small, 0.1-0.5 mm opaque grains are frequent accessory minerals. In reflected light, these are seen to be ilmenite, magnetite, and magnetite with exsolved lamellae of ilmenite.

Two bulk chemical analyses of these rock are given in Table 4. One analysis is for the sample discussed here (location #1); the other analysis is for a coarse-grained monzonite located 20 miles to the south. The similarity of the chemical compositions is apparent; none of the oxide values for the two samples differ by more than the uncertainties claimed by the analyst. The potassium values implied are 2.64 and 2.74%.

These are somewhat below the values of 2.79 and 2.77 obtained for these two samples by the isotope dilution techniques. The isotope dilution measurements of potassium are between the upper and lower limits for potassium which the analyst gives.

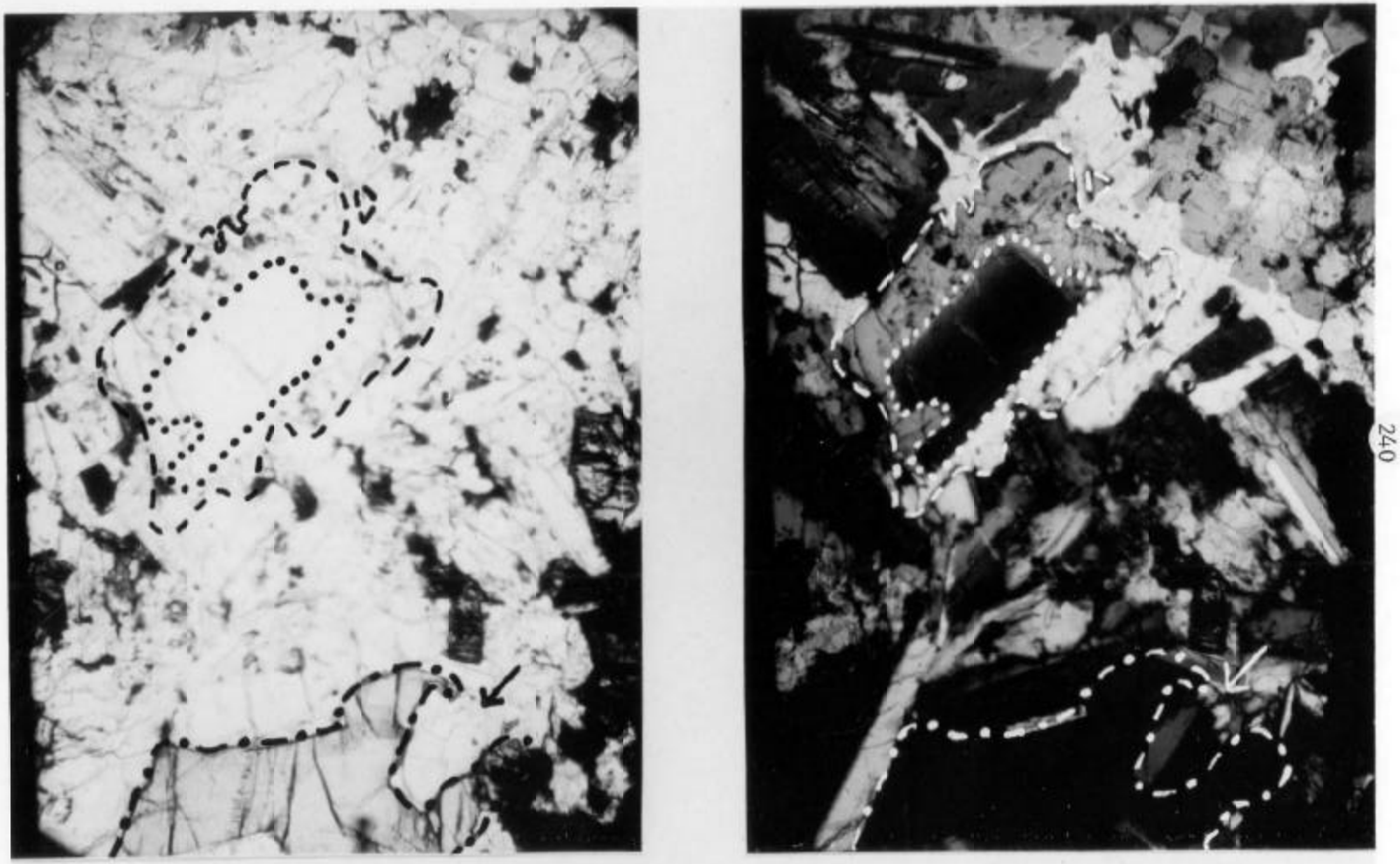

FIG. 18

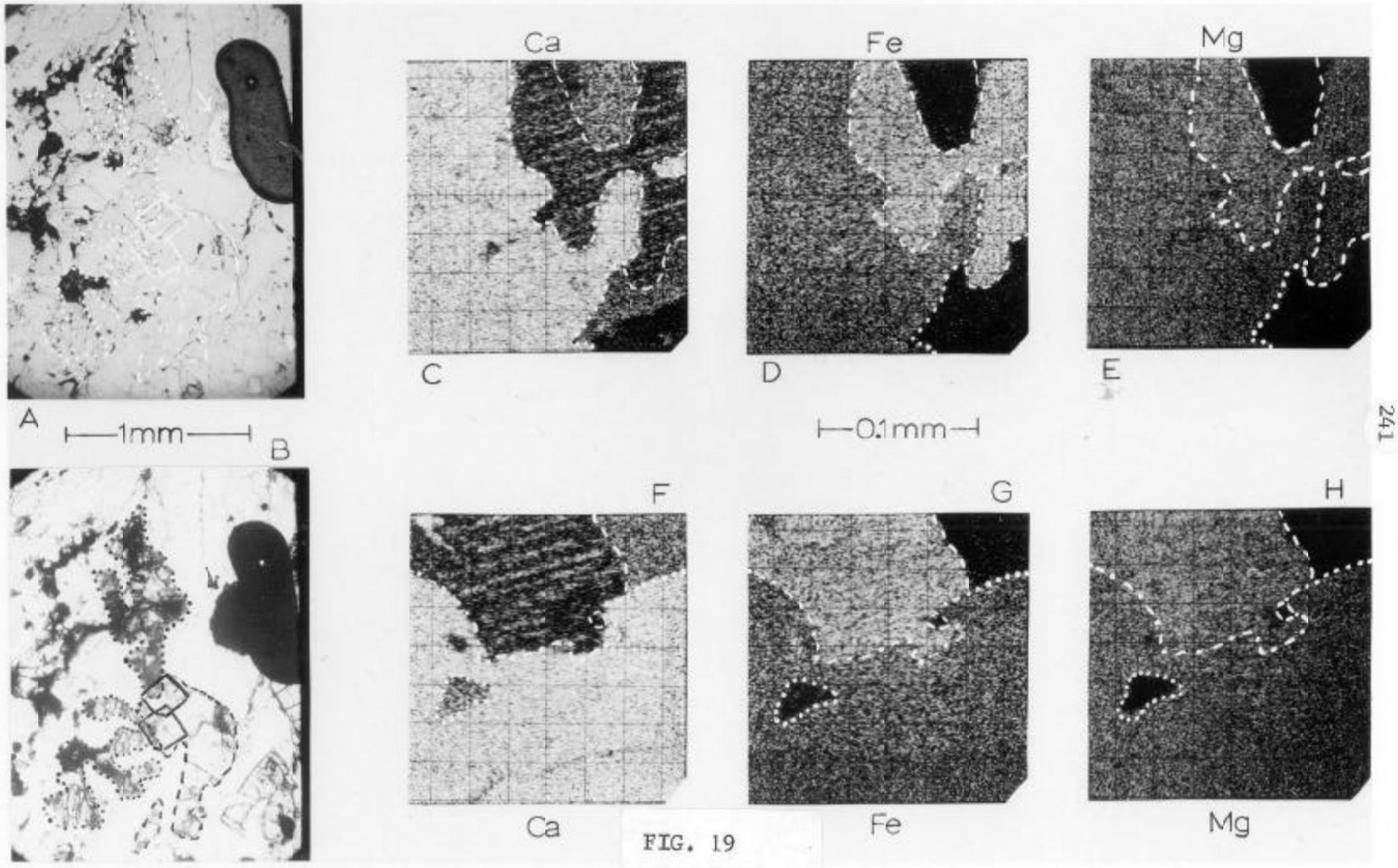

FIG. 19

FIGURE 18.

Rimmed Plagioclase in the Monzonite

A: View of inset 1 (Fig. 16) in transmitted light. Dotted line outlines the calcic core of a rimmed plagioclase grain. Dashed line outlines the edge of the sanidine rim. Dots and dashes outline an augite grain in the lower part of the picture. Note that the core of the rimmed grain is cleaner, i.e. it has less included material than the rimming feldspar.

B: View of inset 1 (Fig. 16) under crossed Nicols. Patterns are the same as in A. The Carlsbad twin plane of the plagioclase core lies approximately in the plane of the photo so that this core, even though it is twinned, appears to have only one optical orientation. Note that the rimming sanidine has two orientations. The different orientations of the rim are aligned with the different orientations of the Carlsbad twin members in the core. A small, unrimmed, twinned plagioclase is partly enclosed by augite (indicated by arrow).

FIGURE 19.

Coexisting Pyroxenes in the Monzonite

Scale for A and B as shown. Scale for all other pictures is as shown under picture D.

A and B: View of inset 2 in reflected light and under crossed Nicols, respectively. Arrow points to a magnetite-ilmenite grain. The foot-shaped dark area is a microprobe reference mark. Augite is outlined with dashes; hypersthene and pigeonite are outlined with dots. The small, square, solid white outlines mark the areas scanned with electron beam scans. The lower square outlines a field which includes the boundary of the augite grain with a pigeonite grain. Beam scans for this field are shown in pictures C, D, and E. The upper solid outline marks a field which includes a hypersthene-augite boundary. Beam scans for the upper field are shown in pictures F, G, and H.

C - E: Element maps of lower outlined field. C, calcium radiation; D, iron radiation; E, magnesium radiation. Note that the chemical compositions change abruptly across the pigeonite-augite boundary rather than changing gradually. Lamellae of calcium-rich pyroxene, exsolved from the pigeonite host, are visible in picture C. In pictures C - E, dashes outline the pigeonite grain, dots mark the edge of the hypersthene grain. Contact between the two phases is marked by dots and dashes. Dark areas visible in pictures D and E are feldspars in contact with the pigeonite.

F - H: Pictures F, G, and H are electron beam scans of the area outlined by the upper square in pictures A and B. F, calcium radiation; G, iron radiation; H, magnesium radiation. Augite is outlined with dots; hypersthene with dashes. The contact between the two phases appears as a dot-dash line. Exsolved lamellae of calcium-rich pyroxene in the hypersthene are visible in picture F. These lamellae appear as strings of fine inclusions in picture A. A similarity in chemical compositions of hypersthene and pigeonite in this rock can be inferred from pictures C - H. This similarity is apparent in Table 4.

For all the electron beam scan pictures, the field shown in A and B is a mirror image of the element maps shown. The mirror plane in all cases goes through the left hand edge of the beam scan picture. The upper right edge and the slant-cut corner of the outlines shown on pictures A and B correspond respectively to the left-hand edge and slant-cut corner of the beam scan picture.

TABLE 4.

Chemical Analyses of Materials Associated with the Monzonite[+]

Oxide	(a) Plagioclase Cores (avg.)	(b) Plagio-clase in Augite	(c) Sanidine Potassic Matter	(d) Augite	(e) Hyper-sthene	(f) Pigeon-ite	(g) Loc. 1 Medium Grain	(h) Loc. 4 Coarse Grain	(i) Errors
SiO_2	55.3 ±1	55.5 ±1	65.8 ±1	52.0 ±2	52.9 ±1	53.1 ±1	59.5	59.0	0.5
Al_2O_3	28.8 ±1	28.1 ±2	19.2 ±1	1.76 ±3	0.53 ±20	0.53 ±20	15.8	16.0	0.3
CaO	11.2 ±3	10.8 ±2	0.32 ±20	18.7 ±2	1.82 ±20	2.30 ±7	5.5	5.3	0.3
Na_2O	5.12 ±3	5.19 ±4	3.36 ±3	--	--	--	3.6	3.8	0.2
K_2O	0.46 ±7	0.52 ±8	11.9 ±2	--	--	--	3.2	3.3	0.2
MgO	--	--	--	16.1 ±2	21.1 ±2	19.6 ±5	3.2	3.5	0.3
FeO	--	--	--	10.3 ±2	24.2 ±2	24.6 ±5	1.7	1.9	0.2
TiO_2	0.72 ±30	0.09 ±20	0.08 ±30	0.57 ±10	0.30 ± 10	0.36 ±8	0.65	0.75	0.2
MnO	--	--	--	--	--	--	0.09	0.10	0.02
SO_3	--	--	--	--	--	--	--	--	--
P_2O_5	--	--	--	--	--	--	0.24	0.24	0.05
Fe_2O_3	--	--	--	--	--	--	4.4	4.4	0.2
H_2O	--	--	--	--	--	--	1.8	1.6	0.2
Total	100.9	100.2	100.7	99.4	100.9	100.5	99.68	99.89	

(TABLE 4. -- continued)

+ Oxides as wt. %. ± values indicate standard deviation from mean V (in %).

(a) Indicated composition: $Ab_{.441}$ $An_{.533}$ $Or_{.026}$.

(b) Indicated composition: $Ab_{.451}$ $An_{.519}$ $Or_{.030}$.

(c) Indicated composition: $Or_{0.689}$ $Ab_{0.295}$ $Ca_{0.016}$.

(d) Indicated composition:

$$(Ca_{0.355}\ Mg_{0.448}\ Fe_{0.161})\ SiO_3 \cdot (CaAl_{0.023}CaTi_{0.016})(Si_{0.5}Al_{0.5})O_3.$$

(e) Grain is in contact with the augite grain for which the analysis is given. Composition indicated is:

$$(Mg_{0.584}\ Fe_{0.377}\ Ca_{0.031})SiO_3 \cdot (CaAl_{0.003}CaTi_{0.009})(Si_{0.5}Al_{0.5})O_3.$$

(f) Grain is in contact with augite grain for which analyses are given. Composition indicated is:

$$(Mg_{0.549}\ Fe_{0.387}\ Ca_{0.040})SiO_3 \cdot (CaAl_{0.002}CaTi_{0.010})(Si_{0.5}Al_{0.5})O_3.$$

(g) Bulk analysis, sample location #1 (Fig. 3, Chapter 1, Part I.). Values are for this sample, the medium-grained monzonite.

(h) Bulk analysis values for a coarse-grained sample of the monzonite; map location #4 (20 miles south of location #1).

(i) Errors for bulk analyses in absolute percent. Analyses by M. Weibel, ETH, Zurich, Switzerland. Financial support by National Aeronautics and Space Administration Contract NAS 9-8074 and National Science Foundation Grant GA -12916 awarded to G. J. Wasserburg.

FINE-GRAINED SUB-UNIT OF THE MONZONITE

Sample #31-19-2A

In hand specimen, the rock is very fine grained, massive and black, containing a few vesicles. The rock is too fine grained to distinguish minerals in hand specimen, but a few whitish phenocrysts are visible.

In thin section, the rock is composed of about 70% groundmass and about 30% phenocrysts. The phenocrysts consist of about 50% fine- to medium- grained plagioclase, 35% fine-grained augite granule aggregates, 10% fine-grained diopside, 5% fine-grained opaques and 1% quartz-sanidine intergrowths. The groundmass of the rock consists of about 50% of an intergrowth of fine-grained plagioclase and sanidine, 35% fine-grained augite, 10% fine-grained oxides and about 5% fine-grained pigeonite.

The plagioclase phenocrysts are equant, anhedral and range in size from about 0.1 - 0.5 mm. They usually show albite twinning, and most grains contain numerous inclusions of rounded, 1-2 μ opaques. None of the phenocrysts observed displayed planar features or contained partially isotropic regions. The composition of the plagioclase phenocrysts is about An_{45-50}. The augite clumps are rounded and consist of numerous 2 x 10 μ to 5 x 20 μ, subhedral augite granules. The cores of some of these clumps contain rounded, anhedral quartz or quartz-sanidine intergrowths. The augite phenocrysts are anhedral and equant.

Oxides are generally subhedral.

Augite in the groundmass is subhedral and elongate, about 5 x 50 μ. The optical properties of the augite grains are difficult to determine, and some pigeonite may be misidentified as augite. Some pigeonite is present in the groundmass as equant, anhedral grains. The oxides are equant and subhedral. Feldspar in the groundmass is an intergrowth of plagioclase and sanidine. Laths (2 x 10 μ) of plagioclase are surrounded by sanidine, but the relative proportions of sanidine and plagioclase are difficult to determine.

The texture of the rock groundmass is intergranular. Laths and small grains of pyroxene are randomly oriented and evenly distributed throughout the matrix of intergrown feldspars. The phenocrysts are randomly distributed throughout the groundmass.

A chemical analysis of this rock is shown in Table 5. It can be seen that this rock is chemically quite similar to rocks from the medium-grained and coarse-grained sub-units, apart from the fact that it has a slightly higher CaO content. This rock contains a very small amount of Fe_3O_4 in the norm, according to this analysis. This is indicative of oxidizing (although not extreme) conditions during its formation.

Sample #13-8

In hand specimen, the rock is massive, black and aphanitic. Some vesicles and a few 1 mm - 1 cm whitish inclusions are visible with the naked eye.

In thin section, the rock consists of 70% cryptocrystalline, dark grey groundmass, about 20% fine- to medium- grained mineral fragments, and 10% of 3- to 10 - mm rock fragments. The mineral fragments consist mostly of anhedral plagioclase. Some grains are clear and display albite twinning but no planar features. Other grains are dusty brown and contain isotropic patches and planar features. Some mineral grains in the matrix are greenish, fractured pyroxene. A few grains of tannish quartz with several sets of planar features are also present. Some of the rock fragments contain clear, relatively unfractured minerals with no planar features or low-index areas. These rock fragments are unrecrystallized. Other rock fragments contain tannish grains with low birefringence or isotropic areas and frequent planar features. These latter rock fragments often contain recrystallized mosaic grains. Rock fragments are generally rimmed by a thin layer of greenish isotropic material; the fragments are generally quartz-plagioclase-garnet or plagioclase-garnet-pyroxene rocks.

The rock has a porphyritic texture with minerals and rock fragments randomly distributed throughout the fine-grained groundmass.

A chemical analysis of this rock is shown in Table 5. It is clear that the rock is chemically very similar to other members of the monzonite unit (see Table 4).

TABLE 5.

Chemical Compositions of Rocks Associated with the Fine-Grained Monzonite*

Wt. % Oxide	#16-7-4	#31-19-2A	#13-8
SiO_2	53.9	58.5	56.6
Al_2O_3	27.2	15.5	15.8
CaO	10.3	7.2	5.9
Na_2O	4.8	3.4	3.3
K_2O	0.55	3.2	3.0
MgO	0.7	3.7	4.6
FeO	0.6	3.5	3.4
TiO_2	0.12	0.9	0.75
MnO	0.02	0.1	0.1
Fe_2O_3	0.55	2.5	2.8
H_2O	1.2	1.2	3.6
P_2O_5	0.02	0.20	0.18
Total	100.0	99.9	100.0

* Chemical analyses performed by M. Weibel, E.T.H., Switzerland. Financed by grants awarded to G. J. Wasserburg (National Aeronautics and Space Administration Contract NAS 9-8074 and National Science Foundation Grant GA-12916). Values shown are weight percent of the indicated oxide; estimated errors in these values are the same as shown in Table 1, column g.

DETAILED OUTLINE OF PART II

Detailed Outline of PART II -- Continued.

Detailed Outline of Part II -- Continued.

Detailed Outline of Part II -- Continued.

Detailed Outline of Part II -- Continued.

Detailed Outline of Part II -- Continued.

Detailed Outline of Part II -- Continued.

Detailed Outline of Part II -- Continued.

Detailed Outline of Part II -- Continued.

Detailed Outline of PART II -- Continued.

CHAPTER 1

Geochronology of the Manicouagan-Mushalagan Lakes Structure

Introduction:

Statement of the Problem --

In a Nutshell: The question focused on in this study is briefly: What is the geological history of the Manicouagan-Mushalagan Lakes structure ; how are the shock-metamorphosed rocks present in the structure related to the igneous rocks which occur in the structure?

Observations: The geological studies discussed in PART I of this thesis lead to the following conclusions:

(1) That the basement rocks which underlie the monzonite have been shock metamorphosed, and that some presently observed rocks have been shocked severely enough to produce partial melting. The presence of shock-metamorphosed rocks implies that the area has been impacted by an extraterrestrial hypervelocity body.

(2) The monzonite, which is limited to the interior of the two lakes, shows every sign of having crystallized from a completely molten material. The main mass of this igneous ($\equiv$ as crystallized from a melt) material contains no features ascribable to shock metamorphism. The lower 50-75 feet of the rather flat-lying body contain recognizable inclusions of basement rocks, many of which have been shocked. The majority of rocks from this unit (referred to in this work as the monzonite), however, show no planar features, isotropic phases, or unusual fracturing.

The monzonite has few counterparts in other areas of Grenville Province. It is not obviously related to the basement complex of gneisses, anorthosite, and gabbroic anorthosite, all of which occur elsewhere throughout Grenville Province.

(3) The monzonite and the shocked rocks are very intimately juxtaposed; rocks which show visible shock effects are found only in the circular area covered by the monzonite (see Fig. 2, CHAPTER 1, PART I). The close spatial relation of the monzonite and the shock-deformed rocks strongly suggests that some genetic relation exists between these two rock types.

Theories of Formation: Three modes of formation for this "igneous" material have been suggested, each of which implies a different geological history for the crater:

(1) That shock breccia, which collected in the crater during impact, possessed sufficient thermal energy to remelt the entire mass. Subsequent crystallization then produced the "igneous" material.

(2) That an extrusive or shallow intrusive mass resulted when the meteorite impact "triggered" or induced later volcanic activity at the crater site.

(3) That explosive magmatic activity took place, as suggested by Currie (1965). This "cryptoexplosion" hypothesis has been suggested by many others (e.g. Branco and Fraas (1905); Bucher (1963)) as a mode of origin for other crater-like structures.

Age Relations: It is obvious that a knowledge of the age relations of the shocked basement rocks and the monzonite at Manicouagan would be useful in determining the history of events in this structure. In an attempt to clarify these age relations, a geochronological study has been undertaken in this thesis research.

In order to unambiguously define the history of this structure, one should know (a) when the shock deformation took place and (b) when the monzonite formed. Ideally, one would hope to obtain absolute ages for these events. Whether or not a time difference exists between the events would be clearly indicated, and the most likely history of crater formation could be ascertained.

Method of Attack --

To determine the time of crystallization of the monzonite body, the monzonite itself and mineral-enriched fractions derived from it were analyzed for argon and potassium. Potassium-argon ages were then determined for the rock and its component minerals. The mineral ages determined help clarify the extent to which the whole-rock age is affected by inherited argon and give some suggestion as to the post-crystallization history of the body. The whole-rock monzonite was also used as the monitor in the Ar^{40} - Ar^{39} portion of this study, and the results of stepwise extractions confirm the simple history suggested by the mineral ages. Potassium-argon ages were also determined for the shock breccia underlying the monzonite and for an anorthosite hornfels found as a large block inclusion of anorthosite in the lower

monzonite layers. The ages of the latter units further clarify the monzonite history. Rocks associated with the monzonite are referred to as Group I rocks.

In order to determine the time of shock metamorphism, a series of rocks was chosen from the anorthosite massif. These rocks ranged from unshocked to nearly shock molten, and their potassium-argon ages were determined. The anorthosites were chosen because:

(1) They displayed a wide range of shock effects.

(2) They exhibited no visible signs of purely thermal alteration (e.g., oxidation or recrystallization and melting at grain boundaries).

(3) The homogeneity and approximately mono-mineralic nature of the rocks from this body minimized effects due to differing mineralogy, grain sizes or chemical composition. These are the rocks of the "shock sequence" which are labeled as Group II rocks. It was hoped that the most highly shocked rocks in this sequence, which should also be the rocks most thoroughly outgassed during the shock-metamorphic event, would yield ages converging on the time of shock metamorphism.

Three of the shock sequence rocks, including the mildly shocked (150 kb) anorthosite, the maskelynite anorthosite, and a pseudotachylyte-shocked anorthosite breccia, were stepwise heated; Ar^{40}-Ar^{39} release curves were obtained. It was hoped that these release patterns would yield information about the

extent of outgassing which occurred during the shock metamorphism of these rocks.

Preview of the Results and Problems --

The potassium-argon ages obtained for the igneous monzonite yielded a well-defined time of crystallization for this body. The implications of the Ar^{40}-K^{40} results for the shock sequence were, however, less than unequivocal. A single well-defined time of shock metamorphism was not indicated by the ages of the shock sequence rocks. Although the Ar^{40}-Ar^{39} release patterns clarify some questions, these data do not resolve the questions of interpretation inherent in the Ar^{40}-K^{40} ages. Another problem which arises is whether or not there have been any thermal events in this area which postdate the monzonite crystallization.

The general question of determining a time of shock deformation will probably receive more attention in the future since both lunar and terrestrial studies suggest that impact processes are much more important than previously assumed. Shock processes in nature are very complicated; they involve both extreme mechanical deformations and extreme thermal disturbances of the shocked systems. Very little, exact experimental data is available with which the thermal and mechanical effects of shock processes can be evaluated. As will be seen, the major problem encountered in this work is that of distinguishing the thermal effects due to shock processes and the effects of purely thermal processes. The problems encountered

in this work may at least indicate what problems must be dealt with in future attempts to determine times of shock metamorphism.

Complete petrographic descriptions of the samples from Groups I and II are found in the Appendix to PART I. Abbreviated descriptions of these samples are presented in this chapter.

A description of the techniques used in the argon and potassium isotopic determinations is presented in the Appendix at the end of PART II.

Age of the Monzonite:

General Statement --

The isotopic data and sample locations for rocks and minerals related to the monzonite are given in Table 1. These include: two whole rock monzonites; pyroxene, sanidine and plagioclase separates from one of the monzonites; anorthosite fragments from the lower layers of the monzonite; the matrix material and fragments of shocked rock from a breccia which underlies the layer of monzonite. All but two of the ages measured lie within the range of 206 to 212 m.y.

Experimental Results --

Whole-Rock Monzonite: Potassium-argon ages were obtained for two samples of whole-rock monzonite. The monzonite is essentially a sanidine-plagioclase-hypersthene-augite rock. About 90% of the potassium and argon in this rock reside in the sanidine phase. A complete description of this rock is given in PART I.

(Map Locations 1 and 4 of Table 1 correspond respectively to the locations of Samples #5-32-1 and #24-7-11 in Fig. 3, CHAPTER 1, PART I.) The two samples of monzonite yielded 210 and 212 m.y. ages.

Mineral separates, including a sanidine fraction, a pyroxene-enriched fraction, and a reasonably pure plagioclase separate were prepared from the monzonite from Location #1 (Sample #5-32-1).

Sanidine Fraction: The sanidine fraction yielded an age of 206 m.y. Sanidine in the monzonite contains most of the argon in the rock and largely determines the argon content of the whole rock. The similarity in the whole rock and sanidine ages is, therefore, not surprising.

The sanidine separate prepared contains predominantly potassium feldspar rims of the feldspar grains; about 10% of the separate consists of impurities of a low-density, iron-magnesium silicate. These impurities are probably altered pigeonite. Splits of this separate were run repeatedly during the course of the potassium-argon work and served as an internal standard for the work. As can be seen from Table 1, the gas amounts determined for the sanidine standard show a good degree of internal consistency ($\pm$ 1% total scatter from the mean); this indicates that the argon analyses were reproducibly executed.

Plagioclase Separate: The plagioclase separate yielded an age of 209 m.y. Over 99% of this separate consists of the calcic plagioclase cores from the feldspars and, at most, 10% of its age is determined by impurities of sanidine. The 209 m.y. age provides

TABLE 1.

Group I.
Rocks Related to Overlying "Igneous Material

Sample No.	Description	Sample Wt.(gm)	Ar^{40} Air(%)	Ar^{40*} (10^{-8}ccSTP)	Sample No.	Sample Wt.(gm)	μ Gms. Analyzed	K%	Age
146	"Igneous" Material: Whole Rock Sample Map Location 1	0.5264	0.89	2468.8	35	0.47205	147.4	2.785	210 ± 3 m.y.
131	Plagioclase Cores from Feldspars	0.9145	2.31	630.9	32	0.4271	237.4	0.7154	
148	Map Location 1	0.8983	2.54	622.1	30	0.9293	117.1	0.7080	209 ± 2 m.y.
107	Pyroxene Separate from "Igneous"	0.7325	70.06	74.0	21	0.36275	4339	0.09819	
109	Material Map Location 1	0.72055	61.96	77.7	22	0.7341	12315	0.09950	190 ± 12 m.y.
111		0.7090	53.06	84.6					
64		0.2467	4.36	5102.3					
66	Sanidine Separate: Consists	0.2463	5.10	5096.6					
69	of Sanidine from Feldspar Rims	0.2467	5.85	5093.6					
71	and an Iron Silicate Impurity;	0.24565	5.21	5079.4					
73	Used as an Internal Calibration	0.2299	5.84	5075.4					
75	Standard	0.2641	6.75	5059.0					

(TABLE 1. -- Continued)

Sample No.	Description	Sample Wt.(gm)	Ar^{40} Air(%)	Ar^{40*} (10^{-8}ccSTP)	Sample No.	Sample Wt.(gm)	μ Gms. Analyzed	K%	Age
	Map Location 1								
87		0.2571	2.03	5088.0	18	0.2343	78.47	5.822	
100		0.26595	24.81	5129.3	33	0.2378	52.07	5.947	206 ± 3 m.y.
121		0.22815	6.81	5087.0					
137		0.24015	0.99	5154.3					
152		0.2749	0.88	5127.4					
135	Anorthosite Inclusion in Lower Layers of Monzonite Map Location 2	0.8418	17.64	373.6	41	0.83420	623.8	0.4093	
150		0.8294	19.04	359.0					212 ± 6 m.y.
83	Whole Rock "Igneous" Material, Outcrop 20 Miles South of # 1 Map Location 4	0.9374	2.19	2474.3	8	0.7870	823.4	2.7533	
85		0.89535	2.71	2472.6	9	0.92375	435.6	2.7969	
91		1.0943	2.50	2470.5	4	1.1935	1729.6	2.7572	212 ± 2 m.y.
					12	1.0700	474.4	2.7494	
					13	0.8426	418.8	2.7625	

(TABLE 1. -- continued)

Sample No.	Description	Sample Wt.(gm)	Ar^{40} Air(%)	Ar^{40*} (10^{-8}ccSTP)	Sample No.	Sample Wt.(gm)	μ Gms. Analyzed	%	Age
115	Breccia: Lithic Fragments of	0.46735	10.07	3911.5	23	0.46055	77.96	4.578	
123	Hornblende Plagioclase Biotite Gneiss Map Location 3	0.45655	7.56	3943.5	37	0.45545	185.3	4.474	206 ± 4 m.y.
127	Breccia: Reddish Matrix Material	0.45015	6.80	1761.1	24	0.3714	79.41	2.141	
137	Enclosing Lithic Fragments Map Location 3	0.4566	14.47	1746.4	40	0.45325	241.3	2.093	197 ± 4 m.y.

an independent measurement which correlates with other ages obtained for the monzonite.

Pyroxene Separate: The Pyroxene separate yielded a mean age of 190 ± 12 m.y. Uncertainties in the large, normal argon corrections for the pyroxene samples makes the 6% error inherent. It is difficult to obtain a pure pyroxene separate since impurities are generally sanidine feldspar and contain 10-50 times as much argon and potassium as the pyroxene. In this separate, 3-30% of the argon may be due to sanidine impurities. It can be inferred that a separate free of impurities might yield an age as low as 180 m.y.

The low age obtained for the pyroxene separate, compared to the whole-rock age, is somewhat perplexing. The pyroxene argon content was analyzed in triplicate, and the three runs produced reasonably consistent results. The potassium content of the split was analyzed twice and yielded reproducible values (see Table 1). It seems unlikely that the low age indicated for the pyroxene is due to analytical errors.

Kistler and Dodge (1966) have reported discordantly low pyroxene ages from a pyroxene-bearing granite in the Sierra Nevada. They attribute the low ages to gas loss by diffusion. More frequently, pyroxene contains "excess" argon (Hart and Dodd, 1963) rather than having lost argon. For want of a better explanation, the low age of pyroxene from the monzonite has been attributed to

diffusional argon loss after cooling of the rock.

Anorthosite Hornfels Inclusion: Large numbers of inclusions of all sizes (including anorthosite) occur in the lower layers of the monzonite. A whole rock specimen of an anorthosite was obtained from an inclusion 10-20 meters in a dimension. This hard, aphanitic material yielded an age of 212 m.y. The rock is an anorthosite hornfels.(This sample, #16-7-4, is described in the Appendix of PART I. Map Location 2, referred to in Table 1, is the same as the location of Sample #16-7-4 in Fig. 3, CHAPTER 1, PART I.)

In thin section, the rock is seen to have undergone complete recrystallization. The thermal relaxation time of a 20-meter block (10^2-10^3 yr.) is much less than the cooling time of the monzonite body (10^5-10^6 yr.). These considerations suggest that the included block attained thermal equilibrium with the surrounding monzonite and recrystallized during cooling of the monzonite body. Such a history is compatible with the observed texture of the rock.

The anorthosite may or may not have been shocked prior to heating. Many hornfelses retain relicts of their original texture. The texture of the anorthosite hornfels may be a relict of the unshocked anorthosite texture, or it may represent recrystallization of previously shock-damaged plagioclase and garnet. At any rate, the recrystallization of this rock has been complete and must have postdated any shock metamorphism of the rock.

The 212 m.y. age determined for the anorthosite hornfels

indicates that the heating and recrystallization of the inclusion occurred at the same time (within experimental error) as the cooling of the monzonite.

Shock Breccia: In a thin, variable layer underlying the monzonite, a shock breccia outcrops. This breccia contains a reddish, fine-grained matrix of small fragments of rock and crystals; the matrix encloses larger, distinct, lithic fragments of a quartz-feldspar-biotite-hornblende gneiss. These lithic fragments are probably chunks of the basement gneiss incorporated into the shock breccia at the time of impact. The shock breccia is described in CHAPTER 1 of PART I and in the Appendix of PART I (see Sample #2-32A). The Map Location 3, referred to in Table 1, corresponds to the location of Sample #2-32A in Fig. 3 of CHAPTER 1, PART I.

(a) Lithic fragments. A whole rock sample was cut from a 5-cm rock fragment included in the shock breccia. This lithic fragment was strongly heated and the mafic minerals within it have been oxidized. The sample yielded an age of 206 m.y. The 206 m.y. age of the lithic fragment suggests that heating of the fragment and consequent argon loss from its minerals took place at the same time (within experimental error) as did the cooling of the monzonite.

(b) Matrix. The reddish matrix of the shock breccia yielded an age of 197 m.y. The matrix is fairly compact but contains a large amount of material with very small grain sizes. It is very

likely that the fine-grained material does not quantitatively retain argon. The low age of the matrix, compared to the age of the fragments it encloses, is probably the result of diffusive argon loss from the friable, fine-grained material after its original heating.

Ar^{40}-Ar^{39} Release Characteristics of the Monzonite: A sample of 0.71605 gm. of whole-rock monzonite chips was stepwise heated, and an Ar^{40}-Ar^{39} release curve was obtained.

The data for the monzonite stepwise extraction are shown in Table 2A. This table lists the ratios observed for each one-hour temperature release, with Ar^{40} used as a reference isotope. The ratios have been corrected for electrometer scale irregularities and for spectrometer discrimination. Absolute amounts of gas released are also listed. These have been calculated on a direct intensity basis, assuming a constant machine sensitivity. The machine sensitivity was determined at intervals by measuring known amounts of Ar^{40} from a calibration pipette attached to the mass spectrometer. The data in Table 1B are derived quantities inferred from this data: these quantities include Ar^{39}, fraction air, Ar^{40*}/Ar^{39}, the Ar^{40*}-Ar^{39} age^{++} and $Ar^{39}/Ar_o^{37}$$^{+}$. The Ar^{40*}-Ar^{39} ages calculated for each extraction have been plotted versus the cumulative Ar^{39} release observed (Fig. 1). Temperatures of the extraction as well as K/Ca ratios (which are proportional to the Ar^{39}/Ar_o^{37} ratio of the material from which the gas is released)$^{+}$

are also plotted in Fig. 1. The errors in the ages involve not only scatter in the Ar^{40*}/Ar^{39} ratios but also the uncertainties due to the Ar^{39} background. The latter uncertainties become large when the amount of isotope released in the step is small compared to 0.005×10^{-8} ccSTP**.

Footnotes for above text:

* Ar^{40*} refers, in the standard way, to radiogenic argon which is the total Ar^{40} with the atmospheric Ar^{40} subtracted.

+ Ar^{37}_o is the Ar^{37} observed which has been corrected for the decay of Ar^{37} (which has a half-life of 35 days). The Ar^{39}/Ar^{37}_o ratio is a characteristic of the K^{39}/Ca^{40} ratio of the site which releases the gas. If the atomic ratio of K/Ca is X, then the Ar^{39}/Ar^{37}_o will be

$$Ar^{39}/Ar^{37}_o = (0.931 \times \sigma_{39\text{-}39} + 0.0064\, \sigma_{42\text{-}39})/0.9997\, \sigma_{40\text{-}37} \cdot$$

$$\sigma_{39\text{-}39}/\sigma_{40\text{-}37} = 1.87.$$

(See Table 5) For most cases, $X < 0.1$ and $K/Ca = 0.57\ Ar^{39}/Ar^{37}_o$. For the maskelynite of composition

An_{55} ($K/Ca = 0.054$), $Ar^{39}/Ar^{37}_o = 0.10$ (compatible with observed value).

++ Ar^{40*}- Ar^{39} ages are calculated in the standard fashion

$$\text{Age} = \ln\left[\frac{Ar^{40*}}{Ar^{39}} \cdot J + 1\right] \qquad J = \frac{\exp(\text{monitor age}/\tau)-1}{(Ar^{40*}/Ar^{39})_{\text{monitor average}}}$$

Brereton (1970). (τ = mean life of K^{40}).

** Errors include two sources: (1) Variations in ratios read on the charts. (2) Errors due to background Ar^{39} (a 5×10^{-11} ccSTP value assumed) and errors in the Ar^{40*} and Ar^{36} due to 2.5×10^{-11} ccSTP background at Ar^{36}. Percentage errors from sources above were Pythagorean summed and are shown in % in table.

TABLE 2A.

Monzonite Monitor (5-32-1)**

Extraction Step	Ar^{40*}	Ar^{39}	Ar^{38}	Ar^{37}	Ar^{36}	Ar^{40} Total
125 ma	131.49	0.527 (285.36) -0.7 +1.2	--	0.176 (856.31) ± 0.6	0.064 (2353.1) -0.9 +4.1	150.37
170 ma	312.58	1.244 (259.75) -0.3 +0.5	--	0.281 (1149.13) ± 0.6	0.035 (9140.0) -1.6 +7.4	323.02
250 ma	536.23	2.173 (250.33) -0.2 +0.3	--	0.279 (1951.87) ± 0.4	0.026 (21143.3) -4.4 +10.9	543.83
350 ma	493.20	1.986 (252.91) -0.1 + 0.3	--	0.179 (2800.89) ± 0.6	0.030 (16507.1) -1.9 +8.5	502.19
450 ma	111.17	0.456 (299.70) -3.4 +3.6	--	0.248 (551.80) ± 0.7	0.087 (1579.6) -1.3 + 3.2	136.75

(TABLE 2A. -- continued)

Extraction Step	Ar^{40*}	Ar^{39}	Ar^{38}	Ar^{37}	Ar^{36}	Ar^{40} Total
550 ma	36.95	0.161 (332.92) -0.4 +3.1	--	0.521 (102.81) ± 3.9	0.056 (952.7) -3.0 +5.5	53.56
700 ma	10.91	0.055 (486.07) -2.0 +9.4	--	0.135 (197.32) ± 0.4	0.053 (499.7) -1.1 +4.9	26.71
875 ma	6.49	0.028 (8099.76) -5.9 + 18.6	--	0.059 (3933.53) ± 1.0	0.759 (304.1) -0.3 +0.5	230.64
1050 ma	0.54	0.007 (2281.06) -2.5 + 75.0	--	--	0.049 (306.5) -0.3 +5.2	14.94

* Radiogenic argon.

** Gas amounts in ccSTP x 10^{-8}. Measured ratios of isotope to A^{40} are indicated in parentheses. Errors are indicated in percent.

TABLE 2B.

Monzonite Monitor (5-32-1)

Extraction Step	Temperature	Ar^{40*}/Ar^{39}	Ar^{39} Cumulative Release	Age+	Ar^{39}/Ar^{37}_{o}	Fraction Air
125 ma	600 °C	249.52 -0.7 +13	0.0794	212.8	1.077	0.1256
170 ma	820 °C	251.35 -0.3 +0.6	0.2668	213.3	1.583	0.0323
250 ma	920 °C	246.83 -0.2 +0.3	0.5942	209.6	2.742	0.0140
350 ma	1080 °C	248.39 -0.1 +0.3	0.8935	210.9	3.868	0.0179
450 ma	1180 °C	243.63 -3.4 +3.7	0.9622	207.1	0.637	0.1871
550 ma	1310 °C	229.66 -0.4 +3.7	0.9864	195.8	0.107	0.3102

(TABLE 2B. -- continued)

Extraction Step	Temperature	Ar^{40*}/Ar^{39}	Ar^{39} Cumulative Release	Age+	Ar^{39}/Ar^{37}_{o}	Fraction Air
700 ma	1450 °C	198.61 -2.0 +11.7	0.9947	170.5	0.140	0.5914
875 ma	1590 °C	227.80 -5.9 +21.9	0.9989	194.3	0.161	0.9719
1050 ma	1680 °C	81.98 -2.5 +158.9	1.0000	72.2	--	0.9641

* Radiogenic argon. + Age = $\tau \ln(A^{40*}/A^{39} \cdot J + 1)$ $J = 4.7658 \times 10^{-4}$

τ = mean life (1.88 b.y.)

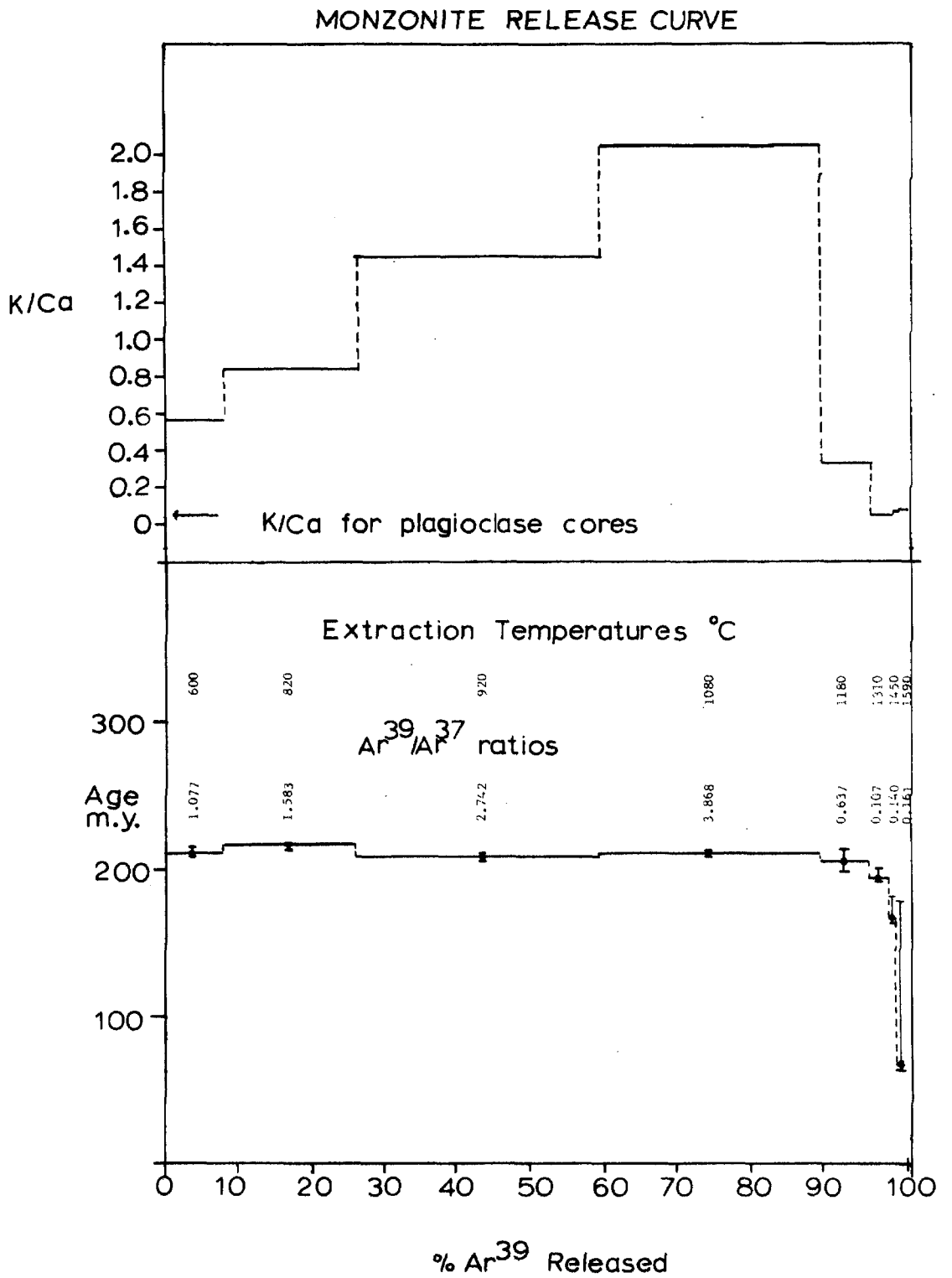
MONZONITE RELEASE CURVE
K/Ca
2.0
1.8
1.6
1.4
1.2
1.0
0.8
0.6
0.4
0.2
0
K/Ca for plagioclase cores
Extraction Temperatures °C
600
820
920
1080
1180
1310
1450
1590
Ar39/Ar37 ratios
Age m.y.
300
200
100
1.077
1.583
2.742
3.868
0.637
0.107
0.140
0.161
0
10
20
30
40
50
60
70
80
90
100
% Ar39 Released

FIG. 1

The Ar^{40*}/Ar^{39} ratios obtained from the monzonite are constant within 5% for most of the release. They have an average value of 247. The average monitor Ar^{40*}/Ar^{39} was used to obtain a J value with which to calculate the ages. At very high temperatures (1350°C), the ratio drops about 20% below the average value. Because of the large errors associated with measuring the small amounts of Ar^{39} released in the 1350°C step (0.028 and 0.007 x 10^{-8} ccSTP), it is uncertain if this low ratio is significant. The Ar^{39}/Ar^{37} ratios peak near 1020°C(K/Ca = 2.2). This is near the temperature at which sanidine is expected to release argon essentially completely. Subsequent releases are characterized by a lower Ar^{39}/Ar^{37} ratio (lower indicated K/Ca) and are probably mostly from the plagioclase cores of grains.

The monzonite releases 98% of its argon before 1230°C, a behavior which is quite different than that exhibited by the shocked anorthosites. The initial releases of the monzonite have nearly the same Ar^{40*}/Ar^{39} ratio as does the rock average. The release curve does not yield any indication of either continuous diffusional loss or secondary thermal metamorphism at a time earlier than 210 m.y. The general flat appearance of the release curve strongly suggests that this rock had a simple one-stage cooling history.

The overall Ar^{40*}/Ar^{39} ratio of 247.28 and the total Ar^{40*} - K^{40} age of 210 m.y. yield a J value of 4.766 x 10^{-4} for this irradiation.

Diffusion Properties of the Monzonite: The amounts of Ar^{39} released in the one-hour heating steps and the temperatures of the extraction steps were used to infer values of D/a^2 at different temperatures. Diffusion from a system of uniform spherical grains was assumed to be occurring for these calculations. The D/a^2 values obtained were then plotted versus $1/T_{abs}$ and values were obtained for D/a^2 at 20°C and the activation energies of the system. D/a^2 values at 20°C for the monzonite range from 10^{-18} - 10^{-21} cm^2/sec, and an activation energy of about 25 kilocalories/mole is suggested for the system.

The diffusion coefficients suggest that the monzonite is susceptible to slight thermal metamorphism but is not a "leaky" argon system. The diffusion properties inferred for the rock also place limits on the duration and degree of any thermal metamorphism which has affected the Manicouagan-Mushalagan Lakes area after the monzonite crystallized.

Conclusions --

Age of the Monzonite: The isotopic data for the Group I samples are shown plotted in Fig. 2. With the exception of the pyroxene and the matrix from the breccia, these samples indicate a well-defined 210 m.y. crystallization age for the monzonite.

The sanidine separate and total rock monzonite from Location 1 are interdependent. Since the sanidine contains 90% of the potassium and argon in the monzonite, the age determined for the whole rock and the age of the sanidine separate from the whole rock should be

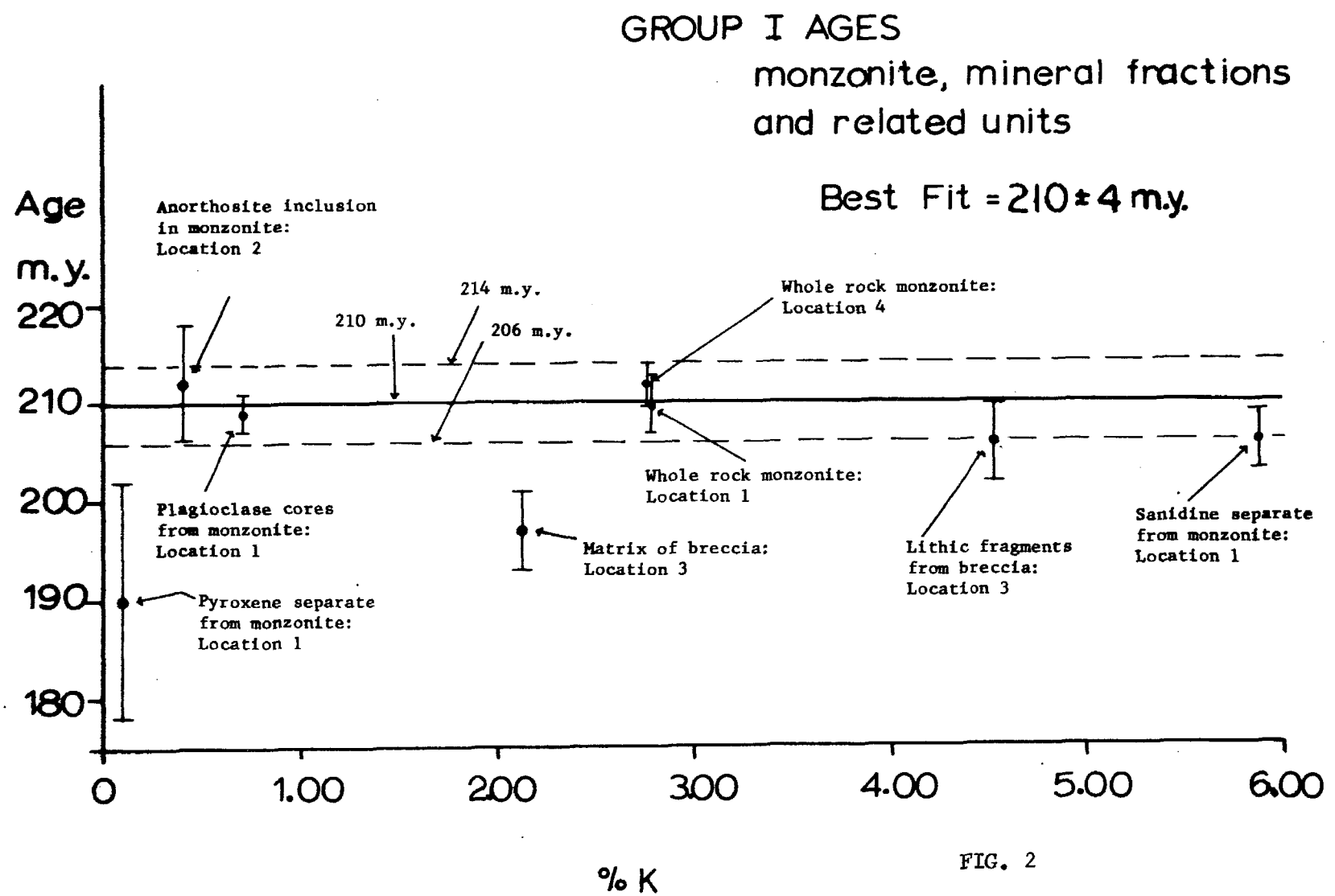
GROUP I AGES
monzonite, mineral fractions
and related units
Best Fit = 210 ± 4 m.y.
Age
m.y.
220
210
200
190
180
Anorthosite inclusion
in monzonite:
Location 2
210 m.y.
214 m.y.
206 m.y.
Whole rock monzonite:
Location 4
Whole rock monzonite:
Location 1
Plagioclase cores
from monzonite:
Location 1
Pyroxene separate
from monzonite:
Location 1
Matrix of breccia:
Location 3
Lithic fragments
from breccia:
Location 3
Sanidine separate
from monzonite:
Location 1
0
1.00
2.00
3.00
4.00
5.00
6.00
% K

FIG. 2

nearly identical. There still remain, however, five independent determinations of the 210 m.y. age. The ages determined for the pyroxene and the matrix from the breccia are 10% and 6% lower, respectively, than the mean age of the monzonite.

The Ar^{40}-Ar^{39} release curve (Fig. 1) for the monzonite is best interpreted as indicating a simple, single thermal event history for the monzonite. The release pattern of the monzonite gives no indication of either continuous diffusional loss or episodic loss of argon from the rock after its crystallization.

The simplest and probably the best conclusion that can be drawn from the data is that the monzonite formation, recrystallization of the anorthosite hornfels, and heating of the underlying shock breccia took place at 210 m.y. ago. Subsequent to that time, no major metamorphic events took place in the area.

As was discussed in PART I, the monzonite must (1) be roughly contemporaneous with the shock event or (2) postdate the shock event. The 210 m.y. age of the monzonite indicates that the meteorite impact took place in the time interval from 440-210 m.y. ago. Four hundred and forty million years is the lower age limit for the impact event, established by the presence of deformed Middle Ordovician limestone in the crater.

Post-Monzonite Thermal History of the Area: The monzonite monitor yields a flat release curve, and there is no evidence for continuous diffusional loss of argon or for an extensive episodic heating at some time later than 210 m.y. The release curve

indicates that gas loss $>$ 5% has not occurred. This fact can be combined with diffusion parameters obrained from the monzonite to place limits on the thermal history of the Manicouagan area. The Ar^{39} diffusion data for the monzonite suggests that D/a^2 at 20°C for this rock is in the range of 10^{-18} - 10^{-21} sec^{-1}. D/a^2 values of 10^{-10} sec^{-1}, 10^{-12} sec^{-1} and 10^{-15} sec^{-1} at temperatures of 300, 200, and 100 °C can be inferred from the monzonite data. These values suggest that any metamorphic or metasomatic event affecting the monzonite and involving 100°C temperatures must have lasted less than 10^5 yrs. A similar event, involving temperatures of 200°C, must have lasted less than 100 yrs; events involving temperatures $>$ 200°C can be excluded since they would have to have occurred for an unreasonably short geological time span. It can be seen that

$$\left.\frac{\lambda}{D/a^2}\right|_{20^\circ C} \gtrsim 10^2 - 10^4.$$

Continuous diffusional loss, greater than a few percent, would not be expected (Wasserburg, 1954). This prediction is confirmed by the Ar^{40}-Ar^{39} thermal release curve of the monzonite.

It should be pointed out that the 20°C diffusion parameter of the monzonite (10^{-18} - 10^{-21} sec^{-1}) is significantly greater than the estimated $\left.D/a^2\right|_{20^\circ C}$ for the maskelynite ($10^{-27} sec^{-1}$). Any low-grade

metamorphic event which affects the maskelynite would affect the monzonite even more strongly. Since the monzonite does not appear to have been thermally metamorphosed, if a metasomatic zeolitization affected the anorthosites in the central massif (as has been suggested by Murtaugh and Currie (1969)), then this event either (1) took place before or during the monzonite cooling, or (2) it somehow did not affect the monzonite.

Time of Shock Metamorphism:

Introduction and Preview --

In order to determine the time of the meteorite impact at Manicouagan, potassium-argon ages were obtained for a series of anorthosites which had experienced varying degrees of shock metamorphism. These anorthosites, which constitute a "shock sequence", yielded ages ranging from 932 to 200 m.y.; several highly shocked anorthosites indicated ages of 280 to 320 m.y. Although the data do not uniquely indicate a time of shock metamorphism, this time is thought to fall within the above interval.

Ar^{40}-Ar^{39} release curves were obtained for three of the shocked samples. These release patterns are difficult to interpret, but the data suggests that argon losses from the shocked rocks could have occurred between 110 and 320 m.y. ago. With the present data, it is not possible to say with certainty how these argon loss occurrences correlate with shock-metamorphic or thermal events in the area.

Estimates of diffusion parameters of the shock-sequence rocks were obtained using the Ar^{39} release data. These estimates suggest that argon loss due to heating of shock-sequence rocks by later thermal events might have been fairly extensive for some rocks.

Shock-Sequence Experiment --

Rationale of the Experiment: If a solid material is subjected to shock-wave deformations, both the in-shock and residual temperatures of the material become progressively greater with increasing shock intensities. As the shock temperatures of the material increase, any gas present would be more easily lost by diffusion. Shock-melted materials would probably lose all, or nearly all, of the gas they contain.

One can consider a set of materials, each of which has been subjected at some previous time to a shock deformation of different intensity. One can arrange these materials according to the degree of shock deformation which they have experienced. Their argon contents would then be expected to decrease concurrently with increasing shock pressure from (1) a value defined by pre-shock argon retention to (2) a value defined by post-shock argon retention. Those materials which were most highly shocked would define a constant, asymptotic value, i.e. the potassium-argon shock age. This simple theory of argon loss during a shock event is the first-order theory upon which the shock-sequence experiment in

this work is based.

Materials of the Shock Sequence: The shock-sequence (Group II) materials consist of anorthosites which have undergone various degrees of shock metamorphism but which retain similarities in textures, mineral phases and mineral phase compositions. As was previously indicated, similarities among the anorthosites strongly suggest that they were derived from a homogeneous anorthosite body, and that the differences among them are due to the occurrence of shock metamorphism subsequent to the original formation of the body. Anorthosites were used to define the shock sequence because: (1) They show a wide range of shock effects. (2) They are free from visible thermal alterations. (3) They exhibit uniformity in texture, mineralogy and chemical compositions. (4) They can be considered to be approximately monomineralic rocks for the purpose of this experiment.

(a) Samples used. The rocks chosen for the shock-sequence experiment exhibit deformations characteristic of shock pressures ranging from 0 to over 600 kb. These samples are: Sample A, an unshocked anorthosite; Sample D, a slightly shocked anorthosite; Samples B and C, maskelynitized anorthosites; Samples E and F, highly shocked anorthosites; Samples G and H, pseudotachylyte-shocked anorthosite breccias. Estimates of the shock intensities experienced by these rocks are shown in Fig. 4, CHAPTER 1, PART I. Complete petrological descriptions are given in the Appendix to PART I.

(b) Lack of thermal alteration. The Group II materials displayed no visible alteration due to heating by the monzonite. The locations in the central massif from which these samples were taken are topographically higher than the highest presently exposed level of the monzonite. These samples are, therefore, least likely to have undergone thermal alterations caused by the monzonite body. Although the thermal effects present in the shock-sequence rocks are thought to be due predominantly to shock heating, minor heating by the monzonite body cannot be entirely ruled out. Lack of knowledge concerning this latter effect is, in fact, a major difficulty involved in determining the precise time of shock metamorphism.

(c) "Monomineralic" nature of the anorthosite. The anorthosites used in the shock sequence have been treated generally as though they were "monomineralic" rocks. Mineralogically, this is not true (see Appendix, PART I). For the purpose of the argon and potassium analyses in this work, however, approximating the anorthosites as "monomineralic" systems is valid.

For a typical anorthosite, about 85% of the rock consists of plagioclase (An_{55}) with a potassium content of ~ 0.44% (see Table 3, CHAPTER 2, PART I). Potassium is uniformly distributed throughout the plagioclase grains as is apparent from electron beam scan pictures of these grains (see Samples A and C in Appendix to PART I). Total rock potassium analyses of the maskelynite yielded a value of 0.45% which is very close to the potassium content of the plagioclase grains. It can be deduced that the potassium present

in phases other than maskelynite (plagioclase) represents only 2 to 4 % of the total potassium in the rock.

Electron beam scanning pictures reveal that the anorthosites contain calcium-poor feldspar between plagioclase grains. In some rocks, this feldspar is more potassic than the plagioclase; in others, it is more sodic. In the maskelynitized anorthosite referred to above, the intergranular feldspar is sodic and is actually potassium depleted with respect to the plagioclase. In other rocks, the intergranular phase is potassium enriched and is one of the major argon-containing components.

A maximum of about 1% of any anorthosite mode consists of intergranular, calcium-depleted feldspar. If it is assumed that this potassium-rich, intergranular feldspar contains 5-10% potassium, then a maximum of 10-20% of the whole-rock argon is contained in this phase. A maximum of some 20% of the anorthosite consists of garnet or pyroxene; if these minerals contain $\sim$ 0.1% potassium, then they will account for some 4% of the potassium and argon in the rock.

From the above discussion, it is clear that the percentage of the whole-rock argon contained in the plagioclase (or maskelynite) phase of the shock-sequence rocks ranges from about 75% in anorthosites with potassium-rich, intergranular feldspar to about 95% in anorthosites with sodium-rich, intergranular feldspar. Since most of the argon and potassium in the shock-sequence rocks is contained in the plagioclase, the rocks behave, to a good

approximation, as if they contained only plagioclase.

(d) Uniformity of the anorthosites. The uniformity of rocks from the anorthosite massif is apparent from the rock descriptions presented in the Appendix to PART I. Textural uniformity of the rocks is often a very important means of inferring the original textures of severely shock-deformed anorthosites. Uniformity among the shock-sequence anorthosites insures that argon-release features of these rocks resulting from minerals other than plagioclase are, to some extent, consistent between samples. Reasonable corrections for such effects can thus be made.

Experimental Results: The potassium and argon data for the members of the "shock sequence" are shown in Table 3. In most cases, the average value listed in the table is the result of replicate determinations. The map locations referred to in the table are shown in Fig. 3, CHAPTER 1, PART I.

(a) Outside anorthosite. A sample of unshocked anorthosite from Map Location A, exterior to the two lakes (see Fig. 3, CHAPTER 1, PART I), yielded an age of 932 m.y. This rock is referred to as Sample A in Table 3.

The anorthosite outside the crater is fresh, unaltered rock with very few fractures visible in thin section. A petrographic description of this rock (Sample A) is given in the Appendix to PART I.

It has been shown that some feldspars lose argon by continuous diffusion (Wetherill et al., 1955; Wasserburg et al., 1956). The question therefore arises whether or not the above age represents a minimum age for its formation time. Since this rock presumably recrystallized during the Grenville Orogeny, and its measured age of 932 m.y. is compatible with other measured ages of Grenville Province rocks (i.e., 900-1150 m.y.; Stockwell, 1970), extensive continuous-diffusional argon loss from this rock did not occur.

(b) Slightly shocked anorthosite. A sample of anorthosite from Map Location D was analyzed. A potassium-argon age and an Ar^{40}-Ar^{39} release curve from the sample were obtained.

In thin section, this sample is extensively fractured; it displays abundant planar features and contains amorphous material of index 1.500 but no clear maskelynite. A complete petrographic description of this rock (Sample D) is given in the Appendix to PART I, and a discussion of the shock features is given in CHAPTER 1, PART I.

The slightly shocked anorthosite is believed to have experienced shock pressures of 150-250 kb. The rock is thought to have experienced a temperature between 60-220 ^{o}C during the shock, and a post-shock temperature between 40-110 ^{o}C.

i. Ar^{40}-K^{40} age -- A total argon age of 532 $\pm$ 8 m.y. was obtained for a split of the 60- to 80- mesh sieve fraction of the whole-rock anorthosite from Location D. Even at the relatively low shock pressure experienced by this sample, a large percentage

TABLE 3.

Group II
Anorthosite Shock Sequence

Sample No.	Description	Sample Wt.(gms)	Ar^{40} Air(%)	Ar^{40} 10^{-8} ccSTP/gm	Sample No.	Sample Wt(gms)	μ Gms. Analyzed	K%	Age
94	Anorthosite from 5 Miles N.W. of	0.57965	14.20	2179.9	1	0.33755	1212.2	0.4502	
96	Mushalagan Lake Map Location A	0.67105	9.39	2167.8	7	0.6825	2672.4	0.4543	
					10	0.5906	1638.2	0.4491	932 ± 7 m.y.
					20	0.65345	777.3	0.4525	
					2	0.32410	1176.6	0.4523	
140	Slightly Shocked Anorthosite: Fractures, Planar Features, Small Amounts of Glass Map Location D	0.51685	15.18	957.9	36	0.5252	300.3	0.3925	
					38	0.5451	303.3	0.3878	532 ± 8 m.y.
79	Totally Maskelynitized Anorthosite	0.6629	11.49	603.9					
81	from Eastern Half of Central	1.1097	8.45	617.4	6	0.7200	3668.6	0.4397	321 ± 4 m.y.
89	Massif Map Location B	0.80810	9.92	618.0	11	0.4293	2314.9	0.4397	
133	Maskelynite Anorthosite from	0.65605	14.30	582.1	27	0.6499	146.4	0.4109	
154	Eastern Summit of Central Massif Map Location C	0.65380	14.32	583.1	31	0.6178	184.1	0.4172	323 ± 3 m.y.

(TABLE 3. -- continued)

Sample No.	Description	Sample Wt.(gms)	Ar^{40} Air(%)	Ar^{40*} 10^{-8}ccSTP/gm	Sample No.	Sample Wt.(gms)	μ Gms. Analyzed	K%	Age
119b	Anorthosite Containing Thermal	0.72265	54.50	782.2	26	0.7329	457.9	0.4904	
125	Glass, Low 2V Plagioclase and Heterogeneous Garnet Map Location E	0.72180	49.82	794.1	29	0.7028	181.4	0.4734	371 ± 9 m.y.
144	Anorthosite with Heterogeneous Garnets, Low 2V Plagioclase, Some Thermal Glass Map Location F	0.66605	21.10	537.4	34	0.6915	213.7	0.4531	
					39	0.6209	381.2	0.4563	275 ± 4 m.y.
165	Pseudotachylite with Shocked Anorthosite Inclusions, Greyish Matrix Map Location H	0.8947	11.75	514.6	42	0.8891	2228	0.6149	
					46	0.8952	2506	0.6045	202 ± 3 m.y.
163	Pseudotachylite with Inclusions Reddish Matrix Map Location G	0.6730	31.90	568.3	45	0.6863	1508	0.4726	280 ± 3

Note: Sample wts. in gms. Gas amounts in 10^{-8}ccSTP.

of the original radiogenic argon in the sample was apparently released.

ii. Ar^{40}-Ar^{39} ages -- A sample, consisting of whole-rock chunks (ranging from 1- to 3- mm in size), of anorthosite from Location D was stepwise heated and its Ar^{40}/Ar^{39} ratios measured. The absolute amounts of the different argon isotopes released in each of the extraction steps are shown in Table 4A. The direct intensity technique used to measure these amounts is discussed in the Appendix. Temperatures, Ar^{40*}/Ar^{39}_{o} ratios, and ages for each release are given in Table 4B. A plot of the Ar^{40}-Ar^{39} ages of each temperature fraction versus the cumulative Ar^{39} release is shown in Fig. 3.

The whole-rock chunks of anorthosite used for the Ar^{40}-Ar^{39} analyses could be somewhat different in chemical composition and mineralogy than the whole-rock sieve fraction used for the Ar^{40}-K^{40} studies. It is improbable, however, that there is a large difference between the material used for the Ar^{40}-K^{40} analyses and the material used for the Ar^{40}-Ar^{39} heating experiment. These two materials were obtained from parts of the same hand specimen separated, at most, by 2 cm.

of the original radiogenic argon in the sample was apparently released.

ii. Ar^{40}-Ar^{39} ages -- A sample, consisting of whole-rock chunks (ranging from 1- to 3- mm in size), of anorthosite from Location D was stepwise heated and its Ar^{40}/Ar^{39} ratios measured. The absolute amounts of the different argon isotopes released in each of the extraction steps are shown in Table 4A. The direct intensity technique used to measure these amounts is discussed in the Appendix. Temperatures, Ar^{40*}/Ar^{39}_{o} ratios, and ages for each release are given in Table 4B. A plot of the Ar^{40}-Ar^{39} ages of each temperature fraction versus the cumulative Ar^{39} release is shown in Fig. 3.

The whole-rock chunks of anorthosite used for the Ar^{40}-Ar^{39} analyses could be somewhat different in chemical composition and mineralogy than the whole-rock sieve fraction used for the Ar^{40}-K^{40} studies. It is improbable, however, that there is a large difference between the material used for the Ar^{40}-K^{40} analyses and the material used for the Ar^{40}-Ar^{39} heating experiment. These two materials were obtained from parts of the same hand specimen separated, at most, by 2 cm.

A J value of 4.661×10^{-4} was used to calculate the ages from the Ar^{40}/Ar^{39} ratios. This value was determined from the overall average Ar^{40}/Ar^{39} ratio and the total age of the rock. The J value obtained by using the monzonite J value and the flux map

TABLE 4A.

Slightly Shocked Anorthosite**

Extraction Step	Ar^{40}* 10^{-8}ccSTP	Ar^{39} 10^{-8}ccSTP	Ar^{38} 10^{-8}ccSTP	Ar^{37} 10^{-8}ccSTP	Ar^{36} 10^{-8}ccSTP	Ar^{40} Total
115 ma	47.45	0.173 (1437.18) -1.9 +3.4	1.072 (232.12) ± 4.9	0.453 (548.95) ± 0.1	0.682 (365.1) -0.2 +0.4	248.90
150 ma	17.19	0.074 (369.49) ± 0.7	0.032 (855.10) ± 27.6	0.205 (133.36) ± 0.5	0.035 (793.3) +1.6 -7.4	27.39
200 ma	17.55	0.075 (426.37) -1.5 +6.8	0.040 (797.66) ± 6.9	0.159 (201.10) ± 0.35	0.049 (655.7) -1.2 +5.3	31.95
250 ma	25.49	0.078 (486.21) -0.7 +0.4	0.027 (1372.58) ± 2.0	0.139 (271.93) ± 0.4	0.041 (912.4) -2.7 +6.7	37.70
325 ma	221.67	0.197 (1204.80) -1.4 +2.9	0.338 (703.49) ± 10.2	0.341 (697.16) ± 0.3	0.054 (4386.0) -2.1 +5.1	237.69

(TABLE 4 A. -- continued)

Extraction Step	Ar^{40*} 10^{-8}ccSTP	Ar^{39} 10^{-8}ccSTP	Ar^{38} 10^{-8}ccSTP	Ar^{37} 10^{-8}ccSTP	Ar^{36} 10^{-8}ccSTP	Ar^{40} Total
400 ma	234.86	0.197 (1274.93) -1.7 +3.0	0.236 (1064.18) ± 11.2	0.459 (548.21) ± 0.1	0.057 (4434.6) -1.0 +4.5	251.63
475 ma	51.18	0.086 (751.48) -1.3 +5.9	0.075 (866.47) ± 11.9	0.369 (175.03) ± 0.2	0.046 (1416.0) -2.4 +6.0	64.67
550	98.38	0.141 (841.97) -0.8 +3.6	0.058 (2060.45) ± 8.7	0.578 (204.91) ± 0.3	0.068 (1733.0) -0.8 +3.8	118.53
650	78.53	0.105 (957.85) -1.1 +4.8	0.037 (2715.38) ± 17.9	0.429 (234.19) ± 0.3	0.074 (1350.1) -1.5 +3.7	100.53
750	20.16	0.030 (1744.26) -1.8 +16.5	0.118 (443.34) ± 52.6	0.123 (425.25) ± 0.5	0.109 (481.2) -1.0 +2.5	52.26

* A^{40*} = radiogenic argon. ** Gas amounts in 10^{-8}ccSTP . Ratios of measured isotope to A^{40} indicated in parentheses. Errors indicated in percent. Gas amounts are for the 0.8425 gm sample, not per gm of sample.

TABLE 4B.

Slightly Shocked Anorthosite

Extraction Step	Temperature	Ar^{40*}/Ar^{39}	Age+	Cumulative Ar^{39} Release	Ar^{39}/Ar^{37}_{o}	Fraction Air
115 ma	600°C	273.99 -1.90 +3.77	226.6	0.1501	0.120	0.8094
150 ma	790 °C	231.85 -0.74 +7.97	193.4	0.2140	0.112	0.3725
200 ma	870 °C	234.23 -1.47 +7.98	195.3	0.2787	0.147	0.4506
250 ma	950°C	328.75 -0.71 +7.05	268.8	0.3460	0.172	0.3239
325 ma	1070 °C	1123.63 -1.40 +2.90	793.9	0.5168	0.177	0.0674
400 ma	1180 °C	1189.98 -1.67 +3.03	831.8	0.6877	0.131	0.0666
475 ma	1275 °C	594.66 -1.27 +6.05	461.2	0.7619	0.070	0.2087

(TABLE 4B.-- continued)

Extraction Step	Temperature	Ar^{40*}/Ar^{39}	Age^{+}	Cumulative Ar^{39} Release	Ar^{39}/Ar_o^{37}	Fraction Air
550 ma	1360°C	698.40 -0.78 +3.68	531.2	0.8835	0.073	0.1705
650 ma	1455°C	748.21 -1.05 +4.92	564.0	0.9741	0.073	0.2189
750 ma	1530°C	673.14 -1.82 +16.87	514.4	0.9999	0.073	0.6141

Ar^{40*} = radiogenic argon 40. + Age = $\tau \ln(A^{40*}/A^{39} \cdot J + 1)$ $J = 4.661 \times 10^{-4}$

τ = mean life = 1.88 b.y.

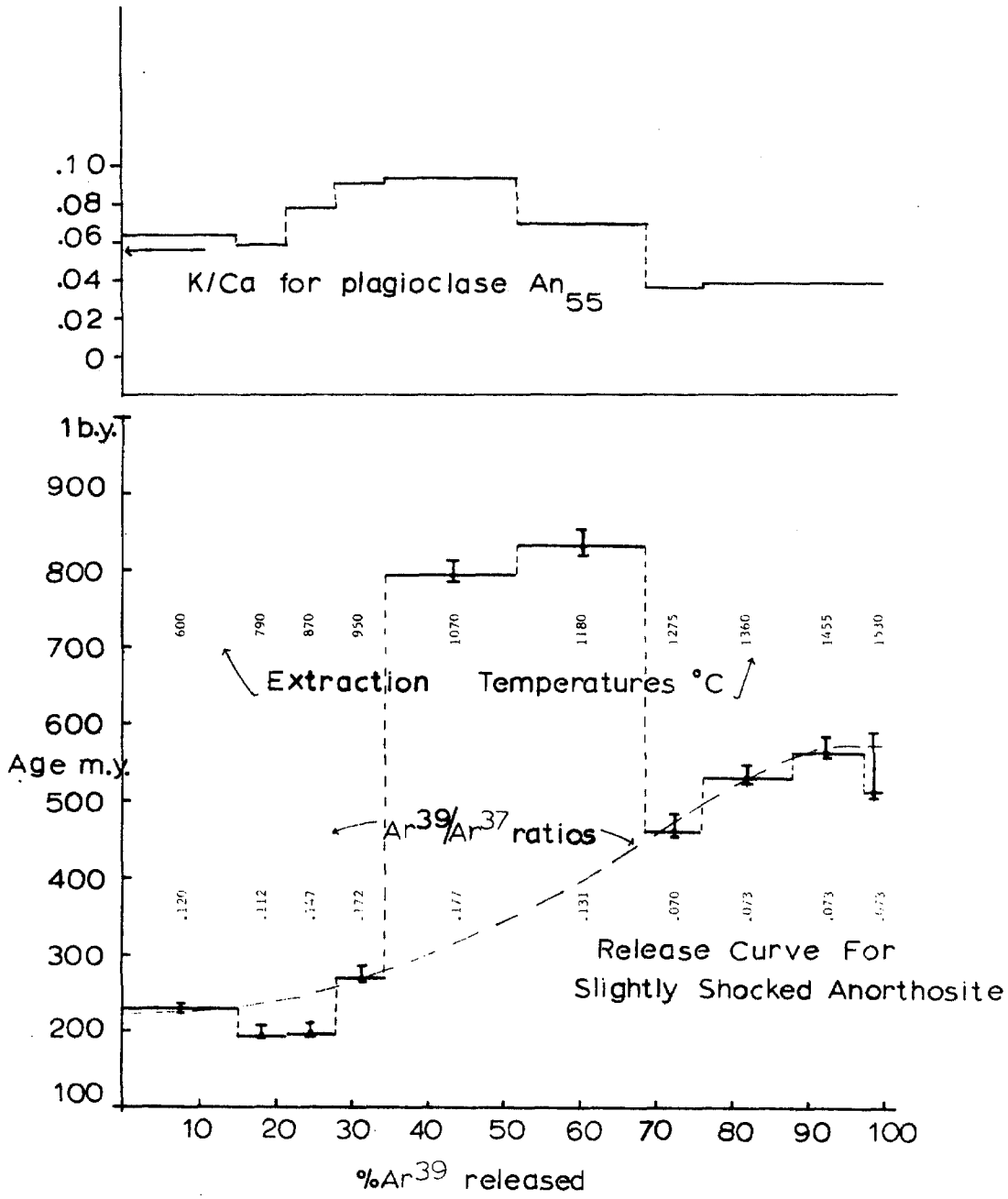
.10
.08
.06
.04
.02
0
K/Ca for plagioclase An55
1 b.y.
900
800
700
600
Age m.y.
500
400
300
200
100
600
790
870
950
1070
1180
1275
1360
1455
1530
Extraction Temperatures °C
Ar39/Ar37 ratios
.129
.112
.147
.172
.177
.131
.070
.073
.073
.073
Release Curve For
Slightly Shocked Anorthosite
10
20
30
40
50
60
70
80
90
100
%Ar39 released

Fig. 3

(see CHAPTER 2) is 4.430×10^{-4}, i.e. about 5% lower. The error in the J value is conservatively estimated at $\pm$ 5%, and hence the value of all ages calculated for the curve may be 5% higher or lower than shown. The J value uncertainty does not affect the relative ages of different temperature fractions; these may be in error with respect to each other only by the amounts shown by error bars on the release curve.

The general features of the Ar^{40}-Ar^{39} behavior of the rock are apparent from Fig. 3. The first release, which is rather large (15% of the sample), indicated a 226-m.y. age. The two subsequent releases yielded ages near 193 m.y. The 950°C argon fraction indicated an age of 269 m.y. while the temperature fractions at 1070 and 1180 °C indicated drastically older ages which are close to 800 m.y. The fractions of radiogenic argon released above 1180°C showed an abrupt drop in age to a value of about 461 m.y.; subsequent releases indicated ages which progressively increase to 546 m.y. The highest temperature argon release indicated a somewhat lower age of 514 m.y.

The release curve suggests that this rock experienced partial argon loss at some time in the past. This is possibly, but not clearly, due to the shock event. It is clear, however, that the Ar^{40}-Ar^{39} release curve of the slightly shocked anorthosite is <u>not</u> totally amenable to interpretation (as discussed by Turner, 1968) as resulting from partial thermal outgassing of a system of spherical grains. The total Ar^{40}-K^{4}

age of 532 m.y. obtained for Sample D represents an average of high and low ages of material from the rock.

The release curve obtained for this anorthosite differs from the release curves of the models discussed by Turner (1968) in that: (1) the curve shows a significantly lower age in the releases subsequent to the initial release; (2) two of the temperature fractions yielded ages drastically older than the bulk of ages from the rock. Another unexpected feature of this release curve is that some 25% of the sample argon is released above 1300°C, whereas plagioclase would normally be expected to have totally released its argon in a one-hour heating at this temperature. The peculiarities of this release curve are also observed in the release curves of the other shocked anorthosites. A generalized discussion of these peculiarities is presented in CHAPTER 2.

The lower ages indicated by the 790 and 870 °C gas fractions are difficult to understand. Generally, any species which loses argon easily at low temperatures (whether by continuous diffusion or episodically during a low-grade metamorphism) will have Ar^{40} depleted from its less retentive sites. It will therefore yield low Ar^{40}/Ar^{39} ratios in the initial stages of a laboratory stepwise-heating experiment. Subsequent laboratory releases in the stepwise heating would degas the more retentive sites which should be <u>less</u> depleted in Ar^{40}.

These releases would therefore indicate higher Ar^{40}/Ar^{39} ratios than the previous releases.

A possible intepretation of the observed behavior is that a phase with a low Ar^{40}/Ar^{39} ratio (and therefore low age) dominates the gas releases of the 790 and 870 °C temperature fractions. As will be discussed in CHAPTER 2, a "low-age" mineral with the appropriate activation energy and diffusion coefficient could dominate the argon releases from a rock at temperatures between 800-900 °C.

The gas released at 950°C has an indicated age of about 268 m.y., while the releases at 1070 and 1180 °C give drastically older ages of 793 and 831 m.y. The high ages may, in analogy with the "low-age" release, be interpreted as resulting from argon with a high Ar^{40}/Ar^{39} ratio released by a "high-age" phase. This "high-age" phase yields the bulk of the gas released from the rock in these two temperature fractions; the total rock system therefore releases argon with a high Ar^{40}/Ar^{39} ratio. These two ages are slightly on the low side of a "Grenville" age and may be due to mildly fractured grains that did not lose much Ar^{40*} during the shock. Relatively undamaged plagioclase grains would be expected to release argon predominantly in the temperature range of 900-1150 °C (see Fig. 4 and discussion of maskelynite). The latter range is, in fact, where the high age releases are observed.

Argon released after 1180°C indicates gradually increasing ages, after an abrupt drop from 800 to 461 m.y. at 1200°C. After the 1200°C extraction step, 23% of the argon remains. The fact that the system retains a significant fraction of its gas at temperatures above 1200°C suggests the presence of a highly retentive phase.

The last 3% of the sample gas released is characterized by a somewhat, but not significantly, lower Ar^{40}/Ar^{39} ratio than the prior release. The lower ratio probably results from large errors involved in measuring the isotopic ratios of small amounts of argon.

The Ar^{39}/Ar_o^{37} ratios and the K/Ca ratios calculated for each release are shown in Fig. 3. The K/Ca ratios were calculated using the relation $K/Ca = 0.53\ Ar^{39}/Ar_o^{37}$ (see discussion of monzonite release curve). The overall average K/Ca ratio of the rock is 0.056, but the values measured for different temperature fractions range from 0.038 to 0.092. The highest K/Ca ratios are observed for the fractions yielding ages near 800 m.y. The variation observed in the K/Ca ratios is slightly puzzling, since petrologic examination of this rock suggests that plagioclase, An_{45-55}, is the major argon-containing phase. If this is the case, then all the argon released would be from the plagioclase, and the K/Ca ratios of gas released from different temperature fractions should not vary. It is possible that argon is being released from sites with different

K/Ca ratios than plagioclase, possibly from hornblende. Hornblende is somewhat more abundant in the slightly shocked anorthosite than in the other shock-sequence anorthosites (see Appendix, PART I). The releases above 1110°C have very similar Ar^{39}/Ar^{37}_{o} ratios, suggesting that they are all from the same material.

A tentative interpretation of the release curve of the slightly shocked anorthosite is suggested by the dashed line in Fig. 3. The release curve is thought to characterize a rock system, originally about 900 m.y. old, which was partly outgassed at around 225 m.y. The outgassing process left some grains which suffered very little gas loss and caused partial gas loss and removal of grain defects in others. The very slightly outgassed grains account for the 794 and 832 m.y. ages observed in the 1070 and 1180 °C temperature fractions. The gas released at 1275, 1360 and 1455 °C is probably from the annealed, highly retentive grains.

The outgassing event was probably a shock-metamorphic event. If the age indicated by the first release is taken to be the time of partial shock outgassing, then this shock time was about 226 m.y. ago. This age is greater than the monzonite age of 210 m.y., although the significant difference between the two ages is very small.

A possible interpretation of the two low-age fractions is that they are due to gas released from a small amount of a mineral introduced into the anorthosite system during an event later than 193 m.y. As will be shown in CHAPTER 2, this mineral must have a higher activation energy than the plagioclase in order to explain the observed features of the curve. The later event probably caused some gas loss in the least retentive fractions of the shocked rock, and the time of the shock outgassing may actually be somewhat earlier than the 226-m.y. age indicated by the initial argon releases.

The idea that a secondary phase is responsible for the low ages is grasped at rather than embraced. It is possible that the phase yielding a low age in this rock is a secondary zeolite. Zeolites may have higher activation energies than plagioclase (Musset, 1969) and were occasionally observed in thin sections of this anorthosite. Murtaugh and Currie (1969) have shown that some anorthosites in the central massif have been severely zeolitized. In order to explain the observed features, however, the secondary zeolite would have to comprise about 15% of the rock . The observed mode of zeolite in this anorthosite never exceeded 2%. A smaller amount of secondary, high-potassium zeolite, or lower-age zeolite, would also explain the observed features. The presence of high-potassium zeolite is unlikely, however, because the K/Ca ratio of the phase is about 0.060. A high-

potassium zeolite would have a K/Ca ratio of about 2.

iii. Diffusion properties of the slightly shocked anorthosite -- Using the amounts of Ar^{39} released at different temperatures, and assuming that the slightly shocked anorthosite behaves as a system of spheres with uniform grain size, values of D/a^2 at different temperatures were calculated. These values were then plotted on an Arrhenius plot; values of $D/a^2\Big|_{20^\circ C}$ and activation energies were inferred from this graph. Below 950°C, the anorthosite behaves as a system with a very low activation energy ($\sim$ 6 kcal/mole) and $D/a^2\Big|_{20^\circ C} = 10^{-8}$-$10^{-9}$. Above 950°C, the anorthosite behavior is similar to that of a system with $D/a^2\Big|_{20^\circ C} = 10^{-24}$ and $E_a = \sim 30$ kcal/mole.

The diffusion properties of the slightly shocked anorthosite suggest that part of the argon in the rock is either contained in very fine grains or adsorbed on grain surfaces; argon present in these sites is released very easily. The remainder ($\sim$ 2/3) of the argon in the rock is contained in grains which, although possibly fractured, have diffusion characteristics closer to those of plagioclase (i.e., $D\Big|_{100^\circ C} = 10^{-15}$, $E_a = \sim 30$ kcal/mole). The low value of $D/a^2\Big|_{20^\circ C}$ inferred for this sample suggests that the rock will lose argon very easily, either by continuous diffusion or by heating due to a slight thermal metamorphic event.

(c) Maskelynitized anorthosite. Potassium-argon, total-rock ages were obtained for two samples of maskelynitized anorthosite from Locations B and C (see Fig. 3, CHAPTER 1, PART I). An Ar^{40}-Ar^{39} release curve as well as diffusion parameters were measured for Sample C. Both anorthosite samples are composed almost entirely of clear, isotropic glass of n = 1.535 (maskelynite) with a little fractured garnet and pyroxene. Petrographic descriptions of these two rocks and a discussion of the shock effects present in them are found in PART I. The maskelynitized anorthosites have probably experienced shock pressures between 250-350 kb and an in-shock temperature between 220-600 °C. Subsequent to the shock-wave passage, the temperature of the material is believed to have adiabatically cooled to between 80-400 °C. (Fig. 8). It is worth noting that neither the in-shock temperature nor the post-shock temperature of this rock is sufficiently high to cause melting of the plagioclase.

i. Ar^{40}-K^{40} age -- Samples B and C yield total argon ages of 323 and 320 m.y., respectively (see Table 3). The remarkable similarity in appearance and argon ages of these two maskelynitized anorthosites, which were located six miles apart, may be more than coincidence. The process of maskelynitization might involve some well-defined thermal history during shock which results in repeatable outgassing patterns for the maskelynitized rocks.

The maskelynitized anorthosites, which are produced by moderate (~ 350 kb) shock pressures, yielded ages ~ 300 m.y.; they therefore appear to have lost more than 80% of their pre-shock argon. (It will be shown later that the shock event probably occurred between 300 and 210 m.y. ago.) The slightly shocked anorthosite experienced a shock pressure of ~ 200 kb and lost more than 50% of its pre-shock argon. These facts suggest that argon loss increases rapidly with increasing shock pressure in the region from 0-300 kb.

ii. Ar^{40}-Ar^{39} release data -- A split of irradiated 60- to 80- mesh maskelynitized anorthosite (Sample C) was stepwise heated and an Ar^{40}-Ar^{39} release curve obtained. The material used for the Ar^{40}-Ar^{39} analysis was a split of the sieve fraction used for the total argon extraction. The amounts of argon isotopes released during each temperature step are shown in Table 5A. The Ar^{40}/Ar^{39} ratios and ages and the Ar^{39}/Ar^{37}_{o} ratios derived from the values in Table 5A are presented in Table 5B. "Ages" for each temperature fraction were calculated from the Ar^{40*}/Ar^{39} ratios using a value of $J = 5.165 \times 10^{-4}$. The Ar^{40}-Ar^{39} ages for each release step are shown plotted as a function of the cumulative Ar^{39} released by the sample in Fig. 4.

The J value used for calculating the Ar^{40}-Ar^{39} ages in Fig. 4 (5.165×10^{-4}) was computed using the overall average Ar^{40}/Ar^{39} ratio of the sample and the total argon age measured for the sample. Since both the average ratio and the total argon age were measured on splits of the same whole-rock mesh fraction,

TABLE 5A.

Maskelynite Data**

Extraction Step	Ar^{40*} 10^{-8}ccSTP	Ar^{39} 10^{-8}ccSTP	Ar^{38} 10^{-8}ccSTP	Ar^{37} 10^{-8}ccSTP	Ar^{36} 10^{-8}ccSTP	Ar^{40} Total
125 ma	6.76	0.046 (1416.3) -3.6 +11.4	0.110 (598) ± 3.1	0.178 (369.1) ± 0.6	0.200 (329.3) -0.8 + 1.5	65.83
150 ma	12.08	0.047 (432.6) -1.2 +10.6	0.008 (2631) ± 7.1	0.132 (154.3) ± 0.9	0.028 (724.5) -2.0 +9.2	20.41
200 ma	42.00	0.124 (398.7) -0.9 +4.1	0.011 (4679) ± 21.1	0.431 (115.0) ± 0.3	0.026 (1940.2) -0.9 +4.2	49.55
250 ma	82.97	0.229 (395.9) ± 23.0	0.012 (7879) ± 15.0	0.720 (125.9) ± 3.1	0.026 (3474.3) ± 23.0	90.68
350 ma	38.22	0.085 (581.0) -0.6 +5.9	0.028 (1777) ±62.0	0.308 (161.3) ± 0.2	0.039 (1282.3) -0.6 +6.2	49.66

(TABLE 5A -- continued)

Extraction Step	Ar^{40*} 10^{-8}ccSTP	Ar^{39} 10^{-8}ccSTP	Ar^{38} 10^{-8}ccSTP	Ar^{37} 10^{-8}ccSTP	Ar^{36} 10^{-8}ccSTP	Ar^{40} Total
450 ma	64.76	0.134 (536.4) -0.8 +3.8	0.018 (4021) ± 18.8	0.489 (147.3) ± 0.2	0.024 (2948.0) -2.3 +10.7	71.97
550 ma	31.68	0.084 (492.7) -3.3 +6.9	0.008 (5031) ± 26.7	0.293 (140.8) ± 0.2	0.032 (1275.6) -1.8 +8.1	41.23
650 ma	49.49	0.138 (485.4) -1.2 +3.8	0.026 (2594) ± 13.0	0.505 (132.2) ± 0.2	0.059 (1140.3) -1.9 +4.8	66.81
750 ma	3.60	0.022 (953.6) -2.5 +22.6	0.010 (2102) ± 5.6	0.064 (335.5) ± 1.8	0.060 (355.3) -0.9 + 4.4	21.40
900 ma	2.23	0.014 (1122.7) -8.0 +36.9	0.019 (822) ± 2.9	0.052 (305.9) ± 8.7	0.046 (343.9) -2.5 +6.1	15.86

** Gas amounts in ccSTP x 10^{-8}. Measured ratios of A^{40} to isotope indicated in parentheses. Errors are standard deviation in %. Gas amounts shown are from the 0.5893-gm sample, not the amounts released per gm.

TABLE 5B.

Maskelynite Results

Extraction Step	Temperature	Ar^{40*}/Ar^{39}	Age+	Cumulative Release	Ar^{39}/Ar^{37}_{o}	Air Fraction
125 ma	600°C	145.4 -3.6 +15.9	136.5	0.0498	0.105	0.8973
150 ma	790 °C	256.2 -1.2 +12.3	234.2	0.1008	0.142	0.4078
200 ma	870°C	337.9 -1.0 +4.5	303.3	0.2351	0.114	0.1523
250 ma	940°C	362.2 -22.9 +23.0	323.3	0.4832	0.125	0.0851
350 ma	1070°C	447.1 -0.6 +6.2	391.6	0.5753	0.108	0.2304
450 ma	1250°C	482.7 -0.8 +4.0	419.6	0.7205	0.107	0.1002
550 ma	1340 °C	378.6 -3.3 +7.3	336.6	0.8115	0.111	0.2317

(TABLE 5B -- continued)

Extraction Step	Temperature	Ar^{40*}/Ar^{39}	Age+	Cumulative Release	Ar^{39}/Ar^{37}_{o}	Air Fraction
650	1450°C	359.6 -1.2 +4.1	321.2 -1.2 +4.1	0.9610	0.105	0.2592
750	1560°C	160.6 -2.5 +30.8	150.2 -2.5 +30.8	0.9848	0.135	0.8316
900	1640°C	158.0 -8.0 +50.0	147.9 -8.0 +50.0	1.000	0.104	0.8593

+ Age = $\tau \ln(A^{40*}/A^{39} \cdot J + 1)$ $\quad J = 5.165 \times 10^{-4}$

* Ar^{40*} = radiogenic argon 40. $\quad \tau$ = mean life = 1.88 b.y.

the computed J value should be quite accurate. This value was only about 6% higher than the J value obtained for the sample by using the J value of the monzonite and the flux map for the sample canister (4.861×10^{-4}) (see CHAPTER 2). The agreement between the two different J values is satisfactory, and the uncertainty in the value used is estimated to be about ± 6%. Due to this uncertainty, the mean age of the release curve may be in error by about 18 m.y.; also, the 110-m.y. initial age inferred for the rock is within 6 m.y. of the actual age of the thermal event thought to have affected the rock.

The release pattern for the maskelynite can be divided into three regions: (1) Between 600 and 870 °C, the ages increase rather rapidly from about 136 to 303 m.y. (2) For extraction temperatures between 940 and 1250 °C, there is a progressive increase in indicated age to a value of 420 m.y. (3) The 1340 and 1450 °C temperature fractions are characterized by a lower age of approximately 330 m.y. The gas released above 1350°C has low indicated ages with large uncertainties associated with them.

As was the case for the slightly shocked anorthosite, the maskelynite release curve is much more complicated than the release curves discussed by Turner (1968).

The maskelynite release curve is not flat, and it is clear that the whole-rock, Ar^{40}-K^{40} age of the maskelynite <u>is not</u> the age of a uniformly outgassed system with a well-defined time of gas loss. It is difficult to associate this curve with any of the

partially outgassed model systems discussed by Turner (1968). None of the release curves discussed by Turner have high-temperature gas fractions with lower Ar^{40}-Ar^{39} ages than previous gas fractions, although such low-age, high-temperature fractions are clearly present in the maskelynite release curve. Despite the obvious complications present in the maskelynite system, several observations can be made from the release curve.

A smooth curve drawn through the ages of the first three temperature fractions of the maskelynite has a "zero release" intercept of 110 m.y. (see Fig. 4). Three possible interpretations of this "age" can be made:

(1) That this time represents a real event in the history of the rock, i.e. the rock was partially outgassed about 110 m.y. ago.

(2) That this age is only apparent, and more heating steps with smaller Ar^{39} amounts released in each step would show a curve with a continuous-diffusion profile.

(3) That the age is apparent, and that more heating steps would show a release curve which indicates episodic argon loss at zero time. Argon loss at zero time could be caused by heating during the irradiation.

The $D/a_2\Big|_{20^\circ C}$ estimated for the maskelynitized anorthosite is 5-6 orders of magnitude lower than the $D/a^2\Big|_{20^\circ C}$ value obtained for the monzonite. If the low initial ages of the maskelynite are

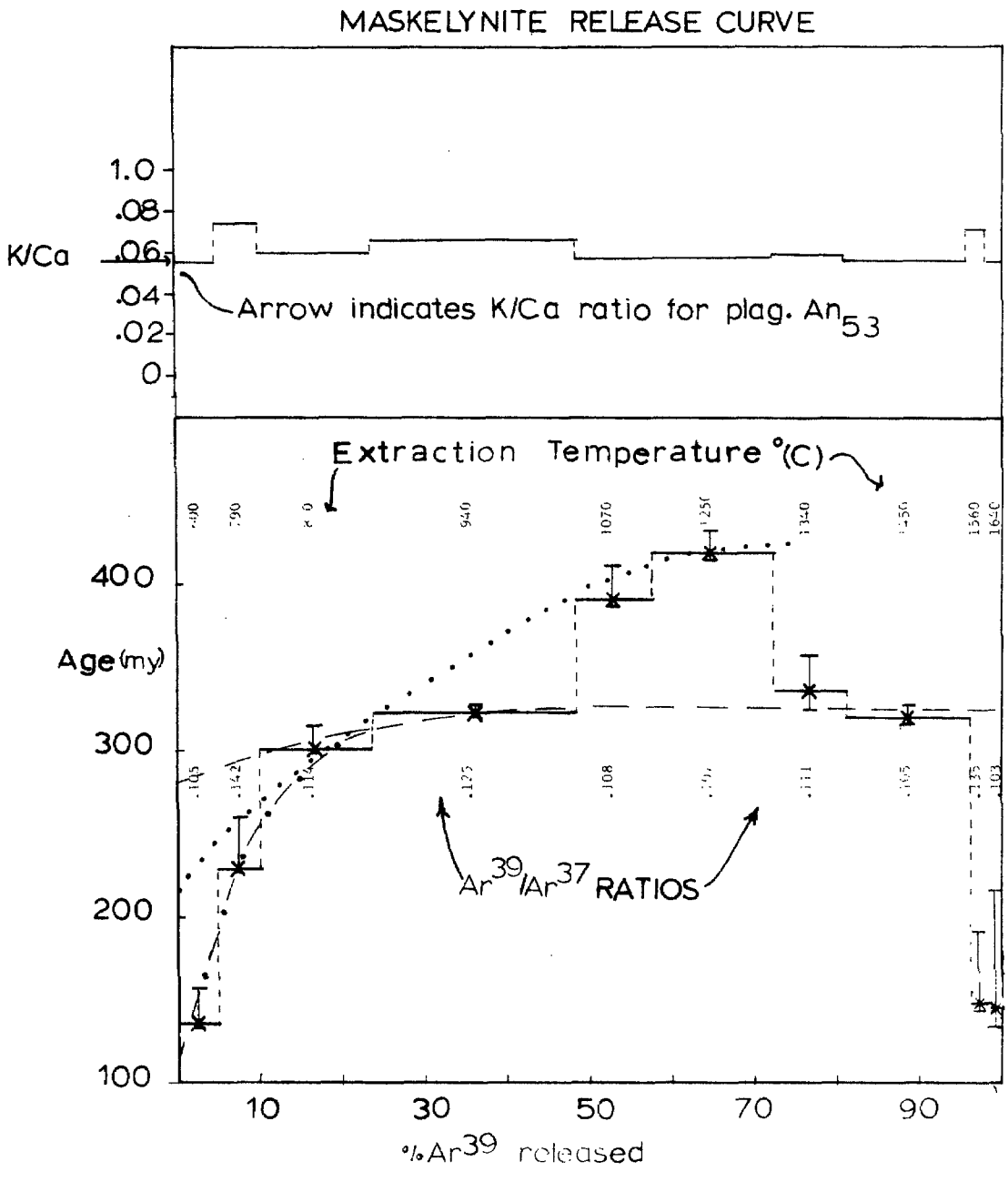
MASKELYNITE RELEASE CURVE
1.0
.08
K/Ca
.06
.04
.02
0
Arrow indicates K/Ca ratio for plag. An53
Extraction Temperature °(C)
940
1070
1250
1340
1560
1640
400
Age (my)
300
200
100
Ar39/Ar37 RATIOS
10
30
50
70
90
%Ar39 released

FIG. 4

due either to continuous argon diffusional loss or to heating losses in the reactor, then low ages for initial releases of the monzonite should also be observed. Since such low-age, initial releases are not observed for the monzonite, it would seem that the first explanation listed above is the most likely.

The higher Ar^{40}-Ar^{39} ages observed in the 1070 and 1250 ^{o}C argon fractions may be regarded in two ways: (1) They may be considered to be distinctly higher ages superimposed on a more-or-less uniform set of ages from the most argon-retentive sites of the rock. (2) These two ages may be considered as part of a generally increasing trend in ages from more retentive sites of the rock.

In the first case, the high ages can be interpreted as coming from plagioclase grains with high Ar^{40}/Ar^{39} ratios (i.e., those grains which still retain much of their pre-shock radiogenic argon). If the high ages are considered part of a general trend of the Ar^{40}-Ar^{39} ages from the more retentive sites, then they can be interpreted as characterizing argon from the most highly retentive sites of the partially outgassed rock. In the second case, it must be assumed that some abnormally high-retentivity material is produced during the outgassing. In order to account for the lower ages of the high-temperature fractions, it must also be assumed that this abnormally high-retentivity material has an Ar^{40}/Ar^{39} ratio lower than the ratio of the least-outgassed lattice sites in the original rock.

The Ar^{40}/Ar^{39} ratios of the 1340 and 1450 °C temperature fractions are distinctly lower than the ratios obtained for the previous fractions. A similar, but not as marked, drop-off is present in the Ar^{40}/Ar^{39} release curve of Lunar Rock 12013 (Turner, 1970). Turner et al. (1971) have also observed this behavior for other lunar shock breccias.

A decrease in the Ar^{40}/Ar^{39} ratios for high-temperature argon releases is not predicted in the partial loss models discussed by Turner (1968). At the present time, no satisfactory explanation exists for this drop-off in ages.

For the maskelynitized anorthosite, the K/Ca ratios of the argon released at all temperatures is nearly identical. In particular, the gas released above 1250°C has the same K/Ca ratio ($\sim$ 0.056) as the gas from other temperature fractions, and this K/Ca ratio is similar to that of plagioclase (An_{53}). The phase which releases the argon above 1250°C, therefore, probably has the same composition as plagioclase.

Apart from its low age (compared to previous releases), the portion of the release curve above 1250°C is unusual in that it implies argon is still present in the rock. Fechtig et al. (1960) have measured diffusion properties for anorthite. Extrapolations of their data suggest that D at 1150°C is in excess of 10^{-6} ($D/a^2 = 10^{-4}$ for 1-mm grains). A one-hour heating of plagioclase at 1150°C would then be expected to totally release argon present in that mineral. Unirradiated maskelynitized anorthosite also has high retentivity at high temperatures; about 25% of the gas in the unirradiated

sample was released above 1200°C (see next section).

It is unclear what is responsible for the high argon retentivity of plagioclase in the shocked anorthosites. This question is considered in more detail in CHAPTER 2. One possible explanation is that the shock process not only fractures grains but also anneals imperfections producing some grains with large, effective, diffusion path lengths. These large grains would have K/Ca ratios characteristic of An_{55} and small D/a^2 values. They would therefore be highly gas-retentive phases. It is possible that the high retentivity is characteristic of both shocked and unshocked plagioclase from Manicouagan. This seems unlikely, but the possibility must be investigated before these high-retentivity phases are conclusively attributed to shock production.

The last 4% of the gas release is characterized by low Ar^{40}-Ar^{39} ages. Large errors are involved in measuring the small amounts of Ar^{40} and Ar^{39} released in the last two extraction steps. These errors arise because the mass spectrometer background levels at mass 36 and mass 39 represent a significant, but unknown, part of the total isotope levels at these masses. The Ar^{40}/Ar^{39} ratios measured for these extraction steps may not be significantly lower than the Ar^{40}/Ar^{39} ratios of the preceding temperature step.

The Ar^{39}/Ar_O^{37} ratios (hence, the K/Ca ratios) measured for all the extraction steps of the maskelynite are constant to within ± 20% and indicate a K/Ca ratio of about 0.054. A K/Ca ratio of 0.054 is compatible with the measured composition of

An_{55}(K/Ca = 0.056) (see Appendix; also, CHAPTER 1 of PART I). The similarity of the K/Ca ratios in the different fractions suggests that all of the argon releases are from material chemically similar to plagioclase, An_{55}.

Two tentative interpretations of the general features of the maskelynite release curve are as follows:

(1) The maskelynite release curve may represent a variation of the release curve for a system of grains which experienced fairly complete outgassing about 280 m.y. ago. The dashed line in Fig. 4 indicates the general form expected for the release curve of such a system. During the gas loss event, some plagioclase was transformed to a highly retentive material with very little of its original pre-shock argon remaining. This highly retentive material is evidenced by the portion of the maskelynite release curve at temperatures above 1200°C. Some of the plagioclase grains in the original rock retained relatively large amounts of their original pre-shock argon. The high Ar^{40}/Ar^{39} ratios of the argon released from these grains during the laboratory extraction results in the distinctly higher ages of the 1070 and 1250 °C temperature fractions. A secondary gas loss event which occurred about 110 m.y. ago partially outgassed some of the less retentive grains in the rock. This secondary gas loss event is responsible for the low ages indicated in the initial temperature steps of the laboratory release. The dot-dashed curve in Fig. 4 indicates the expected effect of the secondary heating on the curve of the original system.

(2) Alternatively, the maskelynite release curve may be interpreted as a variation of the release curve of a system which was partially outgassed about 210 m.y. ago. The dotted line in Fig. 4 shows the general form of a release curve for this system. The outgassing event left some argon-retaining sites in the rock with a fairly "old" Ar^{40}/Ar^{39} ratio. Ratios in these sites correspond to an age of about 419 m.y. The outgassing event also produced some highly retentive plagioclase which lost some, but not all, of its pre-shock argon. This highly retentive plagioclase yields Ar^{40}-Ar^{39} ages of about 320 m.y. A secondary thermal event which occurred about 110 m.y. ago was superimposed on the original outgassing event.

An Ar^{40}-Ar^{39} release curve similar to that of the maskelynite anorthosite could characterize a system which has experienced a number of possible histories. Any history which includes (1) an outgassing event later than about 280 m.y. and (2) a superimposed, secondary thermal event at about 110 m.y. will, under appropriate conditions, produce gas loss in a rock such that its release curve resembles that of the maskelynitized anorthosite. A 210-m.y. age for the original outgassing event is suggested by the argument that the 210-m.y. monzonite formed at the time of shock; not from consideration of the release curve data.

iii. Diffusion characteristics of the maskelynitized anorthosite -- Two experiments were performed in order to obtain information about the argon-retention characteristics of the maskelynite.

(1) A thermal release experiment was carried out by heating a split of the maskelynite (Sample C) for one hour at various temperatures and measuring the yields and compositions of the argon released (see Fig. 5).

(2) D/a^2 values for different temperatures were calculated. The D/a^2 values were plotted as a function of inverse temperature; values of $D/a^2\Big|_{20^\circ C}$ and activation energies of the maskelynite were then inferred from the plot.

The fractional losses of argon from the unirradiated maskelynite are shown plotted versus temperature in Fig. 5. Fractional releases of radiogenic argon from a typical anorthite are also shown for comparison in Fig. 5. The anorthite releases have been calculated from the data of Fechtig et al. (1960), assuming a grain radius of 1 mm.

Three features of the maskelynite gas release behavior are apparent from Fig. 5.

(1) Air composition (Ar^{40}/Ar^{36} = 295.5) argon is essentially totally released at about 600°C. The amounts of air argon released at temperatures higher than this are zero (within error limits) after the extraction blank is subtracted.

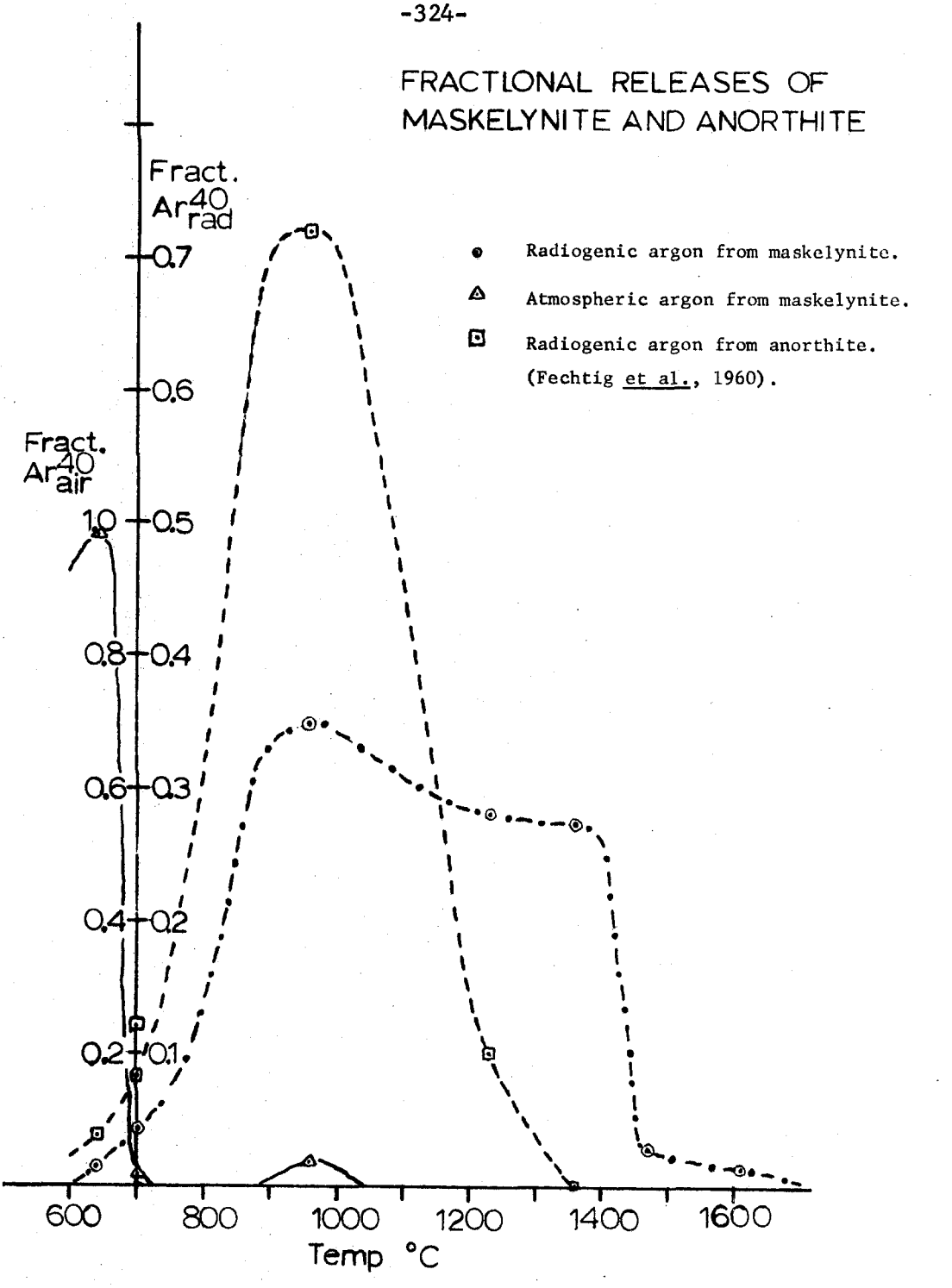
FRACTIONAL RELEASES OF
MASKELYNITE AND ANORTHITE
Radiogenic argon from maskelynite.
Atmospheric argon from maskelynite.
Radiogenic argon from anorthite.
(Fechtig et al., 1960).
Fract. Ar40 rad
Fract. Ar40 air
0.7
0.6
0.5
0.4
0.3
0.2
0.1
1.0
0.8
0.6
0.4
0.2
600
800
1000
1200
1400
1600
Temp °C

FIG. 5

(2) Radiogenic argon (Ar^{40}/Ar^{36} = 1000 - 15,000) is released over a broad range of temperatures from 700°C up to the melting temperature of the maskelynite.

(3) Complete radiogenic release occurs only above 1300°C. It can be seen that a rock composed of 1-mm grains of anorthite, heated with the same temperature steps as the maskelynite, releases its argon completely by the time it has reached 1150°C. This suggests that the maskelynite rock has a higher argon retentivity than the chemically (though not mineralogically) similar anorthite rock.

Using the data for the fractions of argon released at different temperatures and assuming that volume diffusion from uniform spherical grains was effective, values of the diffusion parameter D/a^2 were calculated for the maskelynite at the different temperatures. For the unirradiated maskelynite, these data involved the releases of radiogenic Ar^{40} from the rock; for the irradiated maskelynite, the Ar^{39} fractions released during each temperature step were employed. Logarithims of the D/a^2 values from the maskelynite are shown plotted versus $10^3/T$ in Fig. 6. The D/a^2 values indicated by the unirradiated maskelynite are consistently about one order of magnitude lower than those obtained from the irradiated maskelynite. This difference is thought to be due to consistently low extraction temperature estimates made for the irradiated material rather than to differing diffusion properties of Ar^{40} compared to Ar^{39}.

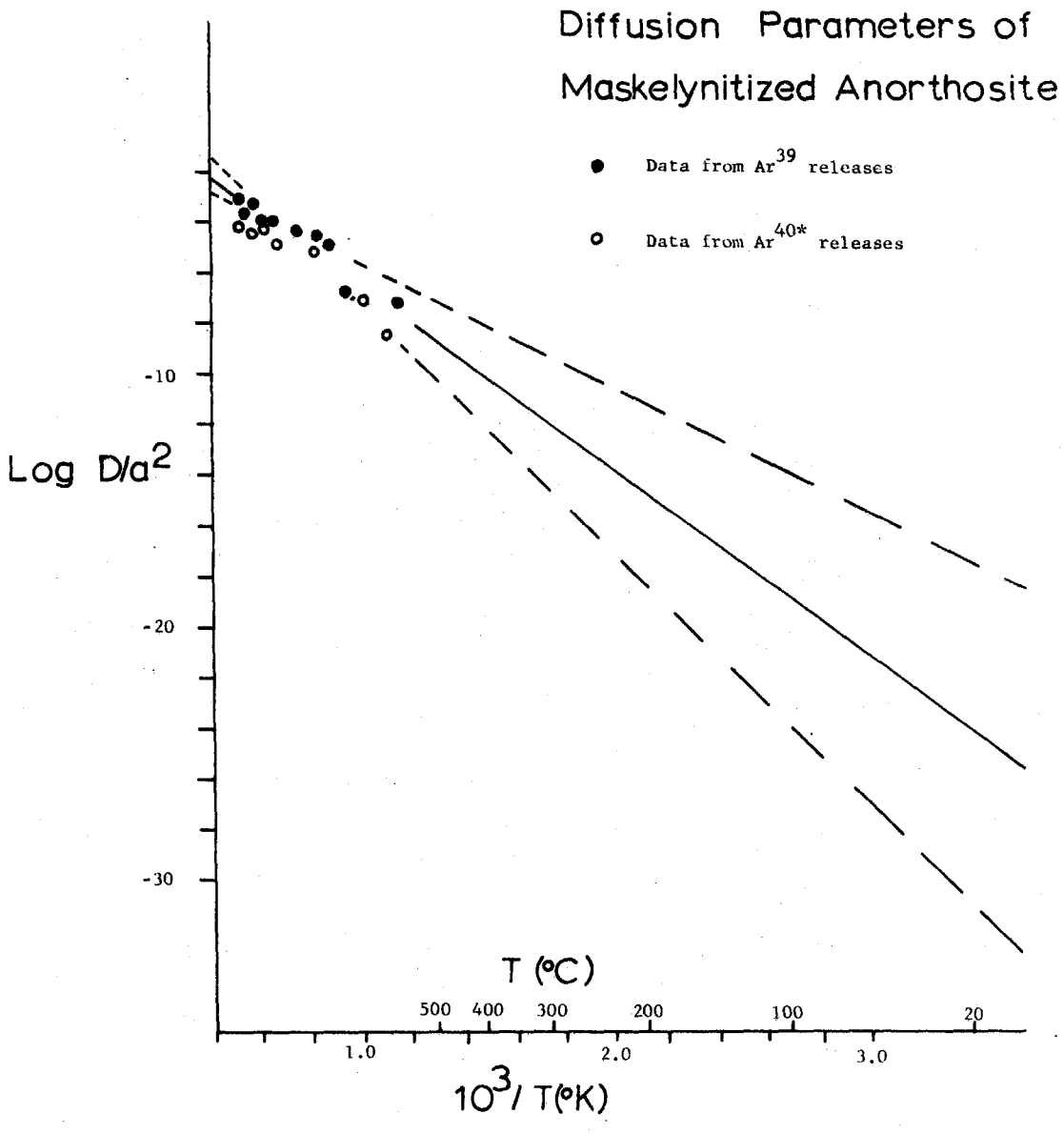
Diffusion Parameters of
Maskelynitized Anorthosite
Data from Ar^{39} releases
Data from Ar^{40*} releases
Log D/a^2
-10
-20
-30
T (°C)
500 400 300 200 100 20
1.0
2.0
3.0
$10^3/T(°K)$

FIG. 6

Although the data show a wide scatter, a linear fit is justified. Estimates of $D/a^2\Big|_{20^\circ C}$ range from about 10^{-18}/sec to about 10^{-30}/sec. Median values of $D/a^2\Big|_{20^\circ C}$ and activation energy for the maskelynite are about 10^{-25}/sec and 30 kcal/mole, respectively.

It is worth noting that the mean $D/a^2\Big|_{20^\circ C}$ value estimated for the maskelynite is about 5-6 orders of magnitude lower than estimates of $D/a^2\Big|_{20^\circ C}$ for the monzonite. An extreme interpretation of the diffusion data suggests that $D/a^2\Big|_{20^\circ C}$ values for the two rocks might be about equal. Estimates of $\frac{\lambda}{D/a^2\Big|_{20^\circ C}}$ for the maskelynite range from 10^1 - 10^{13} with a most probable value of 10^7. Continuous diffusional argon loss from this rock, therefore, is possible but not expected.

It is notoriously difficult to determine low-temperature diffusion properties of rocks from high-temperature release data, and any conclusions based on extrapolated diffusion data are therefore tentative. A simple interpretation of the measured diffusion properties of this rock, however, suggests that maskelynite is <u>not</u> extremely susceptible to argon loss, and that it is at least as argon retentive as the monzonite.

(d) Highly shocked anorthosites. Two highly shocked anorthosites (see Map Locations E and F, Fig. 3, CHAPTER 1, <u>PART I</u>) from the central anorthosite massif were analyzed for argon and potassium. The analyzed samples (referred to as E and F) consisted of the

60- to 80- mesh sieve fractions of the crushed whole rocks. Samples E and F yielded ages of 371 and 275 m.y., respectively.

Both anorthosite samples are characterized by lack of planar features, maskelynite or signs of plastic flow. Both samples contain chemically heterogeneous garnets which are believed to be the result of thermal breakdown of garnet within the grain. Petrographic descriptions and a discussion of the shock-metamorphic textures of these rocks are presented in PART I. Both of these anorthosite specimens are estimated to have experienced shock pressures of 450-600 kb. These shock pressures probably resulted in in-shock temperatures of the rocks ranging from 1100-2200 ^{o}C and post-shock temperatures ranging from 400-1200 ^{o}C (see Fig. 9).

There is a difference of nearly 100 m.y. in the ages of these two samples, even though they are believed to have experienced similar shock pressures. The reason for this age discrepancy is not understood. Sample E was analyzed in duplicate with reasonably consistent results (see Table 3), and there is no reason to believe that Sample F has larger than normal (normal = $\pm$ 1-2%) errors associated with its age.

A simple theory of argon loss during shock predicts that the two highly shocked anorthosites should have ages lower than the less highly shocked maskelynitized anorthosites. The age of Sample F is compatible with the above interpretation, but the high age of Sample E clearly is not.

One possible explanation of the 371-m.y. age is that the shock features in these anorthosites have been misinterpreted; that the anorthosites actually experienced shock pressures of between 200-300 kb. If this were the case, then these anorthosites would be expected to have a higher age than the maskelynite. The 371-m.y. age of Sample E would be expected, while the 275-m.y. age of Sample F could be attributed to post-shock diffusion loss from the latter sample.

The shock pressures experienced by Samples E and F are difficult to determine because few features capable of correlation with well-studied shocked systems are present. Chemically heterogeneous garnet, which is probably due to high shock-induced temperatures, is present in Samples E and F but absent from Samples A, D, C and B. This is thought to be strong, if not conclusive, evidence that anorthosites E and F have experienced higher shocks and more intense shock heating than anorthosites A, D, C and B.

If the shock-pressure assignment for Samples E and F is correct, then the 275-m.y. age can easily be interpreted as being due to nearly complete argon loss during the shock event. The 371-m.y. age of Sample E is more difficult to interpret. This age may be due to incomplete gas loss during the shock. If this is the case, however, Sample F would likewise be expected to be incompletely outgassed and would yield an age higher than

280 m.y.

(e) Pseudotachylyte-shocked anorthosite breccias. Two samples of a pseudotachylyte-shocked anorthosite breccia were collected from Map Locations G and H in the central anorthosite massif (see Fig. 3, CHAPTER 1, PART I). Samples from Locations G and H are breccias which consist of a pseudotachylyte matrix enveloping fragments of extremely stretched and contorted anorthosite. The pseudotachylyte matrix is grey in H and reddish brown in G. In each case, the matrix is an agglomeration of aphanitic material and very small rock fragments. The sample from Location G is from a breccia lens or pod surrounded by visibly undisturbed anorthosite. The highly shocked anorthosite, Sample E, was obtained from a spot in the undisturbed anorthosite a few inches away from this breccia pod.

Splits of the 60- to 80- mesh sieve fractions from the crushed whole rocks were analyzed for potassium and argon. One- to two-millimeter-sized chunks of the sample from Location G were irradiated and stepwise heated; an Ar^{40}-Ar^{39} release curve for the material was then obtained.

Petrographic descriptions of Samples G and H (the whole rocks and samples of the rocks are referred to interchangeably by their map locations) are provided in the Appendix to PART I; the shock features in these rocks are discussed in CHAPTER 1 of PART I. Both rocks show strong evidence of plastic flow, and they are

believed to have experienced shock pressures between 500-800 kb (see Fig. 4, CHAPTER 1, PART I). At these shock pressures, the rocks probably experienced in-shock temperatures greater than 1400°C; the post-shock temperatures were probably between 700-1300 °C (see Fig. 9).

i. Ar^{40}-K^{40} ages -- The total argon ages obtained for splits of the 60- to 80- mesh sieve fractions from Samples G and H were 280 and 202 m.y., respectively. Both samples are thought to have experienced the same shock intensity; if a simple correlation of shock intensity with extent of outgassing exists, the ages of both samples should be nearly identical. It is unlikely that analytical errors greater than 2% exist in the age measurements; the age difference between the two samples is thought to be real. The reason for this difference is not completely clear.

One possible interpretation of the ages of these two breccias is that the 202-m.y. age of Sample H is a result of almost complete outgassing during a shock-formation event of 210 m.y. ago. Subsequent to this shock event, the breccia sample could have diffusively lost some radiogenic argon from its fine-grained matrix such that it indicates a 202-m.y. age. If this interpretation is accepted, then the 280-m.y. age measured for Sample G can be ascribed to incomplete outgassing of the rock during the shock event. This interpretation sidesteps the question of why similarly shocked rocks are not similarly outgassed.

An alternative interpretation of the experimental data is to assume that Sample G experienced nearly complete outgassing during a shock event around 280 m.y. ago. The lower age of Sample H can then be interpreted in two ways: (1) The low age might be the result of post-shock diffusive loss of argon from the fine-grained matrix of the breccia. Similar diffusive loss might not have affected Sample G. (2) The low age might be due to some secondary potassium addition, perhaps related to the zeolite occurrences in other parts of the massif (Murtaugh and Currie, 1969). The potassium measurements for Sample H provide some tenuous support for the second hypothesis. The secondary potassium enrichment in Sample H would have to be about 30%. Sample H has, in fact, about 30% more potassium than the "average" anorthosite (0.6% potassium for Sample H versus 0.45% potassium for an average anorthosite).

Zeolites, which may be secondary, are present in both Samples H and G and are slightly more extensive in Sample H (see Appendix, PART I). Neither sample, however, displays extensive zeolitization, and the attempt to attribute the observed irregularities in the ages to secondary mineralization is somewhat forced and ad hoc .

ii. Diffusion properties of the pseudotachylyte-shocked anorthosite breccia -- Values of D/a^2 as a function of temperature were calculated for the pseudotachylyte-shocked anorthosite breccia using the Ar^{39} release data from the Ar^{40}-Ar^{39} stepwise extraction. It was assumed, for the above calculations, that the Ar^{39} releases

were occurring from a system of uniform spherical grains.

When graphed on an Arrhenius plot, the D/a^2 values yield two more-or-less linear arrays of points. At temperatures below 1200°C, the D/a^2 values define a line with a $D/a^2\Big|_{20^\circ C}$ value of about 10^{-8}-10^{-9} and a very low activation energy of 5.5 kcal/mole. A straight line fitted to the points above 1200°C indicates a much higher activation energy of about 60 kcal/mole and a much lower $D/a^2\Big|_{20^\circ C}$ value of about 10^{-38}-10^{-42} /sec.

The diffusion properties of the pseudotachylyte-shocked anorthosite breccia are compatible with those of a system which contains (1) material of high gas retentivity and (2) material with a distribution of grain sizes including some very small, low-retentivity grains. The above properties are, in fact, expected for a breccia which contains large chunks enveloped in a matrix of finer-grained material. The slightly shocked anorthosite also exhibited diffusion properties similar to those observed for Sample G. In fact, the values of $D/a_2\Big|_{20^\circ C}$ and activation energy inferred for the slightly shocked anorthosite are nearly identical to those of the pseudotachylyte breccia.

The very low values for $D/a^2\Big|_{20^\circ C}$ inferred for the breccia suggest that diffusional loss of argon at low temperatures may extensively affect this rock. Loss could be due either to a slight thermal metamorphism or to continuous diffusion

$$\left.\frac{\lambda}{D/a_2}\right|_{20^{\circ}D} \sim 10^{-8}$$

Both of the pseudotachylyte-shocked anorthosite breccias, G and H, contain a large percentage of fine-grained matrix material. A high susceptibility to diffusive gas loss would be expected for both these breccia samples. As was previously indicated, diffusive argon loss may be the cause of the age discrepancy between Samples G and H.

iii. Ar^{40}-Ar^{39} release curve of Sample G -- Fragments, about 1- to 2- mm in size, of Sample G were irradiated and then stepwise heated in order to obtain an Ar^{40}-Ar^{39} release curve for the pseudotachylyte breccia. The amounts of each argon isotope released during the different temperature steps are shown in Table 6a (the gas amounts shown are the actual gas amounts released by the sample). Temperatures, Ar^{40}-Ar^{39} ages, and cumulative Ar^{39} amounts for each temperature release are listed in Table 6b. The Ar^{40}-Ar^{39} release curve obtained for the pseudotachylyte-shocked anorthosite breccia is shown in Fig. 7.

It should be noted that the millimeter-sized rock fragments used for the Ar^{40}-Ar^{39} analysis were <u>not</u> splits of the 60- to 80-

mesh sieve fraction used for the total argon studies. Mineralogical and chemical properties of the specimen materials used for the different studies are probably not identical. The materials used in both types of analyses, however, are from the same hand specimen and therefore probably do not differ greatly.

The J value used in the calculation of the Ar^{40}-Ar^{39} ages is 4.861×10^{-4}. This J value has an uncertainty of about $\pm$ 6%, resulting in an uncertainty of $\pm$ 6% in the mean age of the release curve. This uncertainty does not affect the relative ages of the different temperature fractions.

As discussed in CHAPTER 2, this sample has the largest difference between the J value calculated on the basis of a total Ar^{40}-Ar^{39} age and the J value calculated from the monitor-determined neutron flux. The difference was about 30% for Sample G, as opposed to 5-6% for both Samples D and C. This is probably due to the fact that the chunks used for the Ar^{40}-Ar^{39} analysis of Sample G contain a relatively higher proportion of fine-grained matrix material than the 60- to 80- mesh sieve fraction used for the total argon analysis. A total argon analysis of the actual chunks used for the Ar^{40}-Ar^{39} studies would probably yield an age which agrees with the mean Ar^{40}-Ar^{39} age of 212 m.y. The difference between the two J values calculated is thought to be real and not the result of errors in the flux value determination; therefore, the J value determined on the basis of the monzonite monitor flux, $4.861 \times 10^{-4} \pm 6\%$, was used for the age calculations.

TABLE 6A.

Data for Pseudotachylyte-Shocked Anorthosite Breccia**

Extraction Step	Ar^{40*} 10^{-8}ccSTP	Ar^{39} 10^{-8}ccSTP	Ar^{38} 10^{-8}ccSTP	Ar^{37} 10^{-8}ccSTP	Ar^{36} 10^{-8}ccSTP	Ar^{40} Total
115 ma	59.94	0.296 (407.18) -1.8 +2.2		0.397 (303.09) ± 1.1	0.205 (588.2) -0.2 +1.0	120.45
150 ma	29.61	0.191 (257.65) -4.3 +5.0	1.874 (26.20) ± 3.5	0.235 (208.85) ± 1.7	0.066 (744.20) -1.7 +4.2	49.11
200 ma	30.69	0.153 (381.46) -1.1 +3.6		0.258 (226.54) ± 0.5	0.094 (623.1) -0.6 +2.9	58.37
250 ma	22.53	0.103 (395.55) -1.1 +5.2		0.115 (353.23) ± 0.5	0.061 (663.8) -2.9 +5.2	40.61
300 ma	11.54	0.061 (487.03) -2.8 +8.9		0.076 (392.85) ± 1.5	0.062 (481.9) -0.9 +4.4	29.825

(TABLE 6A -- continued)

Extraction Step	Ar^{40*} 10^{-8}ccSTP	Ar^{39} 10^{-8}ccSTP	Ar^{38} 10^{-8}ccSTP	Ar^{37} 10^{-8}ccSTP	Ar^{36} 10^{-8}ccSTP	Ar^{40} Total
350 ma	17.14	0.064 (708.11) -1.8 +8.2	0.081 (559.57) ± 15.7	0.115 (395.54) ± 0.5	0.095 (475.3) -0.6 +2.8	45.32
410 ma	13.07	0.045 (946.04) -1.3 +11.5		0.123 (347.42) ± 0.5	0.100 (425.9) -0.6 +2.7	42.71
495 ma	30.13	0.093 (568.67) -1.2 +5.7		0.211 (249.14) ± 0.6	0.076 (691.1) -0.8 +3.6	52.63
575 ma	91.26	0.243 (635.51) -0.5 +2.2	0.088 (1768.02) ± 4.6	0.565 (275.77) ± 0.3	0.219 (712.6) -0.5 +1.3	155.92
650 ma	7.92	0.030 (1116.99) -1.9 +17.4		0.071 (466.42) ± 0.8	0.085 (388.4) -1.4 +3.4	33.11

* Ar^{40*} = radiogenic argon.

** Gas amounts in 10^{-8}ccSTP, Ratios of Ar^{40} to isotope indicated in parentheses. Errors are indicated in percent. Gas amounts are for the 0.7794 gm sample, not per gram of sample.

TABLE 6B.

Data for Pseudotachylyte-Shocked Anorthosite Breccia

Extraction Step	Temperature	Ar^{40*}/Ar^{39}	Cumulative Ar^{39} Release	Age+	Ar^{39}/Ar^{37}_{o}	Fraction Air
115 ma	600°C	202.64 -1.8 +2.5	0.2314	177.1	0.211	0.5023
150 ma	780°C	155.35 -4.3 +5.6	0.3808	137.3	0.230	0.3971
200 ma	855°C	200.57 -1.1 +4.4	0.5004	175.4	0.162	0.4742
250 ma	960°C	219.46 -1.1 +6.2	0.5809	191.1	0.243	0.4452
300 ma	1010°C	188.38 -2.8 +11.1	0.6286	165.2	0.219	0.6132
350 ma	1140°C	267.86 -1.8 +9.4	0.6787	230.7	0.150	0.6217
410 ma	1230°C	289.60 -1.3 +12.9	0.7138	248.3	0.098	0.6939

(TABLE 6B. -- continued)

Extraction Step	Temperature	Ar^{40*}/Ar^{38}	Cumulative Ar^{39} Release	Age+	Ar^{39}/Ar^{37}_{o}	Fraction Air
495 ma	1330°C	325.52 -1.2 +6.3	0.7866	276.9	0.117	0.4276
575 ma	1395°C	371.96 0.5 +2.3	0.9765	313.3	0.114	0.4147
650 ma	1490°C	267.08 -1.9 +20.0	1.0000	230.1	0.109	0.7609

Ar^{40*} = radiogenic argon 40 + Age = $\tau \ln(Ar^{40*}/Ar^{39} \cdot J + 1)$ $J = 4.861 \times 10^{-4}$

τ = mean life = 1.88 b.y.

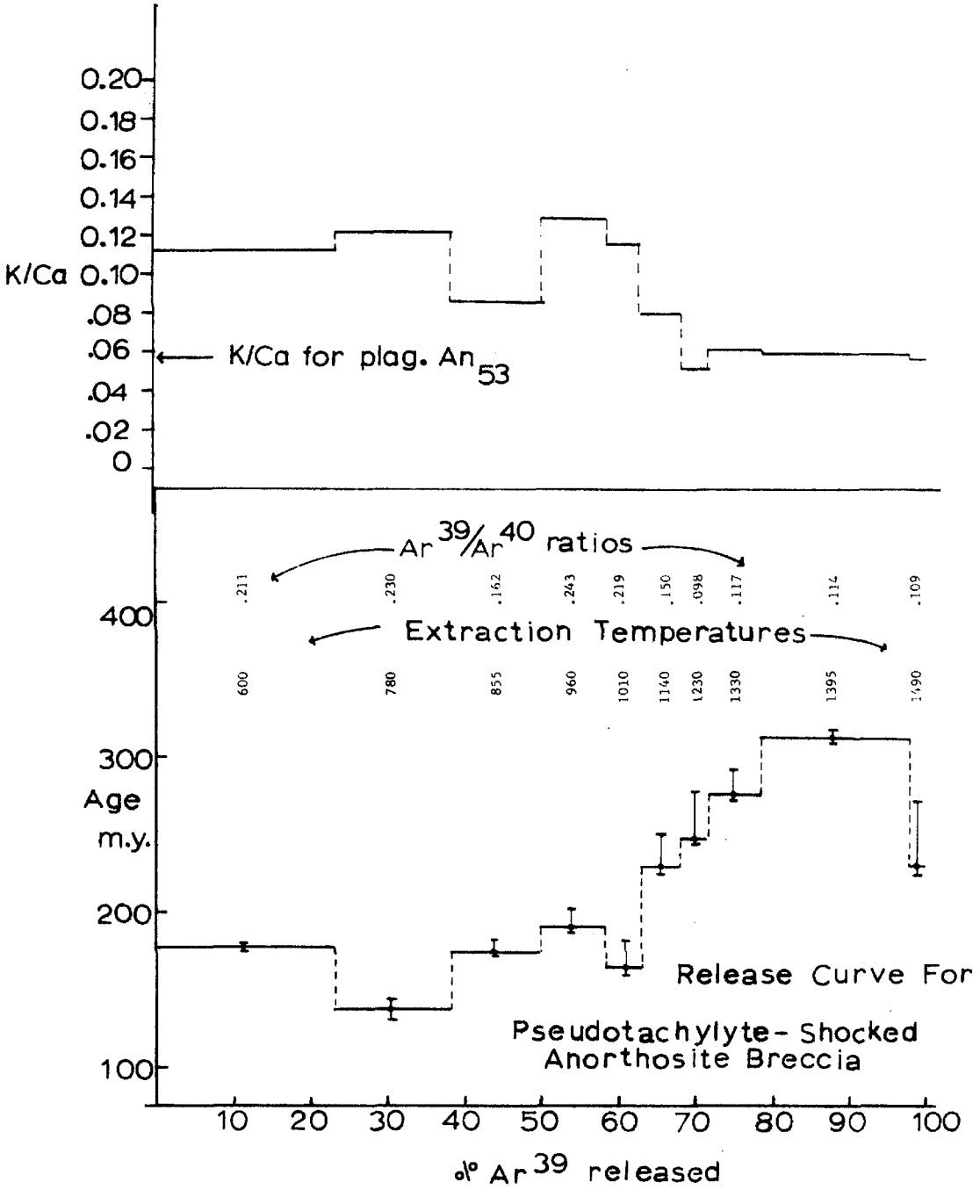
0.20
0.18
0.16
0.14
0.12
K/Ca 0.10
.08
.06
.04
.02
0
K/Ca for plag. An53
Ar39/Ar40 ratios
.211
.230
.162
.243
.219
.150
.098
.117
.114
.109
Extraction Temperatures
600
780
855
960
1010
1140
1230
1330
1395
1490
400
300
Age
m.y.
200
100
Release Curve For
Pseudotachylyte- Shocked
Anorthosite Breccia
10
20
30
40
50
60
70
80
90
100
% Ar39 released

FIG. 7

The 600°C temperature fraction of the breccia yielded a large amount of gas (23% of the sample) and an indicated age of 177 m.y. The second temperature fraction also released a large amount of argon (15% of the sample) but yielded a significantly lower age of 137 m.y. Subsequent temperature releases, with the exception of the 1010°C release, yielded gradually increasing ages. The highest age obtained is the 313-m.y. age for the 1395°C fraction. This latter gas fraction contained 19% of the sample argon. The small amount of gas released at 1490°C indicated a lower age of 230 m.y. and had large errors associated with the age determined.

The Ar^{39}/Ar_o^{37} ratios for each release are listed in Table 6B. These have been corrected for Ar^{37} decay. K/Ca ratios derived from the Ar^{39}/Ar_o^{37} ratios are plotted on Fig. 7. It is clear that the material which releases argon at temperatures below 1000°C has a higher K/Ca ratio than the material which releases gas above 1000°C. The K/Ca ratio indicated by the low-temperature gas fraction is about 0.112, and it is unclear what substance is yielding argon at these temperatures. The K/Ca ratio of the high-temperature gas fractions (0.058), however, is close to that of plagioclase, An_{50-55}. It seems reasonable to attribute these releases to plagioclase grains present in anorthosite fragments in the breccia.

As is the case with release curves for other samples, this curve is markedly different from the model systems discussed by Turner (1968). It is obvious that the total argon age obtained for

Sample G is not the age of a completely and uniformly outgassed system. Two peculiarities of the system are especially remarkable: (1) The curve has dips; two of the temperature fractions indicate lower ages than the gas fraction immediately preceding them. (2) A significant fraction of argon is released above 1300°C.

During the initial temperature step, over 23% of the sample argon is released. This gas has an Ar^{40}-Ar^{39} age of 177 m.y. The age of 177 m.y. is significantly lower than 210 m.y. As discussed above, the maximum error expected in the J value is about 6%; the age of the initial fraction could therefore be no higher than 190 m.y. If the age of the initial temperature fraction is interpreted to be a time of partial outgassing of the sample, as suggested by Turner (1968), then the gas loss event for this sample occurred significantly later than the 210 m.y. monzonite formation.

The large argon releases from this sample at low temperatures are probably from very small grains in the pseudotachylyte matrix, and they suggest that this material may diffusionally lose argon quite readily. This conclusion was also reached during studies of the diffusion properties of the material.

At 750°C this sample releases argon indicating a 20% lower Ar^{40*}/Ar^{39} age than the initial release. A similar drop in age for the second temperature step was observed in the release curve of the slightly shocked anorthosite. As was mentioned in the discussion of the slightly shocked anorthosite, such a drop is not expected

for a simple model system, although systems whose release curves would display such a drop can be imagined (see discussion in CHAPTER 2). It is worth noting that the age indicated by the gas released from the second temperature step is 137 m.y. This age is very similar to the age indicated by the first temperature release of the maskelynite. The similarity of these latter two ages may, however, be coincidental.

As was observed for both of the other shocked samples studied, a fair part of the gas release for this sample takes place at temperatures above those at which anorthite is usually completely outgassed (Fechtig et al., 1960; see Fig. 4). This behavior is possibly indicative of a more "retentive", plagioclase-composition material.

The age of the large fraction of argon which is released at 1395°C is 313 m.y. The breccia is known to contain 4-mm fragments of shocked anorthosite (see Appendix to PART I, Sample G). These fragments are logically expected to be the most highly retentive materials in the breccia ; the K/Ca ratios of the high-temperature releases from the breccia correspond to argon from plagioclase (An_{50}), and the 1395°C gas fraction can be simply interpreted as coming from shocked anorthosite fragments enveloped in the pseudotachylyte matrix. The age indicated by the 1395°C temperature fraction of the breccia is only slightly lower than the age of the corresponding temperature fraction of the maskelynite anorthosite (336 m.y.). This correlation may again be coincidental, but it is worth noting.

Although the release curve exhibits a complicated series of low and high ratios, it has a general regularity. The temperature releases below 1000°C have ages between 140-190 m.y., while above this temperature the ages are higher with a reasonably pronounced plateau present at 313 m.y. The curve can roughly be described as a two-plateau curve, and the ages of the plateaus limit the possible formation times of the material.

One tentative interpretation of the curve is that a major outgassing event took place between 180-313 m.y. ago. It is not known whether the 313-m.y. age of the most retentive phases in the breccia (1) should be interpreted as a relict age for a completely outgassed rock which has experienced a secondary thermal metamorphism or (2) if it is a high age from retentive sites which were only partially depleted during the outgassing event. If the gas loss is assumed to have occurred before 180 m.y., a second event must have also occurred which resulted in partial gas loss from the less retentive, argon-containing sites of the breccia. This second event must be assumed in order to explain the low age of the gas fractions released below 1000°C.

The 138-m.y. age indicated by the 780°C temperature fraction is difficult to interpret. Argon loss due to continuous diffusion or to a mild thermal metamorphism at 138 m.y. would be expected to partially deplete the least retentive, argon-containing sites of the rock. During a subsequent laboratory release, the <u>initial</u> temperature fractions would indicate a 138-m.y. age. The emplacement of a secondary phase in the rock at 138 m.y. could produce the low

second age of the release curve (see discussion in CHAPTER 2). If such a phase is present, its K/Ca ratio must be about 0.115. Some secondary zeolite is present in thin sections of the breccia, but this zeolite comprises only a small fraction of the mode of the rock. It is doubtful that enough "low-age" zeolite is present to account for a 20% lower age in 15% of the argon from the rock.

First-Order Conclusions:

(a) Age vs. shock pressure curve. The whole-rock ages determined for Samples A-H and some of the ages from the Ar^{40}-Ar^{39} release curves of the shocked samples are shown plotted versus the estimated shock pressures for these rocks in Fig. 8. The Ar^{40}-Ar^{39} ages shown include the highest and lowest ages observed; also shown are the ages of the initial and the most retentive fractions. The errors shown for the shock pressure estimates apply both to the total argon ages and to the Ar^{40}-Ar^{39} ages. In order to avoid confusion, error bars have not been attached to the latter.

Three features are immediately apparent from this curve, without considering, at present, either the proper interpretation of the various ages or the temperatures experienced by the shocked samples:

(1) The data show a wide spread of ages and do not define a single-valued age vs. shock-pressure curve. In particular, no well-defined age is indicated by the data at high shock pressures.

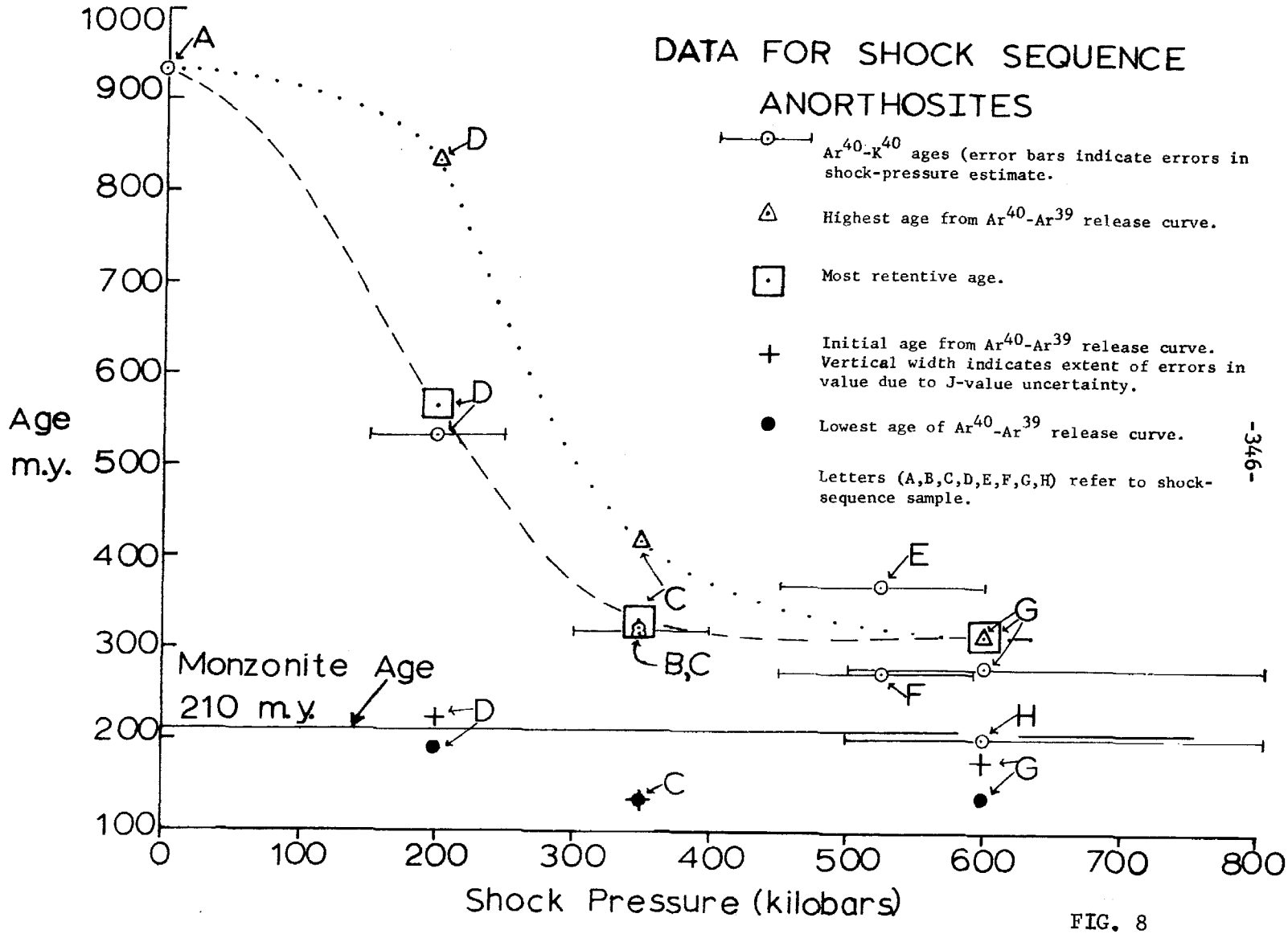
DATA FOR SHOCK SEQUENCE
ANORTHOSITES
Ar^{40}-K^{40} ages (error bars indicate errors in shock-pressure estimate.
Highest age from Ar^{40}-Ar^{39} release curve.
Most retentive age.
Initial age from Ar^{40}-Ar^{39} release curve. Vertical width indicates extent of errors in value due to J-value uncertainty.
Lowest age of Ar^{40}-Ar^{39} release curve.
Letters (A,B,C,D,E,F,G,H) refer to shock-sequence sample.
Age m.y.
1000
900
800
700
600
500
400
300
200
100
Monzonite Age
210 m.y.
A
D
D
C
B,C
E
G
F
H
G
C
0
100
200
300
400
500
600
700
800
Shock Pressure (kilobars)

FIG. 8

(2) Although a well-defined age vs. shock-pressure curve is not observed, the whole-rock ages (exclusive of H) and the highest and most retentive site ages of the Ar^{40}-Ar^{39} release curves all show a general decrease with increasing shock pressure. This decrease in ages is expected on the basis of the simple theory discussed in the introduction to this section.

(3) All of the lowest ages and two of the three initial ages indicated by the Ar^{40}-Ar^{39} release curves are younger than 210 m.y., i.e., the time at which the monzonite body crystallized.

(b) Complications present. Some of the whole rock samples which are believed to have experienced shocks of the same intensity yield very different ages. A first look at the process of argon loss by shock predicts a general decrease in the age of a shocked rock with increasing shock pressure. Such a trend is shown to some extent by the data, but the simple theory does not explain the reason for the double-valued nature of the observed age vs. shock-pressure curve. The fact that the age vs. shock-pressure curve is not single valued is probably not attributable to errors in the estimations of shock pressures experienced by the samples.

The Ar^{40}-Ar^{39} release curves obtained from the shocked samples indicate a reason for the non-uniqueness of the total argon ages from rocks shocked to the same pressure. Consideration of these curves suggest that the shocked rocks are composed of several materials, each of which has a different age. The pseudotachylyte

breccia, for example, consists of low-age (~ 175-m.y.) matrix material with some high-age (313-m.y.) retentive material. Depending upon the relative proportions of these two materials in the rock, breccias such as G and H could have total argon ages which are anywhere between 175-313 m.y. The 202-m.y. age of H might be due simply to higher percentage of grey, low-age matrix present in H relative to G. This argument suggests that total argon ages of the shocked samples may be of very limited value in determining the time of shock.

(c) Limitation of the time. The exact time of the shock event cannot be determined from this data, but some limitations can be placed on this time. Those rocks which have been shocked to pressures greater than 300 kb are expected to be the most thoroughly outgassed rocks of the shock-sequence suite. Ages determined from these samples are all less than 419 m.y. It is therefore reasonable to interpret this data as suggesting that the shock-metamorphic event took place earlier than 419 m.y. ago.

It can be argued on the basis of stratigraphic evidence that the meteorite impact at Manicouagan occurred between 440-210 m.y. ago. The agreement between the stratigraphic age and the shock-sequence age indicates that the shock-sequence approach to determining the impact time is basically correct.

(d) Lack of correlation of shock-sequence ages with the 210-m.y. monzonite formation time. On the basis of geological evidence, it would appear that the formation of the monzonite is the most important thermal event which took place in the Manicouagan area. It is difficult, however, to directly correlate the shock-sequence ages with the geological evidence. Although the initial release of the slightly shocked anorthosite may, within errors, yield the same age as the monzonite (210 m.y.), neither the maskelynite nor the pseudotachylyte gives any indication of a 210-m.y. event in its history.

If 210 m.y. is considered to be the shock-deformation time of these samples, then an asymptotic approach of the ages to this value would be expected at high shock pressures. The present data does not indicate such a trend. The exact extent of the outgassing which occurred in the highly shocked samples is unknown, but it would probably be large. If this were the case, retentive sites in the highly shocked samples would be expected to indicate ages near 210 m.y. Neither the most retentive ages nor the highest ages suggested by the Ar^{40}-Ar^{39} data for the samples shocked to $>$ 300 kb gives any indication of a 210-m.y. age. The initial Ar^{40}-Ar^{39} releases would be expected to indicate an age of 210 m.y. if this were the major outgassing event which affected these rocks. As was pointed out, however, with the exception of the slightly shocked anorthosite, this is not the case.

It is possible that the shock-sequence samples do not indicate a 210-m.y. age because of a later event(s) which left a very strong imprint on the area. If there were a later event, some evidence of it should be present in the Ar^{40}-Ar^{39} release curve of the monzonite. The monzonite, however, gives no indication of a later event although the maskelynite does.

Another possible explanation for the lack of a major 210-m.y. imprint on the data is that no extensive gas loss occurred at this time. The major shock outgassing could have occurred before 210 m.y., and the 210-m.y. monzonite formation might have affected the shocked anorthosites to only a small degree. A later event, limited to the anorthosites, could have produced more significant gas loss among the anorthosites than the monzonite formation event.

(e) Indications of low ages. Perhaps the most surprising feature of the Ar^{40}-Ar^{39} data is that they yield indications of gas loss at times later than 210 m.y. The initial temperature releases for both the maskelynite and the pseudotachylyte breccia yield ages significantly less than 210 m.y. The initial "age" can be simply interpreted as a time of partial gas loss of the system (Turner, 1968). The lowest temperature fraction of the maskelynite yields an age of 138 m.y. The corresponding gas loss event indicated by the release curve would be at about 110 m.y. (see the dot-dash line in Fig. 4).

The "lowest-age" fraction for all three shocked anorthosites is also significantly lower than 210 m.y. For the case in which the lowest age is not from the initial temperature fraction, the meaning of that age is somewhat questionable. A possible interpretation (see CHAPTER 2) is to associate this age with a secondary mineral. If this interpretation is accepted, then the release curves of both the slightly shocked anorthosite and the pseudotachylyte-shocked anorthosite breccia give evidence of a later mineralization.

Shock Release of Argon -- A Closer Look at the Shock-Sequence Experiment --

Introduction:

(a) Limitations of the simple theory. The simple theory of gas loss due to shock, as suggested previously, supposes that increasingly intense shocks cause progressively larger argon releases from materials. Although consideration of a detailed mechanism of gas loss is avoided in this theory, most of the argon loss is presumed to be due to thermal diffusion caused by shock heating of the material.

The potassium-argon data obtained from the shocked samples indicate that this simple theory is generally correct. It is clear from even very elementary considerations, however, that complicating processes also exist. It is well known, for example, that shock processes involve not only temperature increases but mechanical breakdown processes and phase changes as well. The effects of the latter two processes may, in some cases, predominate over the

first. In order to obtain maximum information from the shock-sequence experiment, these complications must be considered in more detail.

(b) Requirements for a good shock age: If the potassium-argon age of a shock-metamorphosed sample is to reflect the time of shock, then a complete loss of argon from the sample must occur during the shock event and the sample must act as a closed system thereafter. The closed system requires that after the shock process (1) the sample must retain argon completely and (2) the potassium concentration must not be changed. The gas retention properties of a shocked material can, at least in principle, be inferred from its presently measured diffusion properties. The amount of argon which the substance has lost during the shock process, however, is much more difficult to infer. The problem of argon loss during a shock event is the main concern of this section.

(c) Potassium alteration subsequent to the shock event. Changes in the potassium concentration of the shock-sequence anorthosites after the shock event, with the possible exception of H, are thought to be minimal. Murtaugh and Currie (1969) have reported zeolitized anorthosite breccias in the central massif of this crater. These breccias contain some shocked anorthosite fragments; therefore, the zeolitization must have occurred

after the shock event. It is not known to what extent (if any) this zeolitization was accompanied by metasomatic alteration of potassium concentrations. None of the samples used in the shock-sequence experiment, however, displayed extensive zeolitization, and potassium-concentration alterations are therefore concluded to be minimal for the samples analyzed.

The chemical composition of anorthosites, both interior and exterior to the crater, show no significant differences (see Tables 1 and 2, Appendix to PART I). This further supports the above conclusion.

(d) Approach to the question of shock outgassing. The question of argon loss from shocked anorthosites will be considered at the following three levels of complication: (1) The shock outgassing of a uniform single crystal of plagioclase. (2) Gas loss during shock from a rock consisting mainly of plagioclase but also containing some other minerals. (3) The actual problem of gas loss from a rock mass. At the end of this section, the major factors presumed to have affected the anorthosites studied will be considered.

Argon Loss -- The Behavior of Argon During a Shock Process:

(a) Argon loss from a uniform solid. As a first approximation to the gas-loss problem, one can consider a uniform single crystal of plagioclase imbedded in a medium of the same shock impedance and shocked under vacuum in the laboratory. The crystallographic

orientation of the sample is arbitrary.

At least three ways in which the shock will affect the argon content of the crystal exist: (1) In-shock and post-shock elevation of the temperature can produce argon loss from the sample. (2) Mechanical breakdown of the sample may lower its post-shock, gas-retention properties. (3) Phase changes produced during the shock process might either raise or lower the post-shock gas retentivity of the plagioclase. These problems are considered in turn.

i. Shock temperatures -- If the Hugoniot of a substance and the shock pressure it has undergone are known, one can in principle determine the shock-produced temperatures the substance has experienced. Experimental Hugoniot data for plagioclase, An_{20}, have been measured by Ahrens et al. (1969). These authors have also calculated in-shock and some post-shock temperatures for the plagioclase (see Fig. 9).

ii. Loss due to in-shock temperatures -- The in-shock temperature of a material depends upon the difference between the shock-state enthalpy and the isothermal enthalpy of the material at the shock pressure. In-shock temperatures are relatively amenable to calculation, and the in-shock temperatures for plagioclase calculated by Ahrens et al. (1969) are shown in Fig. 9.

In-shock temperatures for plagioclase at 400 kb are about

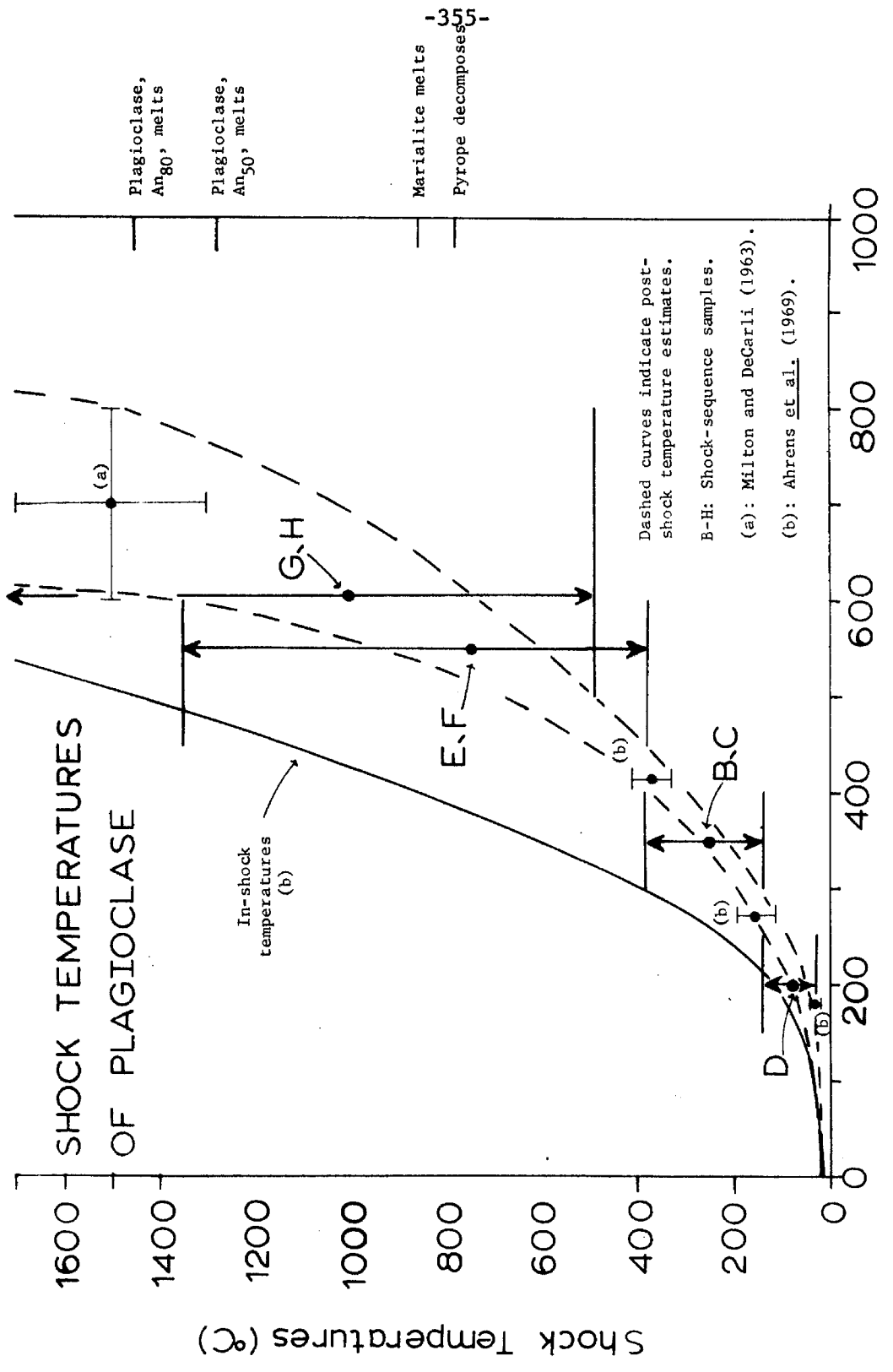
SHOCK TEMPERATURES
OF PLAGIOCLASE
Shock Temperatures (°C)
Shock Pressure (kilobars)
1600
1400
1200
1000
800
600
400
200
0
0
200
400
600
800
1000
Plagioclase, An80, melts
Plagioclase, An50, melts
Marialite melts
Pyrope decomposes
In-shock temperatures (b)
Dashed curves indicate post-shock temperature estimates.
B-H: Shock-sequence samples.
(a): Milton and DeCarli (1963).
(b): Ahrens et al. (1969).
G,H
E,F
B,C
D
(a)
(b)

FIG. 9

850°C, and gas loss from a sample might be expected at these temperatures. The high temperature, however, is maintained only during the passage of the shock wave, and that time is probably too short (i.e., a few microseconds to a few seconds) for complete gas loss to take place. No experimental data bearing on the in-shock gas loss are available, however, and the actual loss which occurs is unknown.

iii. Post-shock temperatures -- As the material relaxes from its high-pressure condition, the states it attains lie along an adiabatic release curve, and the thermal energy remaining in the material after release is

$$\frac{(P_s+P_o)(V_s-V_o)}{2} - \int_{\text{adiabat}} P_s dV = E_{ps} = \int_{T_o}^{T_{ps}} Cp(T)\,dT \quad .$$

This energy can be used to calculate the post-shock temperature attained by using the specific heat as shown above. In order to estimate the post-shock temperatures, release adiabat data is necessary. Release adiabat data is more difficult to obtain than shock Hugoniot data; this explains the paucity of well-measured, post-shock temperatures for plagioclase. Ahrens et al. (1969) give residual temperatures of 30, 170 and 360°C for shocks of 180, 272 and 417 kb, respectively. In general, residual shock temperatures can be expected to increase rapidly with shock

intensities above 400 kb, even if no phase change occurs. For plagioclase shocked to 400 kb, Ahrens et al. (1969) postulate that a phase change occurs during shock to a hollandite-structure mineral with subsequent shock release to a zero pressure density of 3.81 and later reversion to an amorphous mixture of phases. This release path implies that the residual or post-shock temperatures would rise very rapidly for shocks $>$ 350 kb.

The post-shock temperatures for oligoclase (An_{20}) calculated by Ahrens et al. (1969) are shown in Fig. 9 along with a temperature estimate by Milton and DeCarli (1963). This latter point is based upon their observation of the melting of plagioclase (An_{80}) at a 600-800 kb shock intensity. The points shown in Fig. 9 can be used to outline a broad range of post-shock temperatures for plagioclase as indicated by the dashed lines. It can be seen from Fig. 9 that shock pressures of 500 kb cause residual shock temperatures of 600°C while 600-kb shocks leave the material at about 900°C. Ahrens (1971) has indicated that the post-shock temperatures calculated by Ahrens et al. (1969) are probably underestimates of the true post-shock temperatures of plagioclase. The curves of post-shock temperature versus pressure shown in Fig. 9, therefore, probably underestimate the actual temperatures.

iv. Post-shock cooling and gas loss -- The shocked plagioclase will cool from its after-shock temperature with a time constant, r^2/K, which depends on the specific conductivity, K, of the material

as well as on the characteristic dimension, r, of the shocked sample. For plagioclase, $K \sim 10^{-2}$ cm^2/sec*, and therefore for shocked samples a few centimeters in size, the time which will be required for cooling is on the order of a few minutes. For samples which have been shocked to more than 500 kb, the post-shock temperature may be high enough so that a significant fraction of the gas in the plagioclase is lost by thermal diffusion during these few minutes. Larger samples will cool more slowly and thus lose a higher percentage of their original argon.

v. Effects of brecciation and mechanical breakdown -- Extensive microfracturing of shocked materials is well documented. Laboratory shock-loaded quartz, for example, is recovered as a fine powder (Hörz, 1968). Short (1968) has used microfracturing to make quantitative estimates of the pressures which shock-loaded samples have experienced. An obvious effect of a high-fracture density is a decrease in the effective grain size of the shocked material. The reduced grain size will, in turn, increase the value of D/a^2 characteristic of the material. If very small grain sizes are produced by the shock, $D/a^2\Big|_{20^\circ C}$ may be on the order of 10^{-17}/sec

* This value is based on the thermal conductivity of orthoclase, $K = 10 \times 10^{-3}$ cal/cm-°C-sec, given in Clarke (1966) and the heat capacity for plagioclase, $C_p = 0.23$ cal/gm, given by Barth (1970). These values and the densities of plagioclase yield a value of $K = 1.7 \times 10^{-2}$ cm^2/sec.

for these grains.

Material with such a large D/a^2 value would be expected to lose significant amounts of argon by continuous diffusion. If $D/a^2\Big|_{20^\circ C} \sim 10\lambda$ or greater, the plagioclase will not retain argon and will yield a steady-state, approximately zero Ar^{40}-K^{40} age (Wasserburg, 1954).

vi. Effects of phase changes -- Phase changes are known to occur in intensely shocked materials. The argon retentivity of a shock-produced phase may be quite different from that of the original phase. If the shock-produced phase remains after the shocked material relaxes to zero pressure, and this phase is of different retentivity, then the post-shock,argon-retention characteristics of the shocked material will obviously be different than those of the original pre-shock material.

It is known that plagioclase shocked to pressures $\sim$ 300 kb transforms to maskelynite. The maskelynite is stable and remains after the shocked system relaxes to zero pressure (Milton and DeCarli, 1963). Maskelynite, as previously pointed out in this study, probably has different diffusion properties than the plagioclase from which it was formed.

Another possible effect of a phase change would be to effectively remove crystal grain boundaries and anneal imperfections which exist in the original material. If a region in the original sample, which contained both grain boundaries and crystal imper-

fections, transforms uniformly to a new phase that remains after passage of the shock front, the effective grain size in this region of the shocked sample would then be increased over that of the original material. If the original phase and the shock-produced phase have approximately the same diffusion coefficient, then the D/a^2 value of the shocked system would be decreased (i.e., the shocked material would become more retentive).

(b) Rock systems shocked in the laboratory. The next set of complications which are considered are those present in a real rock, shocked under vacuum in the laboratory. Four further complicating factors must be considered in the case of a shocked rock system. (1) The rock consists of a set of grains rather than one uniform crystal. (2) The rock contains more than one mineral species. (3) Transfer of argon within the rock may occur during the shock. (4) The rock system contains imperfections and irregularities.

i. Effects of grains -- In contrast to the case of the single crystal, discussed previously, a real rock consists of discreet mineral grains with different crystallographic orientations. These mineral grains generally display some variation in size. The grain boundaries present in the rock would be expected to produce shock-wave reflections and rarefaction fronts which are not produced in a homogeneous, single-crystal sample. These reflections and rarefactions would then interact resulting in non-uniformity and different shock pressures in different parts of the rock sample.

ii. Effects of more than one mineral -- A real rock consists of more than one mineral species, and each species has a different Hugoniot. Mass conservation within the rock requires that particle velocities within each mineral grain in the rock must be nearly equal. Since the Hugoniots of each mineral are slightly different, each mineral would experience a different in-shock pressure. The in-shock and post-shock temperatures experienced by separate minerals would therefore vary somewhat. In general, the pressures and temperatures experienced by minerals within the same rock do not differ greatly provided the rock does not contain a large amount of pore space. The reason for this is that most silicates possess approximately the same Hugoniot. Hugoniots of the different rock phases will, to a first approximation, depend on the densities of these phases. Therefore, large pressure differences among phases and local "hot" or "cold" spots can occur in rocks which have coexisting mineral species with rather different densities.

Mineralogical grain boundaries will produce shock-wave reflections and rarefaction fronts. Interactions of these rarefactions and reflections will cause localized high and low shock-pressure areas within the grains of the rock.

iii. Argon transfer during shock -- The presence of different minerals within the rock introduces the possibility that different argon concentrations exist in these different minerals. This is

typically the case for a rock with concordant potassium-argon mineral ages among mineral species which have different potassium concentrations. The possibility of localized argon concentrations is improbable in the case of the uniform, single-crystal, shocked substance.

Argon concentrations of the different minerals may, to some extent, equalize either during the shock or immediately afterwards, while the rock is still hot. The process of argon transfer between grains is similar to the "shock implantation" discussed by Turner et al. (1971). This process results in an increase in the argon concentration of some phases which, previous to the shock, contained lower argon concentrations. It is not known to what extent this process takes place. Argon diffusion is normally controlled by grain boundaries and imperfections in crystals. These imperfections and boundaries result in a net argon transfer between grain interiors and the exterior of the rock rather than between different grains within the rock. Shock compression of the rock may, however, lead to the annealing of the crystal imperfections and grain boundaries so that net argon transfer during the shock actually takes place between phases.

iv. Rock inhomogeneities-- Real rock systems contain fractures and non-homogeneous distributions of mineral phases. These features could be expected to result in differences in shock velocity along different directions of the rock and also cause localized highs

and lows in the shock pressure throughout the rock. The latter result from interactions of shock-wave reflections and rarefactions from the non-homogeneities.

(c) The real problem -- a natural rock mass. If a naturally occurring rock mass is shock loaded during a meteoritic impact, three additional complicating factors should be considered: (1) The rock mass is shock loaded in air and not in vacuo. (2) The shocked rock mass is a much larger system than any laboratory shocked system. (3) Large-scale inhomogeneities will probably be present in the rock mass.

i. Rocks shocked in air -- Shocks due to a meteoritic impact occur in the presence of at least a partial atmosphere. Since the atmosphere contains about 1% Ar^{40} (along with smaller amounts of Ar^{36} and Ar^{38}), it is pertinent to ask (1) whether or not Ar^{40} is implanted in a system during a shock and (2) how this implanted argon might affect the gas ages of the shocked system.

Fredriksson et al. (1964) have shown that atmospheric-composition argon (Ar^{40}/Ar^{36} = 296) is implanted in a shocked chondritic meteorite. The chondrite sample was shocked to about 600 kb under a total pressure of 1 bar of atmospheric argon. Furthermore, their data shows that subsequent heating of this chondrite released argon of very nearly atmospheric composition as well as some radiogenic Ar^{40}. The simplest interpretation of their data is that rocks shocked in the presence of argon incorporate some of the external argon present.

ii. Large masses of shocked rock -- If a volume of rock on the order of 1 km in size is more-or-less uniformly shocked, the rock will attain a uniform, post-shock temperature throughout the mass. The time required for the heated mass to thermally relax from this elevated temperature will be $\sim 10^5$ yrs. Even though the mass may have experienced only moderate post-shock temperatures, gas loss from the heated mass during the period of cooling may be complete or nearly complete. This argument suggests that, in general, large masses of moderately shocked rock may experience complete gas loss.

A more quantitative estimate of the probable extent of outgassing in large masses of shocked rock can be formulated by requiring that the diffusional release time of the rock at its post-shock temperature be the same as the thermal relaxation time of the shocked rock volume, i.e.

$X D\Big|_{T_{ps}} r^2 = Ka^2$. Here, $D\Big|_{T_{ps}}$ is the diffusion coefficient of the shocked rock at the post-shock temperature it attains, and r is an appropriate dimension of the shock-heated system. K and a are the thermal diffusivity and the effective grain size of the shocked rock, respectively. The factor, X, is a numerical factor which accounts for the cooling history of the sample. X = 1 implies that the shocked mass remains at its

post-shock temperature during the entire thermal relaxation period and then cools immediately. In real cases, X varies from about 0.1 for a slab of plagioclase shocked to 500 kb to about 0.023 for a hemispherical mass of anorthosite shocked to 400 kb. A conservative value of X = 0.01 will be assumed.

The above criterion for outgassing can then be formulated more succinctly as

$$g = \frac{D/a_2 \Big| T_{ps}}{K/r^2} \sim 10^2 \quad .$$

iii. Large-scale irregularities -- Large-scale irregularities such as faults, folds or rock layers of different composition can exist in the shocked rock mass. These irregularities would be expected to result in shock-wave reflections and rarefactions within the mass. Interactions of the reflections and rarefactions would produce localized highs and lows in the shock pressure throughout the shocked rock body.

(d) Summary. The preceding discussion contains many allusions to possible argon behavior during shock, but few definite statements. It is worthwhile to summarize the effects which are considered most significant.

i. Predominant outgassing effects during shock -- Aside from the experimentally verified implantation of argon,

very little is known about actual gas behavior in materials during shock. If argon loss or transfer takes place while the material is in its high-pressure shock state, the time period during which these processes occur is short, ranging from a few microseconds to a few seconds. The conditions which exist after passage of the shock wave are maintained for a much longer period of time and are therefore thought to be of more importance in the overall argon-release process. In order to simplify the problem, gas loss from the rock during the shock will be disregarded. At worst, this approach will underestimate the extent of outgassing which the sample experiences.

The thermal diffusivities and gas retentivities of shocked materials are amenable to direct measurement, and post-shock temperatures for these materials can, at least, be estimated. The size of a shocked region can also be estimated, and the thermal relaxation time of the shock-heated region can therefore be computed. These parameters of the shocked system allow an estimate (or an underestimate) of the extent of gas loss during shock to be made for the system. For a large rock mass, complete outgassing is expected if $g \sim 100$.

ii. Retentivity of shock-produced phases -- It has been suggested that the shock process might produce phases of both lower and higher retentivity than the original pre-shock phase. The more highly retentive material is probably produced at shock pressures sufficiently great to produce an in-shock phase change

over a region in the original rock containing many imperfections. For plagioclase, a phase change to maskelynite occurs between 300-400 kb. Phases with low retentivity can be produced at lower shock pressures since they probably involve only extreme fracturing and brecciation.

iii. Large-scale irregularities -- Irregularities in a natural rock system will cause different regions of the system to experience different shock pressures.

Argon Implantation in the Shock-Sequence Anorthosites --

The amount of shock-implanted argon present in the anorthosites of the shock sequence is unknown. Fredriksson et al. (1964) have shown that when air argon (Ar^{40}/Ar^{36} = 295.5) is implanted in a chondritic meteorite, subsequent extractions release argon of unaltered isotopic composition. For the extractions made in this study, therefore, air corrections routinely made on the samples effectively subtract-off air-composition (including that which is implanted) argon. Implanted argon present, therefore, will not affect the age determined for the rock.

All of the shocked samples contained air-composition argon which amounted to 10-30% of the total argon. Argon released from the extraction crucible (10-20 x 10^{-8} ccSTP) accounted for only 1-5% of this air argon. Some of the air-composition argon present in these samples might, therefore, really have been shock implanted during the impact event.

Probable Extent of Outgassing of the Manicouagan Anorthosites --

Post-Shock Temperature Estimates for the Samples: The post-shock temperatures which the members of the shock sequence are believed to have experienced are indicated in Fig. 9. The large uncertainty in these estimates is due to uncertainties in both the shock-pressure estimates and the post-shock temperatures calculated for plagioclase. A probable range of post-shock temperatures for each sample, nevertheless, can be estimated. Post-shock temperatures of 50-130°C, 120-400°C, 400-1200°C and 750-3000°C are estimated for Samples D, B and C, E and F, and G and H, respectively.

Absence of Molten Materials in the Shock Sequence: None of the samples of the shock sequence consist of uniform glasses quenched from a melt. Blobs of thermal glass are formed during an impact event from shock-melted and rapidly cooled rocks. Bombs of shock-molten rock, similar in composition to the basement rocks, are found (among other places) in the Ries Basin of Germany (Hörz, 1965); these are the so-called Flädlen. These molten rocks have been used to date the time of the impact of the Ries-kessel (Gentner et al., 1963) at about 15 m.y. Blobs of shock-melted anorthosite similar to the Flädlen of the Ries would, no doubt, be the materials most likely to yield a correct impact age for the Manicouagan Crater.

Although shock-melted glass blobs exist at Manicouagan, they are found in the layer of shock breccia underlying the monzonite. Since most of the outcrops of this shock breccia are only 10^1 to 10^2 meters below the monzonite contact, secondary or possibly simultaneous heating of the shock breccia would probably determine the potassium-argon age of the glasses. Their ages would probably indicate the age of the monzonite rather than the time of shock melting.

The temperatures estimated for Samples E and F include the range where marialite (scapolite) is observed to melt at zero pressure and pyrope decomposes (Deer et al., 1963). The temperatures estimated for Samples E and F are not, however, sufficiently high to melt the plagioclase of the sample.

The temperature values based on the shock-pressure estimates for Samples G and H include the melting temperatures of plagioclase. Although Samples G and H both contain droplets and grains of apparently melted and flowed plagioclase, most of these samples consist of non- shock-melted material.

The Large Shocked Region of the Anorthosite Body: Although none of the anorthosite samples used in the shock-sequence study underwent complete melting, Samples E, F, G and H are believed to have experienced post-shock temperatures greater than 400°C. These samples occur in a large mess of shocked rock. During the

cooling of the mass from its post-shock temperature, some parts of the mass must have remained at elevated temperatures long enough to effect nearly complete argon loss in the highly shocked anorthosite specimens. An estimate of the extent of outgassing which anorthosites in the shock sequence suffered during the shock event can be made using the known parameters for these rocks. The parameters involved in these estimates are best known in the case of the maskelynitized anorthosite.

It is difficult to determine the original sizes of shocked regions within the crater. One simple model is to suppose that the impact left a series of nested, hemispherical shells, each of which experienced about the same shock pressure. Shells further from the point of impact would have experienced a lower peak-shock pressure than those nearer the impact point. In the central region of the present crater, these shells would form approximately horizontal layers. If this model is assumed, then the meteorite impact must have left a rock layer with a 0.25-km thickness, shocked to between 300-400 kb, in the region of the present central massif. The residual temperature of this volume would be 150-400 ^{o}C (see Fig. 9). The 0.25-km estimate for the thickness of the layer is based on the field observation that Samples B and C, the two maskelynitized anorthosites, occurred about 6 miles apart and were vertically separated by about 800 feet. A minimum estimate for the thickness of the layer, shocked to the pressure which the maskelynite experienced, is therefore about 0.25 km. In fact,

most of the rocks observed in this layer appear to have been shocked to higher pressures.

The diffusivity expected for plagioclase-composition rock is about 1×10^{-2}. The thermal relaxation time for the volume of shocked rock containing maskelynite is therefore about 10^{10} seconds.

Estimates of the post-shock temperature of the maskelynitized anorthosite range from 100-400°C, with 250°C as a median value. At these temperatures, D/a^2 values estimated from the thermal release properties of the maskelynite range from 10^{-19} - 10^{-10}/sec, with a best estimate of 10^{-14}/sec (see Fig. 6).

The value of $g = D \Big|_{T_{ps}} r^2/Ka^2$, suggested by the above considerations, is between 10^{-9} and 1, with a median value of 10^{-4}. These values suggest that the maskelynite probably did not lose much argon during its post-shock thermal relaxation. It should be noted, however, that the upper limit of g is 1. If the post-shock temperature experienced by anorthosite shocked to 350 kb is higher than 400°C, as suggested by Ahrens (1971), then the value of g for the maskelynite may be significantly > 1.

An estimate of g can also be made for Samples E and F. The post-shock temperature estimates for the highly shocked anorthosites, Samples E and F, range from 400-1200 °C, with a best estimate of about 600°C. Arguments similar to those made for the maskelynite can also be made for the highly shocked anorthosites. The size of the shocked region in which they occur is comparable to that of the maskelynite;

the diffusion properties of the highly shocked anorthosites are assumed, somewhat simplistically, to be comparable to those of the maskelynite. The value of g for these samples, calculated using the above parameters, is about 10^3. Samples E and F, therefore, are expected to have been nearly completely outgassed during their post-shock cooling period.

The dimensions of the shocked regions assumed in the above calculations are uncertain because the original geometry of the crater is not well known. This problem can, to some extent, be circumvented by using a model of the crater. In this model, hemispherical shock isobars are assumed. Buktovich (1965) has shown that, for the Hardhat nuclear explosion, the peak shock pressures decrease as the inverse square (actually, as $r^{-1.94}$) of the radial distance from the explosion point. A similar decrease in pressure from the impact point is assumed to have occurred in the Manicouagan Lakes structure. The shock pressure at the limit of the original crater, i.e., 35 km from the impact point, is (under)estimated to be 1 kb. In this case, hemispherical regions around the impact point of 1.4, 1.5, 1.8 and 3.0 km in radius will have experienced peak shock pressures of 600, 500, 350 and 150 kb, respectively. The diameter of the 150-kb region estimated by this method (~ 6 km) is about the size of the central massif region. It is known from field studies that most rocks outside the central massif have experienced pressures lower

than 150 kb (see Fig. 3, CHAPTER 1, PART I). This estimation scheme, therefore, seems compatible with the observational evidence.

Values of g for shocked anorthosites in the above model can be calculated using: (1) the above dimensions of the shocked regions of the model crater; (2) the D/a^2 values of the maskelynite; (3) the post-shock temperatures shown in Fig. 9. With these assumptions, values of g obtained for rocks shocked to 350 kb (maskelynitized anorthosites), 500 kb (Samples E and F) and 600 kb (Samples G and H) are 10^{-2}, 10^4 and 10^6, respectively. These values suggest, as did the arguments based solely on field information, that the maskelynitized anorthosite is probably not totally outgassed by the shock whereas the more highly shocked anorthosites are.

The general implications of the above argument are that Samples E, F, G and H have been significantly outgassed shortly after (10^4 yrs.) the shock event. This is due to the fact that a large volume of rock was left at a moderately elevated temperature at the time of shock, and subsequent thermal relaxation of this large rock volume was slow enough to allow nearly complete loss of pre-shock argon from the mass. The period of relaxation (10^4 yrs.) is negligible compared to the time spans which require resolution (10^6-10^7 yrs.). The gas loss during this period can be considered, on a geological time scale, to have occurred simultaneously with the shock event. There is then reasonable

hope of obtaining true impact times from samples found on the central massif which have been shocked to $>$ 350 kb.

Factors Affecting the Post-shock Argon Retention of the Manicouagan Anorthosites --

Diffusion Characteristics: As was pointed out in the discussion of the diffusion characteristics of the shocked anorthosites, there is evidence for the presence of material of very low retentivity in both the slightly shocked anorthosite and the pseudotachylyte-shocked anorthosite breccia. Both anorthosites indicate values of $D/a^2\Big|_{20^\circ C}$ 10^{-8}-10^{-9}/sec, and these large values of the diffusion parameter suggest that both of these anorthosites would be highly susceptible to argon loss during a slight regional metamorphism or by continuous diffusion.

In contrast to the relatively large values of the room-temperature diffusion parameter estimated for the slightly shocked anorthosite and the pseudotachylyte breccia, a median value of $D/a^2\Big|_{20^\circ C} = 10^{-24}$/sec was estimated for the maskelynitized anorthosite; a range from 10^{-18}/sec - 10^{-30}/sec is possible. This value indicates that the maskelynite is probably not a "leaky" argon system, and that it is at least as immune to episodic argon loss or continuous diffusion loss as the monzonite. The above value is in rough agreement with a value of $D/a^2\Big|_{20^\circ C} = 10^{-24}$ obtained by Fechtig et al. (1960) for anorthite (assuming a 1-mm grain size for the anorthite).

Possible Post-Shock Thermal Events: In this area of Grenville Province, the last severe, regional, thermal metamorphism took place during the Grenville Orogeny. The total argon age obtained for Sample A suggests that this orogeny took place 932 m.y. ago.

(a) Zeolitization event. Some workers (Currie, 1965; Murtaugh and Currie, 1969) have pointed out the presence of zeolitized anorthosite breccias in this crater; they interpret these as indicating metasomatism and low-grade metamorphism. The zeolitized breccias include shocked anorthosite fragments; therefore, the zeolitization must have occurred either after the shock event or roughly contemporaneously. The exact time of the event with which this zeolitization is associated, however, is not known.

The zeolitization event might be associated with the formation of the monzonite. If this were the case, however, zeolitized rocks should be associated with the monzonite, but no such rocks have been observed.

The event which produced the zeolitized anorthosite breccias may be related to the low (i.e., < 210) ages indicated by the Ar^{40}-Ar^{39} data for the shocked anorthosites. It would be expected that a metasomatic event which occurred after the monzonite crystallized would have somewhat affected that rock. There is, however, no suggestion of events after the monzonite formation time in the Ar^{40}-Ar^{39} release curve of the monzonite, and it is unclear why the effects of a later event

should be limited to the anorthosites.

(b) Monzonite formation. Heating due to the monzonite formation might reasonably be expected to have partially outgassed less retentive phases in some shocked anorthosites, especially those anorthosites on the margins of the massif that are nearest the monzonite body. The exact extent of this heating is difficult to evaluate since the configuration of the monzonite layer at its formation time is not well known. The anorthosite body can be assumed to have approximately the form of a disc about 6-km in radius. The thermal relaxation time for an anorthosite mass of this form is about 100 times longer than the time required for thermal relaxation of a 1-km thick layer of monzonite. Heating of the anorthosite during the cooling of the monzonite, therefore, would be minimal; it seems probable that the gas loss in the shocked anorthosites, due to heating by the monzonite, would also be minimal.

Neither the maskelnitized anorthosite nor the pseudotachylyte-shocked anorthosite breccia give evidence of a 210-m.y. partial outgassing in their Ar^{40}-Ar^{39} release curves. The Ar^{40}-Ar^{39} release curve of the slightly shocked anorthosite can, however, be interpreted as indicating that this rock underwent a partial gas loss at 210 m.y. The lack of indication in the Ar^{40}-Ar^{39} data that the shocked anorthosites underwent a heating at 210 m.y. is compatible with the simple estimates of the thermal effects of the monzonite body given above.

Final Evaluation of the Shock-Sequence Data --

After taking the complications of shocked systems discussed above, into consideration, a final evaluation of the ages obtained for the shock sequence does not enable one to significantly refine the first-order conclusions previously drawn. The conclusions from the above discussion which are of concern to the shock-sequence experiment are:

(1) That the anorthosites shocked to pressures above 400 kb have probably lost most, if not all, of their pre-shock argon.

(2) That the shock pressures experienced in different parts of a shocked rock are variable.

(3) That the shock event probably produced phases with both higher and lower retentivity than the original phase. These observations, especially the first, enable a few refinements of the first-order conclusions to be made.

Complete Outgassing and the Possible Time of Shock:

(a) Non- single-valued nature of the shock-age curve. It has been shown that those anorthosites in this crater which were shocked to pressures $>$ 400 kb probably underwent nearly complete outgassing during the shock event. Samples E, F, G and H are all estimated to have been shocked to pressures of $>$ 400 kb and should therefore yield a very good indication of the time of shock. Samples B and C are less likely to have lost a significant fraction of their pre-shock argon. An obvious problem which arises in inferring a time of shock from the data for Samples E-H, however,

is that these samples indicate different ages.

If these anorthosites had been completely outgassed by the shock event, they should yield identical ages. The non-uniformity in the observed ages must therefore be due to another factor. This age discrepancy is tentatively thought to be due to a secondary gas loss event which caused different secondary gas loss in similarly shocked anorthosites. If this explanation is accepted, then it is clear that the total argon ages are useless in inferring a shock time unless a larger number of these ages is available. Only the Ar^{40}-Ar^{39} ages will permit determination of the ages of different shocked phases in the rock. It is also clear, from the above considerations, that much more extensive Ar^{40}-Ar^{39} data is required in order to obtain a well-defined shock age for these anorthosites.

(b) Indications of the "highest-age" fractions. A possible solution to the problem of inferring a shock age is to consider the highest age indicated by the Ar^{40}-Ar^{39} data for a particular rock. The highest Ar^{40}-Ar^{39} age for an anorthosite probably derives from those grains which did not lose all of their pre-shock argon during the shock event. If complete outgassing of the shocked system took place, then all argon-retentive sites in the rock should indicate a uniform age. For a rock which experienced complete shock outgassing, the Ar^{40}-Ar^{39} release curve should be flat with no "highest" age present. A material which suffered partial gas

loss in a secondary event, however, would indicate lower ages for gas fractions from its less retentive sites. The highest age in this latter case would characterize the most retentive sites in the material, i.e., sites whose ages still reflect the time of shock outgassing.

A dotted curve through the highest ages indicated by the Ar^{40}-Ar^{39} release curves of Samples D, C and G is shown in Fig. 8. This curve shows a decreasing trend and has a value of 319 m.y. at 600 kb for Sample H. Since this sample was shocked highly enough to be completely outgassed, it is believed that the 319-m.y. age approximates the time of impact. The whole-rock age of E will also fall on this dotted curve if the minimum shock-pressure estimate compatible with the errors is assumed. The high total-argon age of Sample E can be interpreted as being due to Sample E containing only a very small proportion of material affected by the latter secondary event.

(c) Indications of the retentive phases. An alternative approach to inferring a shock age from the Ar^{40}-Ar^{39} data is to consider the ages of gas fractions from the most retentive sites in the rocks. In the discussion above, it was suggested that a highly retentive phase could form in a shocked material from grains of the original phase which had imperfections annealed during the shock process. The grains which form the highly retentive phase probably experienced the highest shock pressures

occurring in the rock. These grains would also experience the highest post-shock temperatures in the rock. It follows from these arguments that the most retentive phase produced by a shock process would also be the most thoroughly outgassed phases. If a material has been totally outgassed during shock, the age indicated by the most retentive site would be the time of shock outgassing. The highly retentive sites in a rock would also be least likely to be affected by a secondary thermal event. For a shock-outgassed rock affected by a secondary event, therefore, the Ar^{40}-Ar^{39} age of the most retentive site will most closely approximate the time of shock.

A dashed curve through the Ar^{40}-Ar^{39} ages of the most retentive sites in Samples D, C and G* is shown in Fig. . These ages show a decrease with increasing shock pressures. The difference between the "highest" and the "most retentive" ages of these samples also decreases with the shock intensity. The difference between these two ages would be expected to decrease with shock intensity since all gas fractions of a completely outgassed rock would yield identical ages. The most retentive ages of both the maskelynitized anorthosite

* The ages indicated by the last 4% of gas released from these rocks are not used because they are thought to have excessively large errors associated with them.

and the pseudotachylyte-shocked anorthosite breccia are about 310 m.y. Since the latter sample experienced ~ 600-kb shock pressure, it should be well outgassed and its 313-m.y. age should represent the time of shock metamorphism.

Lack of Indication of a 210-m.y. Event:

(a) Ages from the retentive phases. As was mentioned in the discussion of the first-order conclusions, only three of the measured ages for the shock-sequence rocks fall within 20 m.y. of the 210-m.y. time of the monzonite crystallization. Of the anorthosites shocked to more than 300 kb, only the total argon age of Sample H is within the range of 190-230 m.y.

It can be argued that the shock metamorphism of these samples occurred at 210 m.y. According to this view, the 313-m.y. age of the retentive sites in Sample G and the 275 and 371 m.y. ages of Samples E and F are due to incomplete outgassing of these rocks during the shock process. This argument is a self-consistent explanation of the data, but it is not compatible with the previous argument that Samples E, F, G and H have undergone complete gas loss during the shock event. If the argument of complete gas loss is accepted, then the age of either the most retentive fraction or of the highest-age fraction of these samples should indicate the time of shock outgassing. If both the above arguments are accepted, then the age of the most retentive gas fraction from Sample G should be close to 210 m.y.; it obviously is not.

It should be pointed out that the age data obtained from these shocked anorthosites is compatible with any impact (shock-outgassing) time between 313-210 m.y., provided that some subsequent gas-loss event occurred. The 210-m.y. shock time is suggested by the theory that the monzonite formed from a shock-melted breccia; i.e., this shock time was not derived from consideration of the shock-sequence data.

(b) Initial ages of the release curves. Of the shocked anorthosites, only the Ar^{40}-Ar^{39} release curve of the slightly shocked anorthosite yields either an initial or a lowest age within the interval of 190-230 m.y.

It has been shown that heating of anorthosites in the central massif during cooling of the monzonite layer at 210 m.y. probably did not cause extensive gas loss from the anorthosites. The predicted slight heating and minimal gas loss at 210 m.y. seems to be confirmed by the lack of indication of a 210-m.y. thermal event in the Ar^{40}-Ar^{39} release curves in Samples C and G. The slightly shocked anorthosite, which may have been affected by this event, has a large $D/a^2\Big|_{20^\circ C}$; it would, therefore, be expected to be susceptible to gas loss during slight heating.

If the shock event occurred at 210 m.y., then the initial temperature fractions from <u>all</u> of the Ar^{40}-Ar^{39} release curves of the shocked anorthosites should show evidence of this age (Turner, 1968). The fact that initial releases from both Samples C and G

indicate ages significantly lower than 210 m.y. may be interpreted as being due to: (1) the imprint of a later thermal event in the area which erased evidence of the 210-m.y. event in these samples or (2) the absence of a 210-m.y. outgassing event. The second hypothesis is tentatively accepted because the Ar^{40}-Ar^{39} release curve of the maskelynitized anorthosite suggests a system which underwent major outgassing at about 270-280 m.y., rather than at 210 m.y., with a secondary gas loss at about 110 m.y. (see discussion of maskelynite data).

Indications of a later event: As discussed previously, the Ar^{40}-Ar^{39} release curves of the shocked anorthosites show unexpected evidence of ages lower than 210 m.y. The maskelynitized anorthosite and the pseudotachylyte-shocked anorthosite breccia indicate initial ages of ~ 110 and 178 m.y., respectively. The lowest ages measured for all of the shocked anorthosites are well below 210 m.y. The lowest ages of the Ar^{40}-Ar^{39} release curves have a questionable interpretation in the cases of Samples D and G since these ages do not occur for the initial releases of the curve. The age of the initial temperature fraction, however, can be related to an episode of partial gas loss from the rock (Turner, 1968).

The low ages observed for the maskelynite anorthosite can be interpreted as suggesting an epidosic heating of between 100-138 m.y. (see dot-dash curve in Fig. 4). This time interval includes: (1) the time of emplacement of lamprophyre dikes in Newfoundland; (2) the age of a diabase dike on Anticosti Island;

(3) the emplacement of the Monteregian Hills; (4) the age of a lamprophyre dike in Moose River Basin. It is at least possible that the initial age indicated by the maskelynite is related to a minor orogeny which has also affected other parts of the Canadian Shield.

The gas losses caused by a later event would probably not be uniform in different shocked anorthosites. Such non-uniform gas losses are thought to be the cause of the differences observed in the total argon ages of anorthosites shocked to about the same intensity.

Summary:

From the age data for the shock-sequence anorthosites, it is not possible to infer a unique time of shock metamorphism. The Ar^{40}-Ar^{39} data suggest that a slight episodic heating of the shocked anorthosites took place after the monzonite crystallized. This latter event was not expected on the basis of previous Ar^{40}-K^{40} studies. The shock-sequence data alone will fit any history which includes (1) major gas loss by shock in the period of 180-320 m.y. ago and (2) secondary gas loss between 100-138 m.y. ago.

It is thought that some of the anorthosites in the shock sequence probably lost a major fraction of their pre-shock argon during the shock process; these anorthosites yielded ages significantly greater than 210 m.y. The Ar^{40}-Ar^{39} ages of the shocked anorthosites yielded no indication of a 210-m.y. event in the retentive fractions

of rocks which are expected to have been outgassed during shock. Only one of the Ar^{40}-Ar^{39} release curves for the shocked anorthosites yielded any evidence for a 210-m.y. outgassing in its initial temperature fractions. For these reasons, it is felt that the time of shock metamorphism of the anorthosite was distinct from and earlier than the time of the monzonite crystallization. The best estimate of the time of shock metamorphism of these rocks is about 280-320 m.y. This argument suggests that the "igneous rock" in the Manicouagan-Mushalagan Lakes structure is not a pool of melted shock breccia which formed and collected in the crater.

Concluding Remarks:

It should be emphasized that the conclusions drawn in this section are preliminary. A complete evaluation of these experimental data cannot be made until a study of gas loss in an experimentally shocked system (preferably Manicouagan anorthosite) is made. Such an experimentally shocked system would permit determination of argon losses resulting from shock processes to be made without complications due to a super-imposed, secondary thermal event. In the experimentally shocked system, the shock pressures experienced by each sample would be precisely known rather than estimated.

Before a final answer to the question of the time of impact at Manicouagan can be given, it is obvious that more experimental data on shocked anorthosites should be obtained. Ar^{40}-Ar^{39} release curves for shocked samples are of far more value than total argon ages since there are too many complications in the system to be evaluated with the latter alone. It would be well worthwhile to obtain shock-melted glasses which have been only moderately heated by the monzonite from the shock breccia unit. Ar^{40}-Ar^{39} studies of such materials could lead to a more unequivocal definition of the shock time.

CHAPTER 2

Experimental and Interpretational Problems of the Ar^{40}-Ar^{39} Experiment

Introduction:

Purpose and Plan --

Although the Ar^{40}-K^{40} data yield good evidence that the time at which the monzonite crystallized was 210 m.y. ± 4 m.y., they are not interpretable as yielding a well-defined time of shock deformation. These data can be interpreted as (1) suggesting a time of shock deformation at 280-290 m.y. with later monzonite crystallization at 210 m.y. or (2) suggesting that the impact time was 210 m.y.

The main problem addressed in this thesis is whether or not a time difference exists between the shock event and the monzonite crystallization. Since the total argon ages did not resolve this problem, the Ar^{40}-Ar^{39} phase of the study was undertaken in an attempt to do so.

The major problem encountered was in attempting to determine the extent of outgassing which the shocked basement rocks experienced at the time of impact deformation. In order to obtain information on the extent of outgassing of the samples used in the shock sequence, they were irradiated with fast neutrons and then stepwise heated; the argon released in each step was analyzed for its Ar^{40}/Ar^{39} ratio. Turner (1968) has shown that this Ar^{40}- Ar^{39}

method can be of great aid in deciphering the thermal histories of meteorites. This method is potentially very valuable for unraveling terrestrial metamorphic histories; in particular, shock-metamorphic histories.

This chapter is somewhat in the nature of an appendix. The experimental results and some preliminary interpretations of these results are discussed in the preceding chapter on geochronology (CHAPTER 1). This was done in order to retain continuity with the arguments based on the Ar^{40}-K^{40} shock-sequence ages. In this chapter, specific details of the Ar^{40}-Ar^{39} experiment and some possible explanations of the unexpected results of this experiment are presented.

Simplified Theory of the Ar^{40}-Ar^{39} Experiment --

When a sample is irradiated, the Ar^{39} which is produced presumably has the same diffusion characteristics as Ar^{40}. Ar^{39} is, in essence, a measure of the potassium content of the part of the grain where it was produced and trapped. Subsequent stepwise extraction initially releases both Ar^{40} and Ar^{39} from the most easily degassed sites in the grain, with later releases from more retentive sites. The amounts of Ar^{40} and Ar^{39} present in each release step can be used to interpret the previous history of Ar^{40} loss, and hence the thermal history of the material.

A simplified model of gas release during shock supposes (1) that during the shock process irreversible heating of the material causes partial gas loss from the least retentive sites of the crystal lattice, and (2) that more retentive lattice sites retain their original pre-shock argon concentration. If this is the case, then stepwise heating of irradiated, shocked material would yield a series of Ar^{40}-Ar^{39} ratios which would indicate (1) the percentage of pre-shock argon lost during the shock event and (2) the time at which the partial gas loss occurred.

The Execution of the Experiment:

Samples Used --

The samples included in the irradiation package were (1) a "slightly shocked" anorthosite (Sample D); (2) a maskelynitized anorthosite (Sample C); (3) two "highly shocked" anorthosites (Samples E and F); (4) two pseudotachylyte-shocked anorthosite breccias (Samples G and H). A sample of the whole-rock monzonite was also included in the irradiation to serve as a monitor as was a small, quartz tube of $CaCO_3$. The calcium salt was later analyzed in order to determine the effects of isotopes other than K^{39} in producing Ar^{39} and hence correct for these interferences.

The Irradiation Procedure --

The samples to be used for irradiation were wrapped in aluminum foil and packed into an aluminum can. This sample-containing can was mounted inside another can on metal bearing points which allowed the inner can to rotate freely. The whole assembly was

irradiated in the shuttle tube facility at the General Electric Test Reactor in Vallecitos.

The inner canister, as pictured in Fig. 1, contained two levels with seven samples in each. Each level included Ni wires to monitor the fast neutron flux, utilizing the reaction ($Ni^{58}(n,p)C^{58}$, $T_{\frac{1}{2}}$ = 71d). The lower level contained those samples prepared as 1- to 3- mm chunks, while the upper level contained splits of the Ar^{40}-K^{40}-analyzed, 60- to 80- mesh powders. The different sample levels were isolated using aluminum foil. The position of the flux wires and samples in each layer is shown in Fig. 1 (see, also, Fig. 2).

The inner canister was constructed from aluminum and had a squirrel cage rotor on its top. During the irradiation, cooling water passing through the shuttle was supposed to spin the inner tube, thereby smoothing out first-order variations in the neutron flux received by the samples over the radial width of the canister. Vertical variations in the flux were not removed.

The canister received an estimated 1.07×10^{17}, fast n/cm^2 irradiation between 17:01 and 18:47 on November 20, 1970. (This value was quoted to G. Turner by GETR personnel.)

After a one-week period, subsequent to the irradiation, the samples were removed the canister. This period was specified in order to reduce activity from short half-life decays (principally Al^{28} with $T_{\frac{1}{2}}$ = 2.30 min.). The samples were then removed from the aluminum foil tubes used during the irradiation. A portion

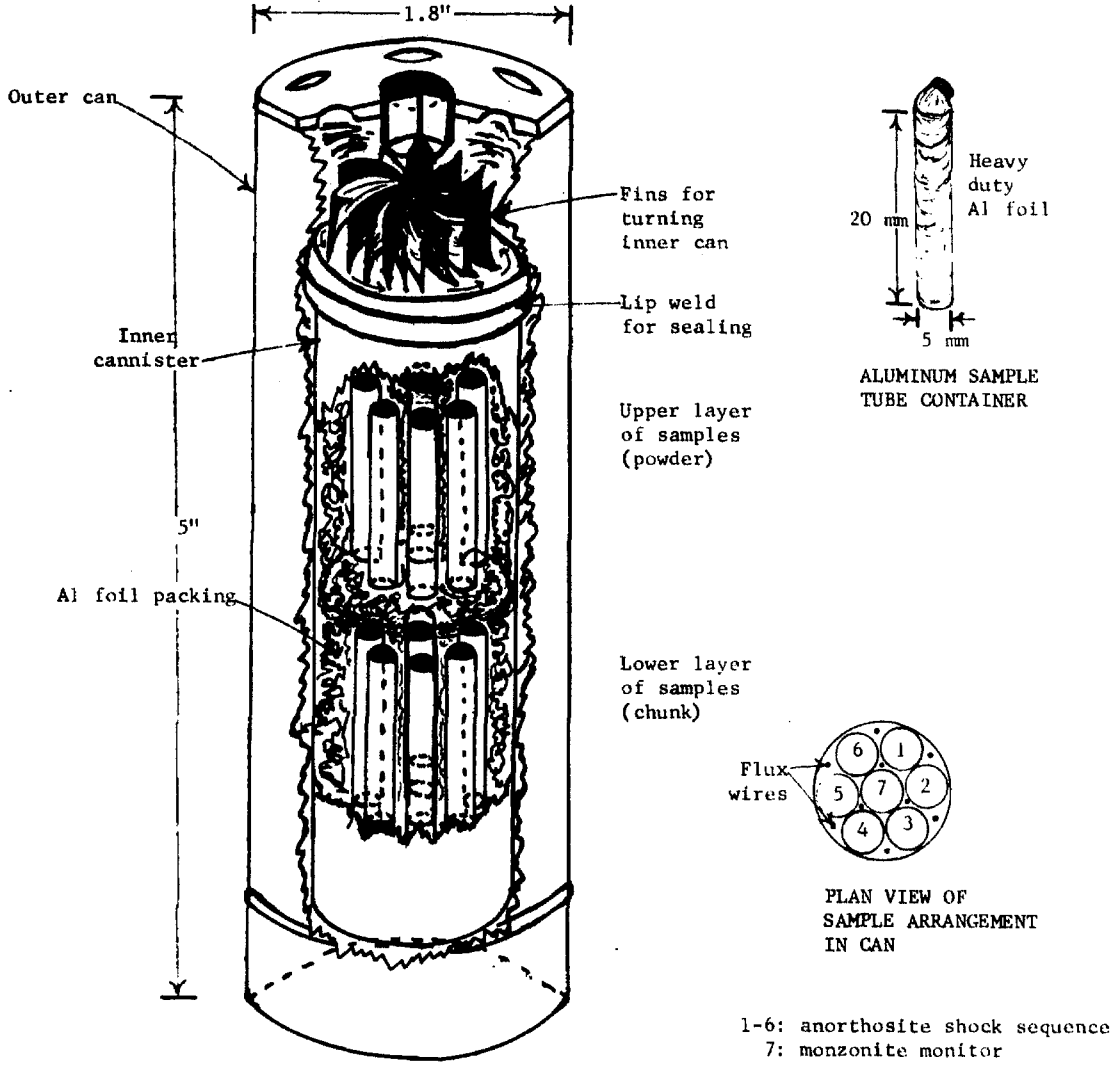

IRRADIATION CANISTER

FIG. 1

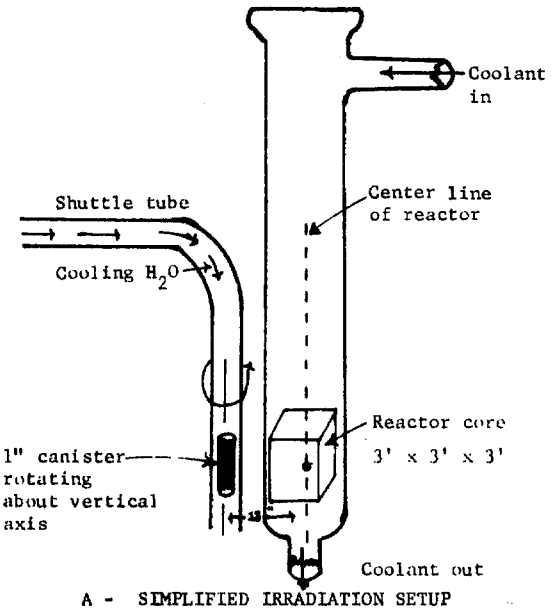

A - SIMPLIFIED IRRADIATION SETUP

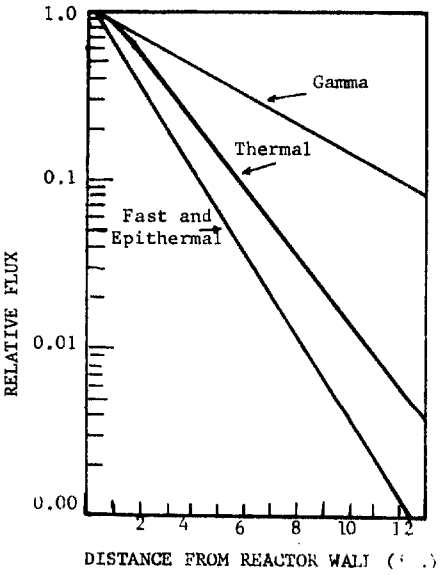

B - VARIATION OF FLUX WITH POSITION

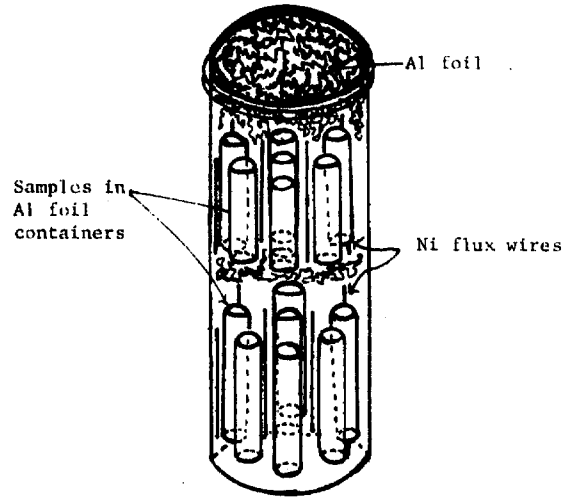

C - INNER CANISTER

Filed notch on can bottom

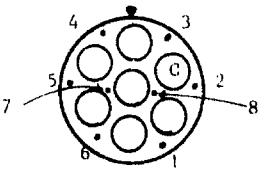

UPPER LEVEL SAMPLES (POWDERS)

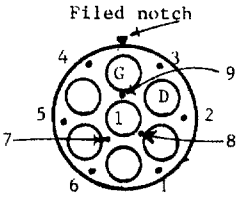

LOWER LEVEL SAMPLES (CHUNKS)

D - PLAN VIEW OF FLUX WIRE LOCATIONS

(Flux wires designated by numbers)

IRRADIATION GEOMETRY AND FLUX VARIATION

FIG. 2

of each sample (about 0.8 gm) was packaged in individual tubes made from a 1- x 2- inch sheet of regular-thickness, aluminum foil. These new sample containers were necessary in order to prevent Ar^{39} (produced during irradiation by trace amounts of K in the original aluminum) from contaminating the Ar^{39} produced in the rock samples. The new sample "boats" were then loaded into the argon-extraction system.

Time limitations only permitted the extraction of (1) the maskelynitized anorthosite; (2) the monzonite whole rock; (3) the slightly shocked anorthosite; (4) the pseudotachylyte-shocked anorthosite breccia.

Sample Gas Analysis --

The techniques used for the extraction of the samples and analysis of the sample-derived argon are described in the Appendix.

Experimental Problems Encountered:

Flux Corrections --

The Vallecitos reactor is a small reactor; the core element being only a 3-foot cube. The shuttle tube facility, in which the canister was irradiated, is 13 inches from the reactor core; the flux variation over the axial width of the sample canister is large, i.e. on the order of 20% (Fig. 2). If the canister is maintained in one position in the flux therefore, a large variation in the neutron dose experienced by various samples will result. This variation will lead to difficulties in estimating the flux dosage and, ultimately, the J values for each sample. In order

to overcome this, water flowing in the shuttle tube is utilized to turn the sample-containing capsule (A set of propellor fins is mounted on the capsule.). Turning the capsule eliminates the 20% flux differences experienced among the samples. A possibility that the capsule fails to rotate during the irradiation exists, however, and Ni flux wires were placed between the samples to monitor the flux experienced (see Fig. 2). In the event that the capsule does not rotate, a flux map can be constructed from the measured activities of the flux wires after the irradiation. Using the map, an estimate can be obtained for the neutron dosage received by each sample. If the capsule does rotate, then the J value for all the samples is considered to be the same as that for the monitor.

When the canister was unpacked, the pre-weighed wires in the various positions were weighed again to confirm their identifications, and γ spectrums of each wire were analyzed. The spectrum from a typical wire shows peaks at 0.511 mev, 0.810 mev, 1.17 mev and 1.33 mev, corresponding to β^+ β^- annihilation; EC of Co^{58} with decay to Fe^{58} ground state; two peaks due to β^- decay of Co^{60} to Ni^{60} with subsequent decay to the Ni^{60} ground state. In order to determine the flux dosage received by the various flux wires and to ultimately infer the flux received by various samples, the γ counts produced by each wire in the .047 mev on either side of the 0.81 mev Co^{58} peak were counted. These counts were then corrected for background, dead time and wire weight and recorded.

Since the Co^{58} is produced by the fast neutron reaction, $Ni^{58}(n,p)Co^{58}$, the number of counts in the .047 mev energy range is proportional to the fast neutron dose received. The locations of the various flux wires and samples are shown in Fig. 2, and the counts measured for each flux wire are listed in Table 1 . The last column of Table 1 shows these counts normalized to the counts estimated for the monzonite monitor in the lower level. Using the data in Table 1 and the sample positions as shown in Fig. 2, the neutron dose received by each sample, relative to the monitor, can be estimated. In Fig. 2, the wires are located in neat niches between the samples; in actuality, however, the uncertainty in the position of the flux wires (± 1/8") means that only a crude flux map can be constructed. The uncertainty in flux value generated by the position uncertainty is about ± 4-5%. This uncertainty in the flux experienced leads to a 4-5% uncertainty in the J values estimated for each sample.

The average flux received in the upper level is estimated to be about 4% higher than that received at the lower level; Sample C received a flux about 2% higher than the monitor (#1). Sample D, the slightly shocked anorthosite, received a flux about 7% lower than the monitor while Sample G, the pseudotachylyte breccia, received a flux about 2% higher than the monitor. A higher flux will imply a proportionately higher J value appropriate for the sample.

TABLE 1.

Flux Wire Data

Wire	Wire Wt.	Normalized Counts $Co^{58}(\gamma)Fe^{58}$	Relative Counts $\frac{1/3(LL-7+LL-8+LL-9)}{1.0}$
		Upper Level	
UL-1	0.1530	523,666	0.9725
UL-2	0.1330	511,890	0.9506
UL-3	0.1014	567,559	1.0540
UL-4	0.10935	578,945	1.0752
UL-5	0.13555	613,109	1.1386
UL-6	0.12865	562,398	1.0444
UL-7	0.13805	575,564	1.0689
UL-8	0.10985	535,879	0.9952
		Lower Level	
LL-1	0.18730	508,017	0.9434
LL-2	0.18495	489,530	0.9091
LL-3	0.18490	504,385	0.9367
LL-4	0.20220	566,475	1.0520
LL-5	0.20110	589,817	1.0954
LL-6	0.16065	554,685	1.0301
LL-7	0.1900	525,011	0.9750
LL-8	0.19390	563,267	1.0460
LL-9	0.15155	527,139	0.9790

The J value calculated from the overall average Ar^{40}/Ar^{39} ratio for the monzonite is 4.766×10^{-4}. Using this measurement and the factors discussed previously, the J values inferred for Samples C, D and G are 4.861, 4.430 and 4.861 (all x 10^{-4}), respectively.

Since measurements of the total Ar^{40}-K^{40} age for each sample are at hand, J values for each sample can also be calculated from the total argon age of the sample and the overall average Ar^{40}/Ar^{39} ratio measured for the irradiated sample. The J values of Samples C, D and G, calculated using these latter measurements, are 5.165, 4.661 and 6.526 (x 10^{-4}), respectively. These J_{self} values can be expected to agree precisely with those in the previous paragraph (J_{monz}) for Sample C only; it is only for this sample that the Ar^{40}-K^{40} and Ar^{40}-Ar^{39} measurements were done on splits of the same material. J_{self} is about 5-6% greater than J_{monz} for Samples C and D but about 30% greater for Sample G.

As discussed previously, the difference between J values for Sample G is thought to be due to differences in the material used for the two types of analyses rather than to errors in the determination of J_{monz} for the pseudotachylyte breccia. For Samples D and C, the differences between J_{self} and J_{monz} (5-6%) are within the expected errors in J_{self}. For Samples D and C, J_{self} is thought to be the most accurate J value while for Sample G, J_{monz} is used. The overall uncertainty in all the J values

is estimated to be ± 6%.

Interfering Isotopes --

During irradiation, the elements present in the sample receive a dosage of neutrons with energies ranging from 0.01 ev to 10 mev, and various stable and unstable argon isotopes are produced. This method assumes that Ar^{39} is an exact monitor of the K^{39} present in the material; this is only approximately true. Isotopes other than K^{39} contribute to the total production of Ar^{39}. If Ar^{39} is used to reflect the potassium concentrations in different sites,"interfering" Ar^{39} from these other isotopes must be accounted for. The amounts of all argon isotopes produced by the irradiation must be known if accurate Ar^{40}/Ar^{39} ages are to be obtained.

One could, in principle, calculate the amount of each argon isotope produced during irradiation and correct for its interference if the following criteria are known: (1) the neutron flux spectrum $\phi(E)$; (2) cross sections for productions of (product) isotope i from (target) isotope j; (3) elemental abundances in the sample. In actuality, however, it is more convenient to irradiate salts of known composition simultaneously with the samples and then measure the amounts of interfering argon isotopes produced. This latter procedure also circumvents the need for detailed knowledge of the reactor neutron energy spectrum.

The reactions which produce argon isotopes are shown in Table 2 (Turner, 1970; Mitchell, 1968). Cross sections for these reactions and argon yields are shown for the product isotopes Ar^{40}, Ar^{39}, Ar^{37} and Ar^{36}. All cross sections are in error because the absolute flux is uncertain. The integrated fast neutron flux (1.07×10^{17} n/cm^2) used for the calculation of the values in Table 2 was quoted to G. Turner by GETR personnel, based on their measurements of the flux. The cross sections shown in the table are normalized to the value of 32.2 mb calculated for $\sigma(Ca^{40}\text{-}Ar^{37})$. Values of the cross sections, shown in Table 2, are discussed in the footnotes to the table.

The effects due to interfering isotopes are small. The K/Ca ratio of the shock-sequence anorthosites is generally about 0.1; hence, using the argon yields in Table 2, $Ar^{39}_{Ca}/Ar^{39}_{K} \sim 0.3\%$*. The Ar^{40} present in the shock-sequence samples is about 500-1000 $\times 10^{-8}$ ccSTP/gm, and their potassium concentration is about 0.5%. Ar^{40}_{Ca}, therefore, is not greater than 0.01% of the total Ar^{40}. For an anorthosite with a 10% air correction, the maximum error which Ar^{36}_{Ca} can produce is about 3%. The data for each temperature release

---

* Subscript refers to the irradiated isotope which is the source of the gas. Ar^{37}_{Ca} is Ar^{37} produced by irradiation of calcium. $(Ar^{39}/Ar^{37})_{Ca}$ is the ratio of calcium-derived Ar^{39} to calcium-derived Ar^{37}.

TABLE 2.

Argon Isotopes in Irradiated Rocks

Product isotope	Production reaction Q value shown in parenthesis	σ in mb*	Amount of isotope produced per gram of target element with 1×10^{17} n/cm^2 (amounts in 10^{-8}ccSTP)
Ar^{41}	$K^{41}(n,p)Ar^{41}$ $Ar^{40}(n,\gamma)Ar^{41}$ $Ca^{44}(n,\alpha)Ar^{41}$	–	Ar^{41} decays to K^{41} with a 1.78-hr. half-life
Ar^{40}	$K^{40}(n,p)Ar^{40}(+2.29)$ $K^{41}(n,d)Ar^{40}(-5.58)$	– 10^{1}-10^{2} (4)	4-10 (3)
	$Ca^{43}(n,\alpha)Ar^{40}(+2.29)$	10^{1}-10^{2} (4)	~ 0.2
	$Ca^{44}(n,n\alpha)Ar^{40}(-8.85)$	10^{-2}-10^{-1} (4)	~ 0.0006
Ar^{39}	$K^{39}(n,p)Ar^{39}(+0.22)$	60.4 (1)	333
	$Ca^{42}(n,n\alpha)Ar^{39}(+0.35)$	3.6 (2)	0.133
Ar^{38}	$K^{39}(n,d)Ar^{38}(-4.1)$ $K^{41}(n,\alpha)Cl^{38}(\beta)Ar^{38}(-0.10)$ $Ca^{42}(n,n\alpha)Ar^{38}(-6.25)$ $Cl^{37}(n,\gamma)Cl^{38}(\beta)Ar^{38}$	–	
Ar^{37}	$Ca^{40}(n,\alpha)Ar^{37}(+1.75)$	32.2 (1)	181
Ar^{36}	$Ca^{40}(n,n\alpha)Ar^{36}(-7.04)$ $Cl^{35}(n,\gamma)Cl^{36}(\beta)Ar^{36}$	0.0098 (2)	0.055

TABLE 2 -- continued.

Footnotes:

* All values shown are normalized to the calculated value of $\sigma(Ca^{40}\text{-}Ar^{37}) = 32.2$. This value is about 10% lower than the value suggested by Turner (1971).

(1) Calculated from monitor data; i.e., 0.71605-gm monzonite sample; 2.785% K; 3.8% Ca; 1.07×10^{17} fast neutron flux produced gas amounts shown in Table 2, CHAPTER 1. Turner (1971) calculates an absolute value for $\sigma(K^{39}\text{-}Ar^{39}) = 68$ mb; hence, the absolute value for $\sigma(Ca^{40}\text{-}Ar^{37}) = 36$ mb. The low values shown in the table probably result from errors in the flux quoted to G. Turner by GETR personnel.

(2) These cross sections are based on the values of Turner et al. (1971); $(Ar^{39}/Ar^{37})_{Ca} = 7.32 \times 10^{-4}$. $(Ar^{36}/Ar^{37})_{Ca} = 3.05 \times 10^{-4}$. The ratios above were measured on a CaF_2 monitor irradiated at Vallecitos, and therefore are produced by neutrons with the same energy spectrum as was used to irradiate the shock-sequence samples.

The values of σ calculated from the above ratios are compatible with the values determined from the irradiated $CaCO_3$. The later values of σ, however, are much less precise.

The isotopic ratios measured for the argon from the irradiated $CaCO_3$ were $Ar^{40}/Ar^{36} > 271$; $Ar^{40}/Ar^{39} > 195$; $Ar^{40}/Ar^{37} \sim 29$. This gas consists of atmospheric argon and calcium-derived Ar^{39}, Ar^{36} and Ar^{37}. After the atmospheric component is corrected for, $(Ar^{36}/Ar^{37})_{Ca} < 0.9 \times 10^{-2}$; $(Ar^{39}/Ar^{37})_{Ca} < 1.5 \times 10^{-2}$. Using the value of $\sigma(Ca^{40}\text{-}Ar^{37})_{Ca} = 32.2$ mb, obtained from the monitor, values of $\sigma(Ca^{42}\text{-}Ar^{39}) \sim 73$ mb and $\sigma(Ca^{40}\text{-}Ar^{36}) \sim 0.29$ mb are obtained.

TABLE 2 -- continued.

In order to determine the amount of Ca^{42}-derived Ar^{39} and Ca -derived Ar^{36}, about 71 mg of spec-pure $CaCO_3$ was irradiated with the samples. Subsequent extraction of this salt yielded about 3×10^{-8} ccSTP of Ar^{37}. This amount is only 50% of the Ar^{37} expected if $\sigma(Ca^{40}\text{-}Ar^{37}) = 32$ mb. The discrepancy between expected and realized amounts is probably due to gas loss from very fine grains of the salt.

The Ar^{39} and Ar^{36} yielded by this sample were of the same order of magnitude as the background, and the errors in the measured Ar^{39}/Ar^{37} and Ar^{36}/Ar^{37} ratios were therefore very large. The values calculated for the cross sections $\sigma(Ca^{40}(n,n\alpha)Ar^{36} = 0.29$ mb ; $\sigma(Ca^{42}(n,n\alpha)Ar^{39} = 73$ mb are, therefore, probably 2 to 20 times higher than the true values.

(3) Turner (1970) suggests values of $(Ar^{40}/Ar^{39})_K = 0.012\text{-}0.031$.

(4) The cross sections of these two reactions are not known, but it can be argued that reactions with similar Q values have cross sections of the same order of magnitude. Hence, $\sigma(Ca^{43}\text{-}Ar^{40})$ should be about the same order of magnitude as $\sigma(Ca^{40}\text{-}Ar^{37})$ and $\sigma(Ca^{44}\text{-}Ar^{40}) \sim \sigma(Ca^{40}\text{-}Ar^{36})$. The isotopic abundances of Ca^{44}, Ca^{43} and Ca^{40} are 0.0206, 0.00145, and 0.970, respectively, and the estimates shown follow from these values.

corrected for the effects of interference isotopes at Ar^{36}, Ar^{39} and Ar^{40} by using the ratios

$$Ar^{36}_{Ca}/Ar^{37}_{Ca} = 2.5 \times 10^{-4};\ Ar^{39}_{Ca}/Ar^{37}_{Ca} = 8 \times 10^{-4};\ Ar^{40}_{K}/Ar^{39}_{K} = 2 \times 10^{-2}$$

suggested by Turner (1970) and the measured Ar^{39}/Ar^{37} and Ar^{40}/Ar^{39} ratios. The corrections to the measured ratios are small because the irradiation dosage was calculated by Turner according to the scheme of Turner (1970) which minimizes the effects of interference isotopes.

Simple Theory --

Elementary View of a Stepwise Heating: Reduced to its simplest terms, the Ar^{40}-Ar^{39} method involves tagging of the amount of potassium present in a particular lattice site by irradiating the sample and making use of the reaction $K^{39}(n,p)Ar^{39}$. Fast neutrons, as described by this reaction, convert some of the K^{39} to Ar^{39} which then remains in the same lattice site as the original K^{39}. When the sample is subsequently heated to different temperatures and extracted during a set of steps in the laboratory, different sites can be differentially drained of argon and information obtained about their Ar^{40}/Ar^{39} ratio (Fig. 3). Since Ar^{40*}/Ar^{39} is proportional to Ar^{40*}/K^{40} and the Ar^{40*}/K^{4} ratio can be interpreted as an age, each heating step will yield an Ar^{40*}/Ar^{39} ratio characteristic of the age of the sites drained.

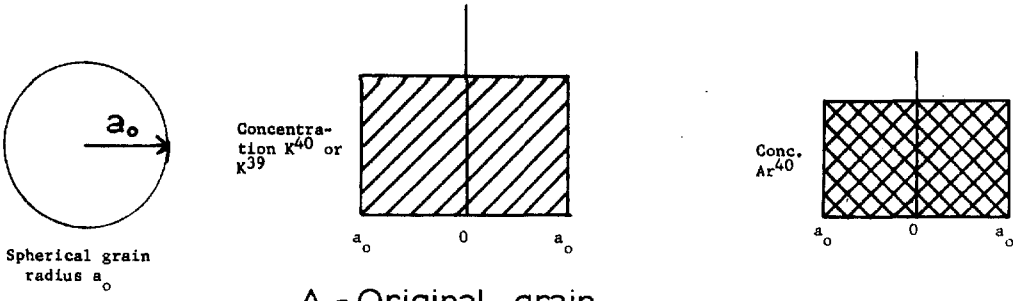

A - Original grain

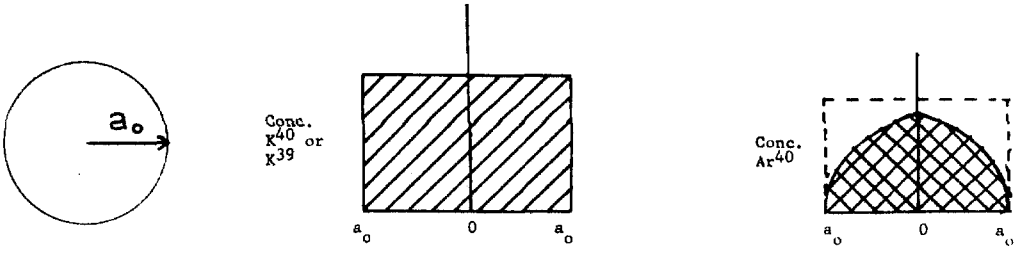

B - Grain after thermal metamorphism produces partial gas loss

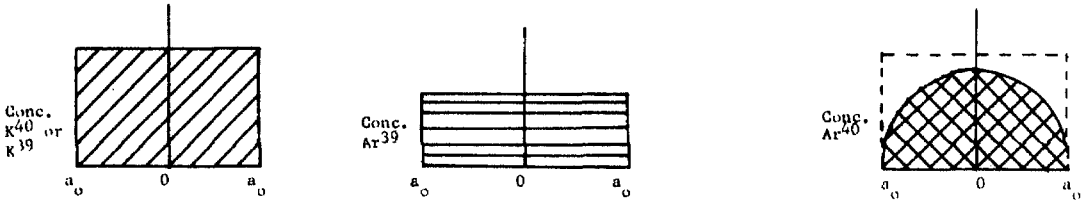

C - Grain after irradiation produces Ar^{39}

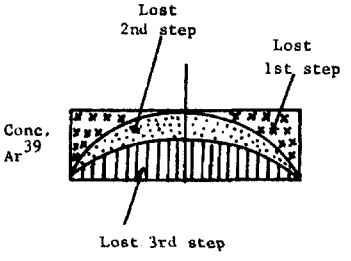

D - Grain during laboratory step heating after irradiation

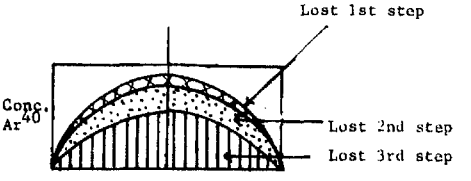

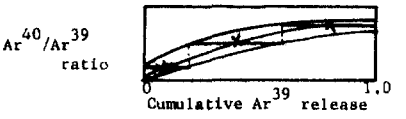

E - 3 step release curve of irradiated grain

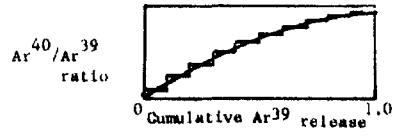

F - Many-step release curve of the same grain

STEPWISE HEATING OF IRRADIATED, PARTLY OUTGASSED GRAIN

FIG. 3

Fig. 3 shows how an irradiated, partially outgassed grain would be expected to behave in a laboratory three-step heating experiment. It can be seen that the first steps of the extraction yield gas with a low Ar^{40*}/Ar^{39} ratio relative to the later steps. The later heatings yield argon with a ratio which is more characteristic of the age of the grain before thermal metamorphism (Fig. 3e).

The stepwise heating experiment shown in Fig. 3e takes three temperature steps in order to extract the sample. An experiment in which many very minute steps are utilized can be imagined; this would more closely approximate a continuous Ar^{40}-Ar^{39} release curve. The continuous curve can be dealt with theoretically. If a continuous curve is to be inferred from a curve with discrete steps, as shown in Fig. 3e, then the Ar^{40}/Ar^{39} ratio for each step should be assigned to the midpoint of the Ar^{39} release rather than to the initial or end point. Plotting a curve through the initial Ar^{39} release value will result in an overestimate of the continuous curve, while using the end value results in an underestimate (Fig. 3f).

Partial Gas-Loss Models of Turner: Turner (1968), using appropriate simplifications, has quantitatively discussed the case of thermal metamorphism and presented curves showing how the Ar^{40}/Ar^{39} ratio observed during laboratory heatings would be expected to vary. In these models (see Fig. 4), an assemblage of spherical grains, originally formed at 4.55 Ae and outgassed at 500 m.y., is studied assuming various partial gas losses at 500 m.y. Turner's calculations

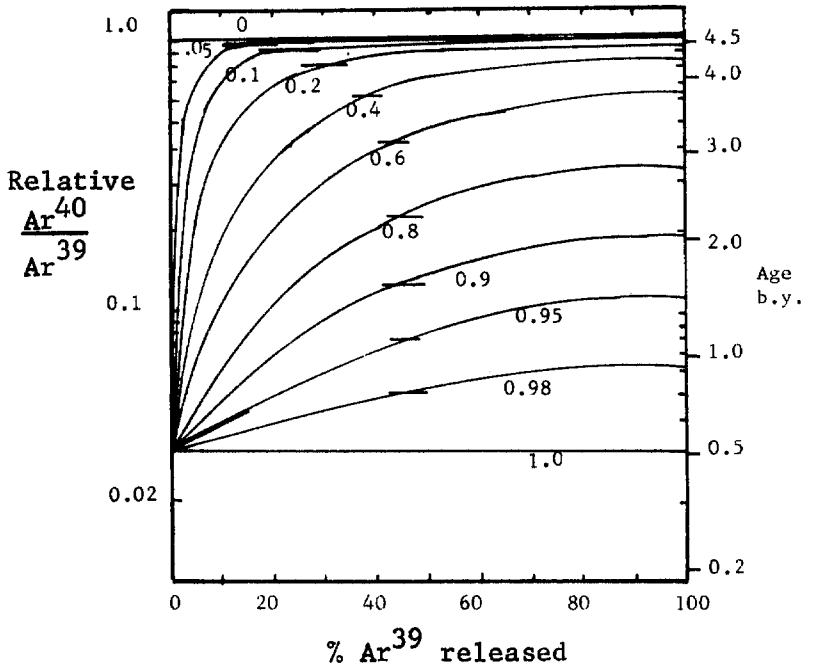

A

UNIFORM SPHERES

Uniform spherical grains of one size

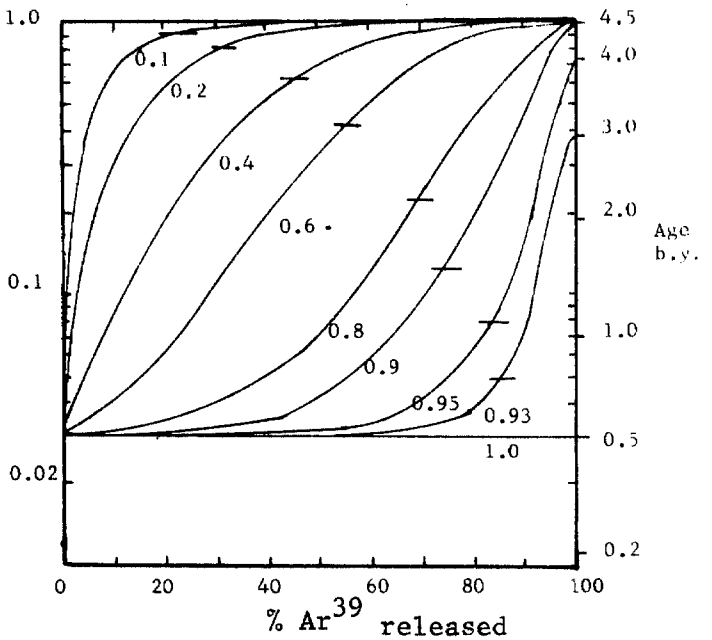

B.

LOG NORMAL DISTRIBUTION

σ = 0.6

Log normal distribution of grain sizes

LABORATORY RELEASE PATTERNS FOR 4.55 AE METEORITE OUTGASSED AT 0.5 AE (after Turner, 1968)

FIG. 4

for a set of uniform spheres and a set of spheres with a log normal distribution of grain sizes ($\sigma = 0.6$; i.e., sizes ranging from $0.36\ a_o < r < 2.8\ a_o$) are shown.

One immediately obvious feature of these curves is that the uniform spheres show less evidence of their original age than the log-normal system of grains. If 80% of the argon is lost from uniform spheres, the maximum age indicated is about 2.8 b.y. By contrast, for the case of a distribution of spheres the larger spheres in the system still give evidence of their original 4.55 b.y. age, even with an 80% gas loss.

Model Calculations for the Shock-Sequence Rocks: Turner's calculations are not entirely appropriate in the case of the shock-sequence anorthosites because of both different ages and different grain-size distributions than those assumed by Turner. In view of this, some simple cases were considered using the same approach as Turner but different ages and slightly different models. A 950-m.y. rock was supposed to consist of: (1) uniform spherical grains; (2) one-half of its mass in the form of spheres $a_o/\sqrt{3}$ in radius and the other half of spheres $\sqrt{3}\ a_o$; (3) one-third of its mass in spheres of radius $a_o/3$, one-third of its mass in spheres a_o in radius and the other third of its mass in spheres of radius $3a_o$. These systems were assumed to have been thermally outgassed to varying degrees at 300 m.y. In each case, a single-volume diffusion process characterized by D was assumed. The curves of indicated age

as a function of the cumulative release of Ar^{39} in a laboratory stepwise heating experiment for these three cases are shown in Figs. 5, 6 and 7

Three general features of these curves, which are quite similar to those established by Turner (1968), are of interest:

(1) For the case of uniform grain sizes, the maximum age indicated by the sample is about 1.2 times its average age; whereas for the case of a mixture of grain sizes, even relatively large (50%) gas losses at the 300-m.y. date do not erase the record of the old age retained in the most retentive sites of the system. The same observation can also be made for Turner's log-normal, grain-size distributions. The important point is that, with a range of grain sizes, the major gas loss occurs from small grains at the time of the thermal disturbance; the larger grains, for the most part, retain their gas. In the laboratory, the Ar^{39} tracer will first release from the smaller, Ar^{40}-depleted grains yielding a low Ar^{40}/Ar^{39} ratio; later in the experiment the larger, retentive grains which are not depleted in Ar^{40} will yield both Ar^{40} and Ar^{39} in a ratio characteristic of the old age. For the uniform spheres there are no sites, in the case of large gas loss, which remain undepleted. At larger losses, almost all the evidence of the original old age is wiped out.

(2) The ratios at releases $<$ 30-40 % are reasonably linear for all cases. It is useful to know this when trying to infer the original time of outgassing, especially if some slight diffusional

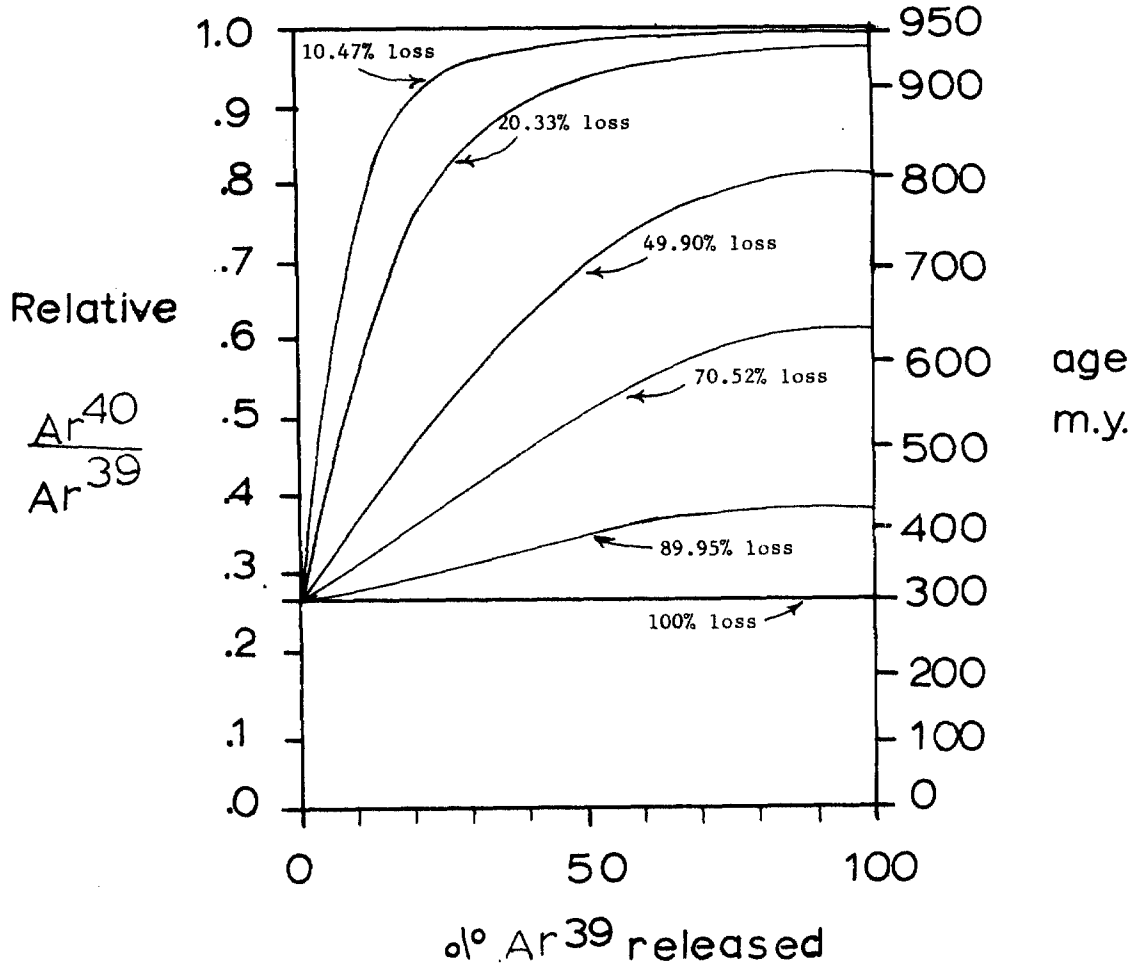

Expected Laboratory Release Curves For 950 m.y. Rock Which Is Uniform Spherical Grains Outgassed At 300 m.y.

FIG. 5

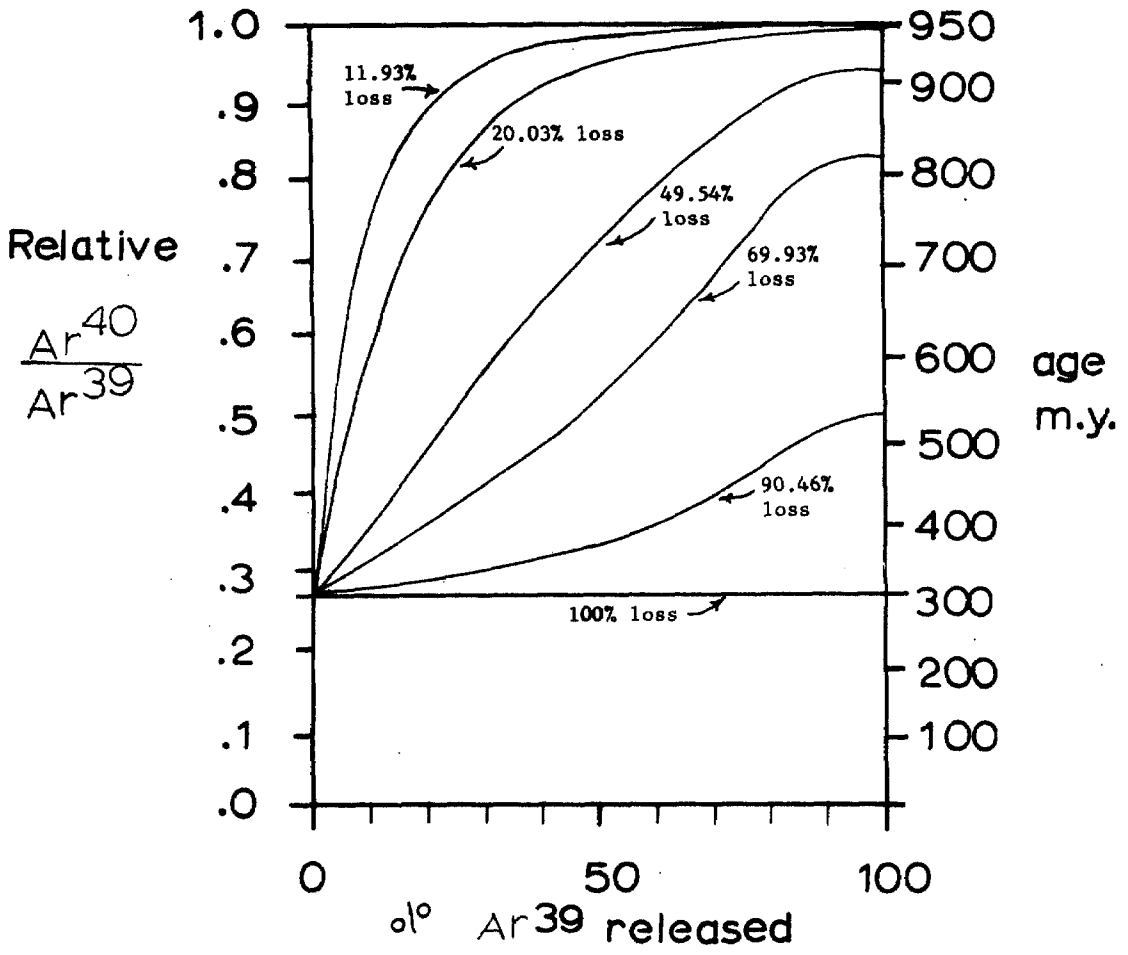

Expected Laboratory Release Pattern For Sample Composed Of 0.5 Mass Fraction Spheres $a_o\sqrt{3}$, 0.5 Mass Fraction Spheres $\sqrt{3}$ a_o

FIG. 6

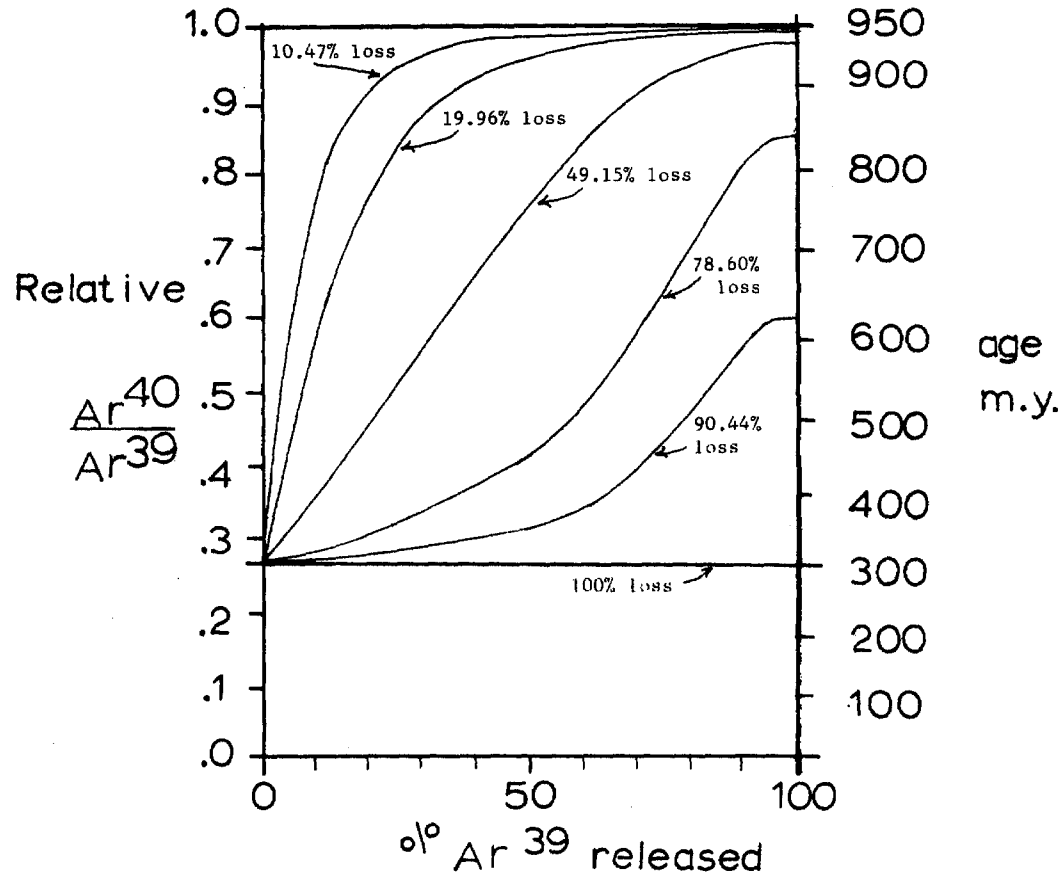

Expected Laboratory Release Pattern For A System: 0.33 Mass Fraction of Spheres $a_0/3$, 0.33 Mass Fraction a_0 Radius, 0.33 Mass Fraction $3a_0$ Radius

FIG. 7

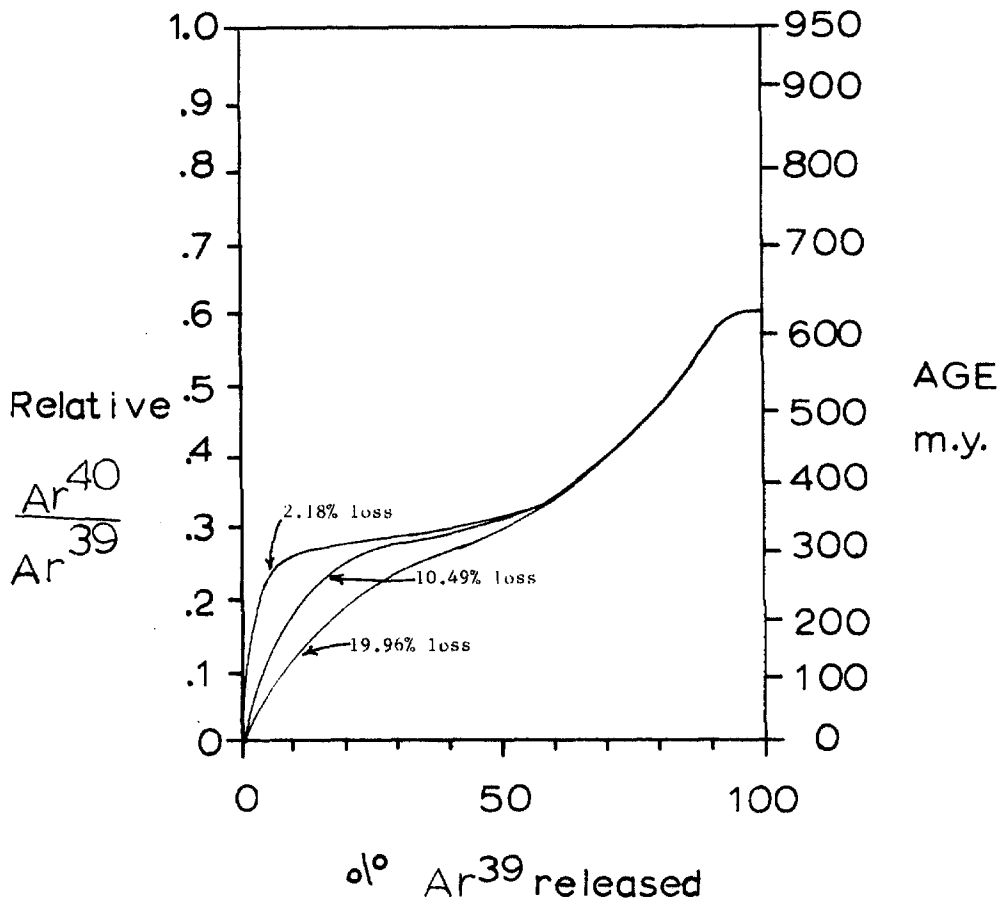

Expected Laboratory Release Patterns for System: 0.33 Mass Fraction Spheres $a_o/3$ Radius, 0.33 Mass Fraction Spheres a_o Radius, 0.33 Mass Fraction Spheres $3a_o$ Radius, 90.44 % Loss at 300 m.y.; Subsequent Continuous Diffusion Loss Thereafter

loss takes place at a later time (see Fig. 8). The later, tertiary loss in this system will take place if there is a heating subsequent to the 300-m.y. metamorphic event or if the material experiences continuous-diffusional loss (Wasserburg, 1954). It is apparent from Fig. 8 that, as the second metamorphic event becomes more severe, it becomes increasingly more difficult to observe evidence of the 300-m.y. event.

(3) For small gas losses (10-20%) at the time of metamorphism, the laboratory release curves have the same shape regardless of the assumptions made regarding grain-size distribution. This is because only the edges of the grains lose argon, and the diffusion process does not affect the grain cores. Thus, no evidence of how large the grains are appears in the release curves.

Complications: Where the Assumptions of the Simple System are In-valid --

Assumptions of the Simple System: The release curves discussed by Turner (1968), in all cases, yield a monotonically increasing (or flat curve) of Ar^{40}/Ar^{39} ratio vs. Ar^{39} release. No dips or drop-offs in the ratio at high Ar^{39} releases are observed.

Three assumptions were made by Turner in his discussion of the model gas-loss systems referred to above: (1) The systems were assumed to consist of a single argon-bearing species with various grain sizes. (2) Argon loss by volume diffusion was assumed to be the sole diffusion process taking place. (3) It was assumed that partial gas loss, which occurs during the metamorphic event, is due

solely to thermal diffusion out of the grains, and that the system, apart from gas concentrations, is the same both before and after the partial gas loss. In this case, partial gas loss will deplete argon-containing sites, during the metamorphism, in order of increasing retentivity of the sites. The laboratory stepwise extraction will deplete progressively more retentive sites in the same fashion that Ar^{40} was depleted from these sites during the original metamorphism. The third assumption is very important because it allows the original Ar^{40} loss behavior to be duplicated by the Ar^{39} behavior during the laboratory extraction. The provision that long-term, low-temperature diffusion is equivalent to short-term, higher temperature processes must, as always, be made.

Real Rock Systems: The model systems discussed by Turner provide the basis for interpreting metamorphic systems. These models are, however, only a first approximation to systems of geological interest. Real rock systems are not only multi-mineralic; they also undergo more complicated metamorphism.

A real rock system usually consists of more than one mineral species. The overall release curve for such a composite system can exhibit a complicated Ar^{40}/Ar^{39} ratio vs. Ar^{39} released behavior.

The purely thermal metamorphism assumed by Turner is seldom realized. In the case of a regional metamorphic event, a system suffers partial gas loss by heating; new mineral phases usually crystallize, and original mineral phases may undergo alteration and suffer gas loss through chemical disaggregation rather than by thermal diffusion. In this case, laboratory thermal release of Ar^{39} from the post-metamorphic system will not duplicate the Ar^{40} release from the original system during the metamorphic event.

Shocked Systems: If a rock suffers partial gas loss due to shock metamorphism, then argon loss will result from both mechanical disaggregation and thermal diffusion. During the shock process, the chemical compositions of the phases in the original sample do not usually change; however, the physical state of material in the original sample can be drastically altered. Gas loss from the shocked system may depend more critically on the mechanical damage suffered during shock than on gas loss by thermal diffusion. For example, gas loss from a fine-grained breccia produced during shock may occur mainly after the shock event (perhaps by continuous diffusion) rather than during shock. For this system, the release of Ar^{39} during a laboratory heating would clearly not duplicate the release of Ar^{40} from the system during the original shock event. The system would yield low initial ages in its release curve, even

though these ages have no relation to the time of shock.

Release Curves of the Shocked Anorthosites --

Observed Features: From the above discussion, it is obvious that real geological systems, and particularly shock-metamorphosed rocks, may yield Ar^{40}-Ar^{39} release curves which can be very complicated. No attempt is made to consider all the features of the curves which could be observed. Some possible explanations of the release-curve features observed for the shock-sequence anorthosites will, however, be discussed.

Four notable features of the Ar^{40}-Ar^{39} release curves of the shock-sequence anorthosites continuously recurred.

(1) A sharp decrease in the Ar^{40}/Ar^{39} ratio of high-temperature gas fractions, compared to the ratio from lower temperature fractions, was observed in the release patterns of Samples D and C.

(2) Ages indicated by the initial temperature fractions of both Samples D and G are higher than the ages indicated by the subsequent temperature fractions.

(3) All the samples released a significant portion of their argon well above those temperatures at which plagioclase normally outgasses completely.

(4) The ages of the small amounts of gas released from the rock during the highest-temperature heating steps are distinctly lower than the ages of temperature fractions at lower temperatures.

The above features will be discussed.

Ratio Drop-off in the Highest Temperature Fractions: All of the samples used in this study show a large drop-off of the Ar^{40*}/Ar^{39} ratio at high temperatures. The errors associated with determining the Ar^{40*}/Ar^{39} ratio for small amounts of gas which is composed mostly of air-composition (blank) argon are quite large. The background at masses Ar^{39} and Ar^{36} is 5×10^{-11} ccSTP and 2.5×10^{-11} ccSTP, respectively. For a sample consisting of about 90% air with a true Ar^{40}/Ar^{39} ratio of 500 and about 5×10^{-8} ccSTP of Ar^{40}, the background in the Ar^{39} is 80% of the unknown peak and the Ar^{36} background is 20% of the Ar^{36} peak. Ratios involving these errors will be very uncertain. For this reason, the low ratios observed are thought to be products of errors rather than evidence of some consistent behavior. For some cases, however, they are significantly lower than the preceding ratios.

It is possible that a phase which releases argon at high temperatures and has a lower "age" is responsible for the low ratios in the last parts of the extraction. The Ar^{39}/Ar^{37} ratios generally observed for these releases are similar, however, (within errors) to those observed for previous releases; this does not support the idea that these releases come from a different phase.

Evidence of a Highly Retentive Phase: A noteworthy and surprising feature of all the shocked samples extracted in this study is that they retain significant (> 25%) fractions of argon at temperatures above 1150°C. As pointed out earlier (see Fig. 5, CHAPTER 1), typical plagioclase behavior (inferred from the data of Fechtig et al., 1960) is for it to lose about 98% of its argon at around 1250°C. For the samples studied, the K/Ca ratios for these high-temperature releases are similar to those of plagioclase, An_{50-55}, which is also the main argon-containing phase in the rocks. The material releasing gas at the high temperatures is probably, therefore, of plagioclase composition and not garnet or pyroxene.

Three possible explanations for this apparently abnormal behavior are: (1) Gas retention at high temperatures is a regional characteristic of plagioclase from this anorthosite massif. (2) It is possible that during the extraction the imperfections in the plagioclase, which determine the effective D/a^2, were annealed at some temperature less than the melting temperature. This would result in the production of a uniform phase with very long path lengths and correspondingly high retentivity. The imperfections annealed might be within a grain, or grain boundaries, but the theory postulates that they would anneal at about 1100°C. (3) A third possibility

is that an effective increase in grain size takes place during the shock metamorphism and that, in some regions of the original material, the imperfections have been removed so that D/a^2 at any particular temperature is smaller than that of the original material. The process which does the annealing is unclear, but it may be that during the shock a phase transformation takes place in a large region of the material; i.e., one whole grain, or several grains, of the rock. When the shocked material relaxes to one atmosphere, the lack of imperfections of the in-shock phase persists over the same region in the zero-pressure phase. This process would be somewhat similar to "recrystallization" during the shock process. At very high shock intensities, globs of thermal glass, which can be expected to have large diffusion path lengths, are produced.

Whether or not the highly retentive sites in the plagioclase from these anorthosites is a regional characteristic of the anorthosites cannot be concluded from the present data. A stepwise extraction must be made on a sample of the outside anorthosite before any definite conclusions can be made as to whether or not shock processes produce retentive phases.

The "crucible-lump" explanation of the highly retentive phase does not adequately account for some of the observations. Diffusion parameters obtained from the Ar^{39} releases of the maskelynite (Fig. 6, CHAPTER 1) show no abrupt decrease around 1150°C as would be expected from the "crucible-glass" theory.

Plagioclase cores from the monzonite released about 99% of their argon at 1250°C, suggesting that crucible welding for unshocked plagioclase, An_{55}, does not take place.

Decrease in Ages of the High-Temperature Gas Fractions: The release curves of both the maskelynitized anorthosite and the slightly shocked anorthosite exhibit a pronounced drop-off of their Ar^{40}/Ar^{39} ratios at temperatures above 1200°C. The release curve obtained by Turner (1970) for Lunar Rock 12013 and release curves of Apollo 14 lunar breccias (Turner et al., 1971) also display this peculiar characteristic. The drop-off in ages is more pronounced in the latter case. This feature of the release curve is peculiar since it implies that the more retentive sites of the present system, i.e., those releasing gas at high temperatures, lost more gas during the original outgassing event that did the less retentive sites. It is difficult to envision how any purely thermal process which produces partial gas loss in a rock system could produce such a loss pattern. At the present time, no satisfactory explanation for this drop-off in ages exists.

If the rock system is supposed to be a composite system, it could be assumed that the high-temperature decrease in ages is due to a low-age, high-retentivity mineral which dominates the gas releases at high temperatures. This explanation may hold in some cases, but it does not account for the observations

of this study. The K/Ca ratios of the high-temperature releases for the shock-sequence anorthosites suggest that these releases are from the same material that releases the bulk of the argon from the rock ; not from a mineral of higher retentivity which probably also differs in chemical composition.

A question arises as to whether the drop-off in the high-temperature ages is part of a decreasing trend in ages from high-retentivity sites or if it is due to the absence of high ages superimposed on a different trend. While this point is semantical to some degree, it affects the way an observed curve may be interpreted. Since the temperature steps used in the Ar^{40}-Ar^{39} extractions integrate gas releases from many argon-containing sites, the same feature may appear differently on two different release curves. For example, if the temperatures of the steps used for extracting the slightly shocked anorthosite had all been 50°C higher, the resulting release curve would have appeared to have a regular decrease in ages at high temperatures rather than an abrupt drop-off in ages.

For both the maskelynite and the slightly shocked anorthosite, it seems best to interpret the highest ages of the release curve as ages superimposed on a more general trend from other fractions of the rock. The "general trends" in ages for these two samples are suggested by the dashed curves in Figs. 4 and 5. The above observation suggests that these shocked systems should be treated

as two subsystems: one subsystem yielding the high ages; the other yielding the general age trend.

It is possible to interpret the high ages observed in the above release curves as being due to argon released from grains which have undergone distinctly less outgassing than the majority of grains in the rock. The former grains are probably only mildly fractured and were not extensively heated during the shock process. The shock process can be assumed to act on two subsystems in the original rock. In one of these subsystems, the shock process merely fractured grains and caused only slight gas loss. In the other subsystem, grains suffered more extensive thermal outgassing, and some of the most extensively outgassed grains were simultaneously transformed into a more retentive phase. The high ages observed during the laboratory stepwise heating of the rock are produced by argon released from the mainly fractured subsystem; the thermally outgassed system produces the general trend observed in ages. For both the maskelynite and the slightly shocked anorthosite, releases from less damaged plagioclase would be expected to occur between 1000-1200 ^{o}C (see Fig. 5, CHAPTER 1). This is, in fact, where the "hump" in these release curves occur. The K/Ca ratios of the high-age releases of the maskelynite are similar to K/Ca ratios of An_{55}; this observation is compatible with the belief that these releases are from mildly outgassed

Low Ages Observed After the Initial Step: A puzzling feature which was observed in the release curves of both the pseudotachylyte-shocked anorthosite breccia and the slightly shocked anorthosite is that gas released at about 700-800 ^{o}C indicates a lower age than gas released during the initial temperature step. This behavior has not been reported elsewhere and is not predicted in the theoretical models discussed by Turner (1968). As mentioned previously, partial gas loss by thermal diffusion depletes the least retentive, argon-containing sites of a rock; subsequent laboratory heating of an irradiated rock would be expected to yield low ages in the initial release with subsequent higher temperature gas fractions yielding progressively higher, rather than lower, ages. At the present time, this feature of the release curves is not fully understood. Two possible explanations are discussed: (1) The dip may be due to the effects of Ar^{39} recoil. (2) The dip may result from the emplacement of a secondary mineral in the anorthosite at a later time.

(a) Ar^{39} recoil. Turner et al. (1971) have suggested that the recoil of Ar^{39} atoms during irradiation of the sample can deplete the Ar^{39} concentration in the outer edges of grains with respect to the interiors of these grains. This depletion predominates in the first gas releases from a sample which include gas mostly from the outer edges of the grains, yielding an artifically high Ar^{40}/Ar^{39} ratio.

Turner et al. (1971) suggest that the recoil range for Ar^{39} atoms is about 0.1 ; hence, one would expect Ar^{39} depletion of the total rock to be significant only in cases where grain sizes are quite small (i.e. about 1-2). As indicated in the discussion of the diffusion parameters for the slightly shocked anorthosite and the pseudotachylyte-shocked anorthosite breccia, both of these rocks probably contain a significant fraction (5-50%) of material with very small grain sizes. For the latter rock, the presence of very fine grains in the matrix material is petrographically discernible. Ar^{39} recoil may, therefore, cause large, apparent increases in the ages of initial gas fractions from the above two rocks.

If the dip in the ages of these rocks is attributed to high initial release ages (rather than to low second-release ages) and Ar^{39} recoil is the cause of the high initial ages, then the general similarity in K/Ca ratios (within a factor of 2) for all gas releases from the rock is understandable.

(b) Secondary "low-age" mineral. A second possible interpretation of the dip in the Ar^{40}-Ar^{39} release curve is that it is due to argon derived from a secondary mineral dominating the gas released in the "low-age" fractions.

It can be supposed that, at some time after the original outgassing of the rock, a secondary mineral was added to the system.

plagioclase grains.

Shocked rocks are known to exhibit large variations in the shock pressure experienced by grains within the same rock (see CHAPTER 1). It is not unreasonable, therefore, to expect that different grains would experience different extents of thermal outgassing, such that the final shocked system would effectively contain two subsystems with each displaying different characteristics. Such variations in the extent of gas loss among grains of the same rock are not possible in the case of equilibrium thermal processes since all grains in the rock will have the same temperature. Geologically important thermal, metamorphic processes are usually equilibrium processes in which no temperature differences exist between grains within the same rock.

A purely thermal gas-loss process can be duplicated by a laboratory outgassing; the Ar^{39} released during laboratory heating of the system should mirror the Ar^{40} release from the original system in the outgassing event. The laboratory thermal outgassing of a shocked system is fundamentally different than the original shock outgassing. The shock process leaves some retentive sites undepleted while the laboratory thermal process outgasses all sites in the rock. It is for these reasons that high-temperature decreases in ages do not appear in the model metamorphic systems discussed by Turner (1968).

This addition could have taken place during a metasomatic event. If the secondary mineral acted as a closed system after its emplacement, then the mineral would, when irradiated, have an Ar^{40}/Ar^{39} ratio corresponding to its time of formation. Under certain conditions, this mineral would comprise the bulk of the argon released from the rock at temperatures from 700-900 ^{o}C. The release curve of the rock would then exhibit its lowest ages in this temperature range.

The circumstances under which the lowest Ar^{40}/Ar^{39} ages for a system are observed after the first release are illustrated by Fig. 9. The present total rock system is considered to consist of two subsystems: (1) the secondary mineral; (2) the original rock. The solid curves in Fig. 9 refer to the parameters of the secondary mineral while the dashed lines refer to those of the original rock system. The fractional releases shown for each subsystem are calculated assuming a one-hour heating at $600^{o}C$, $700^{o}C$, $800^{o}C$, etc. Uniform spherical grains of each phase are assumed to be present, and the diffusion parameters of each phase vary with temperature as shown. Since the secondary mineral has a higher activation energy than the original rock, it releases argon over a narrower temperature range (700-950 ^{o}C) (refer to the inset graph of fractional releases). It is clear from the fractional release pattern of the two subsystems shown that the fractional releases from the secondary,

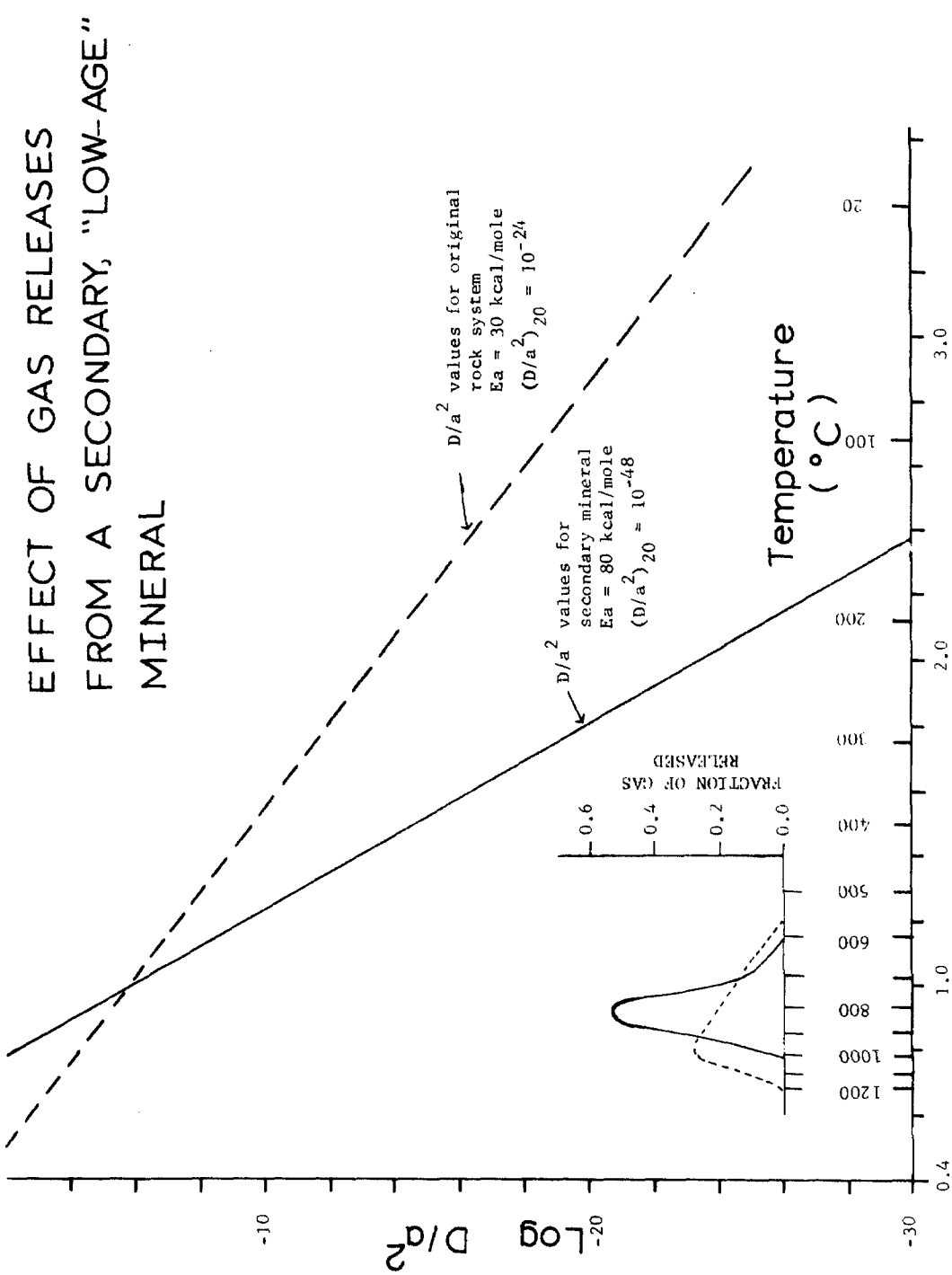
EFFECT OF GAS RELEASES
FROM A SECONDARY, "LOW-AGE"
MINERAL
D/a² values for original rock system
Ea = 30 kcal/mole
(D/a²)₂₀ = 10⁻²⁴
D/a² values for secondary mineral
Ea = 80 kcal/mole
(D/a²)₂₀ = 10⁻⁴⁸
Log D/a²
-10
-20
-30
FRACTION OF GAS RELEASED
0.6
0.4
0.2
0.0
Temperature (°C)
20
100
200
300
400
500
600
800
1000
1200
0.4
1.0
2.0
3.0
10³/T(°K)

FIG. 9

"low-age" mineral peak at about 800°C. The lowest Ar^{40}/Ar^{39} age of the total rock system, therefore, would be observed at about this temperature. If the secondary mineral had a higher activation energy and/or a lower $(D/a^2)_{20}$ than shown, the dip in the release curve would occur at a lower temperature. The important point presented is that two species coexist in the rock system; one has a lower "age" (Ar^{40}/Ar^{39} ratio), a higher activation energy and smaller $(D/a^2)_{20}$ than the other. In this case, the phase which has the younger "age" will dominate gas releases at temperatures greater than that of the first release. The lowest ages of the Ar^{40}/Ar^{39} release curve will then be observed after the initial release.

The magnitude in the dip in ages will depend on the relative amount of the secondary mineral in the rock system and the difference in the Ar^{40}/Ar^{39} ratio of the original rock and the secondary mineral. The releases shown in Fig. 9 are portrayed for equal abundance of the primary rock system and the secondary mineral. The latter difference is a function of the potassium concentrations in the two subsystems of the total system and the age of emplacement of the secondary phase.

Although the above explanation regarding the dip in the release curves is theoretically feasible, it may not apply to the shocked anorthosites studied. Both anorthosites showed only very minor amounts of a secondary phase, and it seems

improbable that the amounts present could account for the dips observed in the release curves. Furthermore, the K/Ca ratios of the gas released in the lowest-age fractions was not grossly different from the K/Ca ratios indicated by other gas fractions of the rock. A greater difference in K/Ca ratios of the lowest-age releases would be expected if these releases were due to a secondary mineral.

APPENDIX

Analytical Techniques

Sample Procurement and Preparation:

The initial phases of the study involved obtaining samples for petrological study. These samples were hand specimens weighing ~ 1 lb. each, which were collected during reconnaissance mapping of the structure.

After suitably defining the problem through preliminary studies, large samples were then collected in amounts which would permit removal of weathered rock from the material used. For many samples, this involved dynamiting the outcrop.

Subsequent sample preparation depended on the experiment being conducted. For the monzonite, 100 lbs. were crushed in a chipmunk rock crusher and then split into four parts. One part was sieved into size ranges of: +35, 35-60, 60-80, 80-115, 115-150, and -150 mesh. The mesh fraction (115-150), which was mostly free of binary mineral grains, was used to obtain the enriched mineral separates used in the monzonite age determinations.

A sanidine separate was first obtained. After removal of iron fragments and magnetite from the total sieve fraction, by using a hand magnet, the sieve fraction was then separated into convenient density ranges. These ranges were chosen to effectively isolate certain minerals. The $\rho > 2.91$ fraction, for example, contained pyroxenes almost exclusively. These separations were effected

using acetone-tetrabromoethane mixtures. To obtain the sanidine, the lightest material ($\rho < 2.55$) of the 115-150 mesh fraction was floated again in the heavy liquids and then passed through the Frantz isodynamic separator. In the Frantz, highly magnetic, altered pigeonite (probably iddingsite or bowlingite) was separated from the sanidine. The result was a sanidine-enriched separate with impurities of augite, altered pigeonite, and some binary grains of plagioclase.

A pyroxene separate was prepared by using the heavy material, $\rho > 2.91$, from the 115-150 mesh material. This density separate was found to contain a few pyroxene-sanidine binary grains. Since the K and, presumably, Ar^{40} contents of the sanidine is about 50 times that of the pyroxene, 2 or 3 binary grains per 100 will cause the separate to have one-half of its age determined by the impurities. Therefore, a very clean pyroxene separate was required. The pyroxene was rolled with a stainless steel bar and plate in order to break it down to a 150-200 mesh size. This size range, which had most of the binary grains broken up, was then passed through the Frantz, using a very low magnet current, permitting removal of some less magnetic sanidine-pyroxene binaries from the main pyroxene mass. The final separate contained about one pyroxene-sanidine binary per 100 grains, each binary being about 30% sanidine. This separate, which contained effectively one sanidine per 300 grains, had between 10-30 % of its age determined by the impurities.

A mineral separate enriched in plagioclase from the cores of the feldspars was prepared. The original material, with densities between 2.55 and 2.71, from the 115-150 mesh fraction was retreated with the heavy liquids. The floats from a $\rho = 2.71$ liquid were taken, and material with $\rho > 2.63$ was separated from this with a 2.63 gm/cm^3 density liquid. This material was then run through the Frantz using a high magnetic current to remove any magnetic pyroxene-binary impurities. The end result was a separate which contained about one sanidine (5% K) grain in 100, and which therefore had only 10% of its age caused by impurities (the plagioclase cores have 0.7% K).

Most of the analyses performed in this study were done on total rock anorthosite samples. These samples were prepared by cutting small blocks about 1" x 2" x 1" from the original hand specimens. These blocks allowed for the trimming off of weathered surfaces. A clean, fresh-looking blank was then chosen and repeatedly crushed with a circular, stainless steel piston and anvil with a ring collar. (The piston press is driven by a 12-ton hydraulic jack.) After each crushing, the powder, which would pass through a 35-mesh screen, was removed and the remaining fraction returned to the crusher. After the sample had been totally ground to -35 mesh, the material (generally 80-100 gms) was sieved into the following fractions: -35, 35-60, 60-80, 80-115, and -115 mesh. For the whole rock analyses, the 60-80 mesh fraction

was washed in acetone (to remove dust-size particles from the larger grains) and then split into representative, sample-sized fractions, generally about 0.2 - 0.8 gms.

When the irradiations were performed, small fragments of the blocks prepared above were crushed once in the piston crusher. This produced powder and chips of rock. Shards, 1-3 mm in a dimension, which were to be used in the irradiation, were then selected and the dust blown off with compressed air.

After the samples had been prepared, the analyses consisted of: (1) argon analyses; (2) potassium analyses.

Gas Analyses:

For the absolute determination of argon, an Ar^{38} tracer of known amount was mixed with the sample, and the isotopic ratios of the mixture measured. For the Ar^{40}/Ar^{39} studies, no spike was used, and amounts of gas were estimated by comparing the signal intensity produced by the sample with the intensity of a standard amount of Ar^{40} in a calibrated pipette attached to the mass spectrometer.

Gas Analysis System:

The gas analysis train consists of three parts: (1) the extraction bottle and gas cleanup system; (2)the Ar^{38} "spike" introduction system; (3) the mass spectrometer and the Ar^{40} calibration pipette. These are discussed in sequence.

The extraction part of the system consists of a bottle with a smaller, inserted quartz glass cup. A tungsten

crucible is mounted in the quartz cup, and the crucible is heated by a 20-kilowatt RF induction heater. A flat glass surface which permits viewing of the crucible through a constriction in the bottle (this is open or closed by a steel ball bearing) is built onto the top of the bottle (Fig. 1).

The extraction purification train consists of a CuO getter, a Ti getter, a cold trap, and several fingers filled with charcoal for gas collection. The purification line is connected directly to a sample collection system which has sample tubes containing activated charcoal attached. Granville-Phillips, Type C, ultra-high vacuum valves are used between the extraction and purification line, between the purification line and the sample collection line, and between the pumping system and the purification line. These high-vacuum valves are referred to as #3, #2, and #1, respectively (see Fig. 1).

During the extraction, the rock sample, which is wrapped in aluminum foil, is pushed into the tungsten crucible and heated. The gases evolved pass into the purification train. Two activated charcoal fingers, held externally at 77°K(LN_2 temperature) ,collect the argon and gases with molecular weight < 25. Two getters are attached to the train which simultaneously remove reactive components of the sample gas. The getters consist of welded stainless steel cans containing the active gettering agents. These cans are attached to the pyrex glass line by means of a welded-on kovar-pyrex graded tube join and are externally heated to the desired

temperature with electric coil heaters. One getter contains CuO maintained at about 400°C, which oxidizes H_2 and produces H_2O which, in turn, is frozen out in the cold trap (maintained at -78°C with dry ice) also connected to the purification train. Another getter contains purified titanium sponge held at 850-900 °C. This getter reacts with any O_2 or N_2 in the system, and when cooled to about 450°C it becomes an efficient hydrogen getter. During the extraction and cleaning steps, the sample collection line is isolated in order to prevent contamination of the charcoal in the sample tubes by the high partial pressures, 0.1 - 0.3 mm, of reactive gases such as H_2O, Co, H_2 attained during the initial extraction procedure. During the purification, the gas adsorbed on the charcoal fingers is released by warming the charcoal to about 70-80 °C. The released gases are thus exposed to the getters, and the purification process is completed.

After the purification, the non-reactive gases (composed mainly of argon) and some unremoved CO are introduced into the sample collection line and collected, in a sample tube, on charcoal which is held at LN_2 temperature. During most of the extractions, the sample tube in which the argon was frozen was sealed and removed from the line; then later attached to the mass spectrometer for analysis. A few of the samples were transferred to the mass spectrometer through a long glass tube which was installed for the Ar^{40}-Ar^{39} stepwise extractions.

Previous to all extractions, all components of the system (including the charcoal, Ti, CuO, and the tungsten crucible) were vacuum heated to drive off occluded gases. During the actual extractions, residual pressures in the extraction line ranged from $1 - 5 \times 10^{-7}$ mm. During this "cleanup" process, the glass tubing was wrapped with heating tapes, while the getters were maintained 50-100 ^{o}C hotter than normal. The sample tubes, which are enclosed in an insulating chamber,were baked at 300^{o}C and maintained at this temperature until they were clean. The tungsten crucible was heated with the RF furnace to 1900^{o}C and maintained at this temperature until an hour's heating at 1750^{o}C liberated only $5 - 10 \times 10^{-8}$ ccSTP of air composition argon. When residual pressures in the system were $1 - 5 \times 10^{-7}$ mm, the system was considered to be clean and ready to begin the extraction procedure.

The Ar^{38} Pipette:

For the argon measurements made during the course of the Ar^{40}-K^{40} analyses,an Ar^{38} tracer of known amount mixed with the sample argon released during the extraction. Ar^{40} was then calculated by mass spectrometrically measuring the isotopic ratio Ar^{40}/Ar^{38}. The Ar^{38} spike delivery system designed for this work is shown in Fig. 2.

TABLE 1.

Typical Steps Followed During Extraction and Spiking of a Sample

Time (min.)	Manipulation	Purpose
-35	Open #2, #3, if closed; open safety valve Y; CO_2 on dry ice traps.	Pump out spike volume; prepare for extraction.
-25	Raise spike measuring cutoff to appropriate calibration point. Open X; lower pipette below tip of pipette volume tube.	Start equilibration of Ar^{38} reservoir with pipette volume, Vp, desired.
- 5	Measure and record meniscus to calibration point distance; raise pipette cutoff; close X.	Isolate Ar^{38} spike in pipette volume tube.
0	Close #1, #2; lower spike measuring cutoff; LN_2(78°K) on charcoal-collecting fingers.	Start collection of Ar^{38} spike in extraction system.
10	Push a sample boat into the extraction vessel crucible.	Put sample in crucible.
20	Raise spike measuring cutoff; start increasing RF heater current.	Isolate spike; start extracting.
20-80	Slow incremential increases in RF heater current; frequent pyrometer readings of crucible temperature.	
80	Set RF current $\tilde{=}$ 175A.	Start heating period at 1600°C.
105	Begin reduction of RF heater current; H_2O (70°C) on charcoal collection fingers.	End sample heating; release gas from charcoal for purification.
115	Turn Ti electric furnace heater off.	Start cooling Ti through region (~ 450°C) where it getters H_2.

(TABLE 1. -- continued)

Time (min.)	Manipulation	Purpose
125	LN_2(78°K) on one charcoal collection finger.	Collect gases in system.
135	Cool warm charcoal finger with LN_2.	Argon collection.
155	Open #1. (only certain samples)	Allow pumpout of extraneous H_2 in the system.
155	H_2O (70°C) on previously cold charcoal finger; open #2; LN_2(78°K) on charcoal in sample tube.	Start collecting sample.
200	Burn off sample tube.	Obtain sample.
205	Open #1, check pressure surge.	Ascertain amount of H_2, He, other residual gases from extraction.
210	Heat Ti to 900°C; warm cold traps and charcoal fingers to room temperature.	Allow getters, traps to outgas.

In operation, the level of the Hg measuring cutoff column is lowered until the U-tube becomes conducting, the nupro isolation valve Y is opened, and the sustem is pumped out for a few minutes. Valve Y is then closed, and the level in the measuring cutoff is raised and then adjusted until it is within 1 mm of one of the calibrated volume marks (A-H) (see Fig. 2). The mark used depends upon the volume of Ar^{38} desired. The level of the mercury pipette cutoff is then lowered below the tip of the pipette volume tube and the nupro isolation valve opened; Ar^{38} is allowed to equilibrate in the volume Vp. When equilibration is complete, the distance between the mercury meniscus in the measuring cutoff and the calibration point being used is measured (using a milimeter scale and hard lens) and recorded. The pipette cutoff level is then raised past the cutoff tip, isolating a volume Vp of Ar^{38}. Isolation valve X is closed, Y is opened, and the measuring cutoff lowered to the bottom of the U-tube. The Ar^{38} spike then passes through the cold trap held at -78 C (to prevent Hg contamination of the extraction system) and to the extraction system where it is collected on charcoal at 78^{o} K. After collection is complete, the measuring cutoff is raised, isolation valve Y is closed, and the sample heating begun. A record is kept of the amount withdrawn each time in order to calculate depletion factors for the reservoir.

The air pressure above the mercury in each cutoff reservoir is easily and conveniently controlled by using a set of valves with an "H" configuration (Fig. 2). The slightly greater than atmospheric pressure required to set the measuring cutoff to calibration points A and B is supplied by a hand squeeze bulb attached to the air inlet leg of the H. The normal level of the pipette cutoff is about 76 cm (Ar^{38} pressure in the reservoir is ~ 0.001 mm), and this level is above the pipette volume tube tip, preventing accidental pumping out of the Ar^{38} reservoir.

Original calibration of the pipette proceeded in four steps: (1) A similar pipette system to the one shown was constructed and the volumes, Vp, for different calibration points of both were measured. These measurements were made using Hg to fill the volumes at a monitored temperature and then weighing the mercury. The reproducibility of the volumes calculated in this way was, in all cases, better than 0.25%. (2) The reservoir of the pipette shown was filled with Ar^{38}, while the remaining system was attached to a glass calibration line in which the pressure of Ar^{40} (introduced from a bottle of refined air argon) could be monitored by several Macleod gauges. (3) With the pressure in the line at about 0.3 mm, a volume of Ar^{40} was isolated in the Ar^{40} pipette. This Ar^{40} volume (about 7×10^{-5} ccSTP) was then mixed with a volume of Ar^{38} from the Ar^{38} pipette prepared as indicated above. The isotope mixture was allowed to equilibrate and was then frozen off, in a sample tube, on charcoal at LN_c temperature. (4) The mixture was

spectrometrically analyzed, and the delivered volume of Ar^{38} per unit volume of Vp was determined. The reproducibility of the results so obtained for this value was $\pm$ 0.5%.

This pipette can deliver amounts of Ar^{38} which are variable. The most frequently delivered amount is ~ 7.52×10^{-6} ccSTP (mark "C") and the smallest amount is 3.19×10^{-6} ccSTP. Delivery of amounts up to about 5×10^{-5} ccSTP is possible, and theoretically, using the technique of measuring the distance of the mercury meniscus from a calibration point and calculating the volume Vp, any designated volume of Ar^{38} could be delivered. In practice, the linearity of the capillary tube was not well known, and amounts delivered were kept close to the volumes defined by the calibration points. In this manner, errors due to non-linearity of the tube bore were involved only in volume corrections and not in the first-order volume determinations.

The sanidine separate taken from the monzonite was repeatedly analyzed for argon throughout the work, once during each extraction series and six times initially, in order to check the overall consistency of the sample preparation- extraction-analysis procedure. The Ar^{40*}/gm for these analyses are shown in Table 1 (Chapter 1). These data have not yet been corrected for the small (1%) depletion of the Ar^{38} reservoir during the course of the work. The total spread of this data is about $\pm$ 1% , and, after correction for the Ar^{38} depletion, this becomes about $\pm$ 0.5%. It seems, therefore, well justified to say that Ar^{40*} elemental abundance measurements,

using 0.5 gm samples of rock with 0.5 to 5% K, can be made with a reproducibility of ± 0.5% and an accuracy of probably better than ± 2%.

Mass Spectrometer:

The mass spectrometer used in these measurements is a single-focusing, Nier source machine with a 6" radius of curvature and a 52^{o} sector magnet.

This instrument was built by C. R. McKinney and G. J. Wasserburg. It has both a simple collector and an electron multiplier and, at present, is used only in the static mode. A pipette system (designed by P. Eberhardt), which delivers a reasonably reproducible amount of normal argon (~ 5.5×10^{-6} ccSTP), is attached to the mass spectrometer manifold. This pipette is used for both machine discrimination checks and first-order sensitivity calibrations. Although the behavior of some pipettes of this type is erratic, the system on the mass spectrometer functions fairly reproducibly. Extensive calibration of this pipette has not been performed, but its delivery is predictable to better than 5%. The sensitivity of the machine is ~ 6 mv/10^{-8} ccSTP/ma emission using a $10^{11}\Omega$ feedback resistor. This machine, with a 100-v electron accelerating potential and a 4-kv ion accelerating potention, has a resolution of about 1/130.

Typical Ar^{40} Analysis:

For a more-or-less typical Ar^{40} analysis, a split of the sample to be analyzed was prepared. This generally consisted of a portion of the acetone-washed 60-80 mesh sieve fraction of the powdered whole rock. This sample was then poured into a folded aluminum foil container which was then folded shut after the sample was introduced. The aluminum foil "boat" was weighed previous to and after adding the sample, thus obtaining the sample weight. Between 3 and 10 samples and material for a repeat analysis of each one, along with a sanidine standard sample, were loaded into the sample arm of the extraction bottle (Fig. 1). The extraction bottle and crucible were cleaned previous to loading, and putting the samples in the bottle arm is the final preparatory step for the run. The arm is sealed and the system pumped down.

The system is then cleaned until the background argon generated during extraction conditions is reduced to a satisfactory level. The charcoal in the sample tubes is maintained at 300°C, and the getters are held at 500 and 950 °C (CuO and Ti, respectively) until extraneous entrapped gases in the system are driven off. The tungsten crucible is heated to between 1900 and 2000 °C until contaminant gases are driven off. The cleanup procedure is continued until a dry run extraction, which involves maintaining the tungsten crucible for 1 hour at 1700°C, produces no more than 5 - 15 x 10^{-8} ccSTP of air argon. The system is then considered ready for extraction, and the residual pressure is generally

about 1 - 5 x 10^{-7} mm.

The sequence of operations performed during a typical extraction is presented in Table 1. Some trouble was experienced with arcing while increasing the RF generator current to its maximum. This problem is distinguished from discharging which occurred with only three samples at very low temperatures. Arcing generally occurred with the crucible around 1200-1400 ^{o}C and was possibly due to sparks initiated in a high vapor pressure of aluminum. The arcing problem was generally circumvented by increasing the RF current very slowly through the region of 120-150 RF amperes (1200-1400 ^{o}C). If arcing started, the current was decreased until it stopped and then slowly brought up again.

For the breccia samples analyzed, as well as for some of the other shocked anorthosites, copious quantities of gas were released at very low temperatures, i.e. 5-600 ^{o}C. These gases were gettered only very slowly, and the argon samples obtained from them were found to contain a much larger than normal mass 28 signal, probably due to contaminant CO. These samples probably contained large amounts of CO and H_2, along with other reactive gases; H_2 and CO being removed only poorly by the getters.

The procedures shown in Table 1 were followed for each sample extraction, and after the sample system had "cleaned up" a "re-extraction" was performed. Procedures followed for these are identical with those shown in Table 1, except that the maximum RF generator current was higher, corresponding to a temperature of

about 1800°C. There was, of course, no sample dropped during "re-extractions". Re-extractions generally yielded about 15-30 x 10^{-8} ccSTP of air argon, and, in no case, did the Ar^{40}/Ar^{36} ratio of a re-extraction exceed 330°C. All extractions appeared to be at least 99% complete. The re-extractions generally produced only about 50% more argon than a blank.

After the spiked samples were obtained, the sample tubes, with a slug for breaking the breakoff seal, were glass blown onto the mass spectrometer manifold for analysis, in groups of about five. A few samples were analyzed in the on-line fashion used for the Ar^{40}-Ar^{39} analyses.After the mass spectrometer manifold had pumped down, the sample was broken and exposed to the 400°C Ti getter on the line in order to remove excess H_2 in the sample. The total sample was then admitted into the mass spectrometer tube and five or ten sets of isotopic ratios obtained by manually scanning the magnetic field. These charts were then drawn, peak heights measured, and ratios calculated. The ratios obtained were corrected for reed and scale factors, plotted vs. time and a value of the reference/isotope ratio at the beginning of the analysis obtained. The scatter in the values of the initial ratio obtained for a typical sample was about 0.5%.

As mentioned, the discrimination and sensitivity of the mass spectrometer was continuously monitored by running frequent calibration volumes of normal argon. The sensitivity was found to

vary in a regular manner, and the discrimination remained constant at about 0.5% per mass unit. ($(Ar^{40}/Ar^{36})_{measured} = 301.5$ vs. 295.5 actual.)

Ar^{40}/Ar^{39} Analyses:

The Ar^{40}/Ar^{39} method involves an irradiation of the samples used. The procedures used for the irradiation are discussed in CHAPTER 2.

Ar^{40}-Ar^{39} Gas Analyses:

The gas analysis system used for the Ar^{40}-Ar^{39} experiments is nearly identical to the system employed for the Ar^{40}-K^{40} work (Fig. 1). The one difference is that the sample collection part of the system used during the total argon extractions was connected

to the mass spectrometer manifold by means of a 10-meter pyrex glass tube and high vacuum valve. The tube and valve permitted the mass spectrometer and extraction line to be used either independently or in an interconnected, on-line fashion. The long glass tube has the disadvantage of having a low conductivity, and a long period (45 min.) is required for nearly complete sample transmission to the mass spectrometer.

The schedule for extractions is shown in Table 2. One extraction step involves a one-hour heating of the sample at some temperature, a gas cleanup period of about 60 min., a sample transfer time (which, because of the long length of the tube, takes about 90 min.), and time to measure the isotope ratios on the mass spectrometer. When several temperature extractions are being performed successively, as was the case for most heatings of the samples, one can begin the extraction of the next step after isolating the sample gas from the original step in the mass spectrometer manifold. Measurement and extraction procedures for the two steps are then simultaneously executed.

This nesting of the extraction steps can save a great deal of time; however, during the first two or three heatings of the shocked anorthosites, large amounts of H_2O, CO, and H_2 were released. It was, therefore, found convenient to delay the start of the next extraction step until completion of the mass spectrometer measurements of the previous sample. This allowed the getters time to outgas partly and decreased contamination of the next step.

TABLE 2.

Sequence of Operations for
$Argon^{40}$-$Argon^{39}$ Stepwise Extraction

Time (min.)	Manipulation	Purpose
-20	Warm up RF generator; CO_2 + ethanol on CO_2 traps; LN_2 on charcoal fingers.	Prepare for extraction; maintain traps at proper temperature, LN_2 = 78°K, CO_2 + ethanol = -78°C.
0	Close #1, #2; push sample into crucible if first step; set RF plate current.	Start heating step; gas being adsorbed on charcoal at 78°K.
0-60	Various observations of RF plate current and pyrometer readings of crucible temperature.	
60	Start RF generator down to Oma; H_2O(70°C) on charcoal.	Stop heating; release adsorbed gas from charcoal.
70	Turn Ti getter coil furnace off.	Cool Ti from 900°C to 450°C range in which it getters H_2 most effectively.
90	Cool one charcoal finger to 78°K with LN_2.	Collect argon on charcoal.
100	Warm charcoal with 70°C H_2O; CO_2 tethanol (-78°C) on the other charcoal finger.	Release argon; extract heavy hydrocarbon impurities.
110	Cool warm charcoal to 78°K with LN_2.	Collect argon sample.
120	Open #1.	Pump out ungettered H_2.

(TABLE 2. -- continued)

Time (min.)	Manipulation	Purpose
125	Close #1, open #2, close mass spectrometer isolation valve; LN_2(78°K) on two sample tubes on collection manifold; warm charcoal finger with 70°C H_2O.	Transfer argon sample to collection manifold and connection line section of extraction line.
170	Isolate mass spectrometer manifold; open mass spectrometer isolation valve; close #2; H_2O(70°C) on extraction line sample tubes; LN_2(78°K) on mass spectrometer charcoal collection finger.	Transfer argon sample to mass spectrometer manifold.
180	Heat Ti getter to 900°C; open extraction line #1; warm extraction line traps and charcoal fingers.	Start preparation of extraction line for next heating step.

Note: Next extraction step can be initiated any time after #2 is closed and extraction line is isolated from mass spectrometer manifold.

215	Close mass spectrometer isolation valve.	Begin mass spectrometric measurement.
220	Lower Ti getter furnace.	Cool spectrometer Ti getter.
230	Open spectrometer manifold pumpout valve.	Pump extraneous H_2 out of mass spectrometer manifold.
233	Close spectrometer manifold pumpout valve; remove LN_2 from manifold charcoal finger.	Isolate mass spectrometer manifold; release sample argon from cold charcoal.
235	CO_2^+ tethanol on manifold charcoal finger.	Prevent release of heavy hydrocarbons from manifold charcoal finger.

(TABLE 2. -- continued)

Time (min.)	Manipulation	Purpose
236	Close mass spectrometer tube pumpout valve; open tube sample inlet valve; begin scanning magnet current.	Admit argon sample to mass spectrometer tube; begin ratio measurements.
236	Measure.	Obtain sufficient number of isotopic ratios.
End	Open tube pumpout valve; close tube inlet valve; open manifold pumpout valve; warm Ti getter.	Pumpout mass spectrometer.

The temperature during the extraction was set by controlling the plate current of the RF generator. This was a workable, although not entirely satisfactory, method. At settings below 125 ma, the crucible did not heat significantly; thus, temperatures between 500-600 ^{o}C were unattainable. Another problem which was manifest during all of the extractions was the instability of the RF generator; spontaneous jumps or drops of 100 ma in the plate current often occurred at settings of 500-600 ma leading to crucible temperature fluctuations of 50-100 ^{o}C. The instability problem was somewhat rectified by constant observation and adjustment of the RF current. On the whole, the setup functioned reasonably well, although three to four 20-hour days were required to completely analyze each sample. Temperatures attained were measured using an optical pyrometer. Uncertainties are present in such readings due to a thin film of evaporated aluminum and silicates which collected on the observation window over a period of time. Uncertainties also exist in regard to the emissivity of tungsten.

Potassium Analyses:

The potassium analyses performed for this study were made on ~ 1 gm. splits of the samples prepared for the argon analyses. Aliquots of the dissolved whole rock were mixed with a K^{40} + K^{41} isotopic tracer and mass spectrometrically analyzed. Refined techniques for potassium analysis used in this laboratory have been discussed by Tera et al. (1970).

A split of the material used for each argon analysis, generally 0.3 - 1.3 gm., was dissolved in a carefully washed 150-ml. teflon beaker using 5 ml. of 48% HF, 5 ml. of distilled $HClO_4$, and about 10 ml. of distilled H_2O. The sample was allowed to digest for 24 hours, and the HF was then gently fumed off. $HClO_4$ was then fumed from the mixture until a semi-dry cake was obtained. This curd was then resolved using HCl and distilled H_2O. Slight residues of undissolved materials, which were sometimes obtained from samples, consisted largely of magnetite.

The resolved solution was placed in a pre-weighed nalgene bottle (125-180 ml.), a convenient amount of H_2O added, and the solution and bottled weighed. By using the same technique of weighing the solution in a pre-weighed, carefully washed nalgene bottle, a 5- to 10-ml. aliquot of the original sample was diluted by a factor of 10-50. Since the K content of the rock samples ranged from 0.5 - 5% K, with the sample weights used, the original solution contained about 50-500 γ K/gm. After dilution, the second solution had about 1-50 γ K/gm. A mixture was prepared of about one gm. of K^{40}-K^{41} tracer (0.2226 μ moles K^{41}/gm) and one to four ml. of the diluted sample solution from above. This mixture, which had a K^{39}/K^{41} ratio of 0.25 - 1.0, was then dried in a nitrogen-cleansed drying vessel (Sanz and Wasserburg, 1969), and a portion loaded on a previously outgassed Ta filament. The filament block and source plates were then loaded into a 12" radius of curvature solid source mass spectrometer.

The sample was then analyzed by obtaining five to six sets of isotope ratios at each of several filament temperatures at which the ion beam behaved stably and had sufficient intensity for analysis. Most of the ratios were obtained using the electron multiplier, but some samples analyzed on a different machine were measured using the Faraday Cup (when sufficient intensity was present). Ratios obtained for one temperature were averaged and the machine discrimination and normal potassium content of the sample obtained from the average. Potassium concentrations were calculated from the values of discrimination and normal potassium content obtained at each temperature. The final potassium content was averaged from these values. Variations in the ratios observed at each temperature were generally about ± 0.5%, while variations in the calculated K abundances at different temperatures (or intensities) were about ± 1.0%. Reproducibility of replicate determinations was generally within ± 2% and, for most samples, within ± 1% (see Tables 1 and 2, Chapter 1).

The spike used for this study had the composition: 0.867 K^{41}; 0.0783 K^{40}; 0.0500 K^{39}. This composition was determined by a spectrometric composition run. The concentration of the tracer was determined by dissolving a weighed amount of KCl in a one-liter bottle. The weight of the solution was determined by weighing the bottle both when empty and full, thus allowing an accurate determination of the normal potassium concentration. Aliquots of this solution were

then diluted to a convenient concentration, and a "spike" and normal mixture with K^{39}/K^{41} about three was prepared. This mixture, when analyzed, indicated a spike concentration of 0.2226 moles K^{41}/gm. This value is very similar to other determinations of the spike concentration made in the laboratory.

No proper measurement of the potassium blank due to the measurement procedure was made. (The filament broke while loading the blank.) Since no correlation seems to exist between high measured K values and small measured samples, and since consistent, clean procedures were employed, the blank is thought to be small. An upper limit for the blank can be estimated from the data. The actual amounts of K measured in a sample ranged from 0.5 to 25 μ gms. Two different samples of the plagioclase cores (0.7% K) were run, in which 0.8 μgm K and 2.0 μ gm K were analyzed. For these runs, the smaller sample yielded a lower rather than a higher measured potassium concentration. A higher value of the concentration obtained with smaller measured samples would be observed if contamination were significant. The error due to potassium background must be less than 3% of the smaller sample mentioned above, i.e. $\sim$ 0.025 μgm K. For all of the 1μ gm samples analyzed, smaller samples yielded lower values; this fact supports the reasoning above. A blank of 0.025μ gm implies errors in potassium concentration less than 3% for all of the samples and less than 1.5% for most of them.

Filament background proved to be something of a problem. The potassium signal for a freshly made tantalum filament sometimes exceeded one volt. Even after heating the filament ribbon white hot in vacuo for two hours, the background potassium signal still remained. It was found that placing a negatively charged screen grid above the filament while heating in the vacuum chamber proved very effective in reducing this background below objectionable levels. The background levels of outgassed filaments were checked before loading the samples several times during the course of the work. These checks showed that the grid method was satisfactory.

Potassium concentrations were calculated using the isotopic ratios of normal potassium determined by Nier (1950) . The ages were calculated using the total decay and branching ratios for potassium suggested by Aldrich and Wetherill (1958). A computer printout of the values of $(\lambda_{\epsilon} / \lambda_{tot})(e^{\lambda t} - 1)$ for different values of t was employed when converting the calculated A^{40}/K^{40} ratios to ages.

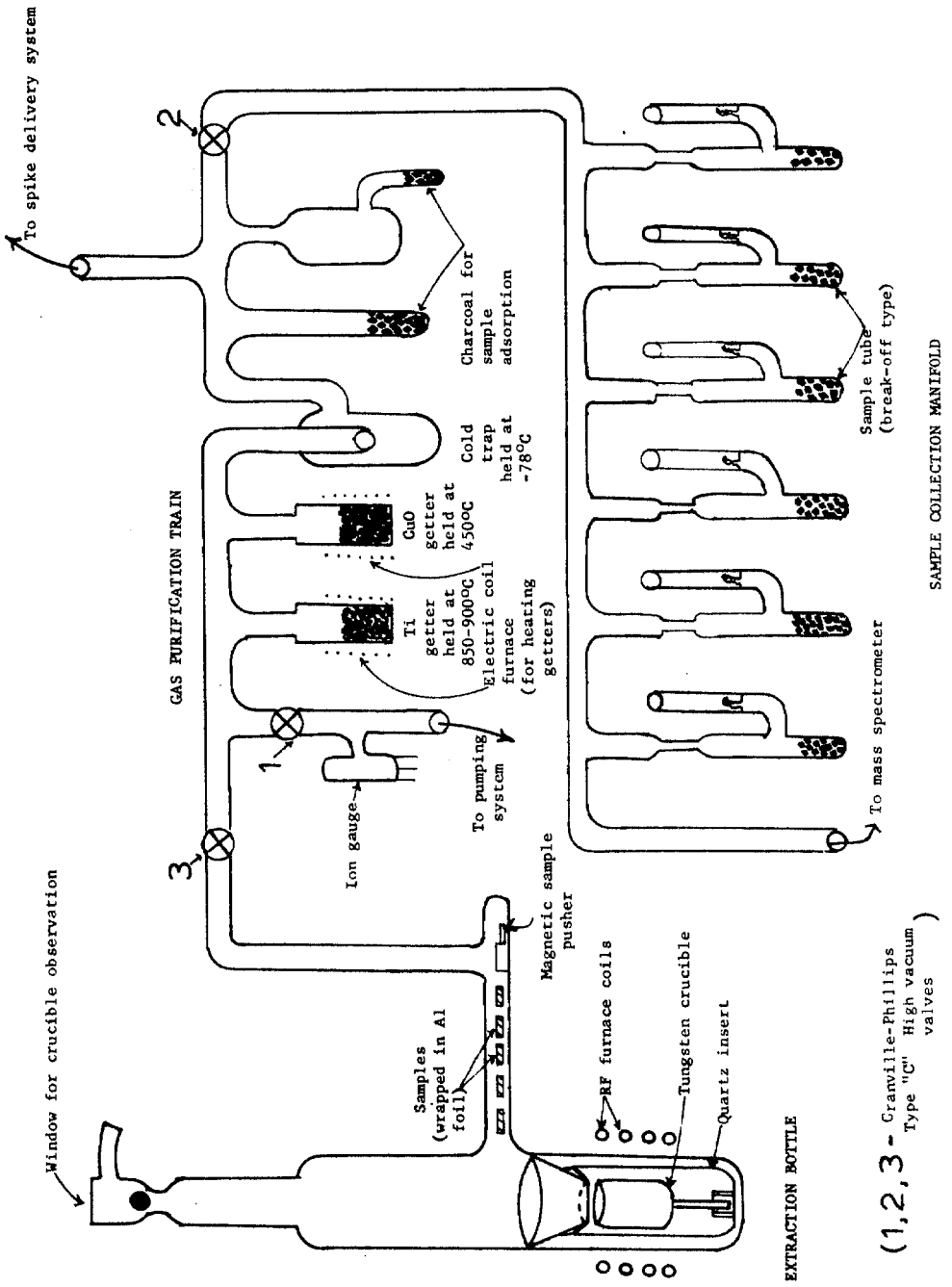

SAMPLE EXTRACTION SYSTEM

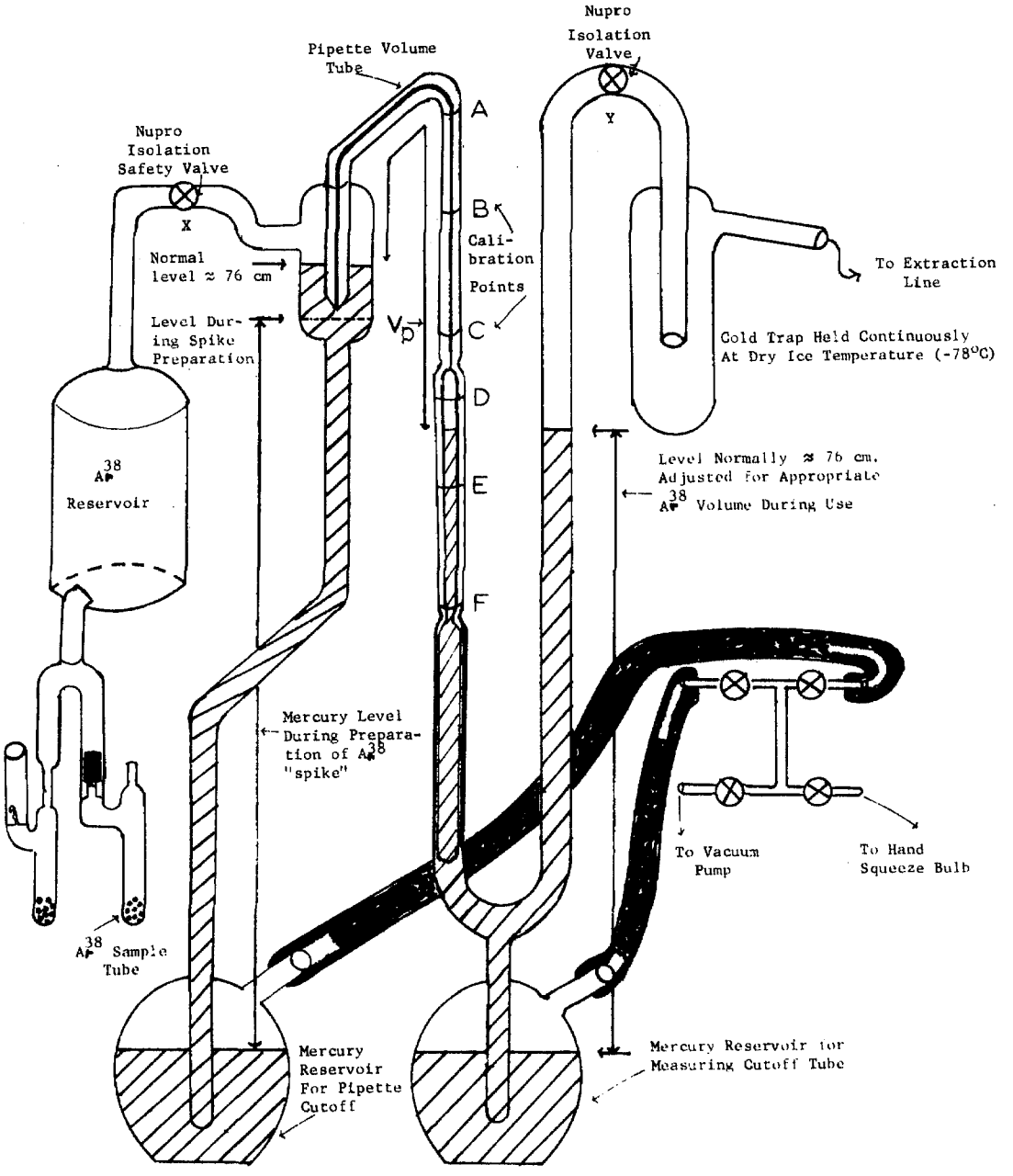

'SPIKE' DELIVERY SYSTEM

REFERENCES

Ahrens, T. J., Private communication, 1971.

Ahrens, T. J., C. F. Petersen, and J. T. Rosenberg, Shock compression of feldspars, J. Geophys. Res., 74, 2727-2746, 1969.

Ahrens, T. J., and T. J. Rosenberg, Shock metamorphism experiments on quartz and plagioclase, in Shock Metamorphism of Natural Materials, edited by Bevan M. French and N. M. Short, pp. 59-81, Mono Book Corp., Baltimore, Maryland, 1968.

Aldrich, L. T., and G. W. Wetherill, Geochronology by radio-active decay, Ann. Rev. Nucl. Sci., 8, 257-298, 1958.

Baldwin,R., The Measure of the Moon, 488 pp.,Univ. Chicago Press, Chicago, Illinois, 1963.

Baldwin, Ralph B., The Face of the Moon, 239 pp., Univ. Chicago Press, Chicago, Illinois, 1949.

Beals, C. S., The identification of ancient craters, Ann. N.Y. Acad. Sci., 123, 904-914, 1965.

Beals, C. S., M. J. S. Innes, and J. A. Rottenberg, Fossil meteorite craters, in The Moon, Meteorites, and Comets, The Solar System, Vol. IV, edited by B. M. Middlehurst and G. P. Kuiper,pp., 235-284, Univ. Chicago Press, Chicago, Illinois, 1963.

Bence, A. E.,and A. L. Albee, Empirical correction factors for the electron microprobe analysis of silicates and oxides, J. Geol., 76, 382-403, 1968.

Berard, J., Summary geological investigations of the area bordering Manicouagan and Mouchalagane Lakes, Quebec Dept. Natural Resources P.R. No. 489, 14 pp.,1962.

Branca, W., and E. Fraas, Das Kryptovolkanische Becken von Steinheim, Akad. Wiss. Berlin, Phys.-Math. Kl., Abh. I, 64 pp., 1905.

REFERENCES -- continued

Brereton, N. R., Corrections for interfering isotopes in the $^{40}Ar/^{39}Ar$ dating method, Earth Planet. Sci. Lett., 8, 427-433, 1970.

Bucher, W. H., Cryptoexplosion structures caused from without or from within the earth? ("Astroblemes" or geoblemes"?), Am. J. Sci., 261, 597-649, 1963.

Buddington, A.F., and D. H. Lindsley, Iron-titanium oxide minerals and synthetic equivalents, J. Petrol., 5, 310-357, 1964.

Bunch, T. E., Some characteristics of selected minerals from craters, in Shock Metamorphism of Natural Materials, edited by Bevan M. French and N. M. Short, p. 413-432, Mono Book Corp., Baltimore, Maryland, 1968.

Bunch, T. E., A. J. Cohen, and M. R. Dence, Natural terrestrial maskelynite, Am. Mineral., 52, 244-253, 1967.

Bunch, T. E., A. J. Cohen, and M. R. Dence, Shock-induced structural disorder in plagioclase and quartz, in Shock Metamorphism of Natural Materials, edited by Bevan M. French and N. M. Short, p. 509-518, 1968.

Butkovich, T. R., Calculation of the shock wave from an underground nuclear explosion in granite, J. Geophys. Res., 70, 885-892, 1965.

Carslaw, H. S., and J. C. Jaeger, Conduction of Heat in Solids, 510 pp., Oxford University Press, Oxford, England, 1959.

Carter, N. L., Basal quartz deformation lamellae -- a criterion for recognition of impactites, Am. J. Sci., 263, 786-806, 1965.

REFERENCES -- continued

Carter, N. L., Dynamic deformation of quartz, in Shock Metamorphism of Natural Materials, edited by Bevan M. French and N. M. Short, pp. 453-474, Mono Book Corp., Baltimore, Maryland, 1968.

Carter, N. L., C. B. Raleigh, and P. S. De Carli, Deformation of olivine in stony meteorites, J. Geophys. Res., 73, 5439-5461, 1968.

Chao, E. C. T., Pressure and temperature histories of impact metamorphosed rocks -- based on petrographic observations, in Shock Metamorphism of Natural Materials, edited by Bevan M. French and N. M. Short, pp. 135-158, Mono Book Corp., Baltimore, Maryland, 1968.

Chao, E. C. T., Shock effects in certain rock-forming minerals, Science, 156, 192-202, 1967.

Chao, E. C. T., Odette B. James, Jean A. Minkin, and Judith A. Boreman, Petrology of unshocked crystalline rocks and evidence of impact metamorphism in Apollo 11 returned lunar samples, in Proceedings of the Apollo 11 Lunar Science Conference, Vol. I, Mineralogy and Petrology, edited by A. A. Levinson, 990 pp., Pergamon Press, Oxford, England, 1970.

Chow, T. J., and C. R. McKinney, Mass spectrometric determination of lead in manganese nodules, Anal. Chem., 30, 1499-1503, 1956.

Clarke, Sydney P., Handbook of Physical Constants, Geol. Soc. Am. Memoir 97, Geol. Soc. Am., N.Y., 587 pp., 1966.

Cullity, B. D., Elements of X-ray Diffraction, 514 pp., Addison-Wesley, Reading, Mass., 1959.

REFERENCES -- continued

Cummings, D., Kinkbands: shock deformation of biotite resulting from a nuclear explosion, Science, 148, 950-952, 1965.

Currie, K. L., The origin of igneous rocks associated with shock metamorphism as suggested by geochemical investigations of Canadian craters, J. Geophys. Res., in press, 1971.

Currie, K. L., Analogues of lunar craters on the Canadian Shield, Ann. N.Y. Acad. Sci., 123, 915-940, 1965.

Currie, K. L., On the origin of some 'recent' craters on the Canadian Shield, Meteoritics, 2, 93-110, 1964.

Dachille, F., P. Gigl, and P. Y. Simons, Experimental and analytical studies of crystalline damage useful for the recognition of impact structures, in Shock Metamorphism of Natural Materials, edited by Bevan M. French and N. M. Short, pp.555-570, Mono Book Corp., Baltimore, 1968.

Dalrymple, G. B., and M. A. Lanphere, Potassium-Argon Dating, 258 pp., W. H. Freeman, San Francisco, California, 1969.

Deer, W. A., R. A. Howie, and J. Zussman, Rock-forming Minerals, 4, Framework Silicates, 435 pp., John Wiley & Sons, New York, N. Y., 1963.

Deer, W. A., R. A. Howie, and J. Zussman, Rock-forming Minerals, Vol. 1, Ortho and Ring Silicates, 333 pp., John Wiley & Sons, New York, N.Y., 1963.

REFERENCES -- continued

Dence, M.R., The extraterrestrial origin of Canadian craters, Ann. N.Y. Acad. Sci., 123, 941-969, 1965.

Dence, M. R., Shock zoning at Canadian craters; petrography and structural implications, in Shock Metamorphism of Natural Materials, edited by Bevan M. French and N. M. Short, pp. 169-184, Mono Book Corp., Baltimore, Maryland, 1968.

Dietz, R. S., Astroblemes: Ancient Meteorite-Impact Structures on the Earth, in The Moon, Meteorites, and Comets, Vol. IV, The Solar System, edited by B. M. Middlehurst and G. P. Kuiper, pp.285-300, Univ. of Chicago Press, Chicago, Ill., 1963.

Dietz, R. S., Cryptoexplosion structures: a discussion, Am. J. Sci., 261, 650-664, 1963b.

Dietz, R. S.,Shatter cones in cryptoexplosion structures (meteorite impact?), J. Geol., 67, 496-505, 1959.

Dietz, R. S., The meteorite impact origin of the moon's surface features, J. Geol., 54, 359-375, 1946.

Duke, M. B., The Shergotty meteorite: magmatic and shock metamorphic features, in Shock Metamorphism of Natural Materials, edited by Bevan M. French and N. M. Short,pp.613-621, Mono Book Corp., Baltimore, Maryland, 1968.

Dworak, U., Stosswellen metamorphose des Anorthosits vom Manicouagan Krater, Quebec, Canada, Contrib. Mineral. Petrol., 24, 306-347, 1969.

El Goresy, A., H. Fechtig, and J. Ottemann, The opaque minerals in impactite glasses, in Shock Metamorphism of Natural Materials, edited by Bevan M. French and N. M. Short, 531-553, Mono Book Corp., Baltimore, Maryland, 1968.

REFERENCES -- continued

Engelhardt, W. v., J. Arndt, D. Stöffler, W. F. Muller, H. Jeziorkowsky, and R. A. Gubser, Diaplektische Glaser in den Breccien des Ries von Nördlingen als Anzeichen fur Stosswellenmetamorphose, Contrib. Mineral. Petrol., 15, 93-102, 1967.

Engelhardt, W. v., and W. Bertsch, Shock-induced planar deformation structures in quartz from the Ries Crater, Germany, Contrib. Mineral. Petrol., 20, 203-234, 1969.

Engelhardt, W. v., F. Hörz, D. Stöffler, and W. Bertsch, Observations of quartz deformation in the breccias of West Clearwater Lake, Canada, and the Ries Basin, Germany, in Shock Metamorphism of Natural Materials, edited by Bevan M. French and N. M. Short, pp.475-482, Mono Book Corp., Baltimore, Maryland, 1968.

Engelhardt, W. v., and D. Stöffler, Stages of shock metamorphism in crystalline rocks of the Ries Basin, Germany, in Shock Metamorphism of Natural Materials, 159-168, edited by B. M. French and N. M. Short, Mono Book Corp., Baltimore, Maryland, 1968.

Eugster, H. P., Reduction and oxidation in metamorphism, in Researches in Geochemistry, edited by P. H. Abelson, 397-426, John Wiley, New York, 1959.

Evans, B. W., D. M. Shaw, and D. R. Haughton, Scapolite stoichiometry, Contrib. Mineral. Petrol., 24, 293-305, 1960.

Fahrig, W. F., F. H. Gaucher, and A. Larochelle, Paleomagnetism of diabase dykes of the Canadian Shield, Can. J. Earth Sci., 2, 278-298, 1965.

Fahrig, W. F., and R. K. Wanless, Age and significance of diabase dyke swarms of the Canadian Shield, Nature, 200, 934-937, 1963.

Fairbairn, H. W., G. Faure, W. H. Pinson, P. M. Hurley, and J. L. Powell, Initial ratio of strontium 87 to strontium 86, whole-rock age, and discordant biotite in the Monterregian Igneous Province, Quebec, J. Geophys. Res., 68, 6515-6522, 1963.

REFERENCES -- continued.

Fechtig, H., W. Gentner, and S. Kalbitzer, Argon bestimmungenun Kaliummineralen - IX. Messungen zu der verschiedenen Arten der Argon diffusion, Geochim. Cosmochim. Acta, 25, 297- 311, 1961.

Fechtig, H., W. Gentner, and J. Zähringer, Argonbestimmungen an Kaliummineralen - VII. Diffusionsverluste von Argon in Mineralien und ihre Auswirkung auf die Kalium-Argon-Altersbestimmung, Geochim. Cosmochim. Acta, 19, 70-79, 1960.

Fechtig, H., and S. Kalbitzer, The diffusion of argon in potassium-bearing solids, in Potassium-Argon Dating, edited by O. A. Schaeffer and J. Zähringer,pp. 68-107, Springer-Verlag, Berlin, Germany, 1966.

Fleischer, R. L., J. R. M. Viertl, and P. B. Price, Age of the Manicouagan and Clearwater Lake Craters, Geochim. Cosmochim. Acta, 33, 523- 527 , 1969.

Fredriksson, K., P. DeCarli, R. O. Pepin, J. H. Reynolds, and G. Turner, Shock-emplaced argon in a stony meteorite, J. Geophys. Res., 69, 1403- 1411, 1964.

French, B. M., Sudbury Structure, Ontario: some petrographic evidence for origin by meteorite impact, Science, 156, 1094-1098, 1967.

French, B. M., and N. M. Short, editors, Shock Metamorphism of Natural Materials, Mono Book Corp., Baltimore, Maryland, 644 pp. 1968.

Gentner, W., H. J. Lippolt, and O. A. Schaeffer, Argonbestimmungen an Kalium mineralien-XI. Die Kalium-Argon-Alter der Glaser des Nördlinger Rieses und der Bohmisch-mahrischen Tektite, Geochim. Cosmochim. Acta., 27, 191-200, 1963.

Geological Survey of Canada, Geological Map of Canada, Map 91A, 1913.

REFERENCES -- continued.

Gold, D. P., and M. Vallée, Field Guide to the Oka Area, Dept. Nat. Res., Mines Br., Geol. Expl. Serv., Quebec, Canada, 37 pp., 1969.

Hammond, W. P., Geology of the Mouchalagane Lake Area, Saguenay County, New Quebec, M.S. Thesis, University of Toronto, Canada, 304 pp., 1945

Hörz, F., Statistical measurements of deformation structures and refractive indices in experimentally shock-loaded quartz, in Shock Metamorphism of Natural Materials, edited by Bevan M. French and N. M. Short,pp. 243-255, Mono Book Corp., Baltimore, Maryland, 1968.

Hörz, Friedrich, Untersuchungen an Riesglasern,Beitrage zur Mineralogie und Petrographie, 11, 621-661, 1965.

Hörz, F.,and T. J. Ahrens, Deformation of experimentally shocked biotite, Am. J. Sci., 267, 1213-1229, 1969.

Kelly, A. O., and F. Dachille, Target: Earth, Target: Earth Publishers, Carlsbad, Calif., 264 pp., 1953.

Kish, Leslie, Geology of Upper Hart-Juane River Area, Saguenay County, Quebec Dept. of Nat. Res., Geol. Expl. Serv., Prelim. Rept. #538, 10 pp., 1965.

Kistler, R. W., and F. C. W. Dodge, Potassium-argon ages of coexisting minerals from pyroxene-bearing granitic rocks in the Sierra Nevada, California, J. Geophys. Res., 71, 2157, 1966.

REFERENCES -- continued.

Kranck, S. H., and G. W. Sinclair, Clearwater Lake, New Quebec, Geol. Surv. Can., Geol. Surv. Bull., 100, 25 pp., 1971.

Kretz, R., Distribution of magnesium and iron between orthopyroxene and calcic pyroxene in natural mineral assemblages, J. Geol., 71, 773-785, 1963.

Krinov, E. L., Giant Meteorites, trans. from Russian by J. S. Romankiewicz, 397 pp., Pergamon Press, Oxford, England, 1966.

Krinov, E. L., The Tunguska and Sikhote-Alin Meteorites, in The Moon, Meteorites, and Comets, The Solar System, Vol. IV, edited by Middlehurst and G. P. Kuiper, pp. 208-234, Univ. of Chicago Press, Chicago, Illinois, 1963.

Kulp, J. Laurence, and Heinrich Neumann, Some potassium-argon ages on rocks from the Norwegian basement, Annals of N.Y. Academy of Sciences, 91, 469-475, 1961.

Kumarapeli, P. S., and V. A. Saull, The St. Lawrence Valley system: A North American equivalent of the East African Rift Valley system, Can. J. Earth Sci., 3, 639-658, 1966.

Kuno, H., Differentiation of Basalt Magmas in Basalts, Vol. II, edited by H. Hess and A. Poldervaart, pp.623-688, Interscience, New York, 1968.

Larochelle, A., and K. L. Currie, Paleomagnetic study of igneous rocks from the Manicouagan structure, Quebec, J. Geophys. Res., 72, 4163-4169 , 1967.

Larochelle, A., Paleomagnetism of the Monteregian Hills, S. E. Quebec, Can. Dept. of Mines and Technical Surveys, Geol. Surv. Can., Geol. Surv. Bull. 79, 1961.

REFERENCES -- continued.

Larsen, E. S., Some new variation diagrams for groups of igneous rocks, J. Geol., 46, 505-520, 1938.

May, P. R., Pattern of Triassic-Jurassic diabase dikes around the North Atlantic in the context of predrift position of the continents, Bull. Geol. Soc. Am., 82, 1285-1292, 1971.

McGetchin, T. R., Geology of the Moses Rock Dike, Thesis (Ph.D), Calif. Inst. Technol., 308 pp., 1968.

Milton, D. J., and P. S. DeCarli, Maskelynite: formation by explosive shock, Science, 140, 67-68, 1963.

Mitchell, J. G., The argon-40/argon-39 method for potassium-argon age determination, Geochim. Cosmochim. Acta, 32, 781-790, 1968.

Muller, W. F., Electronenmikroskopischer Nachweis amorpher Bereiche in stosswellenbeanspruchtem Quarz., Naturwissenschaften, 56, 279-280, 1969.

Muller, W. F., and M. Defourneaux, Deformationsstrukturen in Quarz als Indikator fur Stosswellen: eine experimentelle Untersuchung an Quarzeinkristallen, Z. Geophys., 34, 483-504, 1968.

Murtaugh, J. C., Geology of Tétépisca Lake Area, Saguenay County, Quebec Dept. Nat. Res., Prelim. Rept. 536, 6 pp., 1965.

Murtaugh, J.C., and K. L. Currie, Preliminary study of the Manicouagan structure, 9 pp., Quebec Dept. Nat. Res., Prelim. Rept. 536, 1965.

REFERENCES -- continued.

Mussett, A. E., Diffusion measurements and the potassium-argon method of dating, Geophys. J., Roy. Astr. Soc., 18, 257-303, 1969.

Nier, A. O., A redetermination of the relative abundances of the isotopes of carbon, nitrogen, oxygen, argon, and potassium, Phys. Rev., 79, 789-793, 1950.

Norris, A. W., and B. V. Sanford, Paleozoic and Mesozoic geology of the Hudson Bay lowlands, in Earth Science Symposium on Hudson Bay, edited by Peter J. Hood, pp. 169-205, Geol. Surv. Can. Paper, 68-53, 1968.

Observatories Branch, Dept. of Energy, Mines and Resources, Ottawa, Canada, Bouguer Gravity Anomaly Map of Canada, 1970; Geology and Economic Minerals of Canada, Part II, Maps and Charts, edited by R. J. W. Douglas, 1970.

Papike, J. J., and N. C. Stephenson, The crystal structure of Mizzonite, a calcium- and carbonate- rich scapolite, Am. Mineral., 51, 1014-1027, 1966.

Papike, J.J., and T. Zoltai, The crystal structure of a marialite scapolite, Am. Mineral., 50, 641-655, 1965.

Peck, D. L., A. B. Griggs, H. G. Schlicker, F. G. Wells, and H. M. Dole, Geology of the central and northern parts of the Western Cascade Range in Oregon, U.S. Geol. Surv. Prof. Paper, 449, 56 pp., 1964.

Poole, W. H., Geology of southeastern Canada, in Geology and Economic Minerals of Canada, edited by R. J. W. Douglass, pp. 296-301, Dept. Energy, Mines and Res., Ottawa, Canada, 1970.

Poole, W. H., B. V. Sanford, H. Williams, and D. G. Kelly, Geotectonic Correlation Chart for Southeastern Canada, in Geology and Economic Minerals of Canada, Vol. II, Maps and Charts, edited by R. J. W. Douglass, Geol. Surv. Canada, Ottawa, 1970.

REFERENCES -- continued

Robertson, P. B., M. R. Dence, and M. A. Vos, Deformation in rock-forming minerals from Canadian craters, in Shock Metamorphism of Natural Materials, edited by Bevan M. French and N. M. Short, pp. 433-452, Mono Book Corp., Baltimore, Maryland, 1968.

Robertson, W. A., Manicouagan, P.Q., paleomagnetic results, Can. J. Earth Sci., 4, 641- 649 , 1967.

Robie, R. A., and D. R. Waldbaum, Thermodynamic properties of minerals and related substances at 298.15°K (25.0°C) and one atmosphere (1.013 bars) pressure and at higher temperatures, 256 pp., Geol. Surv. Bull.,1259, 1970.

Roddy, David J., The Flynn Creek Crater, Tennessee, in Shock Metamorphism of Natural Materials, edited by Bevan M. French and N. M. Short,pp. 291-322, Mono Book Corp., Baltimore, Maryland, 1968.

Rose, E. R., Manicouagan Lake - Mushalagan Lake Area, Quebec, 22 pp. Geol. Surv. Can. Paper 55-2, 1955.

Sanz, H.G., and G. J. Wasserburg, Determination of an internal Rb^{87}-Sr^{87} isochron for the Olivenza chondrite , Earth Planet. Sci. Lett., 6, 335-345, 1969.

Shoemaker, E. M., Impact mechanics at Meteor Crater, Arizona, in The Moon, Meteorites, and Comets, The Solar System, Vol. IV, edited by B. M. Middlehurst and G. P. Kuiper, pp.301-336, Univ. Chicago Press, Chicago, Illinois, 1963.

Shoemaker, E. M., C. H. Roach, and F. M. Byers, Diatremes and uranium deposits in the Hopi Buttes, Arizona, in Petrologic Studies: A Volume to Honor A. F. Buddington, edited by A. E. J. Engel, H. L. James and B. F. Leonard, Geol. Soc. Am., 660 pp., 1962.

REFERENCES -- continued

Short, N. M., Experimental microdeformation of rock materials by shock pressures from laboratory scale impacts and explosions, in Shock Metamorphism of Natural Materials, edited by Bevan M. French and N. M. Short, pp. 219-243, Mono Book Corp., Baltimore, Maryland, 1968.

Short, N. M., Nuclear-explosion-induced microdeformation of rocks: an aid to the recognition of meteorite impact structures, in Shock Metamorphism of Natural Materials, edited by Bevan M. French and N. M. Short, pp.185-210, Mono Book Corp., Baltimore, Maryland, 1968.

Short, N. M., and T. E. Bunch, A world-wide inventory of features characteristic of rocks associated with presumed meteorite impact structures, in Shock Metamorphism of Natural Materials, edited by B. M. French and N. M. Short, pp. 255-270 , Mono Book Corp., Baltimore, Maryland, 1968.

Stacey, Frank, Physics of the Earth, 324 pp., John Wiley and Sons, New York, N.Y., 1969.

Stockwell, C. H., Geology of the Canadian Shield, in Geology and Economic Minerals of Canada, edited by R. J. W. Douglas, pp. 44-54, Dept. of Energy, Mines, and Resources, Ottawa, Canada, 1970 .

Stockwell, C. H., A Tectonic Map of the Canadian Shield, in The Tectonics of the Canadian Shield, edited by J. S. Stevenson, Roy. Soc. Can., Spec. Publ. No. 4, Univ. Toronto Press, 179 pp., 1962.

Stöffler, D., Deformation und Umwandlung von Plagioklas durch Stosswellen in den Gesteinen des Nördlinger Ries, Contrib. Mineral. Petrol., 16, 51-83, 1967.

Stöffler, D., Zones of impact metamorphism in the crystalline rocks of the Nordlinger Ries Crater, Contr. Mineral. Petrol., 12, 15- , 1966.

REFERENCES -- continued.

Taylor, F. C., and M. R. Dence, A probable meteoritic origin for Mistastin Lake, Labrador, Can. J. Earth Sci., 6, 39-45, 1969.

Tera, F., O. Eugster, D. S. Burnett, and G. J. Wasserburg, Comparative study of Li, Na, K, Rb, Cs, Ca, Sr and Ba abundances in achondrites and in Apollo 11 lunar samples, Proc. Apollo 11 Lunar Science Conference, edited by A. A. Levinson, Vol. II, Chemical and Isotope Analyses, pp. 1637-1657, Pergamon Press, New York, N.Y., 1970.

Tschermak, G., Die Meteoriten von Shergotty and Gopalpur, Sitzungsber, Akad. Wiss. Wien, Math. - Naturwiss., 65, 122-146, 1872.

Turner, F. J., and J. Verhoogen, Igneous and Metamorphic Petrology, 694 pp., McGraw-Hill Book Co., New York, N.Y., 1960.

Turner, G., Recoil effects in Ar^{40}-Ar^{39} dating (in preparation).

Turner, G., The distribution of potassium and argon in chondrites, in Origin and Distribution of the Elements, edited by L. H. Ahrens, pp.387-398, Pergamon Press, Oxford, England, 1968.

Turner, G., Argon 40 - argon 39 dating: the optimization of the irradiation parameters, Earth Planet. Sci. Lett., 10, 227-234, 1971.

Turner, G., J. C. Huneke, F. A. Podosek and G. J. Wasserburg, ^{40}Ar-^{39}Ar ages and cosmic ray exposure ages of Apollo 14 samples, Earth Planet. Sci. Lett., in press, 1971.

Wanless, R. K., R. D. Stevens, G. R. Lachance, and R. N. Delabio, Age determinations and geological studies, Geol. Surv. Can., Paper 69-2A, 78 pp., 1970.

Wanless, R. K., R. D. Stevens, G. R. Lachance, and C. M. Edmonds, Age determinations and geological studies, Geol. Surv. Can., Paper 67-2A, 141 pp., 1968.

REFERENCES -- continued.

Wanless, R. K., R. D. Stevens, G. R. Lachance, and C. M. Edmonds, Age determinations and geological studies, Geol. Surv. Can., Paper 66-17, 120 pp., 1967.

Wanless, R. K., R. D. Stevens, G. R. Lachance, and R. Y. H. Rimsaite, Age determinations and geological studies, K-Ar, isotopic ages, Geol. Surv. Can.,Paper 6g-17, 77, 1966.

Wasserburg, G. J., Geochronology and isotopic data bearing on development of the continental crust, Adv. in Earth Science, edited by P. M. Hurley, 431-459, 1966.

Wasserburg, G. J., Argon-40: potassium-40 dating, in Nuclear Geology, edited by Henry Faul, 341-349, John Wiley and Sons, New York, N.Y., 1954.

Wasserburg, G. J., R. J. Hayden, and K. Jensen, Ar^{40}-K^{40} dating of igneous rocks and sediments, Geochim. Cosmochim. Acta, 10, 153-165, 1956.

Wasserburg, G. J., G. W. Wetherill, L. T. Silver and P. T. Flawn, A study of the ages of the Precambrian of Texas, J. Geophys. Res., 67, 4021-4047, 1962.

Wetherill, G., L. T. Aldrich and G. L. Davis, Ar^{40}/K^{40} ratios of feldspars and micas from the same rock, Geochim. Cosmochim. Acta, 8, 171-172, 1955.

Williams, H., The geology of southeastern Canada, in Geology and Economic Minerals of Canada, edited by R. J. W. Douglass, p. 243-261, Dept. Energy, Mines and Resources, Ottawa, Canada, 1970.

Williams, H., F. Turner, and C. Gilbert, Petrography, An Introduction to the Study of Rocks in Thin Sections, W. H. Freeman, San Francisco, Calif., 406 pp., 1958.

REFERENCES -- continued.

Wolfe, S. H., Some aspects of the Manicouagan-Mushalagan Lakes Structure, U. S. Geol. Surv. Astrogeol. Stud., Ann. Prog. Rept., Part B., July 1, 1965-July 1, 1966, 71-78, 1966.

Wolfe, S. H., and F. Horz, Shock effects in scapolites, Am. Mineral., 55, 1313-1327, 1970.

Wrage, E. G., Argonbestimmungen an Kaliummineralien, VIII -- ein Naherungsverfahren zur Losung von Diffusionsproblemen, Geochim. Cosmochim. Acta, 26, 61-66, 1962.

Zartman, R. E., A geochronologic study of the Lone Grove pluton from the Llano Uplift, Texas, J. Petrol., 5, 359-408, 1964.